

Abstract

Title of dissertation: Development of single-neuron proteomics by mass spectrometry for the mammalian brain.

Sam (Bok Dong) Choi, Doctor of Philosophy,
2021

Dissertation directed by: Prof. Peter Nemes, Department of Chemistry and Biochemistry

Single-neuron proteomics holds the potential to advance our understanding of important biological processes during neuron maturation and development. However, to characterize proteins from single neurons, further technological advances are still required. This dissertation discusses the development and application of single-cell mass spectrometry (MS) technologies to investigate proteins and its role in different neurons. The work presented herein demonstrates the strategies to develop and advance single-neuron analysis using capillary electrophoresis (CE)-MS. In addition, this work features several contributions to our understanding of neuron-to-neuron heterogeneity, providing new information to advance cell biology and neuroscience.

Chapter 1 overviews the current state of proteomic analysis for cell biology and neuroscience as well as our animal model for this study.

Chapter 2 describes the development of a capillary electrophoresis nanoelectrospray ionization for high-resolution mass spectrometry (tapered-tip emitter).

Chapter 3 presents the improvement in single-cell analysis workflow with a prefractionation method to enhance protein coverage.

Chapter 4 presents the development of an iterative data-dependent acquisition (DDA) ladder to improve sensitivity.

Chapter 5 presents the integration of electrophysiology with microcapillary CE-ESI-MS.

Chapter 6 details the application of ion mobility mass spectrometry with chemical desalting to distinguish different types of neurons by proteomics analysis.

Chapter 7 summarizes results from this dissertation reflects on potential advancements to drive single-neuron proteomics forward.

Development of single-neuron proteomics by mass spectrometry for the
mammalian brain

by

Sam (Bok Dong) Choi

Dissertation submitted to the Faculty of the Graduate School of the
University of Maryland, College Park, in partial fulfillment
of the requirements for the degree of
Doctor of Philosophy
2021

Advisory Committee:

Associate Professor, Peter Nemes, Chair
Professor, Briken Volker, Dean's Representative
Distinguished University Professor, Catherine Fenselau
Professor, Dorothy Beckett
Professor, Neil Blough
Assistant Professor, Colenso Speer

© Copyright by
Sam (Bok Dong) Choi
2021

Acknowledgements

I would like to express my gratitude to my academic advisor, Prof. Peter Nemes, for allowing me to join his research group. I am very thankful for the experience and knowledge I gained under his mentorship. I sincerely thank you for your patience, for teaching me how to formulate scientific questions and to think critically. In addition, your continuous support and guidance has built me into a better individual, leader, and scientist.

I would also like to express my gratitude to Prof. Colenso Speer, Prof. Neil Blough, Prof. Dorothy Beckett, Prof. Briken Volker, and Prof. Catherine Fenselau for serving on my dissertation committee. I am also grateful to Prof. M. Chiara Manzini and Prof. Abigail Polter for showing and imparting their knowledge and passion for neuroscience.

I am also very thankful to past and current members of the Nemes lab, for sharing many meaningful memories and plenty of snacks during our lengthy group meetings. Many thanks to Dr. Camille Lombard-Banek, Dr. Rosemary Onjiko, Dr. Erika Portero, Aparna Baxi, Vi Quach, Jie Li, Aleena Andrews, Leena Pade, Steven Woolford, Dr. Kellen DeLaney, Ryan O'Neal, John Udara Mendis, Bowen Shen, and Dash Jia for taking their precious time to review my abstracts, manuscripts and presentation rehearsals. I would also like to thank Prof. Efrain Rodriguez, Diane Canter from the Chemistry and Biochemistry Department at the University of Maryland for helping me to easily navigate the administrative path towards graduation.

I am forever thankful to my family and close friends for their constant love and support during this journey. To my father, Sang Yeong Choi, thank you for the unconditional love, encouragement, and sacrifice. It was you who I looked up to when I had the most difficult time. Without your encouraging words, I could not have successfully finished the program. Since the beginning of the program, you were always there for me and I am forever thankful for your unconditional support. Thank you sincerely.

I would also like to thank my friends for being there when I had doubts and cheering me on, Jason Choi, Aaron Lee and James Chu. Thank you for being there for me whenever I had difficulties both emotionally and financially. It was you guys who I had turned to when I was going through so much trouble in my life. Thank you for being there always.

I am also thankful to my brothers Ill Kyu Moon and Ill Hwan Moon for always believing in my ability to succeed and for supporting me from the very beginning. To my close friend, Sarang Han, thank you for being always there for me when I was going through hard times. Thank you for bringing joy to my life when it was much needed.

I am grateful to the funding sources that supported this work and myself over the past several years. The Arnold and Mabel Beckman Foundation Young Investigator Grant and the National Institute of Health (NIH) and the Cosmos Club Foundation Scholar Grant.

Table of Contents

Acknowledgements.....	ii
Table of content.....	iv
List of Tables	vii
List of Figures	viii
List of Abbreviations	ix
Chapter 1: Introduction	1
1.1 Single-cell proteomics.....	1
1.2 Proteomic analysis for cellular biology and neuroscience.....	4
1.2.1 Proteomics by mass spectrometry.....	4
1.2.2 Proteomics for cell biology and neuroscience	7
1.3 Research significance and motivation	10
Chapter 2: Development of custom-built capillary electrophoresis nanoelectrospray ionization for limited population of neurons	12
2.1 Introduction.....	12
2.2 Experimental section.....	16
2.2.1 Materials and reagents	16
2.2.2 Solutions	16
2.2.3 Animals.....	17
2.2.4 Proteomic sample preparation.....	17
2.2.5 CE-nanoESI-MS	18
2.2.6 Data analysis	19
2.2.7 Safety consideration.....	20
2.3 Results and discussion	21
2.3.1 Goal and design.....	21
2.3.2 Mass-limited protein digests	28
2.4 Conclusions.....	33
Chapter 3: Enhancing peptide detection by reversed-phase pre-fractionation with capillary electrophoresis mass spectrometry	36
3.1 Introduction.....	36
3.2 Experimental section.....	40
3.2.1 Chemicals and reagents.....	40
3.2.2 Solutions	41
3.2.3 Neuron culture	41
3.2.4 Bottom-up proteomic workflow	43
3.2.5 Reversed phase peptide separation	43
3.2.6 CE-nanoESI-HRMS.....	44
3.2.7 Data analysis	44
3.2.8 Safety consideration.....	45
3.3 Results and discussion	46

3.3.1 Sensitivity needs for limited neuron populations.....	46
3.3.2 Improved trace-sensitive peptide detection	47
3.3.3 Improved trace-sensitive protein detection.....	54
3.4 Conclusions.....	58
Chapter 4: Development of data-dependent acquisition ladder to support ultrasensitive proteomics	
4.1 Introduction.....	60
4.2 Experimental section.....	64
4.2.1 Materials	64
4.2.2 Buffer and standard solutions	65
4.2.3 Neuron culture	65
4.2.4 Bottom-up proteomics	65
4.2.5 Microanalytical CE-nanoESI-HRMS	66
4.2.6 Data analysis	67
4.2.7 Safety consideration.....	67
4.3 Results and discussion	68
4.3.1 A Technological Gap.	68
4.3.2 Guided Design of the DDA Ladder	73
4.4 Conclusions.....	78
Chapter 5: Single-cell mass spectrometry with patch-clamp electrophysiology extends the bioanalytical toolbox of neuroscience	
5.1 Introduction.....	80
5.2 Experimental section.....	82
5.2.1 Materials	82
5.2.2 Animals and brain section preparation	83
5.2.3 Whole neuron electrophysiology and sample collection	84
5.2.4 Sample processing for bottom-up proteomics	84
5.2.5 Single-cell HRMS and CE-nanoESI-HRMS	86
5.2.6 Data analysis	87
5.2.7 Safety consideration.....	87
5.3 Results and discussion	88
5.3.1 Goal and design.....	88
5.3.2 Electrophysiology based microsampling approach	89
5.3.3 Protein identification from single DA neuron	96
5.4 Conclusions.....	98
Chapter 6: Single-cell proteomics by mass spectrometry with patch-clamp electrophysiology using chemical desalting to enhance proteomic coverage for a single neuron.....	
6.1 Introduction.....	100
6.2 Experimental section.....	103
6.2.1 Materials	103
6.2.2 Animals and brain section preparation	103
6.2.3 Sample preparation for single neuron via bottom-up proteomics.....	104

6.2.4 Single-cell CE-nanoESI-HRMS	106
6.2.5 Data analysis	107
6.2.6 Safety consideration.....	108
6.3 Results and discussion	108
6.4 Conclusions.....	121
Chapter 7: Conclusions and future directions.....	123
7.1 Advancing single neuron proteomics and neuroscience.....	123
7.2 Technological advancements for single-cell proteomics.....	125
7.2.1 Improvements in proteomics detection.....	125
7.2.2 Improvements in measurement throughput	125
7.2.3 Improvements in sample preparation.....	126
7.2.4 Improvements in bottom-up data acquisition	126
7.3 Outlook	127
Appendices.....	129
Bibliography	148

List of Tables

Chapter 4

Table 4.1 Protein identification from control, top 150 excluded and top 250 excluded experimental condition.....	129
--	-----

List of Figures

Chapter 1

Figure 1.1 General MS-based proteomics workflow	5
---	---

Chapter 2

Figure 2.1 The proposed microanalytical methodology for trace-level proteomics	22
Figure 2.2 Configuration of ionization sensitivity	25
Figure 2.3 Ultra-sensitive peptide detection	26
Figure 2.4 Technology validation for trace-level bottom-up proteomics	29
Figure 2.5 Protein identification from 1 ng protein digest.....	30

Chapter 3

Figure 3.1 Experimental strategy for improving protein identifications	48
Figure 3.2 Peptide detection by CE-nanoESI-HRMS	49
Figure 3.3 Multidimensional separation for enhancing peptide identifications	51
Figure 3.4 Metrics of peptide and protein detection	54
Figure 3.5 Case study of analyzing 500 pg of protein digest.....	56

Chapter 4

Figure 4.1 Experimental strategy of the nested DDA ladder.....	69
Figure 4.2 Challenges in trace-sensitive neuroproteomics	72
Figure 4.3 Guided design of the DDA ladder	75
Figure 4.4 Depth of proteome coverage	77

Chapter 5

Figure 5.1 Microanalytical workflow	89
Figure 5.2 Validation of the TMT-label approach.....	94
Figure 5.3 Protein and peptide detection from a section of substantia nigra tissue.....	97

Chapter 6

Figure 6.1 Detection of trace amounts of proteins from single neurons.....	110
Figure 6.2 Salt contamination apparent towards single neuron proteomics	112
Figure 6.3 The effect of crown ether on desalting NaCl from model peptides	114
Figure 6.4 Protein ID improvements from using crown-5-ether	115
Figure 6.5 Neuronal soma extraction by microcapillary sampling.....	118
Figure 6.6 Protein identified among different types of neurons	119

List of Abbreviations

CE	Capillary electrophoresis
MS	Mass spectrometry
LC	Liquid chromatography
TOF	Time-of-flight
HRMS	High resolution mass spectrometry
ESI	Electrospray ionization
IMS	Ion mobility spectrometry
CID	Collision-induced dissociation
EIC	Extracted ion chromatogram
DA	Dopaminergic Neuron
TMT	Tandem mass tag
TIMS-TOF	Trapped-ion mobility spectrometry time-of-flight
DDA	Data dependent acquisition
SCOPE-MS	Single cell proteomics by mass spectrometry
PASEF	Parallel accumulation serial fragmentation
PTM	Post translation modification
qOT	Quadrupole orbitrap
HCD	Higher-energy collisional dissociation
iTRAQ	Isobaric tags for relative and absolute quantification
LFQ	Label free quantification
iBAQ	Intensity-based absolute quantification
MRM	Multiple reaction monitoring
SRM	Single reaction monitoring
PRM	Parallel reaction monitoring
CCS	Collision cross section
FWHM	Full width at half max
FDR	False discovery rate
RP	Reverse-phased
PSM	Peptide spectral matches
MF	Molecular features
BSA	Bovine serum albumin
PVN	Parvalbumin
SR	Serotonin
HCA	Hierarchical cluster analysis

Chapter 1: Introduction

1.1 Single-cell proteomics

Uncovering molecular mechanisms of actions in neurons promises to revolutionize our understanding of complex biochemical events in the brain. To this end, systems biology has enabled the understanding of developmental processes with the comprehensive characterization of groups of biomolecules produced in a neuron (DNA, RNAs, proteins, and metabolites) as it matures in the brain. However, there exists a highly complex molecular profile of neurons as there are over 100 billion of neurons consisting of over 100 trillions of interconnected synapses. To understand the molecular profile of this enormous complexity of the neurons, we need to understand its biomolecules produced first as they can lead to the origin of molecular functions. Currently, the human genome contains ~21,300 protein-coding genes,¹ which gives gene products of ~30,000 proteins spanning a 7-10 log-order in dynamic concentration range². Moreover, the human metabolome database currently reports ~115,000 metabolites with concentration ranging in a similar dynamic range,³ which are known to represent only a small fraction of the total metabolites present in the cell. With recent advancements in technology, genomic studies are now able to profile the genome of single cells which has produced important knowledge of cellular heterogeneity in DNA,⁴⁻⁶ RNA,⁷⁻⁸ proteins⁹⁻¹¹ and metabolites¹²⁻¹³. However, there is conceivable fact that transcript and protein productions are often poorly correlated.¹⁴⁻¹⁵ In addition, how processes of gene transcription, translation, and metabolism interplay in complex molecular systems is yet to be understood due to lack of knowledge of protein and metabolite composition during neuron maturation. There have been tremendous

technological challenges to characterize downstream products of gene translation with sufficient understanding. For example, proteins, unlike DNA and RNAs, have a vast variety of chemical properties that exist at a wide dynamic concentration range and cannot be amplified, making their detection difficult. In addition, proteins can be further modified after their production through post-translation modification (PTMs) which make their detection even more complicated due to over hundreds of modifications that change their molecular weights, the fundamental physical property measured by mass spectrometry.¹⁶

The proteome is viewed as the descriptor of a cell's molecular functions and organization inherent in a cell. The proteome amasses downstream products of intrinsic events, such as transcription, translation and changing phase of the cell cycle as well as extrinsic influences including chemical, physical and biological cues. Therefore, single-cell proteomics gives an important overview of cell's molecular mechanism of action and gives an understanding of molecular state. Currently, high-resolution mass spectrometry (HRMS) is the analytical technology of choice for protein analysis for large numbers of mammalian cells^{2, 17-19}. Recent advancements in MS technologies have now made it possible to routinely measure and quantify thousands of proteins from biological specimens from different model organisms, including the human,²⁰ mouse,²¹ and African clawed frog (*Xenopus laevis*).²² HRMS has great detection sensitivity and specificity. It can also perform both label and label-free quantification. In addition, HRMS can be used to perform both untargeted and targeted proteomic analyses. With recent advancement in MS technology, single cell analysis or the analysis of small samples have now made it possible. With a custom-built capillary electrophoresis (CE)- electrospray ionization (ESI) platform, the Nemes lab was able to detect and quantify over 800 protein groups from less than 5 ng of total protein content from a live embryonic cells^{9 23} and from a single neuron.²⁴ In

addition, more recently, single-cell proteomics by MS (SCoPE-MS)²⁵ was able to achieve adequate ion signals for peptide sequencing and quantification in single mammalian cells by integrating isobaric tandem mass tags (TMT)²⁶ and carrier channel cells to enhance the signal intensity from individual cells. Overall, single-cell proteomics technologies have been readily coupled to separation techniques (e.g., capillary electrophoresis (CE), liquid chromatography (LC), etc.) to enable the analysis of gene products in single eggs²⁷⁻²⁸ and small population of neurons isolated from mouse brains.²⁹⁻³⁰

To this end, a population-averaging method is used for the analysis of proteins to provide a global proteome of a large number of cells. However, this method fails to reveal protein variations at the single-cell level, where important biological processes can be captured. With this limitation, primary cell culture can be useful for neuroscientists but does not relay molecular information of individual cells. In addition, proteins expressed in dissected tissue or cell cultures do not necessarily represent the native state of a live cell due to different responses to cell perturbation, disruption, and removal from original tissue. These biological responses from cells will result in significantly different responses for individual cells. Therefore, a microanalytical approach is required to enable the direct sampling of cells.

Here, I discuss the application of MS for proteomic analysis of cells and neurons for neuroscience and put in perspective the work presented in this dissertation. This chapter highlights the current state of proteomic analyses and their application to neuroscience using mouse brain for this dissertation work.

1.2 Proteomic analysis for cellular biology and neuroscience

1.2.1 Proteomics by mass spectrometry

MS is the analytical technology of choice for detecting and quantifying proteins due to its high sensitivity, specificity, and label-free detection capability. There are multiple approaches to detect a protein using MS, including top-down, middle-down, and bottom-up approach. In the “top-down” approach, entire proteins are detected directly using ultrahigh-resolution mass spectrometry. Using advanced sequencing strategies (e.g., electron transfer dissociation), deep sequencing of proteins has been performed with Fourier transform ion cyclotron resonance (FTICR) mass spectrometers which are able to resolve protein isoforms and post-translational modifications. The middle-down approach uses enzymes to partially digest proteins into mid-sized peptide fragments that are more readily detected by high-resolution mass spectrometers. However, the most common approach is the bottom-up approach, where proteolytic enzymes (e.g., trypsin) are used to digest proteins into smaller sized peptides (e.g., 5-25 amino acids) which are then separated (e.g., by nano-flow LC or capillary electrophoresis), ionized by nano-flow electrospray ionization (nanoESI) and sequenced by tandem MS.³¹⁻³² For this dissertation work, a bottom-up proteomic approach was used and will be described further in the following section.

The general bottom-up proteomics workflow is presented in Figure 1.1 and has recently been reviewed in detail.³¹⁻³² First, cells from biological samples (e.g., cell culture, tissue, etc.) are lysed by chemical and physical perturbation. I used salts and detergent to disrupt the cells and solubilize and denature the freed proteins, and physical perturbation was performed by

sonication. After disruption of the cells, protein disulfide bonds are then reduced and alkylated to promote further unfolding. Resulting proteins are digested into peptides using a proteolytic enzyme. Trypsin is the most common choice of enzyme due to its high specificity (cleaves at the c-terminal of arginine and lysine residues) and because it leaves a positive charge at the end of the cleaved peptides which enhances their ionization. Peptides are typically separated using reversed-phase nano flow liquid chromatography (nanoLC) or capillary electrophoresis (CE). Additional separation by offline fractionation of these peptides has been shown to improve the number of identified proteins.³³⁻³⁵

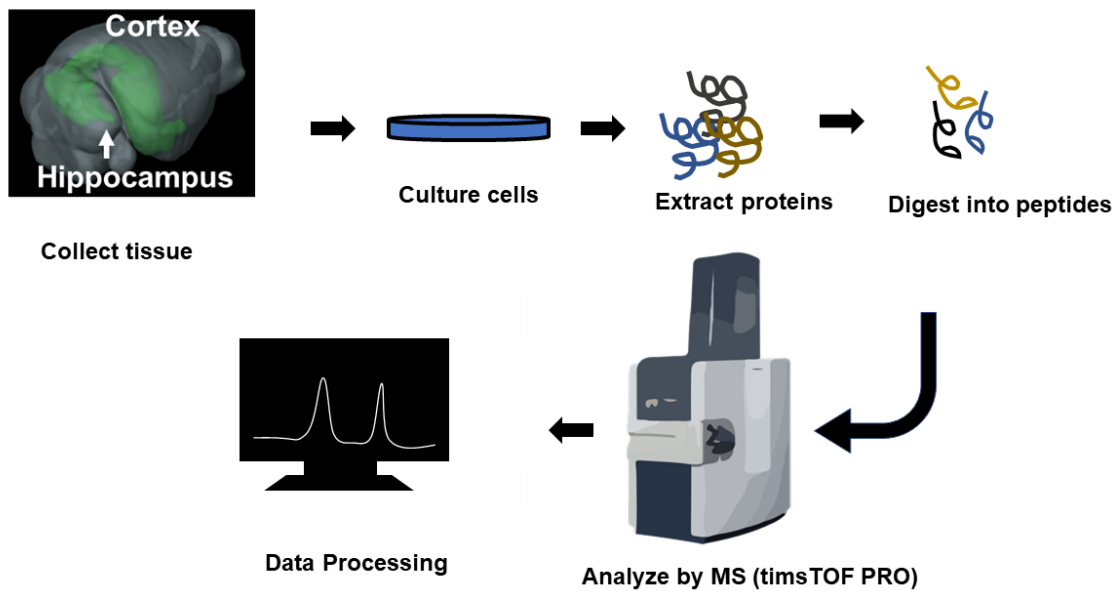


Figure 1.1 General MS-based proteomics workflow for the detection of proteins in biological samples.

Upon separation, peptides are ionized typically by electrospray ionization and detected by different types of mass analyzers. Generally, both nanoLC and CE are coupled to a tapered fused silica nanospray emitter or a tapered-tip stainless steel emitter. Next, the generated peptide ions

are detected using high-resolution hybrid instruments such as quadrupole orbitrap (qOT) or quadrupole time-of-flight (qTOF) mass analyzers for untargeted, discovery analysis. The peptide ions are sequenced in the mass analyzer by using a data-dependent acquisition approach. In this approach, peptide ions are detected on single-stage (full) scans (MS^1) and are sequenced by tandem-MS (MS^2) using collision-induced dissociation (CID), higher-energy collisional dissociation (HCD) or other fragmentation techniques.

Quantitative analysis can be performed using one of several different approaches. One of which is relative quantification, where proteins or peptides from different samples are differentially labeled and mixed together to allow for the simultaneous quantification of these proteins and peptides in a single analysis. One such method involves using designer mass tags that have been developed to barcode proteins or peptides via chemical reactions. Examples include, tandem-mass tags (TMTs)³⁶ and isobaric tags for relative and absolute quantification (iTRAQ)³⁷ that have been commercialized, whereas another type of tagging can be synthesized in house (DiLeu).³⁸ The alternative is label-free quantification (LFQ), which quantifies proteins based on spectral counting or ion signal abundance. Using LFQ with known concentration of protein standards makes absolute quantification possible via intensity-based absolute quantification (iBAQ). There are also different types of techniques like single reaction monitoring (SRM), multiple reaction monitoring (MRM) or parallel reaction monitoring (PRM) to successfully monitor and provide relative and absolute quantification of peptides of interest. However, these techniques are used only with targeted peptides of interests such as biomarkers.

The identification of proteins and their PTMs is often facilitated by advanced bioinformatics software tools that are capable of processing and extracting complex MS data through user-friendly interfaces. This step is often facilitated by publicly available proteomes

from UniProt and in-silico predicted proteomes from experimentally determined RNA expression. Some of the well-established bioinformatics software packages that are used to process raw mass spectrometric data include Proteome Discoverer (Thermo Scientific), ProteinScape (Bruker Daltonics) and MaxQuant³⁹ by executing search engines such as SEQUEST, Mascot and Andromeda. Protein identification strategies used in bottom-up proteomics have been reviewed in the references.^{1, 39-40}

1.2.2 Proteomics for cell biology and neuroscience

Untargeted characterization of protein production in single neurons can facilitate our understanding of biochemical processes involved in neurons during brain development. More specifically, there exists an enormous molecular diversity between neurons which are responsible for functional differences as they develop at the protein level.⁴¹ Uncovering these molecular differences can empower neuroscientists to understand biological processes involved during normal and impaired brain development. However, single-cell analysis requires technologies that can deliver biological characterization at the level of cell function (electrophysiology), gene expression (transcriptomics) and protein production (proteomics) to gather all the information to understand the molecular mechanism of action. At present, there are many technologies for single-cell electrophysiology and transcriptomics that are routinely utilized for physiological investigation. For example, whole-cell patch-clamp electrophysiology can now routinely measure electrophysiological properties of single neurons for neuroscientists.⁴² Although it requires technical skills to manipulate the cell and an understanding of electrical activities of neurons for high-fidelity biophysical analysis, it is the one of the most utilized method to measure the cell's response to electrical activity. For characterizing gene expressions in single

cells, next generation RNA-sequencing technology enables global transcriptomic profiling across different brain regions and neuron types.⁴³⁻⁴⁵ Unfortunately, these types of advancements in technology are not yet available for single-cell proteomics analyses that involve the detection of large numbers of proteins directly from single-neurons, because there is no amplification that is available for single-cell proteomics.

Detecting proteins from directly sampled single neurons would also require a significant enhancement in detection sensitivity for current MS-technology. The average size of single mammalian neurons (~5–50 μm in diameter) with limited total protein amounts available (<500 pg) makes the detection of proteins difficult. Moreover, a wide dynamic range in concentration (~7-log-order in magnitude) for proteins in neurons also makes quantitative measurements challenging for HRMS.⁴⁶ Several technologies were introduced to accommodate these challenges for trace-sensitive analysis. For example, liquid chromatography (LC) technology is one of the mainstream techniques for proteomics studies for HRMS. However, LC technology usually requires 100–1,000 ng of protein digest amounts per measurement, which is ~1,000-fold higher than the amount of protein available in single neurons.⁴⁷⁻⁴⁸

As an alternative approach, CE technology is compatible with limited sample volumes (<10 nL) and is capable of providing online preconcentration to boost peptide ion signals for sensitive analysis. CE can also achieve high separation efficiency to resolve complex molecular samples in short analysis times. Typically, an ~2–3 h measurement time is normal for LC, but CE measurements can be completed in less than 30 min (~4–6 \times faster than LC). With these technological advantages over LC, many reports demonstrate the potential of CE-HRMS technology towards single-cell analysis. Representative cases include a discovery detection of ~200 protein groups from 5 ng of *Pyrococcus furiosus* digest,⁴⁹ ~109 protein groups from 100

HeLA cells (~30 ng of protein),⁵⁰ and ~730 protein groups from 1 ng of hippocampal neuron digest.²⁹ However, CE separates compounds based on their electrophoretic mobility, which depends on the size and charge of the compound while LC separates based on their hydrophobicity indices. Therefore, neither CE or LC can easily resolve co-eluting isobaric (same nominal mass) and isomeric species, which often lead to chimeric tandem mass spectra. This problem significantly hinders peptide and protein identification.⁵¹ To further extend these measurements directly to single neurons, new solutions are needed to separate isobaric and isomeric compounds to enhance the single-neuron proteomic measurements.

One possible option to resolve isobaric and isomeric compounds is to use ion mobility spectrometry (IMS) with HRMS. In this technology, compounds are separated in gas phase based on their collisional-cross section (CCS), which relates to the size and shape of the molecule.⁵² The incoming peptide ions to the MS can be additionally separated in the IMS-HRMS, enabling co-eluting isobaric species to be resolved for improved identification, reducing chimeric spectra problem. Chimeric spectra can be a problematic where two more precursor ions with similar mass and retention time are co-sequenced by MS/MS, thus diminishing the identifiable peptides.⁵³ Introducing this separation mechanism in addition to CE or LC would greatly enhance peptide coverage from complex mixtures. However, as mentioned before, LC technology excels in large-scale proteomics but is not fully applicable to single-cell proteomic analysis. In addition, there exists no technology that integrates CE with IMS-HRMS for shotgun proteomics, especially that is suitable for volume- and mass-limited samples. Although IMS-HRMS promises to alleviate the chimeric spectra problem, the current state of technology calls for new ways to integrate the system with different technologies toward single-neuron proteomics.

1.3 Research significance and motivation

To study proteomics in individual neurons during their early maturation, the Nemes Lab uses the mouse brain, a well-established mammalian model for molecular, cellular and neuroscience studies. This animal model offers several advantages for neuroscience, for example: it is anatomically, physiologically, and genetically similar to humans, the animals are easy to maintain, they have a short life cycle, and abundant genetic resources are available.

Recently, our lab characterized limited population of neurons from cultured neurons and identified important proteins that belong to the types of neurons using CE-ESI-MS. Comparing proteomic profiles obtained from single neurons would enable us to differentiate different types of neurons and test the functional significance of the measured proteomic differences across different types of neurons.

In this dissertation work, I developed single-cell analytical tools and applied them to distinguish types of neurons based on proteomic analysis of single neurons that were identified by electrophysiology. To enable single-cell proteomics, a new generation electrospray ionization source was developed in **Chapter 2** to enhance peptide detection sensitivity. Using a custom-built CE-MS platform, I developed pre-fractionation methodology to further improve the number of peptides detected towards single neuron analysis (**Chapter 3**). In **Chapter 4**, I discuss the development of iterative data-dependent acquisition methodology to deepen proteome coverage by MS. In **Chapter 5**, I discuss the incorporation of a new sampling approach by integrating electrophysiology and microaspiration to characterize proteins in the neuronal soma. **Chapter 6** utilizes this technology with a new chemical desalting methodology

to enhance the detectable proteins from single neurons that were collected from electrophysiological measurements. Finally, **Chapter 7** reflects on the current state of single-cell proteomics with mass spectrometry, emphasizing existing challenges and emerging methodologies that are needed to continue to push the field forward.

Chapter 2: Development of custom-built capillary electrophoresis nanoelectrospray ionization for limited population of neurons

This chapter includes material adapted with permission from:

S.B. Choi, M. Zamarbide, M.C. Manzini and P. Nemes*, Tapered-Tip Capillary Electrophoresis Nano-Electrospray Ionization Mass Spectrometry for Ultrasensitive Proteomics: the Mouse Cortex, *Journal of the American Society of Mass Spectrometry*. 2017, 28, 597-607. <https://doi.org/10.1007/s13361-016-1532-8>

Author Contribution: S.B. Choi processed the sample, analyzed the data, and wrote the manuscript

2.1 Introduction

Unbiased characterization of gene expression has the potential to reveal how the central nervous system establishes enormous cell and tissue diversity. Starting with usually thousands–millions of cells, high-resolution mass spectrometry (HRMS) is able to characterize the encoded proteome and quantify translational and post-translational modifications.⁵⁴⁻⁵⁷ Discovery HRMS enabled drafting of the human proteome⁵⁸ and, recently, cataloging gene expression diversity between tissues and cell types in the mouse brain,⁵⁹ complementing cell heterogeneity information at the transcriptomic level.⁶⁰⁻⁶¹ Extension of proteomics to small populations of neurons would empower brain research, but this requires new microanalytical HRMS solutions capable of measuring trace amounts of proteins.

There have been a handful of reports on proteomics from nanograms–subnanograms of proteins (see recent reviews including references⁶²⁻⁶⁵). Single-cell HRMS was pioneered with the detection of 450 amol (~10 ng) α - and β -globulins from human erythrocytes⁶⁶ and carbonic

anhydrase⁶⁷ in diluted lysates by capillary electrophoresis (CE) Fourier transform ion cyclotron resonance (FTICR). For targeted proteins, gains in detection sensitivity and throughput were possible using microfluidics (two proteins with 12 cells/s)⁶⁸ and mass cytometry (34 proteins with 1000 cells/s).⁶⁹ In parallel, refinements in sample preparation and nano-flow liquid chromatography (nanoLC) HRMS extended mass-limited proteomics to discovery operation. Representative cases include identification of 2000 proteins from cytometry (34 proteins with 1000 cells/s).⁶⁹ Representative cases include identification of 2000 proteins from <400 ng proteins from Langerhans islets,⁷⁰ 145–187 proteins from 500 breast cancer cells (~150 ng protein),⁷¹ and 109 proteins from 100 HeLa cells.⁷² Additionally, porous layer open tubular (PLOT) columns yielded 566 proteins from 50 ng *M. acetivorans*⁷³ and 163 proteins from ~20 cervical cancer cells (~2.5 ng).⁷⁴ Using FTICR, 870 proteins were identified from 50 ng proteins from *D. radiodurans* with an estimated 7 amol lower limit of detection.⁷⁵ Most recently, 1327 proteins were identified from 50 human breast adenocarcinoma cells (~5 ng protein) using focused acoustics-assisted sample preparation and 4-h-long separation on a PLOT column.⁷⁶ These examples demonstrate substantial sensitivity improvements in nano-flow LC to extend proteomics to limited samples.

CE is an alternative technology with orthogonal advantages for trace amounts of proteins. High separation power, compatibility with limited samples, fast separation (<1 h), and remarkable limits of detection were demonstrated early by a coaxial sheath-flow electrospray ionization (ESI) interface supplemented with a nebulizer gas.⁷⁷ Since this milestone work, various CE-ESI designs were developed in pursuit of sensitivity and robustness (see reviews elsewhere⁷⁸⁻⁸⁰). To enhance sensitivity, one group of interfaces eliminates the sheath liquid (“sheathless” designs) to avoid sample dilution in the ion source and maintains nano-flow

electrospray ionization (nanoESI) through pulled and/or coated capillaries.⁸¹⁻⁸⁵ Emitter clogging and loss of electrical contact have been reported to affect the operational durability of these devices. The porous-junction interface⁸⁶ enhanced robustness and sensitivity to 30 amol lower limit of detection for peptides and protein standards,⁸⁷⁻⁸⁸ detecting 385 proteins from 5 ng digest of the extremophile *P. furiosus*⁸⁹ in a bottom-up strategy. Most recently, 5-amol detection was accomplished for targeted peptides by directly hyphenating a CE capillary to an ESI emitter.⁹⁰ Sheathless interfaces have also demonstrated utility for intact proteins from a few hundred nanograms of proteins.⁹¹⁻⁹³

“Sheath-flow” CE-ESI devices are attractive due to easier construction, enhanced robustness, and compatibility with different modalities of CE separation. The broadly successful sheath-flow design [24] surrounds the CE capillary with a sheath liquid at tens of $\mu\text{L}/\text{min}$ to complete the electrical circuit⁹⁴ and a stream of concentric, heated nebulization gas (L/min) to facilitate droplet desolvation. CE-ESI sensitivity was improved by eliminating the nebulizer gas and lowering the sheath liquid rate to 5–10 $\mu\text{L}/\text{min}$.⁹⁵ Further reduction of the sheath liquid rate using an electrokinetic pump and integration of the CE capillary into a pulled nanoESI emitter achieved ~335–600 zmol lower limit of detection for protein standards via multiple reaction monitoring.⁹⁶⁻⁹⁷ Furthermore, refinement to this interface yielded an estimated 1 zmol lower limit of detection on a hybrid quadrupole Orbitrap mass spectrometer, enabling the identification of 60 proteins from 400 fg digest from *E. coli*⁹⁸ in a bottom-up and 30 proteins from *P. aeruginosa* in a top-down approach.⁹⁹ Most recently, 1249 different proteins were identified from 300 ng digest from the *Xenopus laevis* fertilized egg¹⁰⁰ and 2313 phosphorylated peptides in 200 ng protein from human mammary cells¹⁰¹ in discovery MS. The electrokinetically pumped CE-nanoESI interface achieves ultrasensitive operation but requires specialized expertise, including HF

etching, to assemble the ionization source. The recent commercialization of this interface alleviates some of these challenges.

Over the last 6 y, we and others have designed readily constructible, low-cost sheath-flow CE-ESI interfaces for trace-level measurements. Our designs eliminated the nebulizer gas and used blunt-tip metal emitters (260/130 μm o.d./i.d.) to sustain the sheath liquid at 700–1000 nL/min in the stable cone-jet regime to ensure efficient ion generation. CE-micro-flow ESI (μESI) enabled lower limits of detection at 10–50 nM, or 60–300 amol, for metabolites¹⁰²⁻¹⁰⁷ and 3.5–11 nM, or 25–75-amol, for peptides.²⁷⁻²⁸ Large-bore emitters (e.g., 720/420 μm o.d./i.d.) were recently found to compromise the sensitivity of this design to 100 nM, or \sim 1 fmol limit of detection,¹⁰⁸ underscoring that the geometry of the emitter has important impacts on sensitivity. Our CE- μESI interfaces enabled the identification of \sim 1700 and quantification of 500–800 proteins in 10 ng protein digest from single embryonic cells in the 16-cell *Xenopus laevis* embryo, marking the first time metabolomics and proteomics was performed in actual single cells in the cleavage-stage (16-cell) *Xenopus laevis* embryo.^{9, 28}

Here, we report a readily constructible sheath-flow CE-ESI design that is able to operate in the nano-flow regime to enable ultrasensitive bottom-up proteomics of the mouse cortex. We extended CE- μESI into the nano-flow regime (\sim 100–300 nL/ min sheath) and selected a tapered-tip metal emitter to serve as the sheath supply and ESI source. Peptide separation and quantification were reproducible across several weeks with a lower limit of detection estimated at 260 zmol for angiotensin II (156,000 copies) in parallel reaction monitoring. Identification of model proteins from \sim 1 pg amount demonstrated ultrasensitive detection. A 1 ng protein digest from the mouse cortex yielded 217 different protein groups using a quadrupole time-of-flight mass spectrometer. CE-identified proteins included products from many genes that mark major

cell types in the brain, ranging from neurons to oligodendrocytes, astrocytes, and microglia.

Ultrasensitive proteomics by CE-nanoESI-MS raises a potential to characterize gene translation in small populations of cells or single cells to help understand cell heterogeneity during normal brain function and disease.

2.2 Experimental section

2.2.1 Materials and reagents

All materials were purchased at reagent grade or higher from Sigma-Aldrich (St. Louis, MO, USA) unless noted otherwise. Sodium dodecyl sulfate (SDS) was from Amresco (Solon, OH, USA). Reagent-grade ethylenediamine tetraacetic acid 598 S. B. Choi et al.: Tapered-Tip CE-NanoESI-MS For Ultrasensitive Proteomics (EDTA), MS-grade trypsin protease, and LC-MS grade acetonitrile (ACN), methanol (MeOH), formic acid (FA), and water (Optima) were from Fisher Scientific (Fair Lawn, NJ, USA). All standards were prepared in 500- μ L or 2-mL LoBind protein microtubes from Eppendorf (Hauppauge, NY, USA).

2.2.2 Solutions

The lysis buffer was prepared to contain: 20 mM Tris-HCl, 5 mM EDTA, 1% (v/v) SDS, and 35 mM NaCl. Peptide standards were serially diluted from a 200 ng/ μ L stock (in deionized water) using 25% (v/v) ACN containing 0.05% (v/v) FA. Standard bovine serum albumin (BSA, 1 μ g/ μ L) in TEAB buffer (100 mM) was reduced with dithiothreitol (1 M), alkylated with iodoacetamide (1 M), and digested with trypsin [enzyme:protein = 1:50 (w/w)] over 12 h at 37 °C. The digest was lyophilized and reconstituted at 2 μ g/ μ L in 75% (v/v) ACN containing 0.05% (v/v) FA before serial dilution using the same solvent. Solutions were vortex-mixed, centrifuged

at $10,000 \times g$ for 60 s at 4 °C, and stored at -20 °C until measurement by CE-nanoESI-HRMS. The background electrolyte (BGE) consisted of 50% ACN with 1 M FA (yielding pH 2.3).

2.2.3 Animals

All procedures regarding the maintenance and humane treatment of mice were authorized by the George Washington University Institutional Animal Care and Use Committee (IACUC Approval Number A274). Adult male mice (*Mus musculus*) were purchased from Charles River Laboratories (Wilmington, MA, USA) and maintained in a breeding colony. Four-month old adult male mice were sacrificed by cervical dislocation. The brain was surgically removed, placed on ice, and rinsed with ice cold phosphate buffer solution to remove residual blood and contaminants. The posterior half of the cortex was identified in reference to the Allan Brain Atlas, and the tissue was dissected and immediately frozen in liquid nitrogen. The sample was stored at -80 °C until analysis within a month.

2.2.4 Proteomic sample preparation

The dissected tissue was lysed in 500 μ L lysis buffer, facilitated by sonication for 15 min in water bath (~ 4 °C). The lysate was reduced (5 μ L of 1 M dithiothreitol, 30 min at 60 °C) and alkylated (10 μ L of 1 M iodoacetamide, 15 min in the dark) before quenching the reaction (5 μ L of dithiothreitol). To remove cell debris, the lysate was centrifuged at $11,200 \times g$ for 10 min at 4 °C, and the supernatant was aliquoted into a separate LoBind microtube. Proteins in the aliquot were purified by precipitation over 12 h in 2 mL of chilled acetone (-20 °C), followed by centrifugation at $11,200 \times g$ for 10 min at 4 °C. The protein pellet was washed with chilled acetone, lyophilized at room temperature, and reconstituted to 1 μ g/ μ L protein concentration in 500 μ L of ammonium bicarbonate (50 mM) based on the standard bicinchoninic acid (BCA)

assay (Thermo Scientific, Waltham, MA, USA). Aliquots of 50 μL were separated into individual LoBind microtubes to serve as technical replicates. Each aliquot was digested with 1 μL of trypsin (1 mg/mL) over 12 h at 37 $^{\circ}\text{C}$. The digests were lyophilized and suspended in 50 μL of 50% (v/v) ACN containing 0.05% (v/v) AcOH, which was selected to enable on-column preconcentration by field-amplified sample stacking in a higher-conductivity BGE during measurement by CE-HRMS.

2.2.5 CE-nanoESI-MS

The microanalytical CE platform was constructed based on our recent prototypes^{9, 104, 106} and operated for bottom-up proteomics as described elsewhere^{9, 28}. During sample loading, a 1 μL portion of the sample was deposited into a microloading vial, whence 1 nL (\sim 1 ng protein digest) was hydrodynamically injected into the CE separation capillary (90/ 20 μm o.d./i.d., 90 cm length) by elevating the capillary inlet 20 cm above the outlet end for 3 min. Peptides were separated by applying 22–26 kV to the capillary inlet. The CE electrical circuit was completed through a sheath solution (50% MeOH in 0.1% FA), which was fed through a grounded metal emitter and supplied by a low-flow syringe pump (model Pico Plus Elite; Harvard Apparatus, Holliston, MA, USA). The CE-nanoESI interface was built from commercially available parts. The following components were used in the construction (part number, p/n): fused silica capillary for electrospray sheath (360/75 μm o.d./i.d., p/n #106815-0019; Polymicro Technologies, Phoenix, AZ, USA) and for CE separation (90/20 μm o.d./i.d., p/n #106815-0381; Polymicro); metal tapered-tip emitter for nanoelectrospray (320/100 μm o.d./i.d., p/n MT320-100-3.5-5, New Objective, Woburn, MA, USA); sleeves to mount sheath flow (p/n F-172; IDEX Health and Science, Oak Harbor, WA, USA), and CE (p/n F180x; IDEX) capillary; T-union to

mount parts (MicroTee, p/n P-888; IDEX). The CE-nanoESI interface was mounted on a three-axis translation stage to align the emitter tip with the orifice of a mass spectrometer. The Taylor cone was monitored using a long-working distance objective (Plan APO, 20× 0.42 NA, Mitutoyo America Corp., Aurora, IL, USA) and a CCD camera (EO-2018C; from Edmund Optics Inc., Barrington, NJ, USA).

The stability of ion generation was evaluated based on the ion signal recorded by a mass spectrometer. Peptide ions were mass-analyzed between m/z 350 and 2400 by a quadrupole orthogonal acceleration time-of-flight mass spectrometer equipped with a collision-induced dissociation (CID) cell (Qq-TOF, Impact HD; Bruker Daltonics, Billerica, MA, USA). The mass spectrometer was tuned and calibrated according to vendor specifications and operated at 40,000 FWHM resolution. To identify peptides, signals were fragmented via data-dependent acquisition (DDA) with the following settings: data acquisition rate, 4 Hz for MS1 and 1 Hz for MS2 ; survey scan interval, 3 s; fragmentation preference, top most-intense; MS2 threshold, 500 counts per 1000 summations; mass accuracy for dynamic exclusion, 50 mDa; m/z window and CID energy, 8 Da and 20–70 eV depending on charge state; collision gas, nitrogen; and dynamic exclusion, applied; smart exclusion, applied with 5× threshold.

2.2.6 Data analysis

Peptide standards were quantified based on area-under-the curve in selected-ion electropherograms that were generated with 10 mDa window in DataAnalysis. For the standard BSA and cytochrome c, primary MS-MS/MS data were exported into XML in DataAnalysis 4.3 (Bruker Daltonics) and processed in ProteinScape 3.1 using Mascot 2.5.1 search engine. The data were searched against the SwissProt Mammalian proteome database (downloaded on

December 15, 2015). The search parameters were: digestion, tryptic; missed cleavages, maximum 2; minimum number of unique peptides, 1; MS/MS score threshold, 4.5; fixed modification, carbamidomethylation at cysteine; variable modification, oxidation at methionine; and MS tolerance for peptides and fragments, ± 20 ppm and ± 0.1 Da, respectively. For the mouse brain tissue, the raw mass spectrometric data were analyzed with MaxQuant 1.5.3.30 (Max Planck Institute of Biochemistry) executing Andromeda 1.5.3.8 search engine. The MS-MS/MS data were searched against the SwissProt mouse (*Mus musculus*) proteome database (downloaded from UniProt on November 11, 2015) containing 16,792 entries, as well as contaminants from the common Repository of Adventitious Proteins (cRAP) database (downloaded from the Global Proteome Machine¹⁰⁹ on July 28, 2016) containing 115 entries. The search parameters were identical as earlier, except for the following instrument specific parameters: main search peptide tolerance, 6 mDa; TOF MS/MS match tolerance, 30 ppm; isotope match tolerance, 5 mDa; decoy mode, revert. Proteins were identified based on at least one sequence-unique peptide match (see sequence annotations in the Supporting Information document) with false discovery rate (FDR).

2.2.7 Safety consideration

Standard safety protocols were followed when working with chemicals. Capillaries pose poking hazard and were handled with care. All conductive parts of the CE-nanoESI system were shielded or grounded to prevent accidental exposure.

2.3 Results and discussion

2.3.1 Goal and design

The overall goal of this study was to develop a microanalytical HRMS that enables the discovery characterization of protein amounts contained in limited cortical tissues, particularly small populations of neurons. Our experiments based on cultured cortical neurons and a total protein assay (BCA) found that 5–50- μm -diameter neurons contain total protein. As this protein amount is ~ 1000 – $10,000$ -times smaller than common to nanoLC-nanoESI-HRMS analyses, the technology of choice in discovery proteomics, our goal necessitated the development of an alternative approach. One such technology is CE-HRMS, which is compatible with samples limited to ~ 1 – 100 nL, provides exquisite peak capacity, and can be coupled to HRMS.¹¹⁰ Indeed, a microanalytical CE- μ ESI-HRMS platform that we recently built was capable of detecting 1709 and quantifying hundreds of proteins in ~ 20 ng protein digests from single embryonic cells of *Xenopus laevis*.^{9,28} However, as protein amounts contained in a handful of neurons to single neurons are 20–100-times smaller, our goal required significant advances in the sensitivity of CEESI-HRMS.

To bridge this technological gap, we here advanced CE-ESI-HRMS sensitivity to enable bottom-up proteomics from ~ 1 ng protein digest. Our approach (Fig. 2.1) used diluted protein digests from the mouse brain to aid technology development and validation. In this study, the posterior half of the mouse cortex (Fig. 2.1a), which includes the occipital, temporal, and parietal cortical regions, was selected as the model, although any regions of the brain, tissues, or limited populations of cells should be amenable to the workflow. The cortical tissue was dissected, and the proteins were extracted, reduced, alkylated, and trypsin-digested using a standard bottom-up

proteomic workflow (see Methods). The resulting digest was diluted to 1 ng/nL concentration, and a volume containing 1 ng protein digest (1 nL) was used to approximate the total protein content of a handful of mammalian neurons in this study.

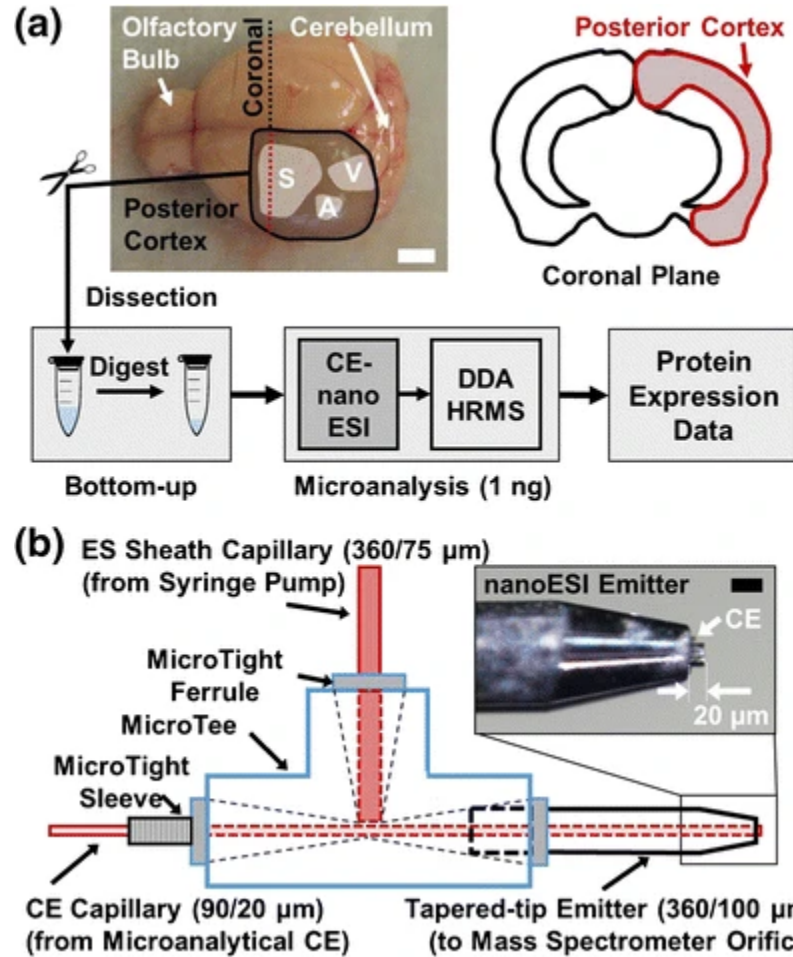


Figure 2.1 The proposed microanalytical methodology for trace-level proteomics in the mouse brain. **(a)** The posterior half of the mouse cortex was identified and dissected free of underlying tissues (see highlight and coronal section). For reference, location of the somatosensory (S), visual (V), and auditory (A) structures are highlighted. Proteins were processed via a bottom-up workflow and the resulting peptides measured. **(b)** Schematics of the tapered-tip capillary electrophoresis (CE) nanoelectrospray ionization (nanoESI) interface for ultrasensitive proteomics. The interface used readily available commercial parts to facilitate broad adoption (see vendor and parts information in the Methods). Scale bar = 2 mm (white), 100 μm (black)

Initially, we tested our sheath-flow CE-μESI interface for measuring this limited protein digest. Based on earlier designs,^{9, 28, 102, 104} we constructed a microsampling stage capable of

reproducibly loading 1 nL, or ~1 ng protein digest into a CE capillary (see Methods for details). The capillary was connected to a CE- μ ESI interface, which featured a 260/133 μm o.d./ i.d. blunt-tip stainless steel tubing (Hamilton Company, Reno, NV, USA). As ESI efficiency depends on electro sprayed droplet size⁹⁴ and droplet size varies with flow rate,¹¹ we proposed that further sensitivity enhancements are possible using this CE- μ ESI device by lowering the sheath liquid rate to the nano-flow regime. The scaling laws of electrospray¹¹¹ suggest that transitioning from 1 $\mu\text{L}/\text{min}$ to ~200–300 nL/min sheath rate, which is the flow rate domain in standard nanoLC nanoESI-MS, reduces electro sprayed droplet size by 50%. However, our tests showed that the electrospray was unstable below ~500 nL/min sheath liquid: the ion current was frequented by low-intensity domains and current spikes. Microscopy of the electrified meniscus captured transitions from the cone-jet regime to the non-axial (multijet) and pulsating (burst or a stable) spraying modes. Additionally, the electrified liquid meniscus was ill-anchored on the rim of the emitter with frequent transitions between the outer and the inner edges of the rim, likely causing unstable droplet trajectories toward the MS orifice. As these factors combined lowered sensitivity, our goals necessitated an alternative sheath-flow design to measure the limited protein digests.

These observations guided the design of a new CE-ESI interface capable of stable operation in the nano-flow regime (CE-nanoESI) for efficient ion generation. The co-axial sheathflow configuration was selected because of its robust operation and compatibility with diverse CE separation modes. An additional consideration was the use of readily available commercial parts and a simplified configuration to aid instrument construction and transferability to other laboratories. To help reproducibly anchor the Taylor cone, we evaluated metal blunt tip emitters (Hamilton) with narrower rim dimensions than earlier as well as emitters

with tapered-tip geometry (New Objective) that essentially eliminates the rim. Using a T-union, the CE fused silica separation capillary (90/20 μm o.d./i.d.) was mounted into blunt tip metal emitters with 210/108 μm (gauge 33) or 235/108 μm o.d./i.d. (gauge 32) or emitters tapered to 100 μm o.d./i.d. (New Objective). The CE capillary was adjusted to protrude 10–20 μm from the emitter tip to minimize sample dilution in the ion source (see tapered-tip design in Figure 2.1b). These CE-ESI constructs were installed in front of a mass spectrometer, and stability of the Taylor cone was imaged in ESI-only (CE turned off) and CE-ESI operation (CE on) using a long-distance microscope (data not shown). At 200–350 nL/min sheath liquid, the tapered-tip design anchored the Taylor cone most stably and produced the most stable ion current, ensuring robust nanoESI for several hours of tested operation.

Therefore, this tapered-tip CE-nanoESI interface was selected for further characterization as an ionization source. Ideally, the ion source is operated in the cone-jet regime, which is the most efficient for ion generation.¹¹²⁻¹¹³ To enhance ionization efficiency, angiotensin II was supplied at 100 nM in 50% MeOH, 0.1% FA through the sheath liquid using a syringe pump, and a long working-distance camera was used to position the CE-nanoESI emitter in front of the mass spectrometer orifice plate to establish the cone-jet regime. The mass spectrometer was used to evaluate the ion yields as a function of emitter-to-mass spectrometer orifice distance ($d_{\text{ES-OR}}$), electrospray potential, and sheath flow rate. Figure 2.2a maps the onset and stability domains of the cone-jet regime. Shorter distances yielded significantly higher ion currents and better spray stability (less error) for the peptide, which we ascribe to more efficient entraining of electrospray droplets into the mass spectrometer. These data suggest further sensitivity enhancements possible with shorter distances; however, electric discharge (corona discharge, sparks, or arc) presents a practical boundary condition at ~ 300 μm distance from the MS orifice using the current emitter

material. Nonconductive emitters, similar to pulled borosilicate¹⁰⁰ or fused silica capillaries, may help reduce d_{ES-OR} in the presented sheath-flow configuration. Afterward, the rate of sheath flow was refined using a mixture of standard peptides in the CE-nanoESI modality (Figure 2.2b). Angiotensin II, leucine enkephalin, and methionine enkephalin were detected in the highest ion signal intensity (electrophoretic peak area) at 300 nL/min sheath, which corresponds to the flow rate domain used in standard nanoESI-HRMS.

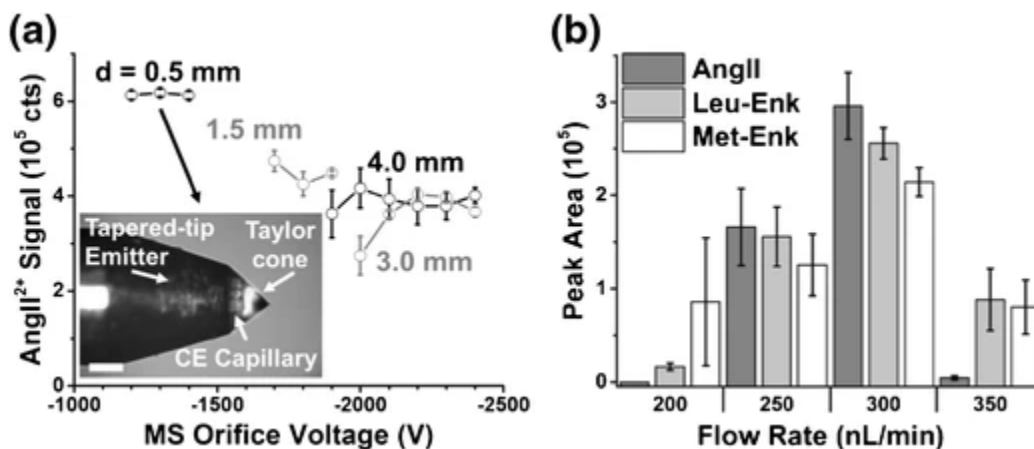


Figure 2.2 Configuration of ionization sensitivity. The CE-nanoESI sheath liquid contained angiotensin II (AngII) to quantify detection sensitivity as a function of spray-to-MS orifice distance (d_{ES-OR}), electrospray potential, and sheath supply rate. (a) On-set and stability domains of the cone-jet spraying regime at 300 nL/min sheath without CE (CE voltage turned off). The inset shows stable anchoring of the Taylor cone at the tapered-tip emitter and the CE separation capillary protruding $\sim 10\text{--}20\ \mu\text{m}$ into the Taylor cone. Scale bar = $50\ \mu\text{m}$. (b) Angiotensin II, leucine enkephalin (Leu-Enk), and methionine enkephalin (Met-Enk) were detected in the highest signal abundance at 300 nL/min sheath rate. Therefore, the final experimental settings in this study were: $d_{ES-OR} = 0.5\ \text{mm}$, electrospray potential = $-1300\ \text{V}$ on MS sampling plate (versus grounded electrospray emitter). Error bars show S.E.M

Next, the interface was evaluated for electrophoretically separating the peptide standards as model for a bottom-up proteomic workflow (Figure 2.3a). Without Joule heating or electrolysis, the CE current is expected to correlate linearly with the applied potential (Ohm's law). Indeed, a broad range of separation potentials ensured Ohmic characteristics with a $\sim 7.64 \pm$

0.06 M Ω net resistance for the CE circuit. A more than 3% deviation from the expected CE current versus voltage correlation was selected to mark the upper limit of the dynamic range of separation potential above \sim 27 kV. Although higher separation voltage provided faster separation, lower CE voltages were advantageous for resolving co-migrating species. For example, the peak-to-peak resolution between the Leu-Enk and Met-Enk improved from 1.13 at 27 kV and 1.35 at 25 kV to 1.61 at 23 kV CE potential, as moderately lower potentials provided slightly longer times for separation to unfold (without causing detectable peak broadening due to diffusion). A stable total ion current signal over an extended period, \sim 90 min (see TIC in inset), confirmed robust CE-nanoESI operation. Technical quadruplet analysis of the angiotensin II standard revealed that the same-day repeatability was \sim 2% relative standard deviation (RSD) in migration time and \sim 20% RSD in quantification based on under-the-peak-areas calculated in selected-ion electropherograms. Angiotensin II was separated with a theoretical plate number of \sim 330,000 in BGE prepared with 1 M FA. These analytical figures of metrics raised a potential to address complex protein digests.

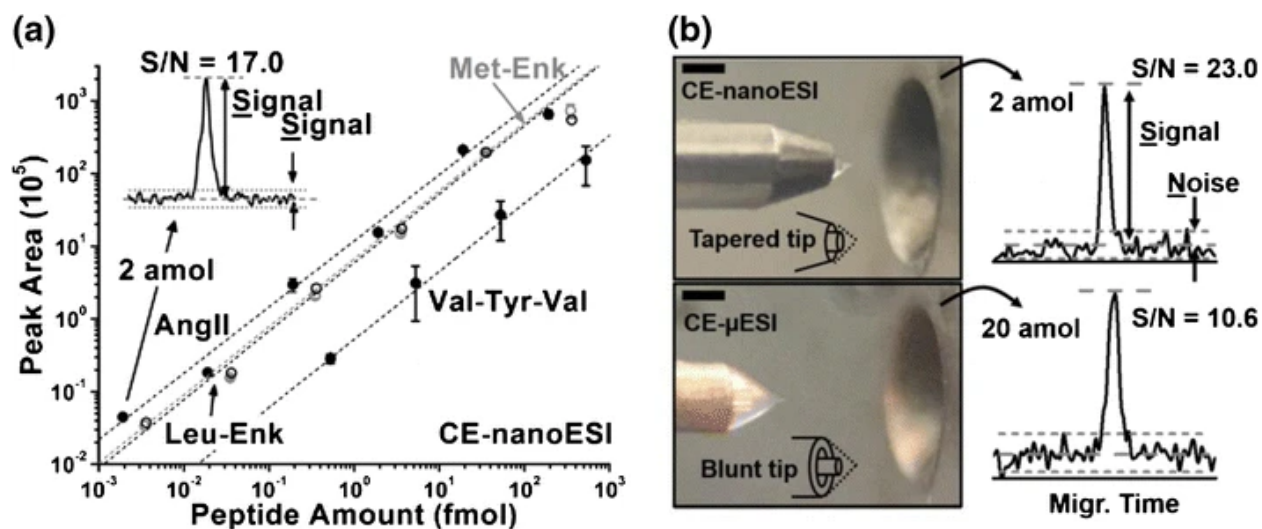


Figure 2.3 Ultra-sensitive peptide detection. (a) CE-nanoESI-HRM separated angiotensin II (AngII), leucine enkephalin (Leu-Enk), methionine enkephalin (Met-Enk), and valine-tyrosine-

valine (Val-Tyr-Val) in high efficiency (330,000 theoretical plates for angiotensin II). Quantification was linear over a 4–5 log-order concentration range ($R^2 > 0.9$ for each different peptide) using single-stage MS. Error bars show S.E.M. **(b)** Sensitivity of CE tapered-tip nanoESI (**top panels**) was evaluated and compared with our earlier blunt-tip CE- μ ESI (**bottom panels**) interface. Optical imaging revealed that the tapered-tip geometry sustained a smaller Taylor cone with stable anchoring on the emitter rim, enabling robust operation (see top panel). Parallel reaction monitoring of the y_2 fragment from angiotensin II indicated a ~ 260 -zmol lower limit of detection (156,000 copies) for the peptide using the tapered-tip versus ~ 5 amol by the blunt-tip. These results confirmed ultrasensitive detection by CE-nanoESI-HRMS. Scale bars = 150 μm . Experimental conditions: $d_{\text{ES-OR}} = \sim 500 \mu\text{m}$, -1300 V spray, 25 kV separation for CE-nanoESI; $d_{\text{ES-OR}} = \sim 1.5 \text{ mm}$, -1700 V spray, 27 kV separation for CE- μ ESI

Detection sensitivity was tested using serial dilutions. Based on under-the-peak-areas in selected ion electropherograms, the peptide mix was quantified over a 4-log-order dynamic range (Figure 2.3b). Two amol of angiotensin II yielded $S/N = 17.0$ (signal height/noise root mean square) in single-stage (MS1) modality, which extrapolates to ~ 350 -zmol ($\sim 210,000$ copies) peptide in a discovery (untargeted) approach at $S/N = 3$. This sensitivity is ~ 70 -fold higher compared with our previous blunt-tip CE- μ ESI design.^{9, 28} To directly compare the sensitivity of these nano- and micro-flow CE-ESI designs under identical experimental conditions, we established stable cone-jet spraying regime for the tapered-tip CE-nanoESI and the blunt-tip CE- μ ESI interfaces and performed parallel reaction monitoring (PRM) for AngII2+ using the same mass spectrometer and data acquisition settings (see Methods). Microscopy imaging revealed (see Figure 2.3b) that CE-nanoESI sustained a Taylor cone of $\sim 100 \text{ fL}$ at 300 nL/min sheath, whereas the liquid cone in the blunt-tip design (260/130 μm o.d./i.d.) measured $\sim 5 \text{ nL}$ at 1 $\mu\text{L}/\text{min}$ sheath. Additionally, the CE- μ ESI interface required larger distance from the orifice of the mass spectrometer to maintain the cone-jet regime (Figure 2.3b). Therefore, tapered-tip CE-nanoESI was anticipated to cause less dilution for peptides migrating into the Taylor cone and also ensure more efficient ion transfer into the mass spectrometer. With the CE-nanoESI

interface, targeted MS/MS on 2 amol of AngII2⁺ generated the b2⁺, b4⁺, and b6⁺ fragments in detectable signal intensity (S/N > 3) and the y2⁺ fragment in high abundance, essentially identifying the peptide sequence (data not shown). A 2 amol of AngII2⁺ yielded the y2⁺ fragment at S/N = 23 in the corresponding selected-ion electropherogram, indicating a 260-zmol lower limit of detection, or 156,000 copies of the peptide. In comparison 20 amol AngII2⁺ yielded S/N = 10.6, suggesting an ~6 amol lower limit of detection using CE- μ ESI. Therefore, the tapered-tip design provided a 22-fold sensitivity improvement compared to CE μ ESI interface, raising a potential for ultrasensitive proteomics.

2.3.2 Mass-limited protein digests

Tapered-tip CE-nanoESI-MS was tested for trace amounts of proteins. Digests of standard BSA and cytochrome c were serially diluted in 75% (v/v) acetonitrile containing 0.05% (v/v) FA, and 1 nL of the standards was analyzed by tandem MS (CID) in DDA. The MS-MS/MS data were searched against the mammalian proteome to identify these proteins in confidence (<1% FDR, Mascot score >30). Figure 4 exemplifies the separation of select peptides from BSA and identification of the proteins based on the peptide information. The theoretical plate number in the complex BSA digest ranged from a median of ~100,000 to 290,000 (see peptide sequence 499–507), revealing efficient separation performance. As expected, lower protein amounts yielded decreasing sequence coverage. With ~8% sequence coverage, the lower limit of identification was <1 pg for BSA with similar performance for cytochrome c. This raises a potential to measure trace amounts of proteins in complex protein digests. We attribute ultrasensitive protein identification by tapered-tip CE-nanoESI to efficient minimization of sample complexity by high-efficiency electrophoretic separation, on-column pre-concentration

via field-amplified sample stacking by CE, and efficient and stable ion generation afforded by nanoESI in the cone-jet spraying regime.

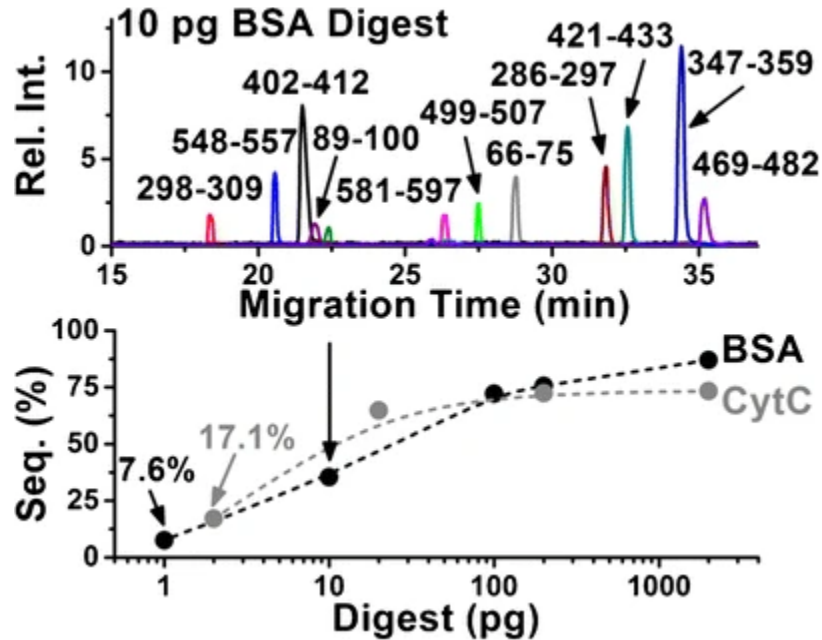


Figure 2.4 Technology validation for trace-level bottom-up proteomics. Digested bovine serum albumin (BSA) and equine cytochrome *c* (CytC) were serially diluted, and the resulting peptides sequenced by CE-nanoESI-MS using a Qq-TOF. Separation of representative peptides is shown from BSA (**top panel**). Numbers specify amino acid location in the protein sequence. Proteins were identified in confidence (<1% FDR) with a <1 pg lower limit of identification (**bottom panel**), confirming ultrasensitive detection by CE-nanoESI-MS

CE-nanoESI-MS was applied to limited amounts of protein digests from the posterior half of the mouse cortex. The tissue was isolated, and the proteins were extracted, reduced, alkylated, and digested using a standard bottom-up protocol that was scaled to the total protein content of the sample (see Methods). Digested proteins were suspended to 1 ng/nL in 75% (v/v) ACN containing 0.05% (v/v) AcOH. One ng of digest was analyzed by CE-nanoESI-MS on the Qq-TOF mass spectrometer using DDA. The base peak electropherogram revealed appreciably complex peptide composition despite the limited amount of sample analyzed (Figure 2.5a). The electropherograms appeared similar between technical replicate measurements

(compare top and middle panels). Indeed, the Pearson correlation coefficient (ρ) was 0.99 for 45 randomly chosen peptides, revealing robust performance. These peptides were separated within a relatively short (~20-min) time window (see bottom panel), agreeing with similarly compact separation also noted in other bottom-up proteomic studies by CE.^{28, 49, 98, 101}

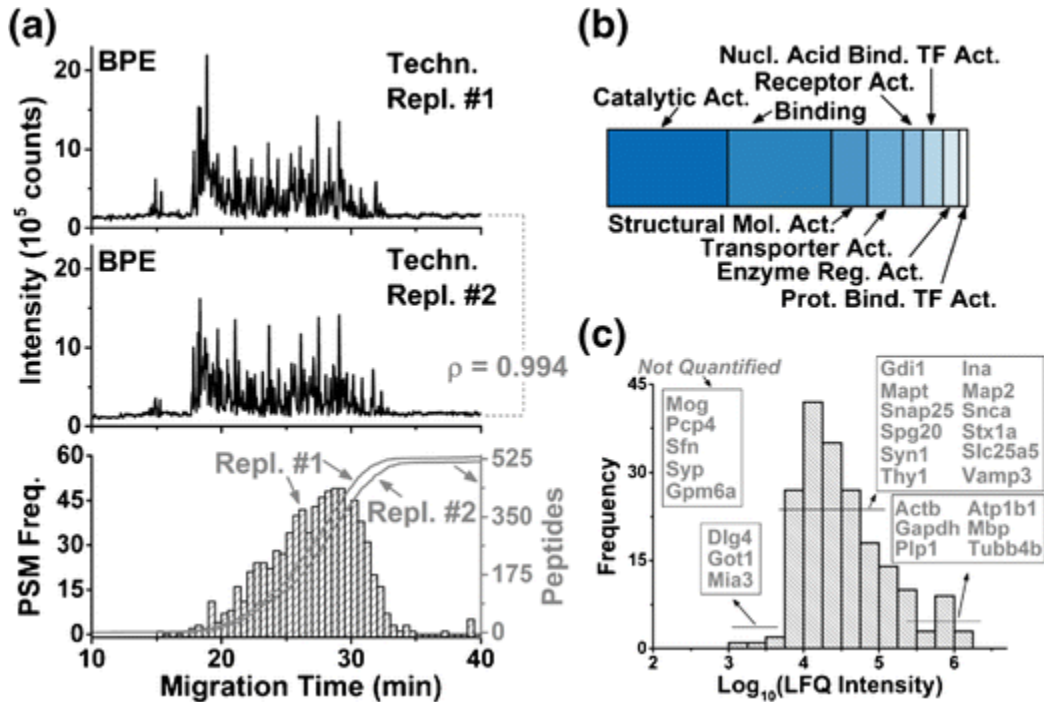


Figure 2.5 Protein identification from 1 ng protein digest from the mouse cortex. (a) Peptide separation was robust, as revealed by a high Pearson correlation (ρ) calculated for 45 randomly selected peptides between technical replicates. Tandem MS enabled rapid acquisition of peptide spectral matches (PSMs) within a ~20-min separation window, identifying ~525 different peptides. Cumulative rate of peptide identification is shown for technical replicates in grey. (b) These peptides were mapped to 217 nonredundant protein groups in the encoded mouse proteome (Supplementary Table S2.1). Gene ontology annotation is shown for these proteins. Key: Act., activity; TF, transcription factor. (c) A total of 192 proteins were quantified, which spanned a ~3-log-order concentration range based on calculated label-free quantification (LFQ) intensities. Representative proteins are labeled and grouped into abundance domains (see Supplementary Table S2.1)

Generated peptide ions were sequenced by tandem MS using DDA. We recently demonstrated that dynamic adjustment of the tandem MS duty cycle depending on precursor ion

intensity enhances peptide sequencing during compact electrophoretic separation.²⁸ Using this strategy, 668 peptide spectral matches (PSMs) were acquired, which identified 407 different peptides, corresponding to ~60% identification rate based on individual MS/MS events. This success rate was enhanced to ~66% by spiking the sheath liquid with 5% (v/v) dimethylsulfoxide, a known supercharging agent.¹¹⁴ As in nanoLC-nanoESI, supercharging enhanced the quality of tandem mass spectra in CE-nanoESI-MS by promoting the formation of peptides with higher charge states (67% versus 73% of ions doubly charged), which are known to fragment better. These results complement our recent observation for CE- μ ESI interface, in which supercharging did not appreciably enhance peptide identifications on the same mass spectrometer, likely due to higher flow rates.²⁸ It follows that peptide identifications appear to increasingly benefit from supercharging in CE-ESI designs that employ low-flow sheath liquid or are sheathless (e.g.,⁸¹⁻⁸⁵).

The peptide sequences led to the identification of 217 different protein groups from the 1 ng protein digest from the mouse cortex. PANTHER (Protein Analysis Through Evolutionary Relationships) Gene Ontology annotation suggested that these proteins had structural molecular, catalytic, binding, and transporter activities (Figure 2.5b). Other categories suggest roles in receptor binding, nucleic acid and protein binding transcription, and enzyme regulation. To estimate the relative abundance of these proteins, we calculated label-free quantification (LFQ) intensities using MaxLFQ.¹¹⁵ About 12% of the identified proteins were not quantifiable based on the MS/MS data (LFQ intensity = 0). The LFQ intensity values for 192 proteins indicated a ~3-log-order concentration range with tailing toward higher LFQ intensities. Representative proteins are grouped into abundance domains in Figure 2.5c. A complete list of identified proteins and their calculated LFQ intensity values are in Supplementary Table S1. For example,

proteins in the low–middle abundance range included transcription and translation regulators and macromolecular assembly (e.g., Efla1, Hspa8), synaptic function (e.g., Dlg4/PSD95, bassoon, and CaMKIIb), and energy production (e.g., Atp9a, Atp5j2). Proteins with high LFQ intensity values were enriched in structural organization (e.g., Tuba1a, Tubb4b, Actb), glycolysis (Gapdh), and myelination (e.g., Mbp, Plp1).

Last, we surveyed the 217 proteins identified by CE-nanoESI-MS based on their known affiliation with neurons, astrocytes, and oligodendrocytes. At least 40 different genes that are commonly used as neuronal markers were readily recognized at the protein level. For example, synaptosomal-associated protein 25 (Snap25), synapsin 1 (Syn1), syntaxin-1a (Stx1a), synaptotagmin 1 (Syt1), vesicle-associated membrane protein 3 (Vamp3/synaptobrevin-3), and GDP dissociation inhibitors 1 and 2 (Gdi1, Gdi2) are implicated in neurotransmitter exocytosis at the synapse.⁴⁸ Other proteins such as microtubule-associated protein 2 (Map2) and alpha-internexin (Ina) are neuronal-specific cytoskeletal components. Oligodendrocyte markers include multiple myelin components, such as myelin basic protein (Mbp) and proteolipid protein 1 (Plp1). Finally, key proteins involved in neurodegenerative disorders were detected by our approach. Microtubule associated protein tau (Mapt) and alpha-synuclein (Snca) accumulate in the brain of patients with Alzheimer's disease, and are mutated in frontotemporal dementia with parkinsonism and Parkinson's disease, respectively.¹¹⁶ Spartin (Spg20) is mutated in a rare form of hereditary spastic paraplegia.¹¹⁷ Combined, these results established that CE-nanoESI-MS is able to characterize protein expression in the mammalian brain with sufficient sensitivity to detect markers of healthy and diseased neurons.

2.4 Conclusions

Here we developed an ultrasensitive, robust CE-nanoESI interface for MS to enable the discovery characterization of protein translation in 1 ng protein digest from the mouse cortex. This sensitivity raises a potential for detecting proteins expressed by a handful of neurons. The CE-ESI design uses a small-bore tapered-tip metal emitter to integrate the CE separation capillary into a nanoESI source via a co-axial sheath-flow configuration. We found that the tapered-tip emitter stabilized the Taylor cone with reduced volume in the nano-flow regime (200–350 nL/min), ensuring efficient and robust ion generation within close proximity of the mass spectrometer inlet for maximal ion collection. Combined, these performance metrics provided an estimated 260 zmol lower limit of detection, or 156,000 copies for peptide standards. Compared with other co-axial sheath-flow interfaces, this sensitivity is ~4000-times higher than those based on large-bore emitters,¹⁰⁸ ~20–100 times higher than our previous constructs based on small-bore blunt-tip emitters (see earlier and ^{9, 28}), and is comparable to electrokinetically pumped interfaces using multiple reaction monitoring.⁹⁶⁻⁹⁷ While specialized low-flow⁹⁸ and sheathless⁸⁶ CE-nanoESI interfaces and nanoLC-nanoESI⁷⁵⁻⁷⁶ systems recently accomplished 1–10 zmol lower limit of detection, microanalytical tapered-tip CE-nanoESI presents analytical advantages. This interface provides fast analysis time (e.g., ~30 min typical by CE versus ~2–5 h typical by nanoLC), can be constructed with minimal-to-no prior experience in <15 min using readily available commercial components (see Figure 1b), offers robust operation (2 mo tested here without detectable performance deterioration), and compatibility to volume/mass-limited specimens (<1 μ L digest deposited here). Combined, these metrics facilitate broad adoptability of the technology for ultrasensitive proteomics also in other laboratories where limited volumes or amounts of protein digests need analysis.

Ultrasensitive peptide detection extends MS-based proteomics to trace amounts of samples. In the work presented here, we demonstrated the identification of 1 pg, or 15 amol of standard proteins. CE-nanoESI enabled the detection of 217 nonredundant protein groups from ~1 ng protein digest from the mouse cortex. In principle, tapered-tip CE-nano-ESI-MS raises sufficient sensitivity to measure hundreds of picograms to few nanograms of proteins contained in small populations of neurons and other single cells. Continuous developments in microscale sampling, protein extraction, and digestion (e.g., by on-column immobilized microreactors,¹¹⁸ fractionation,¹¹⁹ and focused acoustics-assisted sample preparation⁷⁶) can help extend the detectable coverage of the encoded proteome to single cells. To address compact electrophoretic separation, refinements are needed in tandem MS technology. Tandem MS with fast duty cycle using DDA or data-independent acquisition strategies as well as parallelization of MS–MSn scans using new-generation hybrid instruments promise enhanced protein identifications. Last, besides LFQ as demonstrated here, existing strategies in quantitative proteomics, such as iBAQ, TOP3, TMT, TMTc, iTRAQ, and SIN, are adaptable to perform relative or absolute quantification on trace amounts of proteins using tapered-tip CE-nanoESI-MS.

Ultrasensitive proteomics raises a potential to understand how differential gene expression coordinates cell heterogeneity during brain development and function. Many of the proteins identified in this work are expressed from genes that are classically used to mark important cell types in the brain: neurons, oligodendrocytes, and astrocytes. We anticipate that the sensitivity of the presented technology is sufficient to identify key proteins involved in different stages of neurodevelopmental or neurodegenerative disease progression in specific brain regions. This approach can lead to a better understanding of the molecular mechanisms

underlying disease, to the identification of diagnostic or prognostic biomarkers, or to pinpoint novel therapeutic targets.

Chapter 3: Enhancing peptide detection by reversed-phase pre-fractionation with capillary electrophoresis mass spectrometry

This chapter includes material adapted with permission from:

S.B. Choi, C. Lombard-Banek, P. Muñoz-Llanca. M.C. Manzini and P. Nemes*, Enhanced Peptide Detection Toward Single-Neuron Proteomics by Reversed-Phase Fractionation Capillary Electrophoresis Mass Spectrometry, *Journal of the American Society of Mass Spectrometry*. 2018, 29, 913-922. <https://doi.org/10.1007/s13361-017-1838-1>

Author Contribution: S.B. Choi designed the research, processed the sample, measured the samples, analyzed the data, and wrote the manuscript.

3.1 Introduction

The ability to measure gene expression in a small population of cells is critical for understanding molecular players of neuronal differentiation in the developing brain. Empowered by liquid chromatography and late-generation high-resolution mass spectrometry (HRMS), shotgun (bottom-up) proteomics now enables differentiation of neuronal cell types by quantifying the expression of ~13,000 protein groups from primary cell cultures.⁴⁸ To detect the encoded proteome in deeper coverage, ~10–100 µg of proteins are typically harvested from few to tens of millions of cells before analyzing ~100 ng to ~5 µg of protein digest per experiment by nano-flow (ultra) high-performance liquid chromatography (nanoLC) HRMS. Extension of proteomics to small populations of neurons would complement single-cell transcriptomics data,¹²⁰⁻¹²² thus raising a potential to better understand molecular changes as neurons acquire functional phenotypes. Without technologies capable of amplifying the whole proteome,

however, significant improvements are needed in the sensitivity of HRMS to detect proteins from sub-nanograms of total protein amounts expressed in neurons.³⁰

Separation is essential to deepen proteomic coverage by HRMS; separation simplifies molecular complexity along the temporal dimension, thus increasing the total number of tandem mass spectra that can be acquired to identify peptides regardless of limitations in MS/MS duty cycle (e.g., ~10–20 Hz). For example, the recent deep proteome maps of human tissues⁵⁸ and cell types in the brain⁴⁸ were made possible by cumulatively identifying ~300,000 peptides that were separated in multiple measurements with each employing 6-h-long gradient by nanoLC. Another way to improve identifications is by integrating technologies that employ orthogonal mechanisms of separation.^{33, 123-124} For example, the broadly successful multidimensional protein identification technology (MudPIT) is based on the on-line hyphenation of strong cation exchange and reversed-phase (RP) chromatographies into a single nanoLC platform.³³ Alternatively, the sample may be fractionated via ion exchange or RP chromatography followed by offline RP nanoLC under similar or different pH conditions prior to detection by HRMS.¹²⁵⁻¹²⁸ While nanoLC serves as the main stream separation approach for peptides, this technology typically requires ~1,000-fold higher protein digest amounts per measurement than the available protein content in single neurons. Recent developments in nanoLC tailored detection to substantially smaller protein amounts, such as the identification of ~3,700 proteins from 500 breast cancer cells (MCF-7), or 50 ng of total proteins using porous open-layer tubular columns (PLOT)⁷⁶ and ~6,000 proteins from ~500 ng digest of HeLa culture using an automated low-flow fractionator instrument.¹²⁹ Continuous advances in sample handling present a potential to approach protein amounts in single neurons using nanoLC.

Capillary electrophoresis (CE) is an alternative technology for limited samples. CE can achieve outstanding separation efficiency to resolve molecules in complex samples, offers various strategies of online preconcentration to enhance signal-to-noise ratio, and ensures compatibility with limited sample volumes (e.g., <1–10 nL) (reviewed in references¹³⁰⁻¹³³). We and others demonstrated CE electrospray ionization (ESI) HRMS to offer significant sensitivity gains for limited amounts of protein digests via bottom-up^{9, 28, 134} or top-down^{91, 135} workflows compared with nanoLC. Representative examples comprise the targeted detection of hemoglobins in single erythrocytes¹³⁶⁻¹³⁷ and attomoles of carbonic anhydrase from a few erythrocytes^{67, 138} as well as the discovery detection of ~200 protein groups from 5 ng of *Pyrococcus furiosus* digest,⁸⁹ ~100 protein groups from ~16 pg of *Escherichia coli* digest,⁹⁸ and ~109 protein groups from 100 HeLa cells (~30 ng protein).⁷² By performing capillary zone electrophoresis, our custom-designed microanalytical CE-ESI-MS platform identified ~800 protein groups from 20 ng of protein digest from single identified cells in the 16-cell *Xenopus laevis* (frog) embryo, corresponding to ~0.1% of the total protein content of the cell.^{9, 28} Most recently, we developed a nano-flow CE-ESI-MS interface capable of 260 zmol (156,000 copies) lower limit of detection. Using this technology, 217 protein groups were detected from 1 ng of protein digest from cultured mouse neurons, essentially approaching the total protein content of 1–5 neurons.³⁰ Remarkably, protein identifications in these CE-HRMS experiments by us and others relied on the fragmentation of peptide signals migrating across ~20–30 min, which is considerably shorter (compressed) compared with hours of separation typical of nanoLC. Owing to current limitations in MS/MS duty cycle, compressed separation is expected to hinder peptide detection, thus hampering the identification of proteins.

There is a significant interest in advancing peptide and protein identifications by microscale CE-ESI-MS.¹³⁹ In a similar fashion to nanoLC, multidimensional separation can reduce sample complexity prior to CE-ESI-MS. For example, ~3,430 proteins were identified after fractionating 1.5 mg of yeast protein digest into 182 aliquots using RP-nanoLC followed by CE-ESI-HRMS of each fraction.¹¹⁹ Similar strategies recently identified 4,134 proteins by fractionating 600 µg of protein digest from ~50 *Xenopus laevis* eggs¹⁴⁰ and ~1,600 proteins by fractionating 50 µg of protein digest from the mouse brain.¹⁴¹ Other strategies tailored sample handling to lower amounts of protein digests by streamlining fractionation on-line with CE analysis. For example, solid-phase microextraction (SPME) with CE-ESI-MS identified ~370 protein groups from 5 ng of digest from *Pyrococcus furiosus*,⁴⁹ whereas strong cation exchange of 50 ng protein digest detected 799 protein groups from *Escherichia coli*¹⁴² and ~1,000 protein groups from a whole *Xenopus laevis* zygote.¹⁴³ Alternatively, electrophoretic peak capacity can be enhanced by lengthening the separation time, albeit at the risk of diffusion-limited peak broadening deteriorating sensitivity. By minimizing/eliminating the electroosmotic flow using neutral-coated capillaries, a recent study identified ~250 proteins from 50 ng of protein digest from mouse brain, which was improved to ~1,600 protein identification by enabling the analysis of 50 µg of digest with 500 nL loading of sample directly on the separation capillary, remarkably on par with nanoLC MS.¹⁴¹ However, to advance identifications in trace amounts of protein digests by fast CE, the rate of peptide separation and the duty cycles of MS/MS should ideally be matched.

In this study, we evaluated the identification and quantification of peptides by capillary zone electrophoresis HRMS to measure proteins from digest amounts that approximate to ~1– 5 neurons cultured from the mouse forebrain. Our microanalytical approach combined off-line RP

fractionation with a custom-built CE-nanoESI-HRMS platform capable of ultrasensitive detection (260 zmol). Integration of these orthogonal separation mechanisms simplified compressed electrophoretic separation, improving separation performance and detection sensitivity. After processing 1–20 μg of protein digest from a neuron culture, the strategy identified 737 proteins in technical triplicates (\sim 480 proteins/analysis on average) from \sim 1 ng of protein digest, approximating the total protein content from a few neurons. Furthermore, we demonstrated that this approach was scalable to identifying 225 protein groups in technical triplicates (141 proteins/analysis on average) from \sim 500 pg of digest, approaching single neuron protein content. Microscale RP fractionation with CE-HRMS raises sufficient sensitivity toward peptidomics and proteomics in single neurons to help elucidate molecular mechanisms responsible for the formation and maintenance of neuron-to-neuron heterogeneity in the brain.

3.2 Experimental section

3.2.1 Chemicals and reagents

All materials were purchased at reagent grade or higher unless noted otherwise. Dithiothreitol (DTT), iodoacetamide (IAD), hydroxy methylaminomethane (Tris-base), Tris-hydrochloric acid (Tris-HCl), Tris-phosphate buffer solution, potassium chloride, and sodium hydroxide were obtained from Sigma-Aldrich (St. Louis, MO, USA). Papain dissociation system was from Worthington Biochemical Corporation (Lakewood, NJ, USA). Sodium dodecyl sulfate (SDS) was from Amresco (Solon, OH, USA). Ethylenediamine tetraacetic acid (EDTA), LCMS grade acetonitrile (ACN), MS-grade trypsin protease, methanol (MeOH), formic acid (FA), acetic acid, and water (Optima) were from Fisher Scientific (Fair Lawn, NJ, USA). Pierce C18 Zip Tips (P/N 87784) were from Thermo Fisher Scientific (Waltham, MA, USA). Reagent-grade

ammonium bicarbonate was from Avantor (Center Valley, PA, USA). Fused silica capillaries (20/90 μm inner/outer diameter (i.d./ o.d.) for CE separation and 75/350 μm i.d./o.d. for sheath supply) were from Polymicro Technologies (Phoenix, AZ, USA) and used without modification. Stainless steel tapered-tip metal emitters (100/320 μm i.d./o.d.) were from New Objective (Woburn, MA, USA). Poly-L-ornithine, Hank's balanced salt solution (HBSS), phosphate-buffered saline solution (PBS), minimum essential medium (MEM), neurobasal medium, glucose, penicillin-streptomycin, and fetal bovine serum were from Gibco (Grand Island, NY, USA). B27, N-2, Glutamax, and pyruvate supplements were from Thermo Fisher Scientific (Waltham, MA, USA). All standards were prepared in 500 μL or 2 mL LoBind protein microtubes from Eppendorf (Hauppauge, NY, USA).

3.2.2 Solutions

Following protocols described elsewhere [38], the “neuronal plating medium” was prepared to contain MEM with 0.6% (w/v) D-glucose, 10% (v/v) horse serum, 1% glutamine, and 1% penicillin-streptomycin. The “neuronal maintenance media” was neurobasal supplemented with 2% B27, 1% N-2, 1% Glutamax, 1% penicillin- streptomycin, and 1% pyruvate. All media were filtered through a 0.2 μm porous mesh prior to usage. The cell “lysis buffer” contained 5 mM EDTA, 20 mM Tris-HCl, 35 mM NaCl, and 1% (v/v) SDS. The CEnanoESI “sheath solution” contained 50% (v/v) MeOH with 0.1% (v/v) FA.

3.2.3 Neuron culture

All procedures regarding the maintenance and handling of mice (*Mus musculus*) were approved by the George Washington University Institutional Animal Care and Use Committee

(IACUC No. A274). Timed pregnant C57BL/6 dams were obtained from Charles River Laboratories (Wilmington, MA, USA). Primary cultures of mouse hippocampal neurons were prepared as described previously [38]. Briefly, hippocampal neurons were isolated from mouse embryos at Embryonic Day 16 and dissociated using papain solution for 30 min at 37 °C according to manufacturer recommendations (Worthington), followed by trituration and mixing with a plastic pipette in neuronal plating medium. Hippocampal cells were filtered with a 70 µm nylon mesh cell strainer (Falcon) and plated at 1×10^5 cell/cm² on a 24-well plate previously coated with poly-Lornithine (1 mg/mL) in plating medium. After 1 h, the medium was replaced with neurobasal maintenance medium and cultured for 14 d in vitro. Afterward, the cultured neurons were rinsed with ice-cold PBS to remove residual growth media, scraped, and the content of 2 wells was suspended in 150 µL PBS (Thermo Fisher Scientific). Cells were pelleted by centrifugation at $800 \times g$ for 5 min at 4 °C, and stored at -80 °C until further processing for analysis by CE-HRMS. To approximate the extractable total protein amount from an average single neuron in the culture, we combined cell counting and total protein assay. A 10 µL portion of the PBS suspended cultured neurons were mixed with 10 µL of 0.4% trypan blue (Life Technologies, Washington, DC, USA), and stained cells were analyzed in a microfluidic cell counter (model Countess, Invitrogen, Carlsbad, CA, USA). The results revealed a 6.4×10^5 cells/mL cell density, and ~90% of the cells were quantifiably viable. This suspension contained 0.35 mg/mL protein based on the bicinchoninic acid assay (BCA, Thermo Scientific), which approximated to ~500 pg of total protein extractable from a neuron on average.

3.2.4 Bottom-up proteomic workflow

The hippocampal neurons were processed following a standard bottom-up proteomic workflow [39]. In this study, the cultured neurons were lysed in 200 μL of lysis buffer with subsequent ultrasonication for 15 min in an ice-cold water bath to facilitate protein extraction. The resulting sample was reduced (4 μL of 1 M DTT, 30 min at 60 $^{\circ}\text{C}$) and alkylated (8 μL of 1 M IAD, 15 min in the dark) before quenching the reaction (4 μL of 1M DTT). To remove cell debris, the sample was centrifuged at $14,000 \times g$ for 10 min at 4 $^{\circ}\text{C}$, and the supernatant was transferred into a new 2 mL LoBind microcentrifuge tube. Next, proteins were purified by overnight precipitation in 1 mL chilled acetone (-20°C), followed by centrifugation at $14,000 \times g$ for 10 min at 4 $^{\circ}\text{C}$. The resulting pellet was washed with chilled acetone (-20°C), dried at room temperature, and reconstituted in 100 μL of ammonium bicarbonate (50 mM). Protein concentration was estimated based on BCA. A total of ~ 20 or 100 μg of protein amount were digested by trypsin at a 1:50 protein:enzyme ratio (0.4 μL or 2.0 μL of 1 $\mu\text{g}/\mu\text{L}$ trypsin, respectively) for ~ 6 h at 37 $^{\circ}\text{C}$. The resulting peptides were vacuum-dried and stored at -20°C until analysis.

3.2.5 Reversed phase peptide separation

The dried peptides were reconstituted in 0.1% (v/v) FA to a 1 $\mu\text{g}/\mu\text{L}$ peptide concentration, confirmed by the Colorimetric Peptide Assay (Thermo Scientific). An aliquot containing 20 μg (for method development) or 1 μg (for scalability test) peptides were fractionated on C18 ZipTip cartridges (100 μL or 10 μL format, Pierce, Thermo Scientific) following manufacturer instructions. Peptides were sequentially eluted using 10%, 20%, and 30% acetonitrile in water containing 0.1% FA. Each resulting fraction was dried and

reconstituted in 20 μ L (method development) or 2 μ L (scalability test) of 75%(v/v) acetonitrile containing 0.05% (v/v) acetic acid (“sample”) before analysis by CE-HRMS.

3.2.6 CE-nanoESI-HRMS

Peptides were detected in a custom-built microanalytical CE nanoESI- HRMS platform that we recently characterized (see reference³⁰). In this study, capillary zone electrophoresis was performed on 1 nL of digest sample in a 90-cm capillary at \sim 250 V/cm field strength. Peptides were ionized in a CE nanoESI interface operated in the cone-jet spraying mode for efficient ion generation using 50% MeOH (0.1% FA) at 300 nL/min flow rate as sheath liquid and 2.7 kV as electrospray potential. Peptide ions were mass-analyzed using a hybrid quadrupole Orbitrap mass spectrometer equipped with a higher-energy collision dissociation (HCD) cell (Q Exactive Plus, Thermo Scientific). Separating peptide features were surveyed between m/z 350 and 1,800 at 35,000 FWHM resolution (MS1) using the following settings: maximum IT, 50 ms; chromatography peak width (FWHM), 13 s; exclusion mass tolerance, 10.0 ppm; peptide matches, on; ion signals excluded below +2 charge state; ion signal intensity threshold, 1.5×10^3 counts; apex trigger, turned off. Ions that matched these criteria were selected for fragmentation in the HCD cell with the following settings: maximum IT, 60 ms; m/z isolation window for MS2, 1.0 Th; normalized collision energy, 28; MS2 resolution, 17,500 FWHM; TopN, 15; loop count, 15. Fragmented ions were dynamically excluded with 5 ppm accuracy for 9 s before being reconsidered for fragmentation.

3.2.7 Data analysis

Raw mass spectrometric data were analyzed in MaxQuant ver. 1.5.7.4 (Max Planck Institute of Biochemistry) executing the Andromeda 1.5.6.0 search engine³⁹⁻⁴⁰ against the

SwissProt mouse proteome database (downloaded from UniProt on November 11th, 2015) containing 16,792 entries. The search parameters were: digestion, tryptic; missed cleavages, maximum 2; minimum number of unique peptides, 1; fixed modification, carbamidomethylation of cysteines; variable modification, oxidation of methionines; main search peptide tolerance and MS/MS match tolerance, ± 4.5 ppm and ± 10 ppm, respectively; isotope match tolerance, 2 ppm; decoy mode, revert; label-free quantitation, enabled; fractionation, “no” for control (unfractionated samples) and Byes, three fractions[^] for fractionated samples. Proteins were identified with a false discovery rate (FDR) <1% against a reversed sequence decoy database. For each identified peptide, the extent of co-isolation spectral interference was quantified in Proteome Discoverer 2.1 (Thermo Scientific, Waltham, MA. USA) using SEQUEST HT as the search engine against the mouse proteome with identical data processing settings as in MaxQuant. Following reporting guidelines in UniProt, we report proteins as groups based on the parsimony principle unless the MS-MS/MS data provide sufficient evidence to identify isoforms with known biological significance in SwissProt. Common contaminants were manually removed from the reported list of proteins. Label-free quantification (LFQ) intensities were calculated using the MaxLFQ algorithm¹¹⁵ in MaxQuant with LFQ minimum ratio count set to 1 and fast LFQ disabled. For statistical analysis, p-value of less than 0.05 (Student’s t-test) was used to indicate statistical significance. Errors are reported as standard deviation (SD).

3.2.8 Safety consideration

Fused silica capillaries and tapered-tip metal emitters, which pose needle-stick hazard, should be handled with care. Standard safety protocols were followed during the handling of

chemicals. All electrically conductive parts of the CEnanoESI system were grounded or isolated to prevent electrical shock hazard.

3.3 Results and discussion

3.3.1 Sensitivity needs for limited neuron populations

The goal of this study was to advance protein identification from protein digest amounts that approximate to a few mammalian neurons to a single neuron. We and others recently demonstrated that CE-HRMS offers sensitivity benefits for limited amounts of peptides and proteins (see reviews¹³⁰⁻¹³³). For example, custom-built microanalytical CE has allowed us to identify ~800 proteins from ~20 ng of protein digest from single *Xenopus laevis* embryonic cells^{9, 28} and 217 proteins from ~1 ng of protein digest from a cortical neuron culture of mouse.³⁰ These identifications relied on the detection of 829^{9, 28} and 525³⁰ peptides, respectively, migrating over a 20–25 min window. In these experiments, compressed separation challenged the fragmentation of peptides with a limited MS/MS duty cycle, which in turn hindered protein identifications. To improve protein detection for limited populations of neurons, including single cells, using CEHRMS, methodological or technological developments need to balance sample complexity, separation peak capacity, and/or the duty cycle of tandem mass spectrometry.

We proposed that multidimensional separation sufficiently simplifies molecular sample complexity for tandem mass spectrometry to enhance peptide detection from trace amounts of protein digests afforded from limited neuronal populations. Our working strategy adopted the principle that integration of orthogonal separation mechanisms improves the net peak capacity of the system. For example, RP fractionation of 600 µg of digest from fertilized *X. laevis* eggs by RP-LC with analysis of 1.5 µg digest by CE-ESI-MS recently identified ~4,100 protein

groups.¹⁴⁰ However, to extend these measurements to significantly smaller numbers of neurons in this work, substantially smaller starting amounts of proteins and resulting protein digests must be processed. Indeed, by combining cell counting and total protein assay in a neuron culture (see Methods), we approximated an average neuron to yield ~500 pg of total protein extract. RP sorbent C18 columns present an attractive alternative to nanoLC for processing miniscule amounts of protein digest because this platform is scalable (e.g., protein binding up to 8 µg in 10 µL volume), operates sufficiently fast for manual sampling (10–15 min), and can be integrated off- or on-line with CE.

3.3.2 Improved trace-sensitive peptide detection

We evaluated the combination of RP fractionation and CEnanoESI- HRMS for detecting proteins in trace amounts of protein digests. Schematics of the study are presented in Figure 1. After culturing primary hippocampal neurons from mouse, the cells were lysed in 1% SDS lysis buffer, and ~20– 100 µg of proteins were processed via a bottom-up proteomic workflow (see Methods). A protein digest containing 20 µg of peptides was step-wise fractionated on a RP column (ZipTip) using 10%, 20%, and 30%(v/v) ACN containing 0.1% FA (see Figure 3.1). As no peptides were detectable upon additional elution with 40% ACN, 30% ACN was considered sufficient to recover peptides from the RP column. Eluted peptides were dried and reconstituted in 20 µL of 75% (v/v) ACN containing 0.05% (v/v) acetic acid, selected to perform on-column enrichment via field-amplified sample stacking for capillary zone electrophoresis in this work. An identical amount of protein digest served as “control” (without RP fractionation). To analyze digest amounts that approximate extractable proteins from <5 neurons (see Methods), we analyzed 1 ng of total peptides from the control and among the fractions. Last, we designed

experiments to test scalability by RP fractionating 1 μg digest (approximating $\sim 2,000$ neurons) and measuring ~ 500 pg protein digest, essentially approximating protein amounts from a single neuron.

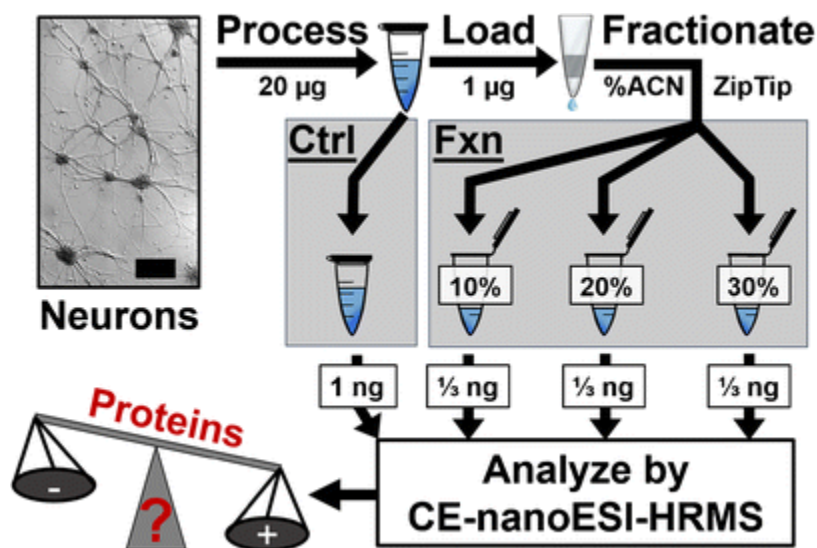


Figure 3.1 Experimental strategy for improving protein identifications from protein digest amounts approximating to 1–5 neurons. A ~ 20 μg of protein digest from cultured neurons was reversed-phase fractionated (ZipTip), and ~ 1 ng of total peptide mixture was analyzed by CE-nanoESI-HRMS. Unfractionated digest served as control. This approach was scalable for fractionating 1 μg protein digest ($\sim 2,000$ neurons) before analyzing 500 pg of peptide mixture, essentially approaching the protein content of a single mammalian neuron

Without RP fractionation, peptide identification was constrained by compressed separation in the control (Figure 3.2). The rate of MS/MS events rapidly increased as migration unfolded with most tandem mass spectra resulting between 20–30 min and 33–37 min (see “MS/MS events”). A portion of these MS/MS events resulted in successful peptide spectral matches (PSM) against the mouse proteome (see “PSMs”). Most PSMs were acquired over a ~ 10 -min window, revealing significantly shorter, or compressed, separation by capillary zone electrophoresis than is typical of nanoLC. Although the MS/MS duty cycle was not exhausted at any point of the separation, the rate of peptide identification was limited at ~ 100 PSMs/min at

the apex of the electropherogram (22–28 min, see arrows); only ~45% of the acquired tandem mass spectra were successfully matched to PSMs in this region (Figure 3.2. top panel).

Furthermore, the primary high-resolution MS-MS/MS data revealed notable spectral interference during fragmentation as a result of ion(s) that were coisolated with the peptide precursor ion with a standard ± 0.5 Th window. Co-isolation interference was quantifiable ($>0\%$, see Methods) for ~65% of PSMs at the most compressed portion of the electropherogram (22–28 min) compared with ~50% of PSMs acquired with interference outside this compressed zone (14–22 min and 28–40 min). Combined, these data suggested possible improvements in protein identification by minimizing spectral interference during peptide separation.

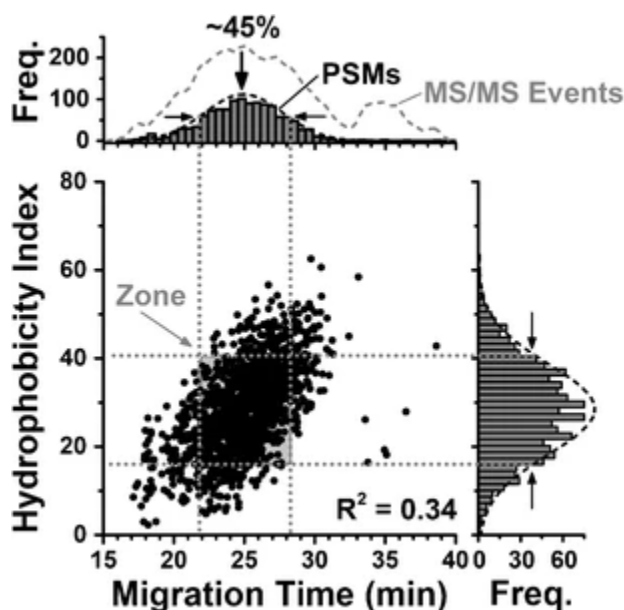


Figure 3.2 Peptide detection by CE-nanoESI-HRMS. Distribution of separation time and hydrophobicity indices calculated for peptides that were detected in the control (unfractionated) digest revealed a zone of compressed separation, which in turn lowered the success rate of MS/MS events leading to peptide identifications. Each data point marks a different identified peptide

RP fractionation offered one such direction toward simplified peptide complexity. We calculated the hydrophobicity index of each identified peptide using the Sequence Specific

Retention Calculator (ver. 3.x–2010). As shown in Figure 3.2, calculated indices suggested broad hydrophobic characteristics for the identified peptides. Additionally, the hydrophobicity indices were poorly correlated with migration time ($R^2 = 0.34$, see Figure 3.2). This result confirmed orthogonality between hydrophobic retention on an RP column and electrophoretic migration using our custom-built CE-HRMS system. Therefore, we expected the integration of RP fractionation and electrophoretic separation to enhance the separation peak capacity of our custom-built CE-nanoESI-HRMS system.

We applied multidimensional separation for trace amounts of neuronal protein digests. We analyzed a total of 1 ng of peptides with fractionation and without (control) (Figure 3.3a); 1/3 ng of total peptides were measured from each of the three fractions (10%, 20%, or 30% ACN), confirmed by a total peptide assay (see Methods). The distribution mean of peptide hydrophobicity indices increased with eluent strength across the fractions (see left panel), thus validating the mechanism of retention as hydrophobic interaction with the stationary phase of the ZipTip column. In contrast, the distribution mean of migration times was indistinguishable between the control and the fractions (see right panel), revealing no detectable effects on electrophoretic mobility by RP fractionation. It follows that RP fractionation prior to CE minimized molecular complexity during capillary zone electrophoresis HRMS.

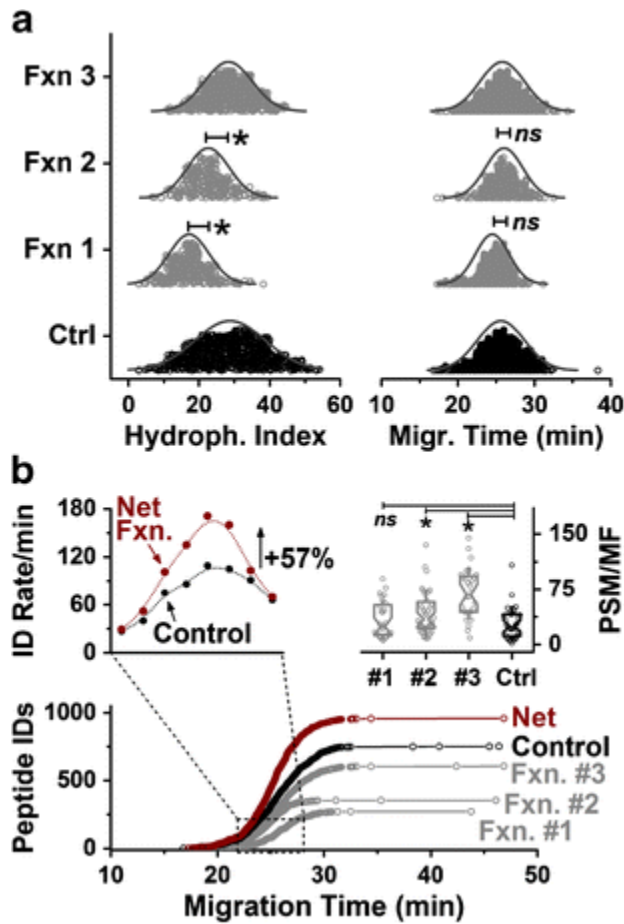


Figure 3.3 Multidimensional separation for enhancing peptide identifications. (a) Peptides were successfully separated on a C18 phase based on hydrophobicity differences (left panel), but not migration time (right panel). Key: * $p < 0.05$; ns, not significant. Each data point corresponds to a different identified peptide. (b) Cumulative peptide identifications rapidly increased during compressed CE separation; the combined fractions (“Net”) outperformed the control (left inset). Fractionation simplified peptide complexity, allowing for a greater portion of molecular features (MF) to be identified as peptide spectral match (PSM) (see PSM/MF, right inset)

Next, we characterized peptide identifications upon RP fractionation. Figure 3.3b monitors peptide identifications as migration unfolded. Cumulative identifications rapidly increased over the most compressed zone of separation. The identification rate, quantified as number of non-redundant peptides identified per unit time, was improved in the “Net Fraction” compared with the control (see left inset). The greatest improvement occurred during the most compressed portion of the electropherogram (see center), where the peptide identification rate

was enhanced by 57%. The fragmentation data from these additional MS/MS transitions allowed a significantly greater portion of detected molecular features (MF) to be identified as PSMs in the Net Fraction compared with the control (see PSM/MF in right inset). Notably, ~90% of these PSMs were acquired with full C-trap fill time (60 ms) in the fractions or the control, revealing ion flux-limited conditions for the quadrupole Orbitrap mass spectrometer. Most recently, independent studies using nanoLC-HRMS found longer fill times (250 ms) advantageous for shotgun proteomics of limited protein digests (e.g., 1–10 ng),¹⁴⁴ suggesting that similar instrumental settings may also further peptide identifications during trace-sensitive CE-nanoESI-HRMS. While the number of identified peptides from the control (624 peptides) exceeded those from each of the fraction in our study (338, 227, 507 peptides in fractions 1, 2, and 3, resp.), the combined fractions with cumulative technical measurements identified substantially more peptides despite consuming an equal amount of total protein digest for analysis: 1,753 peptides were identified in union between the fractions (“Net Fraction”) versus 1,238 peptides in the control. Therefore, RP fractionation helped identify a greater number of peptides by CE-HRMS.

We also assessed the performance of peptide quantification upon fractionation (Figure 3.4). To account for biological variations between cell cultures, we repeated the analysis of 1 ng total protein digest using different neuron cultures ($n = 3$) upon fractionating 20 μg of protein digest from each replicate as described earlier (see also Figure 3.1). The results of technical replicates and cumulative identifications are presented in Figure 4a. Compared with the control, fractionation resulted in a 25% increase in peptide identification (left panel). We ascribe the observed sensitivity improvements to a combination of factors. Electrophoretic separation was notably improved in the fractions compared with the control. Using the 90-cm capillary, the mean theoretical plate number increased from ~274,000 in the control to ~373,000 in Fraction 1,

~412,000 in Fraction 2, and ~314,000 in Fraction 3 with these differences being significant ($p = 2.8 \times 10^{-3}$, 1.2×10^{-6} , and 2.2×10^{-2} , respectively). Additionally, the HRMS data revealed fractionation to effectively remove abundant salts and polar compounds from the culture media. Consequently, by lower salt concentration decreasing the conductivity of the sample, it is possible that field-amplified sample stacking was also improved in the fractionated samples. Furthermore, lower salt concentration in the fractionated samples is expected to have promoted ion generation by minimizing ionization interferences in the CE-nanoESI source. Indeed, signal-to-noise (S/N) ratios were improved by ~2-to-2.5-fold for several randomly selected peptides that migrated in the most compressed zone of the electropherogram, such as EIQTAVR with S/N = 127 ± 8 in Fraction #1 versus 50 ± 5 in the control, AVAVVVDPIQSVK with S/N = 143 ± 7 in Fraction #2 versus 60 ± 2 in the control, and SYELPDGQVITIGNER with S/N = 328 ± 8 in Fraction #3 versus 134 ± 3 in the control in the same experiment. Last, fractionation also minimized chemical complexity, thus likely allowing better utilization of the constrained MS/MS duty cycle to fragment trace-level peptide signals, which are otherwise deprioritized or triaged during data dependent acquisition due to lower S/N.

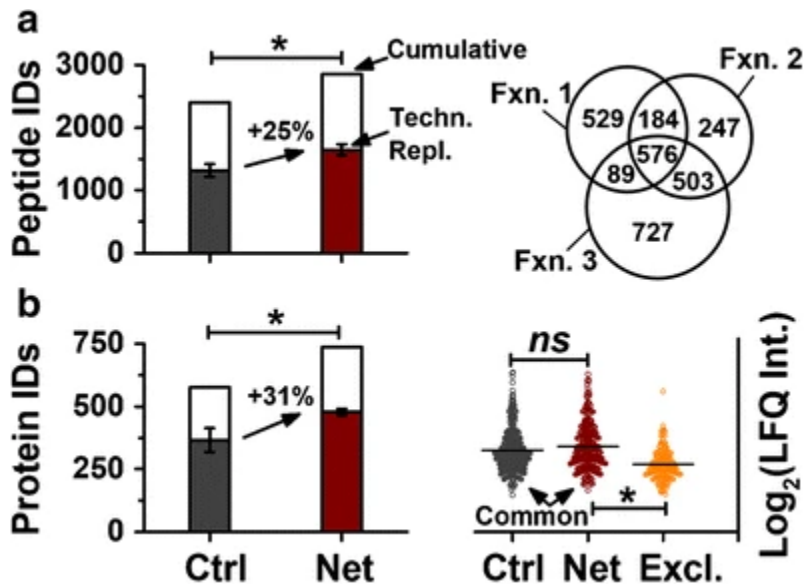


Figure 3.4 Metrics of peptide and protein detection from 1 ng of protein digest. (a) Three-step reversed-phase fractionation with CE-nanoESI-HRMS identified more peptides (see “Net”), significantly improving protein identification than the control (left panel). Comparison of peptides identified in each fraction on the basis of three independent experiments (right panel). (b) Protein identifications against the mouse proteome (left panel). The mean label-free quantification (LFQ) intensity was indistinguishable for proteins between the fractionated and control samples (right panel). Proteins that were exclusively quantified by fractionation (“Excl.”) had significantly lower LFQ intensities, suggesting a sensitivity gain by fractionation. Error bars, standard deviation. Statistical significance, * $p < 0.05$

3.3.3 Improved trace-sensitive protein detection

Higher-sensitivity peptide detection upon fractionation, in turn, improved the identification of proteins. As shown in Figure 3.4b, 31% more proteins were identifiable on average per technical replicate in the Net Fraction than the control with this difference being significant ($p = 6.9 \times 10^{-4}$). Cumulatively, triplicate analyses amounted to 737 protein groups identified in the Net Fraction versus 577 protein groups in the control. The distribution of LFQ intensities calculated for commonly detected proteins (see Methods) had indistinguishable means (see bottom panel), suggesting no quantifiable differences in the protein digest amounts that were recovered by fractionation or analyzed by CE-nanoESI-HRMS. Remarkably, proteins that were

exclusively quantified by fractionation were found to populate the lower domain of the quantitative dynamic range (see right panel) with this difference being significant ($p = 7.4 \times 10^{-21}$). A list of identified and quantified proteins and their calculated LFQ intensity are tabulated in supplementary Table 3.1. Combined, these results established higher qualitative and quantitative sensitivity to detect and identify peptides/ proteins by supplementing CE-HRMS with RP fractionation, particularly for molecules of lower abundance.

Last, we tested the scalability of the approach to process protein digest amounts from a limited population of neurons and a single neuron. We RP-fractionated $\sim 1 \mu\text{g}$ of peptides from the neuronal protein digest, confirmed by a total peptide assay, which approximates to proteins from $\sim 2,000$ neurons. Each fraction was dried and reconstituted in $2 \mu\text{L}$ of sample solvent in a microtube (see Methods). A total of 500 pg of peptide was analyzed by CE-HRMS between the fractions, corresponding to the content of a mammalian neuron. From equal amounts of total digest analyzed, triplicate analysis enabled 225 protein groups to be identified with fractionation compared to 141 protein groups from the control (Figure 3.5). A list of identified and quantified proteins is shown in Supplementary Table 3.2. Considering a 20-fold sample reduction during fractionation and a 2-fold sample reduction during detection (40-fold net reduction) in the workflow compared with the previous portion of this study, these identification numbers are encouraging toward trace-sensitive analysis of single neurons.

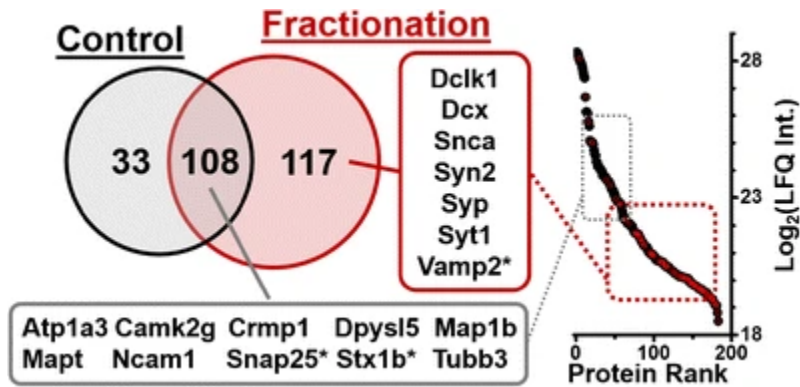


Figure 3.5 Case study of analyzing 500 pg of protein digest amount, approximating a single neuron. Products of many genes used as classical neuronal markers were identified by RP fractionation CE-nanoESI-HRMS. Representative examples are shown (left panel). Fractionation helped quantify proteins of lower-abundance (see red data points marking proteins, right panel). *Proteins from 1 ng digest are included

The identified proteins were enriched in products of many important neuronal genes. Our proteomics data identified 100 protein groups translated from 100 different genes that quantitative single-cell transcriptomics independently found to be differentially expressed during early neurogenesis.¹⁴⁵ A list of these proteins is tabulated in Supplementary Table 3. We identified a combination of proteins involved in neuronal differentiation and function, reflecting the developmental stage of the cultured neurons, which at 14 days in vitro have partially completed differentiation but are still extending processes and forming synapses.¹⁴⁶⁻¹⁴⁷ We found a high relative abundance of neuronal cytoskeletal protein such as Tubulin beta 3 chain (Tubb3), a well-established marker of differentiated neurons,¹⁴⁸ and Tubulin alpha-3 chain (Tuba3a), which is involved in neuronal migration (Figure 3.5, right panel). Mutations of the TUBA3A gene in humans lead to lissencephaly, brain malformations caused by abnormal organization of the hippocampus and cortex.¹⁴⁹ Proteins linked to neuronal migration were identified, mostly belonging to the middle-to-lower domain of protein abundance in our dataset, including proteins critical for neurite differentiation and cytoskeletal dynamics: neural cell adhesion molecule 1

(Ncam1),¹⁵⁰⁻¹⁵¹ microtubule associated protein 1B (Map1b),¹⁵² and the serine-threonine kinase doublecortin-like and CAM kinase-like 1 (Dclk1).¹⁵³⁻¹⁵⁴ Interestingly, Dclk1 and the microtubule-associated protein, doublecortin (Dcx), which is another classic neuronal marker, were only identified with the fractionation approach. Mutations or deletion in DCX also cause lissencephaly in humans,¹⁵⁵ and Dclk1 is highly expressed in regions with active neurogenesis and critical for neuronal survival.¹⁵³ Other interesting family members associated with developmental processes are the isoforms collapsin-response mediator proteins (CRMPs), CRMP-1 (Crmp) and CRMP- 5 (Dpysl5), which are highly expressed in the developing brain and play a role in neurogenesis, axonal guidance, and neuronal physiology.¹⁵⁶⁻¹⁵⁷

A second set of the identified proteins are key for mature neuronal function and have been linked to cognition and neurodegenerative disorders, such as the neuronal sodium/potassium-transporting ATPase $\alpha 3$ subunits (Atp1a3). Mutations in ATP1A3 have been found in individuals with rapid onset dystonia-parkinsonism.¹⁵⁸ The calcium/calmodulin dependent protein kinase type II subunit alpha (Camk2a)¹⁵⁹ and microtubule-associated protein tau (Mapt) have been linked to Alzheimer's disease. Finally, we identified proteins at the core of synaptic function regulation,¹⁶⁰⁻¹⁶² such as synaptosomal-associated protein 25 (Snap25), syntaxin-1B (Stx1b), synaptotagmin-1 (Sy1), synaptophysin (Syp), and synapsin-2 (Syn2). In addition to Syn2 and Syp, lower abundance protein like vesicle-associated membrane protein 2, also known as synaptobrevin-2 (Vamp2), was only identified by fractionation, likely amounting to the simplification of the sample complexity to identify proteins in the lower domain of the dynamic range of protein concentrations (see Figure 5, right panel).

Overall, these results showed that measurement of 500 pg to 1 ng of total peptides after fractionating 20 to 1 μ g of protein digest is sensitive enough to identify neuronal markers

associated with the development or disease of hippocampal neurons. Our findings also reveal sensitivity gains by fractionation to enable the detection and quantification of a greater number of proteins, including many of lower abundance (Figure 5), from trace amounts of protein digests. The agreement between data from ultrasensitive proteomics from this study and single-cell transcriptomics can help query molecular mechanisms during early neuronal differentiation.

3.4 Conclusions

Single-neuron measurements raise a powerful potential to better understand molecular processes as neurons develop in the brain. However, protein amounts contained by single neurons are 1,000- to 10,000-fold smaller (~500 pg/cell) than are typically detectable by standard nanoLC-HRMS. Here, we demonstrated that RP fractionation of 20 to 1 µg of protein digest in a ZipTip column improved the detection and quantification of proteins and peptides from 1 ng to 500 pg protein digests using CE-nanoESI-HRMS. This approach attains sufficient sensitivity toward characterizing protein digest amounts that single mammalian neurons are approximated to yield. We ascribe these improvements in sensitivity and quantification to a combination of factors, including reduced sample complexity, improved separation performance during CE, enhanced ionization efficiency during nanoESI, and higher peak capacity benefiting peptide fragmentation with a limited MS/MS duty cycle. As an example, we demonstrated the identification of 480 proteins/ experiment from 1 ng protein digest (737 proteins by technical triplicates) and 141 proteins per experiment from 500 pg protein digest (225 proteins by technical triplicates), essentially approximating proteins extractable from ~1 to 5 neurons. However, to extend these measurements directly to small populations of neurons or single neurons, continuous advances are needed at nearly all stages of the proteomic workflow,

beginning with the handling of cells, followed by the efficient extraction and processing of their limited protein content, before trace-sensitive characterization of proteins and peptides. The presented work lays down encouraging detection sensitivity by microanalytical RP fractionation with CE-nanoESI-HRMS to open a gate to study mechanisms of gene translation in limited populations of neurons to single neurons in the brain.

Chapter 4: Development of data-dependent acquisition ladder to support ultrasensitive proteomics

Based on material submitted by Sam B. Choi, Pablo Munoz-LLancao, M.Chiera Manzini, and Peter Nemes*

Author Contribution: S.B. Choi designed the research, processed the neuron culture, prepared the sample, and performed the measurements. S.B. Choi also analyzed the data, interpreted the results, and wrote the manuscript.

4.1 Introduction

Ultrasensitive high-resolution mass spectrometry (HRMS) promises new frontiers in biology and health research, including neuroscience. Using high-performance nano-flow liquid chromatography (nanoLC) HRMS, it is now possible to quantify ~13,000 different proteins from neuron cultures.^{56, 163} For deep coverage of the proteome, current protocols in shot-gun proteomics process appreciable amounts of starting material (e.g., milligrams) to analyze ~100 ng–1 µg of protein. These protocols process a sizable population, usually millions of neurons. Extension of HRMS to a few to a single neuron would open new frontiers in neurobiology and neuroscience by appreciating molecular composition at a spatial resolution commensurate with neural circuits. Compared to averaging over an entire cell population, single-neuron analysis would reduce molecular noise from the neighbors.¹⁶⁴ However, a single mammalian neuron yields only ~500 pg of protein extract,²⁹ which is ca. 1000–100,000-fold less than usually analyzed in nanoLC HRMS. To expand analytical neuroscience with HRMS, there is a high need

to innovate technologies and methodologies capable of deep protein detection and quantification from trace amounts of material.

Ultrasensitive proteomic HRMS aims to bridge this technological gap (reviewed in references¹⁶⁵⁻¹⁶⁷). Specialized systems automating volume-limited liquid handling extended nanoLC tandem HRMS instruments to single-cell analyses. More than 2,800 protein groups were identified from a 20 *Saccharomyces cerevisiae* strains using a single LC-HRMS method.¹⁶⁸ From a 100 pg of tryptic protein digest, recent nanoPOTS array (N2) chips were able to identify over ~1,300 proteins from single murine cells.¹⁶⁹ The automated single cell proteomics (SCoPE2) workflow enhanced measurement throughput to ~200 single cells over 24 h using an advanced nanoLC system, while reporting on ~1,000 proteins per cell.¹⁷⁰ These experiments deepened the detectable coverage of the single cell proteome, albeit at the expense of long experimental times (~2–5 h per analysis).

Capillary electrophoresis (CE) equips HRMS with sensitivity, efficiency, and speed. We and others developed robust methodologies and custom-built CE-ESI instruments capable of zeptomole–femtomole sensitivity (reviewed in references¹⁷¹⁻¹⁷²). For example, ~200 protein groups were identified from 5 ng of *Pyrococcus furiosus* digest¹⁷³ and up to 1,209 proteins groups from single embryonic cells dissected from^{28, 174} or analyzed *in situ/vivo*¹⁷⁵⁻¹⁷⁶ in chordate embryos of important biological models (*Xenopus laevis*, zebrafish). A home-built micro-analytical CE platform and a sheath-flow tapered-tip CE-ESI design equipped HRMS with 260 zmol sensitivity (156,000 copies) and robust operation on a quadrupole time-of-flight mass spectrometer, allowing us to identify ~217 protein groups from ~1 ng protein (approximating ca. two neurons).³⁰ An electrokinetically pumped low-flow sheath-flow interface provided 330 zmol sensitivity, identifying ~100 proteins from 16 pg of *E. coli* protein digest¹⁷⁷, 1,249 protein groups

from 300 ng protein digest from *Xenopus laevis* eggs,¹⁷⁸ and recently 4,400 protein groups were detected from 220 ng of K562-cell digest via 2 h of separation.¹⁷⁹ Proteins in these experiments were identified in a short amount of time, usually less than an hour, leading to compressed separation.

We recently argued that compressed electrophoresis challenges protein identification in high-sensitivity (single-cell) CE-HRMS.²⁹⁻³⁰ We and others found peptides to typically migrate as few-second wide peaks over a ~20–30 min effective separation window in bottom-up proteomic experiments. These separations are ~2–10-times faster than those typical in nanoLC. The resulting ion flux is chemically complex but transient, lasting only a few seconds. These conditions challenge the duty cycle of peptide isolation, activation, and fragmentation with a limited MS/MS speed. Indeed, only ~43% of molecular features (MFs: signals with unique m/z and separation time) were identifiable as peptide spectral matches (PSMs) during this portion of the separation, belonging to ~217 proteins.²⁹ Orthogonal separation, e.g., via high-pH fractionation allowed us to reduce the complexity of the chemical space, facilitating tandem MS to identify 225 protein groups from protein amounts estimated in single mammalian neurons.²⁹ Even with orthogonal separation, the resulting MS/MS transitions exhausted DDA capacity (~10–20 Hz) to fragmenting the most abundant peptide ions for better protein identifications, especially on mass spectrometers employing slower mass analyzers (e.g., compare orbitrap and time-of-flight).

Iterative DDA advanced sensitivity in nanoLC HRMS experiments.¹⁸⁰⁻¹⁸² Repeated measurements with DDA take leverage over stochastic selection of complementary sets of peptides to improve identification. Indeed, ~20% more proteins were identified via triplicates, with this gain quickly diminishing after the 5th replicate, reaching 95% saturation by the 10th.¹⁸⁰

Other DDA methods employed iterative strategies to boost identifications, ranging from exclusion or targeted inclusion of ions (mass-to-charge, m/z values) of interest.¹⁸³⁻¹⁸⁶ During precursor ion exclusion (PIE), the identified peptides were progressively excluded in the replicates by dynamically updating the ion exclusion list. The approach allowed nanoLC-HRMS to identify 533 proteins from five replicates of 1 μg of yeast whole cell lysate digest, equating to a 51% improvement compared to the standard approach.¹⁸³ Modified versions of PIE approach also enhanced peptide identification by 52% over four measurements of 16 μg of IgG1 monoclonal antibody digest.¹⁸⁷ Alternatively, post analysis data acquisition (PAnDA) iteratively prioritized unselected peptide features via targeted ion lists.¹⁸⁸ The inclusion ion list was able to identify 1,059 protein groups upon 6 technical replicate measurement of 4 μg of protein digest from *C. elegans*, corresponding to an ~18% increase in identifications compared to the control. In a combination of targeted and discovery approach, a real-time algorithm was developed that monitored the previously known order of nanoLC elution for peptides for targeted inclusion followed by exclusion.¹⁸⁹ This approach boosted identifications by 80% (826 vs. 459) from four mice tissue samples.

Here, we build on iterative DDA to advance ultrasensitive CE-HRMS to protein amounts approximating to ~10 mammalian neurons. A DDA ladder was prepared to iteratively exclude a static list of most abundant peptide-like molecular features during replicate measurement of the protein digest. In simplification from earlier iterative solutions, the DDA ladder requires no prior knowledge of identified peptides or dynamic adjustment of the exclusion list between replicates, as exclusion of ions are based on static ion abundance tiers established upon the first experiment. We demonstrate the potential of the approach for ultrasensitive neuroproteomics estimating to ~5

and 10 neurons. The DDA ladder is a simple and promising addition to the growing family of tandem MS approaches supporting neuroscience.

4.2 Experimental section

4.2.1 Materials

Unless otherwise stated, all materials were purchased at reagent grade from Sigma-Aldrich (St. Louis, MO). Standard lysozyme, myoglobin, and papain dissociation system were obtained from Worthington Biochemical Corp (Lakewood, NJ). Sodium dodecyl sulfate (SDS, 10% v/v) was obtained from Amresco (Solon, OH). Ethylenediamine tetraacetic acid (EDTA), LC-MS grade acetonitrile (ACN), formic acid (FA), acetic acid (AcOH), methanol (MeOH), MS-grade trypsin protease and water (Optima) were supplied by Fisher Scientific (Fair Lawn, NJ). Ammonium bicarbonate was from Avantor (Center Valley, PA). Hank's balanced salt solution, fetal bovine serum, penicillin-streptomycin, minimum essential medium, neurobasal medium, glutamine, and poly-L-ornithine were obtained from Gibco (Grand Island, NY). B27, N-2, glutamax, and pyruvate supplements were obtained from Thermo Fisher Scientific (Waltham, MA). Fused silica capillaries (20/90 μm inner/outer diameter and 75/350 μm inner/outer diameter) were from Polymicro Technologies (Phoenix, AZ) and used as received. The stainless steel tapered-tip metal emitter (100/320 μm inner/outer diameter) was manufactured by New Objective (Woburn, MA). All standards were prepared in 500 μL or 2 mL LoBind protein microtubes from Eppendorf (Hauppauge, NY).

4.2.2 Buffer and standard solutions

The cell lysis buffer was prepared to contain: 5 mM EDTA, 20 mM Tris-HCl, 1% (v/v) SDS, and 35 mM NaCl. The *neuronal plating medium* was prepared as described elsewhere¹⁹⁰ to contain: 0.6% (v/v) D-glucose, 10% (v/v) horse serum, 1% glutamine, and 1% penicillin-streptomycin in 1× MEM. The *neuro-maintain medium* was prepared to contain: 1% penicillin-streptomycin, 1% glutamax, 1% N-2, 2% B27, and 1% pyruvate in neurobasal medium. Prior to usage, all media were filtered through a 0.2 μm porous mesh.

4.2.3 Neuron culture

All procedures regarding the maintenance and humane treatment of mice were authorized by the Institutional Animal Care and Use Committee of the George Washington University (Approval Number A274). Adult pregnant C57BL/6 dams of mice (*Mus musculus*) were purchased from Charles River Laboratories (Wilmington, MA). Primary cultures of isolated mouse hippocampal neurons were prepared as described elsewhere.¹⁹⁰ After 14 days of cell culturing, each plated well was washed three times with 1 mL of SDS (10% v/v), and the cultured neurons were gently scraped to be transferred to a 1 mL LoBind microtube using micropipette with LoBind tip. Collected neurons were centrifuged at 800 × g for 5 min at 4 °C and stored at −80 °C until processing for measurement.

4.2.4 Bottom-up proteomics

The collected cultured neurons were processed using a standard bottom-up proteomic workflow (see reference¹⁸²). A 200 μL of lysis buffer was added to the collected neurons with 15 min of sonication in cold water bath (~4 °C). The lysate was reduced (5 μL of 1 M

dithiothreitol, DTT, 30 min at 60 °C), alkylated (10 μ L of 1 M iodoacetamide, IAD, 15 min in the dark) and quenched (5 μ L of DTT). The lysate was centrifuged at $11,200 \times g$ for 10 min at 4 °C, and the supernatant was transferred into a new 2 mL LoBind microtube. Proteins in the aliquot were purified by precipitation in 1 mL of chilled acetone (-20 °C, $5\times$ volume of sample aliquot) over 12 h, followed by centrifugation at $11,200 \times g$ for 10 min at 4 °C. The protein pellet was rinsed with chilled acetone, vacuum-dried at room temperature, and reconstituted in 200 μ L of ammonium bicarbonate (50 mM). The final concentration of protein content was 0.5 μ g/ μ L based on the standard bicinchoninic acid assay (Thermo Scientific, Waltham, MA). Aliquots of 40 μ L were transferred into 5 separate 500 μ L LoBind microtubes to serve as technical replicates. Each aliquot was digested with 0.8 μ L of trypsin (1 mg/mL) over 12 h at 37 °C. The resulting peptides were vacuum-dried and reconstituted in 40 μ L of 50% (v/v) ACN in 0.05% (v/v) AcOH, chosen to help on-column field-amplified sample stacking.³⁰

4.2.5 Microanalytical CE-nanoESI-HRMS

This study utilized a home-built co-axial sheath-flow CE-nanoESI platform³⁰ with the following settings: CE, 90 cm capillary at 23 kV vs. Earth ground (applied to the inlet); CE-ESI sheath solution, 50% MeOH (0.1% FA) supplied at 300 nL/min; ESI, +2,700 V at 2 mm from the MS inlet, operated in the cone-jet spraying regime for efficient ion generation.¹¹² Peptide ions were detected using a quadrupole orbitrap mass spectrometer (Q Exactive Plus, Thermo Scientific, Waltham, MA) between m/z 350–1,800 at 35,000 FWHM resolution (128 ms transient, 110 ms free fill). Higher-energy collisional dissociation (HCD) was triggered by DDA with the following instrumental settings: peak width (FWHM), 13 s; mass exclusion mass tolerance, 10.0 ppm; isolation window, 0.8 m/z ; peptide matches, on; apex trigger, turned off; ion

signals excluded below +2 charge state; ion signal intensity threshold, 1.5×10^3 counts; maximum ion trap time, 50 ms for MS¹. HCD employed the following conditions: m/z range, 200–2,000; resolution, 17,500 FWHM (64 ms transient) for MS²; normalized collision energy, 32; dynamic exclusion, 5.0 s; maximum IT, 50 ms for MS²; TopN, 15; loop count, 15.

4.2.6 Data analysis

Using MaxQuant¹ (version 1.5.7.4), the MS–MS/MS data were searched against the mouse proteome database containing 16,915 entries (downloaded from SwissProt on September 13th, 2017). The search parameters were: digestion, tryptic; missed cleavages, maximum 2; minimum peptide length, 5; minimum number of unique peptides, 1; fixed modification, carbamidomethylation at cysteine; variable modification, oxidation at methionine; match tolerance for main search peptide tolerance and MS/MS, ± 4.5 ppm and ± 20 ppm, respectively; isotope match tolerance, 2 ppm; decoy mode, revert; label-free quantitation, enabled. Proteins were identified and filtered based on false discovery rate (FDR) <1% against reversed-sequence decoy database. Reported proteins were protein groups filtered and combined based on the closest parsimony principle. Common contaminants were manually curated and filtered from the reported list of proteins. Molecular features were surveyed in MzMine 2.0¹⁹¹ with the following parameters; mass detector, exact mass; noise level, 5,000; chromatogram builder, on; Scans, MS¹; min time span (seconds), 12 s; minimum height, 5,000; m/z tolerance, 0.05 m/z or 20 ppm.

4.2.7 Safety consideration

Metal tapered-tip emitters and fused silica capillaries pose needle-stick hazard and should be handled with care. Handling of chemicals followed standard safety protocols. Electrically

conductive components of the CE-nanoESI-HRMS platform were grounded (Earth) or isolated to eliminate electrical shock hazard.

4.3 Results and discussion

4.3.1 A Technological Gap.

The goal of this study was to enhance CE-ESI-HRMS sensitivity for ultrasensitive neuroproteomics. CE-HRMS enabled the analysis of hundreds to thousands of different molecules in single cells and limited protein digests in exceptional sensitivity, in cases ~200–1,000-times higher than nanoLC.^{28-30, 174-176} Biomolecules in these experiments migrated over a considerably short time frame, typically within a ~15–30 min of effective separation window. For complex ‘omes, particularly a vastly expanded peptidome in bottom-up proteomics, compressed separation taxes identification due to limitations in HRMS-MS/MS sensitivity and speed.²⁹ To enhance detection, electrophoresis employing long separation times¹⁹² or orthogonal dimensions, such as ion exchange¹⁹³⁻¹⁹⁴, size-exclusion¹⁹⁵, or high-pH C18 chromatography³⁰ reduce molecular complexity over time to tailor to the duty cycle of MS/MS. Technological implementation, however, becomes increasingly challenging for trace amounts. Peak broadening due to longer separations is anticipated to reduce sensitivity (Van Deemter). Analyte transfer between separation dimensions risks peptide losses. These technologies also require skilled expertise and access to advanced, often custom-built, instrumentation, further constraining the studies to specialized laboratories.

To advance CE sensitivity to trace amounts of proteins, we proposed to improve the success of HRMS data acquisition. Our experimental rationale is shown in **Figure 4.1**. Protein

amounts approximating to single neurons and subcellular amounts were measured to assess suitability for single-neuron proteomics in this study. We used a home-built (one-dimensional) CE-ESI system³⁰ to analyze ~10 nL of protein digest from 250 nL of sample (see Fig. 4.1).²⁹⁻³⁰ Other custom-made or commercial CE systems with compatibility to limited amounts of samples may be used as an alternative. We reasoned that a microanalytical capability by CE allows for deepening proteomic coverage via repeated measurements if each replicate reports progressively deeper into the proteome, all the while still consuming trace-level net amounts. We envisioned these DDA transitions to form a ladder.

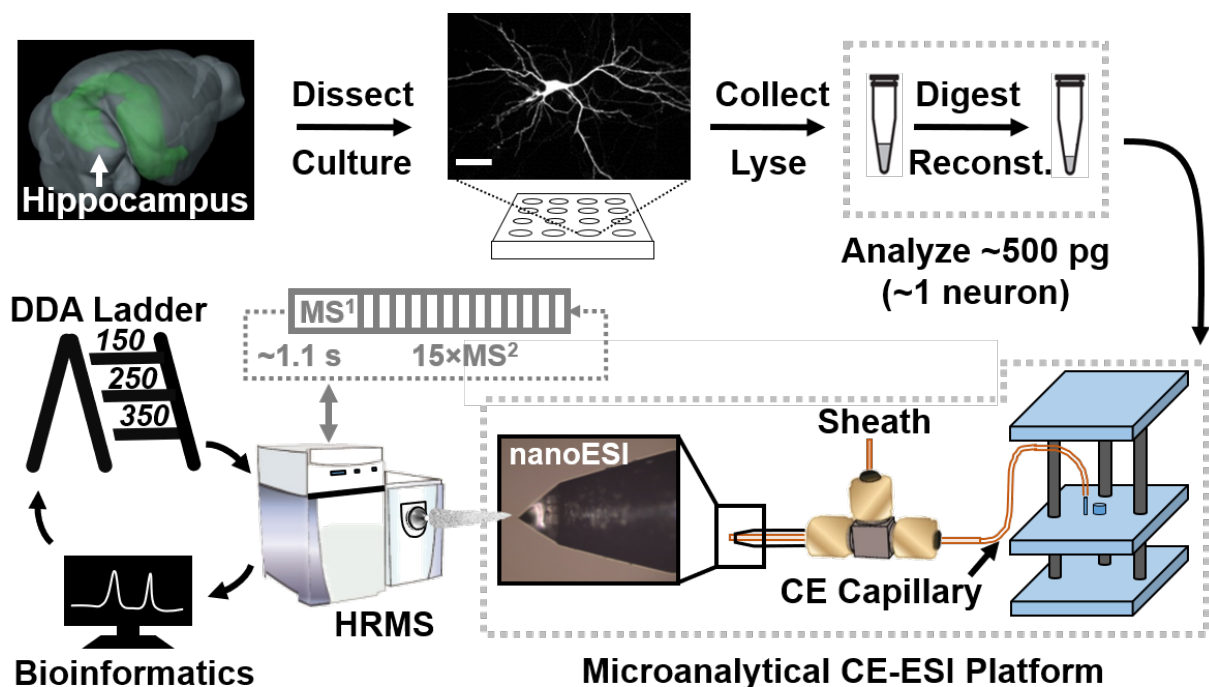


Figure 4.1. Experimental strategy of the nested DDA ladder for ultrasensitive CE-ESI-HRMS. The 150, 250, and 350 most abundant (top) peptides were excluded during replicate measurement of protein digests, with each replicate approximating to a single neuron (~500 pg/cell).

Method development began with control experiments optimizing performance. A protein digest, prepared from a culture of primary hippocampal neurons (mouse), was diluted to yield ~1

ng of protein digest per measurement for method development. This amount estimated the total amount of protein extractable from ca. 2 neurons.²⁹ The peptides were electrophoresed, ionized, and detected in a quadrupole orbitrap tandem mass spectrometer (Q-Exactive Plus, Thermo, see **Methods**). With a robust performance and well-established usage, we chose DDA to govern MS/MS with a preference for more abundant ions. A single-stage MS scan surveyed signals (m/z values), followed by fragmentation of the most abundant signals with a peptide-like isotope pattern. DDA parameters were optimized for identification based on technical duplicate analyses (same sample analyzed twice). A dynamic exclusion of 5 s yielded 380 proteins (vs. 334 proteins at 2 s, 286 at 10 s, and 330 at 15 s), an MS¹ automatic gain control (AGC) of 10^6 counts returned 432 proteins (vs. 364 proteins at 5×10^5 counts), and selection of the top 15 most abundant ions for MS/MS (TopN) gave 518 proteins (vs. 359 proteins at Top12, 474 at Top20). Technical triplicate, consuming 1.5 ng protein digest in total, identified an average 208 proteins per measurement, or 238 proteins cumulatively. Detection of various classical neural markers (see discussions later) agreed with earlier studies, demonstrating robust performance from CE-ESI-HRMS.²⁹⁻³⁰

The MS-MS/MS data were evaluated for potential limitations during data acquisition. In bottom-up proteomics, protein identification is based on peptide spectral matches (PSMs), which depend on MS/MS of molecular features (MFs: signals with unique m/z vs. migration time).

Figure 4.2 assesses these events. During the ~60 min experiment, 707 peptides were detected (<1% FDR) with the majority migrating through the capillary between ~30 min to ~45 min (**Fig. 4.2A**). This short, ~15 min, effective window witnessed a rapidly accumulating number of MFs with time. Their success of assignment as a PSM was substantially varied. At the most compact zone of separation, only ~20–30% of MFs were identified. The rate of identification increased to

~35–50% as molecular complexity relaxed. These results were obtained on a quadrupole orbitrap mass spectrometer in this study, yet agreed with limited identification success (~45%) by a quadrupole time-of-flight instrument.²⁹ **Figure 4.2B** evaluates MS/MS transitions underpinning these PSMs. In response to increasing MFs, DDA successfully boosted the rate of MS/MS transitions to the minimal duty cycle. Notably, ~95.5% of the MS/MS transitions that were made throughout the experiment were found to have exhausted the maximal C-trap fill time that was permitted. Therefore, DDA curtailed MS/MS rate in a trade between sensitivity and protein identification number.

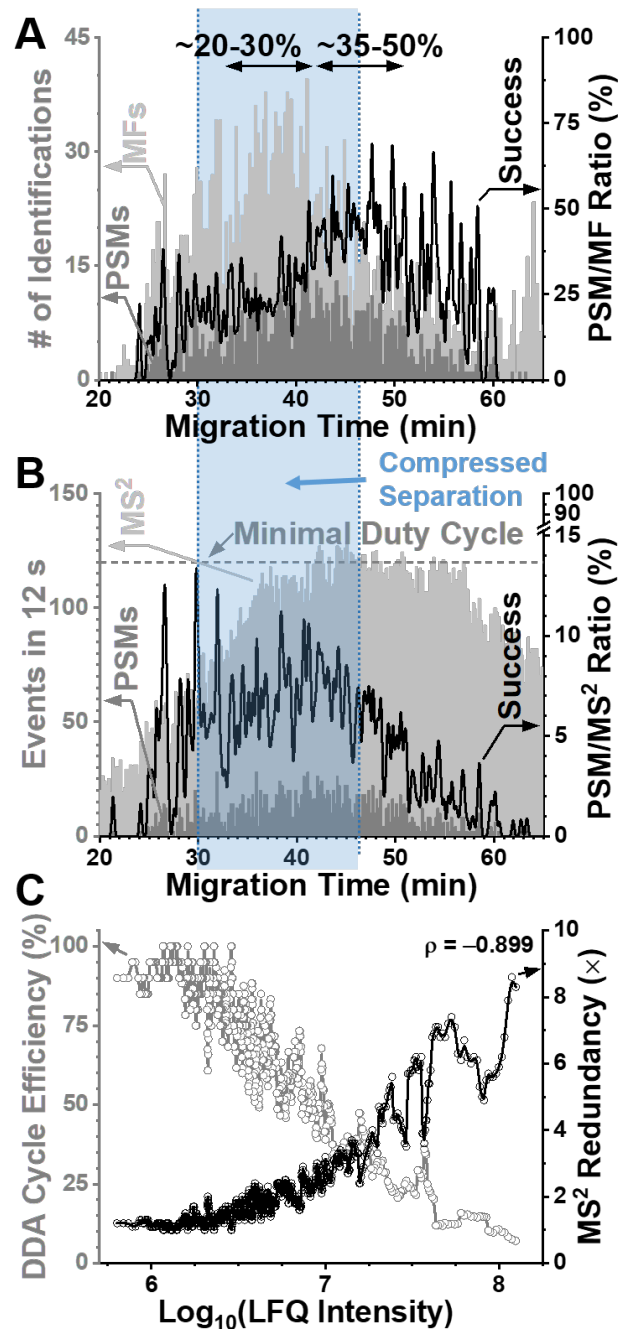


Figure 4.2. Challenges in trace-sensitive neuroproteomics using CE-HRMS with standard DDA. **(A)** Comparison of molecular features (MFs) and peptide spectral matches (PSMs), uncovering rapidly diminishing success at identifying putative peptide signals during the most compressed portion of electrophoresis. **(B)** Evaluation of tandem MS events underlying peptide identifications, showing optimal success at minimal MS/MS duty cycle. **(C)** More abundant peptides were fragmented at increasing redundancy, causing a steep decay in the efficiency of

the DDA cycles identifying peptides. Key: ρ , Coefficient of Pearson product-moment correlation.

How complementary the resulting PSMs were, we asked, as deeper coverage of the proteome depends on the identification of different peptides. In a representative dataset, 2,196 different PSMs were acquired belonging to 1,203 different peptides (peptide groups), revealing that the same peptide was fragmented ~ 1.8 -times on average (MS^2 redundancy). **Figure 4.2C** monitors MS^2 redundancy over peptide abundance using calculated label-free quantification (LFQ) intensities, which are used as a proxy for concentration.²⁸ More abundant peptides were more likely to yield PSMs. This redundancy ca. tripled with each decade of ion signal abundance over the ~ 3 log-order observed dynamic range. For example, HFFTVTDPR (Sideroflexin-3 eukaryotic translation initiation factor 5A-1) was fragmented once, whereas the ~ 100 -times more concentrated NLDIERPTYTNLNR (Tubulin alpha-1B chain) was fragmented 8 times. Repeated fragmentation, in turn, deteriorated the utilization of the DDA cycle time (**Fig. 4.2C**), as also quantified by a strong anticorrelation between the datasets ($\rho = -0.899$, Pearson). An ~ 9 -fold increase in MS^2 redundancy yielded a 15-fold reduction in cycle utilization. Therefore, more abundant peptides were not only more likely to be redundantly fragmented, but they also required increasingly more time, which in turn further depreciated identification success.

4.3.2 Guided Design of the DDA Ladder

As our results revealed abundant MFs to be more redundantly fragmented under optimal CE-HRMS conditions, we reasoned that a DDA method minimizing PSM redundancy would deepen proteome coverage. **Figure 4.3** presents the guided design of the approach. Spectral redundancy is monitored as a function of abundance in **Figure 4.3A**. Ca. 65%, $\sim 75\%$, and $\sim 85\%$ of total signal abundance was produced by the 150, 250, and 350 most abundant (top) peptides,

which yielded ~25%, ~37%, and ~50% of all the PSMs performed, respectively. Based on these results, we posited that exclusion of these redundant features during replicates of the sample, afforded by low sample consumption by our CE-ESI HRMS platform, would free up DDA bandwidth to lower-abundance peptides. We built three DDA methods that formed a nested series of exclusion ions for these peptide ions, ranked by abundance (recall **Fig. 4.1**). These DDA methods offered vantage points at different depths into the proteome, akin to rungs of a ladder; therefore, we termed the method a “DDA ladder.”

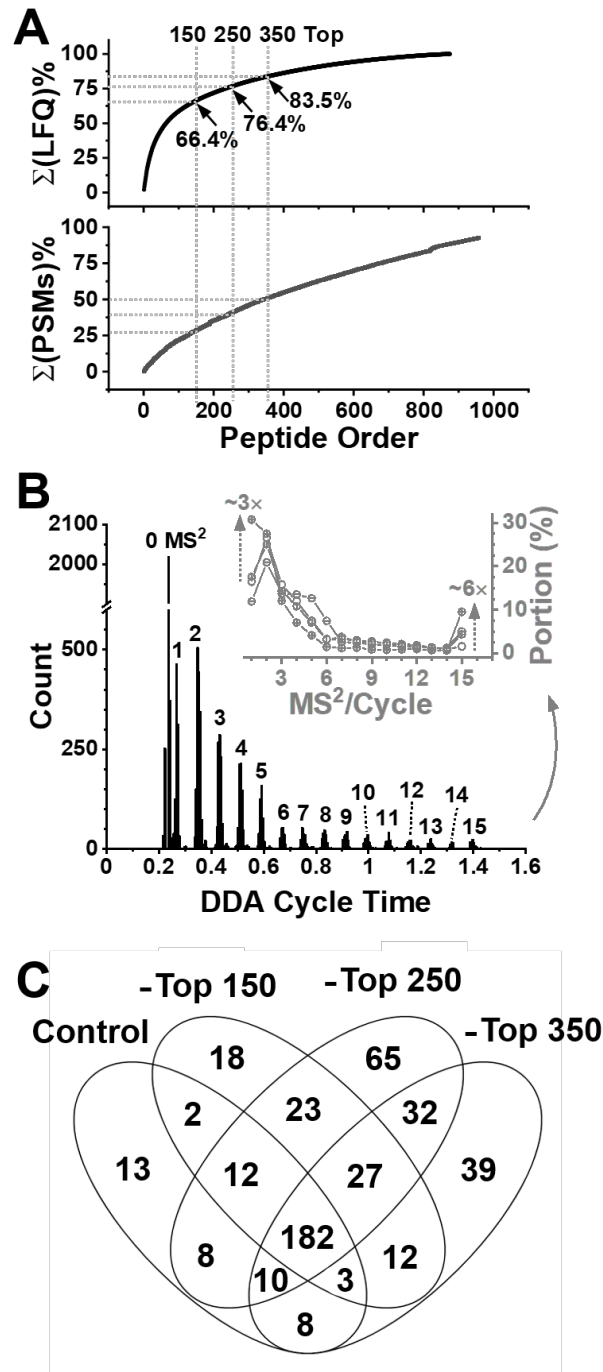


Figure 4.3. Guided design of the DDA ladder. **(A)** The 150, 250, and 350 most abundant peptides accounted for the majority of signal abundance (LFQ intensity) and peptide spectral matches (PSMs) in control experiments (1 ng protein digest analyzed). **(B)** Evaluation of the DDA cycle time, revealing underfilling of the top-15 peptide ions targeted for tandem MS. **(Inset)** Most DDA cycles were completed after fragmenting only 1–5 peptide ions. Exclusion of the top 250 ions improved full utilization of the DDA cycle. **(C)** Exclusion of the most abundant

ions resulted in complementary protein identifications from 500 pg protein digest analyzed per measurement, approximating to a single neuron.

Each rung of the DDA ladder was experimentally tested. Protein amounts of 500 pg, which approximates to a single neuron,²⁹ were measured in triplicate as the control (without exclusion of ions). The resulting proteins were ranked by LFQ abundance, and the triplicate analyses were repeated while excluding the 150, 250, and 350 most abundant peptides. Utilization of the DDA duty cycle is analyzed in **Figure 4.3B**. Ca. 42% of the DDA cycles were completed without peptide ions selected for fragmentation (see 0 MS²). Ca. 10–30% of cycles performing tandem MS selected 1 to 5 peptide ions for analysis (see **inset**). Less than ~2% of the cycles were able to complete 15 MS² scans after the survey (MS¹) scan. Exclusion of the most abundant peptide ions improved these metrics. Disregarding the top 250 ions tripled the fraction of cycles completing one tandem MS scan and boosted the frequency of cycles targeting 15 peptide ions by 6-fold, while reducing cycles in between (see 2–14 MS² scans). As shown in **Figure 4.3C**, these transitions identified a complementary set of proteins. The identified proteins are tabulated in **Table 4.1**. It follows that each rung of the DDA ladder helped coverage.

The DDA ladder was benchmarked for proteins (**Fig. 4.4**). Standard DDA with technical replicates, which is the closest neighboring technology, was chosen as reference. **Figure 4.4A** predicts the cumulative number of proteins on the basis of up to quintuplet replicates (Control). With rapid saturation in identification, repeated analysis provided diminishing returns. While triplicates identified 238 proteins, projected identifications were only 287 at 6, 319 at 9, and 338 at 12 replicates. We considered 3 technical replicates as a satisfactory trade between identification number, sample consumption, and analysis time. These results were outperformed with each additional rung of the DDA ladder. Compared to projections, the number of identified

proteins expanded by ~11%, 30%, and 29% upon exclusion of the top 150, 250, and 350 ions, respectively. The first two rungs (top 150 and 250 ions excluded) were chosen to supplement the control experiments; the DDA ladder was finalized for the remainder of the study. With only ~500 pg/analysis afforded by μ CE and a total of 9 replicates, the method consumed ~5 ng, approximating to ~10 neurons.

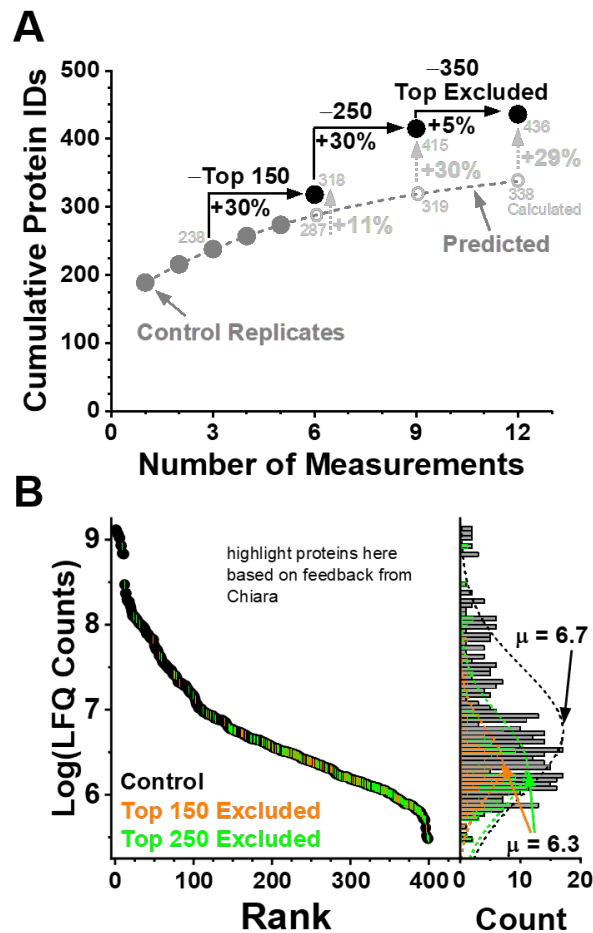


Figure 4.4. Depth of proteome coverage. **(A)** Cumulative protein identifications upon technical replicates by standard DDA (Control) and the DDA ladder. Exclusion of the top 150 and 250 ions was chosen sufficient for this work. **(B)** Expanded dynamic range of quantification by the DDA ladder, revealing quantification of lower-abundance proteins. Proteins only quantifiable by exclusion of the top 150 (orange) and 250 most abundant proteins are marked over the control (black).

We inquired about the depth of coverage of the proteome. **Figure 4.4B** screens the dynamic range of proteins that were quantified based on LFQ. The DDA ladder identified 416 proteins (nonredundant), 396 of which were also quantified (see **Table 4.1**). To minimize potential variations in LFQ between the replicates, the calculated abundance values were scaled using linear regression on the basis of the commonly quantified proteins (control vs. top 150 excluded: $R^2 = 0.93$; control vs. top 250 excluded: $R^2 = 0.90$). Comparison of the proteins based on abundance reveals expansion of the linear dynamic range of quantification upon exclusion of the abundant peptide ions. Proteins that were detected exclusively by the DDA ladder occupied the lower domain of the dynamic range of concentration, with significantly lower Gaussian distribution means than the control (e.g., $p = 0.00009$ for top 150 excluded, Student's t-test). DDA ladder deepened coverage of the neuroproteome.

Many of these proteins are known to fulfil important biological roles. Some of the neural proteins like *Ndrp2*, which may act as tumor repressor, and *Wdr47*, a neuronal enriched MAP interacting proteins, and *Camk2d*, a calmodulin-dependent protein kinase, were likely to be masked by the abundant proteins which made these to be undetected and unidentified in any other measurements. With enhanced sensitivity, the DDA ladder method expands the analytical toolbox of neuroscience.

4.4 Conclusions

This study advanced CE-HRMS to trace-sensitive neuroproteomics. A DDA ladder encompassing two levels (rungs) of filters deprioritized high-abundance ions to expand the quantifiable linear dynamic range of the proteome. The method improved utilization of the limited DDA duty cycle, reduced redundant MS/MS events, and promoted the selection of a

larger number of ions that could be targeted for fragmentation. In turn, these advances were better prepared to measure high peptidome complexity unfolding during compressed electrophoresis. CE-HRMS employing the DDA ladder complements classical nanoLC-based proteomics with fast analysis (~30–45-min separation), high sensitivity, and robust operation. Recent commercialization of CE instruments capable of handling limited amounts of samples (e.g., less than ~1–5 μL) may substitute the custom-built microanalytical CE platform in this study. With well-established usage and commercial availability, we anticipate the DDA method to be readily adaptable to other laboratories analyzing other types or limited amounts of proteins via shot-gun proteomics.

Continuous advances at multiple stages of the proteomic workflow promise further sensitivity improvements possible. Technologies enabling the isolation and handling of miniscule amounts of proteins with reduced losses, for example, by *in vivo* microsampling¹⁷⁵, nanoPOTS¹⁶⁹, and ScoPE¹⁷⁰ offer viable solutions to obtain and process miniscule amounts of proteins from biopsies and limited populations of cells, including single cells. Identification and quantification of 415 nonredundant protein groups from protein amounts estimating ~10 neurons in this study, including many with important biological functions in homeostasis and disease, marks another technological leap in ultrasensitive proteomics, expanding the bioanalytical toolbox of neuroscience.

Chapter 5: Single-cell mass spectrometry with patch-clamp electrophysiology extends the bioanalytical toolbox of neuroscience

Based on material in preparation for submission by Sam B. Choi, Abigail Polter, and Peter Nemes*

Author Contribution: S.B. Choi designed the research, processed the collected neurons, prepared the sample, and performed the measurements. S.B. Choi also analyzed the data, interpreted the results, and wrote the manuscript.

5.1 Introduction

It is imperative to understand the cellular heterogeneity in cells to uncover how each cell establishes functional differences as they mature. In addition, understanding individual cell's susceptibility to diseases and therapeutic treatments would facilitate the development of effective treatments.¹⁶⁴ Many technological developments have contributed to uncover the molecular composition of the individual cells using techniques, such as, patch-clamp electrophysiology¹⁹⁶⁻¹⁹⁹ and high-resolution mass spectrometry (HRMS).^{63, 174, 196, 200} Patch-clamp electrophysiology technique has enabled the measurement of neural electrical activities to monitor and investigate neuronal communication, translating into the cell's physiological characteristics²⁰¹ and the cell's physiological response to treatments.²⁰² Understanding these physiological aspects of individual cells with protein characteristics can empower our ability to deepen the knowledge in developmental processes of these cells.

However, uncovering cell-to-cell heterogeneity in their proteome requires sensitive technologies that are capable of single-cell analysis. Continuance in advancement in high-resolution mass spectrometry (HRMS) with high-performance liquid chromatography (nanoLC)

has now enabled ultrasensitive detections to characterize and quantify the expression of ~13,000 protein groups from millions of cells from brain primary cell cultures.²⁰³ We and others have recently extended the proteomic measurement to limited population of neurons (~5 – 10) using capillary electrophoresis (CE) as an alternative to nanoLC with a zepto-mole (~230 zmol) detection limit for a model peptide standard (angiotensin II).^{30, 204} The hyphenation of CE to HRMS has demonstrated its capability to deliver sensitive measurements of a wide range of volume-limited biomolecules in the past.^{63, 132, 174, 196, 205-206} CE-HRMS has excellent sensitivity and requires miniscule amounts (<1 ng) of sample material for successful analysis, thus being favored by others to utilize the technology for single-cell metabolomic^{63, 196, 207} and proteomic^{174, 206, 208-210} analysis. However careful sampling of the cell content remains a challenge to characterize molecular compounds, especially proteins, directly from a single cell.

The effort to advance single-cell analysis for molecular characterization has been ongoing since the development of whole-cell patch-clamp electrophysiology which was used to measure physiological properties of individual neurons.^{198-199, 211-212} The patch-clamp technique was able to explore individual ion channels in live neurons, providing information on electrical activities of the patched neuron. However, this technique has limitation for chemical analysis as it cannot provide in-depth molecular information. Owing to this limitation, a separation technique (i.e., CE) has been previously introduced to the patch-clamp technique in past studies to demonstrate its feasibility to analyze biological activities and separate chemical compounds to identify receptor agonists but with a low throughput.²¹³ These technologies were developed several decades ago but only recently, the patch-clamp electrophysiology was coupled to CE-HRMS to enable metabolomic measurements from single mammalian neurons. This combined approach was able to detect 60 metabolites from microaspirated glutamatergic cells and gamma-

aminobutyric acid (GABA) from GABAergic neurons, highlighting technology's sensitivity and specificity.²⁰⁰ Another representative case for the application of technology includes, metabolomic analysis using nanoESI-MS for direct sampling of cytoplasmic content from single cells, identifying over 70 molecular features from onion epidermal cells and mouse brain neurons.¹⁹⁶ Although these examples using patch-clamp microsampling with HRMS aimed to deliver metabolomic analysis of specific cells, their application to single-neuron proteomics remains to be a challenge. To address this challenge, we here report an integrated approach combining the whole-cell patch-clamp electrophysiology with single-cell high-resolution mass spectrometry for discovery proteomic analysis from electrophysiologically identified single neurons in the mouse brain.

5.2 Experimental section

5.2.1 Materials

All materials were purchased at reagent grade. Dithiothreitol (DTT), iodoacetamide (IAD), tris-hydrochloric acid (tris-HCl), tris-hydroxy methylaminomethane (Tris-base), potassium chloride (KCl), and sodium hydroxide (NaOH) were obtained from Sigma-Aldrich (St. Louis, MO). Acetonitrile (ACN), trypsin protease, water (Optima), formic acid (FA), ethylenediamine tetraacetic acid (EDTA), acetic acid (AcOH) and methanol (MEOH) were purchased in MS-grade from Fisher Scientific (Fair Lawn, NJ). Ammonium bicarbonate was from Avantor (Center Valley, PA). Sodium dodecyl sulfate (SDS) was from Amresco (Solon, Ohio). Fused silica capillaries (40/90 μm inner/outer diameter) were from Polymicro Technologies (Phoenix, AZ, USA) and used as received. Borosilicate capillaries for electrode

capillaries (0.75/1 mm inner/outer diameter) were from Sutter Instrument (Novato, CA). All standards were prepared in 500- μ L LoBind protein microtubes from Eppendorf (Hauppauge, NY). Tandem mass tagTM reagents and 1 M triethylammonium bicarbonate (TEAB) were obtained from ThermoFisher Scientific (Waltham, MA).

5.2.2 Animals and brain section preparation

All procedures were carried out in accordance with the guidelines of the National Institutes of Health for animal care and use and were approved by the George Washington University Institutional Animal Care and Use Committee (IACUC# A378). C57Bl6/J mice were bred in-house and were maintained on a 12-h light/dark cycle and provided with food and water ad libitum.

General methods were followed to prepare acute brain tissue sections as described elsewhere.²¹⁴ Male mice aged postnatal day (PND) 21-35 were deeply anesthetized with an intraperitoneal injection of ketamine and dexmedetomidine (100/0.25 mg/kg, respectively) and perfused with ice-cold HEPES ringer solution (in mM): 86 NaCl, 2.5 KCl, 1.2 NaH₂PO₄, 35 NaHCO₃, 20 HEPES, 25 glucose, 5 sodium ascorbate, 2 thiourea, 3 sodium pyruvate, 1 MgSO₄, 2 CaCl₂.²¹⁵ Following perfusion, the brain was rapidly dissected and horizontal slices (220 μ m) were prepared in HEPES ringer using a vibratome. Slices recovered for 1 h at 34°C in oxygenated HEPES holding solution and then were held in the same solution at room temperature until use.

5.2.3 Whole neuron electrophysiology and sample collection

Midbrain slices were continuously perfused at 1.5–2 mL/min with artificial cerebrospinal fluid (aCSF) at 28–32°C containing (in mM): 126 NaCl, 21.4 NaHCO₃, 2.5 KCl, 1.2 NaH₂PO₄, 2.4 CaCl₂, 1.0 MgSO₄, and 11.1 glucose. Patch pipettes for recording (2–4 MΩ) and protein extraction were backfilled with ~20 uL 50 mM ammonium bicarbonate in water. Dopaminergic neurons were putatively identified based on their location in the lateral portion of the substantia nigra and their larger size. After obtaining a giga-ohm seal, a 60-second recording in the cell-attached configuration was obtained, and the dopaminergic identity of the neuron was confirmed by the presence of a slow pacemaker firing pattern (Figure 1). Following electrophysiological analysis, the microprobe entered the cell with a steady negative pressure applied at the outlet end of pipette with a syringe to aspirate a portion of neural soma. The neuron was visually inspected during microaspiration under an inverted microscope (40× magnification, Nikon FN1). Electrophysiological recordings were obtained using a Sutter integrated patch amplifier and Sutterpatch software (Sutter Instruments, Novato, CA). Upon completion of microaspiration, the pipette was gently removed from the cell and the contents expelled into a 500 μL Eppendorf LoBind microtube for bottom-up proteomic analysis. A small portion of substantia nigra tissue containing ~50–100 dopaminergic neurons were also collected for TMT labeling approach for sensitivity enhancement.

5.2.4 Sample processing for bottom-up proteomics

A standard bottom-up proteomic workflow requires tissue lysis, reduction, alkylation and protein purification steps prior to trypsin digestion.¹⁸² However, in this study, we modified the protocol to minimize sample losses from added steps. Each collected protein extract from

dopaminergic neuron was added with 5 μL of 50 mM ammonium bicarbonate containing 0.1 μg of trypsin protease for one-step digestion at 60 $^{\circ}\text{C}$ for 1 h. The resulting single-neuron protein digests were vacuum-dried and stored at -80°C until TMT labeling.

For reference, a whole-tissue protein digest was prepared from the substantia nigra and was processed following a standard bottom-up proteomic workflow. The tissue was dissected under the stereomicroscope and lysed in 50 μL of *lysis buffer* (in mM: 5 EDTA, 20 Tris-HCl, 35 NaCl, and 1% (v/v) SDS) facilitated by periodic ultrasonication for 5 min in an ice-cold water bath. The resulting protein extract was reduced by adding 2 μL of 1 M DTT (30 min at 60 $^{\circ}\text{C}$), alkylated by adding 4 μL of 1 M IAD (15 min in the dark), and quenched by adding 2 μL of 1 M DTT. The cell debris was separated from the supernatant by centrifugation at $15,000 \times g$ for 10 min at 4 $^{\circ}\text{C}$, and the supernatant was transferred into a new 500- μL LoBind protein microtubes for overnight acetone precipitation in 300 μL ice-cold acetone (-20°C). Purified proteins were dried at room temperature, reconstituted in 50 μL of 50 mM ammonium bicarbonate and digested for 6 h at 37 $^{\circ}\text{C}$ (1 μg of trypsin protease was added). The resulting peptides were vacuum-dried and stored at -80°C until TMT analysis.

The dried peptides samples were barcoded for quantification. Labeling was done using TMTsixplexTM isobaric labeling kit (ThermoFisher Scientific) following the vendor suggested protocol. More specifically, for single neurons, the dried sample was reconstituted in 1 μL of 100 mM TEAB and tagged with 1 μL of 85 mM TMT label reagent (TMT-128 channel) while the whole tissue sample was added with 20 μL of 100 mM TEAB and tagged with 5 μL of 85 mM TMT label reagent (TMT-131 channel). Each sample was incubated for 1 h at room temperature for successful labeling. After incubation, the reaction was quenched (0.5 μL and 2 μL of 5% hydroxylamine for 15 min at room temperature). Upon quenching of the reaction, the samples

were mixed together, vacuum-dried, and stored at $-80\text{ }^{\circ}\text{C}$ for up to 1 month period until CE-nanoESI-HRMS analysis.

5.2.5 Single-cell HRMS and CE-nanoESI-HRMS

Combined TMT labeled peptides were analyzed on a custom-built micro-loading CE platform that we recently reported.²⁹ However, the platform was modified from our previous version. The separation CE capillary was coaxially fed into a pulled borosilicate capillary, which it served as nanoelectrospray (nanoESI) emitter (0.75/1 mm inner/outer diameter) with $\sim 10\text{--}15\text{ }\mu\text{m}$ tip aperture. An $\sim 20\text{ nL}$ ($< 1\text{ pg}$) of protein digest was separated by capillary zone electrophoresis in a 100-cm capillary at $\sim 220\text{ V/cm}$ field strength. The electrophoretically separated peptides were ionized by a modified nanoESI interface. In this design, the sheath solution (10% MeOH in 0.05% (v/v) AcOH) was supplied throughout the borosilicate capillary emitter, pumped electrokinetically operating at $+1,700\text{ V}$ for stable spray. The emitter was positioned $\sim 500\text{ }\mu\text{m}$ in front of a mass spectrometer for detection and the nanospray source was maintained in the cone-jet regime for efficient ion generation.¹¹²

Peptide ions were mass analyzed from m/z 400 to 1,700 at 35,000 FWHM resolution (MS^1) using a hybrid quadrupole orbitrap mass spectrometer (Q Exactive Plus, Thermo Scientific) equipped with a higher-energy collision dissociation (HCD) cell for fragmentation. The mass spectrometer was operated with the following settings: Chromatography peak width (FWHM), 13 s; AGC target, 1×10^6 counts; Maximum IT, 50 ms; dynamic exclusion mass tolerance, 5.0 ppm; peptide match, on; exclude isotopes, on; dynamic exclusion, 9.0 s; ion signals excluded below +2 charge state; ion signal intensity threshold, 1.5×10^6 counts; apex trigger, off. Ions that passed these threshold criteria were selected for HCD with the following

settings: maximum IT, 60 ms; isolation window, 1.5 Da; normalized collision energy, 36%; MS² resolution, 17,500 FWHM; TopN, 20; loop count, 20; fixed first mass, 110.0 *m/z*; minimum AGC target, 9.2×10^2 counts. Ions that were fragmented under these settings were dynamically excluded with 5.0 ppm accuracy for 9.0 s before re-consideration for another fragmentation.

5.2.6 Data analysis

Primary MS/MS–MS data were analyzed in MaxQuant ver. 1.6.2.10 (Max Planck Institute of Biochemistry) executing the Andromeda search engine ver. 1.5.6.0 search engine¹¹⁵ against the *Mus musculus* proteome (downloaded from UniProt on February 2nd, 2018) as database with the following search parameters: trypsin digestion, up to 2 missed cleavages; variable modification, methionine oxidation; fixed modification, cysteine carbamidomethylation; precursor mass tolerance (MS¹), 20 ppm; fragment mass tolerance (MS²), 4.5 ppm; minimum peptide length, 5. Peptides are reported with <1% false discovery rate (FDR), calculated against a reversed-sequence decoy database. The reported protein groups were clustered based on the parsimony principle. Common contaminants were manually removed from the reported protein list.

5.2.7 Safety consideration

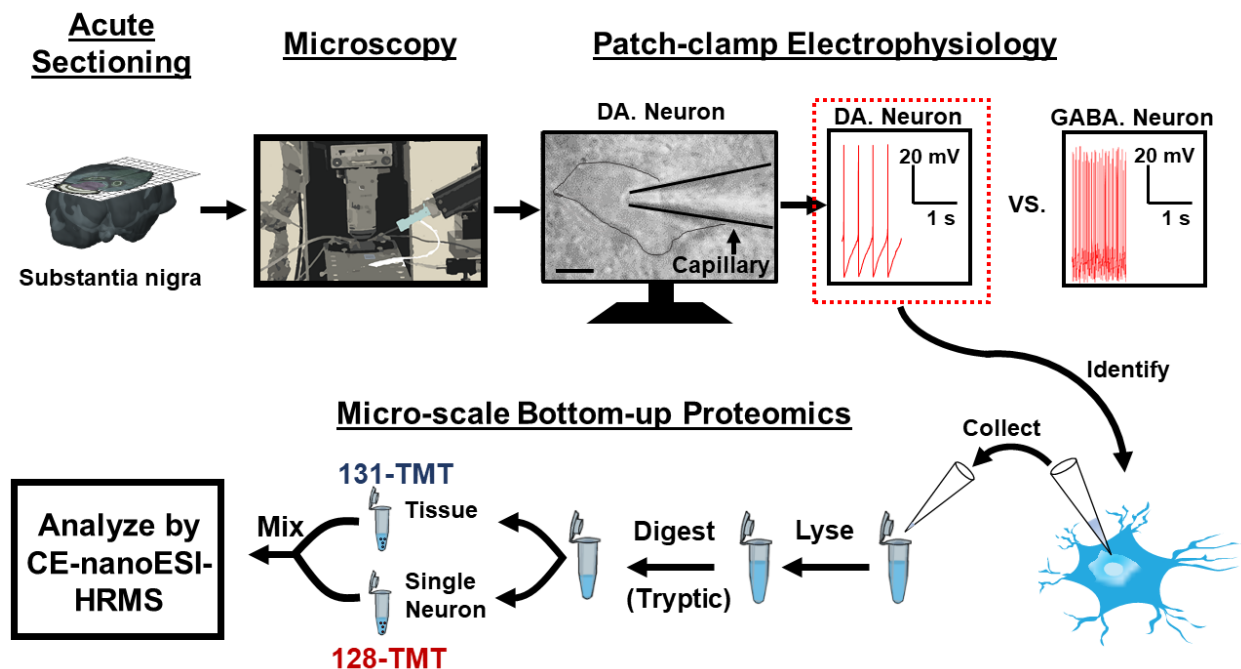
Fused silica capillaries and borosilicate capillary emitters, which pose potential needle-stick hazard, were handled with care. Standard safety protocols were followed during the handling of chemicals. All electrically conductive parts of the CE-nanoESI interface were grounded or isolated to prevent electrical shock hazard.

5.3 Results and discussion

5.3.1 Goal and design

The goal of this study was to use this integrated approach to enable the discovery protein analysis of single tissue-embedded identified neurons in the mouse brain. We combined existing technologies and newly developed technologies to overcome analytical challenges that hindered identification of proteins in single neurons. Here, we chose CE for separation of complex protein digests processed from single neurons, microprobe approach for microsampling of the neuronal soma,²⁰⁷ and redesigned nanoESI interface for trace sensitive analysis. We and others have recently demonstrated that CE-HRMS offers exceptional sensitivity to detect peptides and proteins from small amounts of sample.^{131-132, 205} In our previous CE-HRMS measurements, we identified an appreciable number of protein IDs, identifying 225 protein groups from ~500 pg of a hippocampal neuron protein digest.²⁰⁴ The protein digest prepared in the past studies were from a large collection of neurons, where a serial dilution of the sample was necessary to result in ~500 pg of protein digest. However, significant improvements were necessary in various aspects of the sampling approach to overcome the challenge in handling of limited sample material from single neurons. Therefore, we revised microprobe methodology²¹⁰ to address the sampling challenge by microaspirating the cell content from neuronal soma using the patch pipette. In recent studies, *in situ* microprobe approach was applied in single-cell mass spectrometry for *Xenopus laevis* embryos using pulled borosilicate capillaries to sample a single live embryonic cell to detect ~230 molecular features.²⁰⁷ The reported microprobe approach demonstrated its feasibility and applicability of the technology to our microanalytical workflow. In addition, we

also coupled a redesigned nanoESI ion source to improve the detection sensitivity by modifying the co-axial designed interface with borosilicate emitter for enhanced ionization.²¹⁰



Figures 5.1. Microanalytical workflow for whole-cell patch-clamp electrophysiology followed by single-neuron proteomic analysis. **Top panel:** Neurons were putatively identified based on the anatomical location using microscopy. Then, the identification of DA neuron was confirmed based on its unique slow pacemaker firing pattern from electrophysiological recording. Another example recording of other neurons from substantia nigra is presented (GABAergic neuron) to demonstrate our capability to differentiate neuronal types based on the recordings. The electrophysiologically-identified neurons were microaspirated and processed via a micro-scale bottom-up proteomic workflow. Processed sample was then labeled with distinct TMT channels (131-substantia nigra tissue and 128-single neuron) and analyzed by CE-nanoESI-HRMS platform.

5.3.2 Electrophysiology based microsampling approach

In this study, we also used a technique that was well established for recording electrical activities of single neurons, the whole-cell patch-clamp electrophysiology (**Figure 5.1**). The

purpose of this biological assay was to confidently identify dopaminergic (DA) neurons based on their size, anatomical location, morphology, as well as electrical activity.^{197,216} The substantia nigra tissues from the mouse brain was sectioned and was prepared as described in the methods and was placed in an artificial cerebrospinal fluid for patching (see **Methods**).²¹⁷ We chose substantia nigra brain section as the model tissue for this study because of high population of DA neurons (>70%),²¹⁷ facilitating the selection and identification of the DA neurons. Neurons were putatively identified based on their size and location in the tissue using an inverted microscope (40×magnification, Nikon FN1). With the guide of a micromanipulator, a single identified DA neuron was patched, and its electrical activities were recorded (**Figure 5.1**). Under the canonical buffer solvent condition, the electrophysiological measurements indicated that the patched neurons were healthy DA neuron. However, the solvent content of the buffer solution in the electrode was incompatible with CE-HRMS measurement, due to a high concentration of salt, sodium gluconate. High salt composition in the sample was not ideal because it interferes with ion generation, thus making it unfavorable for mass spectrometry analysis.²¹⁸ Therefore, we revised the composition of the electrode probe solution that was compatible with both electrophysiological recordings as well as CE-HRMS analysis. We tested multiple solvent compositions, and we found out that 50 mM ammonium bicarbonate solution was able to replace the original buffer solution in the electrodes. With this revised set-up, we were able to patch identified DA neurons from substantia nigra in a midbrain slice by applying negative pressure to form a tight seal patching. The electrophysiological properties of the selected neuron were recorded by applying a small current to measure the cell's action potential firing rate, using a standard protocol.¹⁹⁹ The characterization of neuron's intrinsic properties was essential to understand its unique features that are informative of its specific neuronal type. For example, the

subcellular composition of different neurons is known to have distinct electrophysiological properties, and therefore, accurate identification of the type of neuron that is of our interest (DA neuron) was necessary before proceeding with the proteomics workflow. Our measurements revealed an average firing rate of 2.88 ± 0.42 Hz with corresponding half-width of 1.37 ± 0.19 , demonstrating the unique slow pacemaker action potential pattern stereotypic of DA neurons (**Figure 5.1**).²¹⁷ The distinct electrical recordings from neighboring neurons like GABAergic neuron added the confidence in identifying DA neurons and demonstrated our capability to differentiate DA neurons from others based on our recordings. After successful patching and recording, additional negative pressure was applied to the patch pipet, and subcellular component of the neuron (<10 nL) was aspirated using the same patch pipette (**Figure 5.1**). The collected neuron content was then transferred into a LoBind microtube for micro-scaled bottom-up proteomic workflow.

The average size of a DA neuron can be as large as $35 \mu\text{m}$ in diameter²¹⁶. Based on our previous experiments, a neuron of that size (5–50- μm -diameter) typically contains <500 pg of total protein amount.³⁰ This extremely limited amount of starting material necessitates a revised micro-scaled proteomic workflow to overcome technical challenges. One of the primary goals was to avoid multiple steps (i.e., alkylation, reduction and protein purification) that could lead to excessive sample losses. To test this hypothesis, we modified standard bottom-up proteomics workflow by directly adding ~1–5 ng of trypsin protease into the sample collection solvent in the microtube and digested the proteins for 6 h at 37°C .¹⁷⁴ Omitting alkylation and reduction steps may cause a partial incomplete digestion of the peptides due to the existing disulfide bonds between sulfhydryl groups of cysteine side chains,²¹⁹ and therefore we evaluated the performance of the revised workflow. We compared the measurements from pooled neuron

samples under the two conditions: with alkylation, reduction and purification prior to tryptic digestion to serve as a control and without these steps prior to tryptic digestion. Our measurements indicated that, avoiding the series of steps mentioned above retained more proteins, improving the identification by ~2–3 times (20 vs. 46 protein IDs from control and experimental condition respectively from 100 pg of protein digest). This result validated that our revised protocol improved peptide recovery for limited sample material that is prone to protein losses during processing.

Next, we evaluated the compatibility of our workflow to a recently developed carrier protein methodology for targeted analysis.²⁰⁸ In this study, a large amount of BSA digests was used to prevent undesired sample loss, which improved peptide recovery for selected peptides with an average recovery rate of 150% . Therefore, we integrated a similar approach to our study, where we spiked processed single-neuron samples with a high concentration of BSA protein standard (1 μg of digest in 10 μL solvent volume) to serve as a carrier protein and to prevent adsorption of the sample to the surface of microtube. When we assessed the performance of the approach, we were able to identify ~242 protein groups from triplicate measurements from ~100 pg of neuron digest, which corresponds to an ~ 4–5 times improvement in protein IDs when compared to the measurement from control condition. Combined, the revised micro-scaled bottom-up proteomics workflow enabled an ~10-fold sensitivity improvement compared to the traditional bottom-up proteomic workflow for limited sample amounts, raising sufficient sensitivity for single-neuron analysis.

Although the revised microsampling approach and micro-scaled bottom-up proteomic workflow promise to enhance the detection sensitivity in the sample preparation aspect which was validated by our initial measurement (~100 pg of digest), the actual protein content we

extract is expected to be less than 100 pg. Therefore, another level of detection sensitivity enhancement was necessary to characterize proteins from the identified neurons. Here, we utilized the strategy to boost the detectable signal of the peptide ions by combining large number of cells of the same type. In recent studies, the barcoding of multiple single cells and carrier cells has shown to improve the protein identification by increasing peptide ion accumulation from the measurements, resulting in better sequencing of the detected peptides. However, a caveat of this approach indicated that the protein identification improvement was noticeable with less stringent (3% false discovery rate) search parameter owing to the challenge in detection sensitivity for single cells.²⁰⁹ Encouraged by the report, we applied this approach to single DA neurons and a small portion of substantia nigra tissue (~50–100 neurons) using tandem mass tags (TMT) to barcode each separately for analysis. The purpose of this approach to our technology was to alleviate the detection sensitivity limitation especially for lowly abundant peptide ions, which are commonly undetected, and sometime detected with low efficiency in the produced fragmentation ions. Therefore, by integrating this approach, we expected to see an improved the quality of tandem mass spectra which will lead to an enhanced peptide sequencing and protein identification.

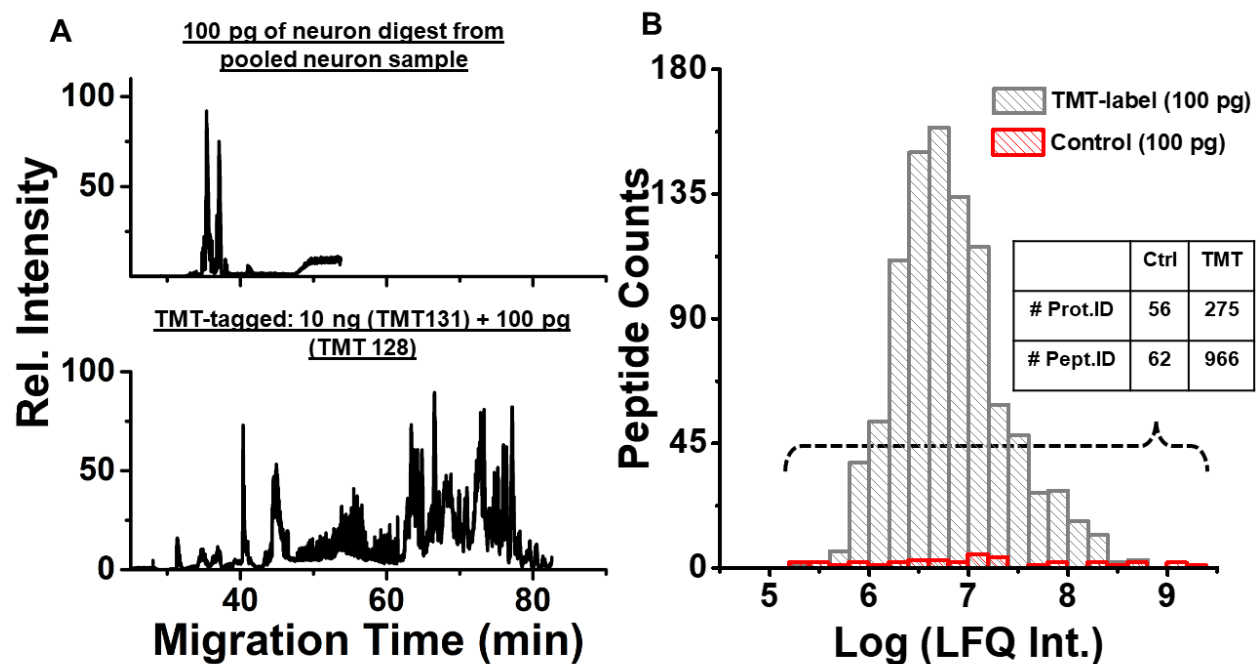


Figure 5.2 Validation of the TMT-label approach for trace-sensitive proteomics via CE-nanoESI-HRMS platform for neuron digest. Comparison of peptides and proteins identified from control (non TMT-labeled) and TMT-approach. About 100 pg of neuron digest was measured in two experimental conditions: with and without TMT-labeling. **(A)** Base peak electropherogram indicates a significant peptide signal boost in TMT approach, resulting in increased number of PSMs from the measurement. **(B)** Identified Peptide abundance distribution across quantified peptides from two experimental condition, control vs. TMT approach. The in-set tabulates display of identified protein and peptide groups using TMT-labeling approach revealing ~5 times and ~15 times improvement in protein and peptide identification from the analysis of 100 pg of neuron digest.

We evaluated the performance gain from this approach by starting with a large quantitative difference in mixed ratio (1:100) of hippocampal neuron digest to resemble the natural abundance ratio variation between a single DA neuron and a portion of the substantia nigra tissue. **Figure 5.2a** shows the representative display of base peak electropherograms from the two conditions. The two electropherograms from each condition revealed a very distinct pattern where the control condition had small number of visually detectable peaks and the TMT-labeled condition included many intense complex peaks. When we compared the number of

PSMs for both conditions, there was a significant improvement in the experimental condition equating to about 5 times in number of PSMs (~200 vs. ~1000 PSMs from control and TMT-experimental condition respectively), suggesting that addition of pooled neurons improved the identification. We reason that this improvement in peptide sequencing comes from the increased overall peptide intensity from 10 ng of protein digest sample, which in turn improved the peptide selection for tandem MS. However, it was critical to examine the quantification of these identified peptides to determine whether these quantified peptides were from a 100 pg or 10 ng of protein digest sample. Therefore, we carefully examined the identified proteins/peptides to determine whether these proteins/peptides belonged to the measurement of 100 pg of neuron digest. To do this, we evaluated each barcoded channel for respective neuron samples, 100 pg and 10 ng, where each sample was uniquely barcoded: TMT-128 for 100 pg of digest and TMT-131 for 10 ng of digest (**Figure 5.2b**). We discovered that the majority of detected PSMs consisted of many quantifiable TMT-128 channel along with the TMT-131 channel. For example, from 10 ng digest, 389 proteins were quantified, and 275 proteins of the quantified proteins were also belonged to 100 pg digest channel, equating to about 70% of overlap between tagged channels. When we compare this to our control condition for 100 pg digest without TMT-label approach, we saw an ~5× improvements in protein IDs and ~16× improvements in peptide IDs. The detection sensitivity was significantly improved using this approach as represented by the peptide quantification distribution (**Figure 5.2b**). These results suggest that the TMT-labeling approach is scalable to single neurons, containing less than 500 pg in total protein content, and can be used to improve the protein identification that is otherwise challenging.

5.3.3 Protein identification from single DA neuron

Last, we applied this combined approach to detect proteins and peptides from single DA neurons to test its applicability. By utilizing the whole-cell patch-clamp electrophysiology technique, we take advantage of the borosilicate electrode tip to extract a subcellular portion of the neuron as described earlier. We integrated carrier protein assisted approach²⁰⁸ to prevent potential adsorption of the extracted cell content to the surface of the LoBind microtube and the TMT-labeling approach to enhance the overall peptide ion signal. A section of the substantia nigra tissue, which is estimated to contain ~50–100 DA neurons, was tagged with the TMT-131 while subcellular extract component from a single DA neuron was tagged with the TMT-128. The purpose of adding tissue to the single neuron sample was to enhance the peptide ion signal, thus increasing the selection of lowly abundant peptide ions for tandem MS. When we mixed the two samples, we expected to have more quantified proteins from the tissue while also having appreciable number of quantified proteins from single neuron. Indeed, over 70% of the identified proteins from the tissue was also quantified in the single neuron. From the replicate measurements ($n = 3$), a total of 213 protein groups were identified from the tissue (Figure 5.3a). Of these, 146 proteins were also quantified from a single neuron.

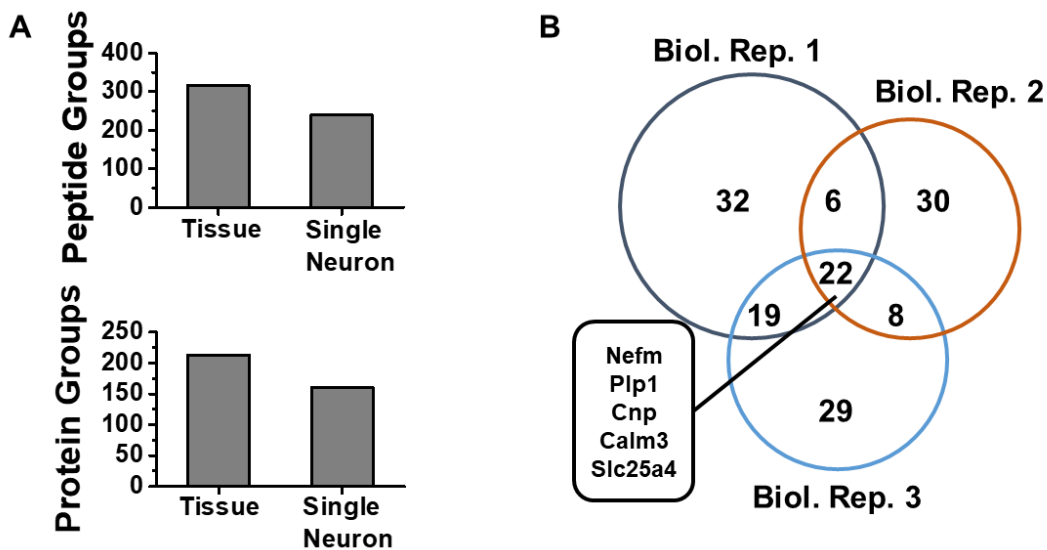


Figure 5.3 Protein and peptide detection from a section of substantia nigra tissue containing ~50–100 neurons and a single neuron using the TMT-labeling method. **(A)** Majority of the identified proteins and peptides from the tissue were also identified in single neuron sample. Our approach enhanced sensitivity for peptide and protein detection in single neurons. **(B)** Comparison of identified proteins in each different DA neuron based on independent measurements. A total of 146 protein groups were identified from 3 biological measurements. Representative proteins are listed and grouped on close parsimony principle (see Supplementary Table S1).

When we survey the identified protein groups from the 3 biological replicates, we observe that commonly identified proteins are primarily associated with the membrane, nucleus, and mitochondria (i.e., *Atp1a3*, *Scn1a*, *Basp1*, *Cs*, and *Atp5f1b*). The detection of these proteins is not surprising, as we would expect our extraction procedures to result in a sample enriched with proteins associated with organelles in the cell body. The high percentage of mitochondrial proteins found in common between the three biological replicates suggests that we are reproducibly aspirating intact mitochondria during microsampling of the neurons. In addition to organelle and cytosolic proteins, we also see membrane-bound proteins, such as ion channels (*Calm3*), transporters (*Gapdh*) and neurotransmitter receptors (*Stx1b*), which suggests that some

cell membrane is included in our aspirate. Several proteins involved in vesicle release from pre-synaptic terminals were detected (Stx1b) as well. There are few potential sources for these proteins; it is possible that these proteins represent newly synthesized proteins during the process of post-translational modification and trafficking to presynaptic terminals. It is also well known that DA neurons release dopamine somato-dendritically, and therefore, it is also possible that these proteins are associated with these release sites. Our measurements revealed the presence of several proteins that we would expect to find in glial and vascular cells rather than neurons (PLP1 and Cnp). To our best knowledge, we reason that these proteins come from the small portions of tissue that immediately surround the aspirated cell may, in some cases, become attached to the tip of the electrode. These could include processes of oligodendrocytes, or endothelial cells from small branches of blood vessels. Combined, these results demonstrated that patch-clamp electrophysiology and CE-nanoESI-HRMS are capable of characterizing protein expression from single DA neuron with high sensitivity to detect neuronal marker proteins.

5.4 Conclusions

In conclusion, we have developed an integrated microanalytical workflow to expand the toolbox of neuroscience by providing electrophysiological and microanalytical CE-nanoESI-HRMS to enable single-neuron proteomic analysis from the mouse brain. This combined approach is well adaptable for trace-sensitive proteomic analysis of individual cells of interest, including but not limited to pyramidal neurons and hippocampal neurons. This approach attains sufficient sensitivity to detect proteins from single neurons. We ascribe this sensitivity

improvements to combination of factors including, revised microsampling approach and micro-scaled bottom-up proteomics process workflow and modified TMT labeling approach. We demonstrated that we were able to identify over 146 protein groups from 3 biological replicate measurements with many key neuronal marker proteins. However, continuous advances are necessary in nearly all stages of proteomic workflows, starting with better handling of single neuron content with protein extraction via microsampling approach and improved detection sensitivity by redesigning CE-nanoESI ion source. We believe that this approach raises new potential to uncover cell heterogeneity from mammalian neurons to understand how neurons establish molecular differences by providing molecular information and physiological properties of the cell.

Chapter 6: Single-cell proteomics by mass spectrometry with patch-clamp electrophysiology using chemical desalting to enhance proteomic coverage for a single neuron

Based on material in preparation for submission by Sam B. Choi, Abigail Polter, Alexander Kisner, and Peter Nemes*

Author Contribution: S.B. Choi designed the research, processed the collected neurons, prepared the sample, and performed the measurements. S.B. Choi also analyzed the data, interpreted the results, and wrote the manuscript.

6.1 Introduction

Mass spectrometry (MS)-based proteomics provide comprehensive and quantitative description of the biological system under investigation²²⁰⁻²²². Single-cell proteomics (SCoPE) by MS has gained popularity due to its complementary information to single-cell transcriptomics by investigating protein abundance and post translational modification status. MS-based SCoPE is known to be able to quantify single-cell proteomics in an unbiased manner. However, sensitivity limitations for MS-based SCoPE have placed a constraint on SCoPE-MS experiments to the analysis of large cells from biological systems that contain enough material for sample preparation and analysis (for example, human oocytes or frog embryos^{27, 223-224}). To this end, many SCoPE-MS analyses focus on using single cell proteomics by mass spectrometry (SCoPE-MS) method that employs isobaric stable isotope labels with a carrier protein channel to analyze single cells.²⁵ Since the introduction of SCoPE-MS, many studies have focused on improving the protein coverage by optimizing sample preparation²²⁵⁻²²⁶, peptide separation²²⁷ and data collection.^{10, 228} One major advancement includes carrier channel protein using isobaric labels (tandem mass tag (TMT)), where chemical tags that have the same intact mass. However, each

tag has a unique mass barcode that are uniquely identified by peptide fragmentation to understand its relative quantification of multiple samples in the same analysis. The major advantage of this approach is that peptides from the same sample appear as one peak in the MS spectrum where it increases signals thus enabling isolation of peptide ions for MS² analyses where the identification and quantification can occur. SCoPE-MS method utilizes this feature to enable the analysis of single-cell proteomes by spiking a carrier sample into a multiplex experiment at levels from 100 x to 200 x of the single-cell proteomes²²⁹. However, high levels of carrier proteome may affect quantitative accuracy and biological conclusions. This is because of the difficulty of analyzing MS measurements of a very small signal in the presence of another very large signal. Therefore, to measure quantitatively accurately, new ways must be improvised.

Another major limitation in analyzing single cell in our previous studies was salt contamination. When microsampling approach was used to analyze electrophysiologically measured neurons, salt contaminants were added into the sample collection. Due to the nature of buffer solution enriched in salt concentration in whole-cell patch clamp electrophysiology, salt contaminant was a major issue in measuring these collected neurons. Salt contamination can be hindering to protein characterization by mass spectrometry because it forms adducts to lower the spectral S/N ratio and also causes ion suppression.²³⁰⁻²³¹ Therefore, having a high concentration of salt can be detrimental in characterizing proteins from single cells especially when there are low amounts of samples present (< ng). There are techniques are available to desalt the sample such as ziptipTM and C18 spin columns which use C18 beads to trap the peptides while washing away salt contaminants.²³² However, these techniques requires at least 10 µg of the sample material to trap the peptides to C18 beads. Furthermore, the recovery rate is about 50–70%, based on our previous study which is an important consideration when handling such small

amounts of samples like that of single neuron content. Here, to address this issue, we provide a chemical desalting methodology by introducing crown-5-ether to react with sodium ions available from our miniscule amounts of sample prior to electrophoretic separation by capillary electrophoresis (CE). Crown-5-ether is known to react with sodium cations to form a complex by numerous previous studies²³³⁻²³⁴. In this study, we evaluated the effectiveness of chemical desalting to reduce salt contaminants from our harvested single neurons by microcapillary sampling with electrophysiology. We combined our custom-built capillary electrophoresis electrospray ionization (CE-ESI) with timsTOF MS to enable an orthogonal separation mechanism to simplify compressed electrophoretic separation which in turn improves separation performance and detection sensitivity. It is common to have compressed electrophoretic separation when using CE as previously studied²³⁵, and therefore having an orthogonal separation mechanism will greatly mitigate the compressed separation afforded by CE. After incorporating chemical desalting with integration of orthogonal separation mechanisms, we were able to identify over 700 protein groups from a single dopaminergic neuron. With careful chemical modification by introducing crown-5-ether to minimize salt contaminant, we were able to achieve over 50% recovery rate for protein IDs from 200 pg of protein digest with similar amounts of salt present as the single neuron content. Furthermore, we demonstrated that this approach was able to differentiate different types of neurons by their proteomic differences by hierarchical cluster analysis (HCA) plot. Chemical desalting with microanalytical CE-HRMS raises sufficient sensitivity in proteomics in single neurons to help understand molecular mechanisms involved in the formation and maintenance of neuron-to-neuron heterogeneity in the developing brain.

6.2 Experimental section

6.2.1 Materials

All materials were purchased at reagent grade. Dithiothreitol (DTT), iodoacetamide (IAD), tris-hydrochloric acid (tris-HCl), tris-hydroxy methylaminomethane (Tris-base), potassium chloride (KCl), and sodium hydroxide (NaOH) were obtained from Sigma-Aldrich (St. Louis, MO). Acetonitrile (ACN), trypsin protease, water (Optima), formic acid (FA), ethylenediamine tetraacetic acid (EDTA), acetic acid (AcOH) and methanol (MEOH) were purchased in MS-grade from Fisher Scientific (Fair Lawn, NJ). Ammonium bicarbonate was from Avantor (Center Valley, PA). Sodium dodecyl sulfate (SDS) was from Amresco (Solon, Ohio). Fused silica capillaries (40/90 μm inner/outer diameter) were from Polymicro Technologies (Phoenix, AZ, USA) and used as received. All standards were prepared in 500- μL LoBind protein microtubes from Eppendorf (Hauppauge, NY).

6.2.2 Animals and brain section preparation

All experiments used male and female mice (9-11 weeks old) in procedures conducted in accordance with National Institutes of Health Guidelines for the Care and Use of Laboratory Animals, and with the approval of the IACUC of The George Washington University (IACUC# A378). Female and male ePet-cre (C57BL/6 background, Strain 12712, The Jackson Laboratory) and PV-cre (C57BL/6 background, Strain 8069, The Jackson Laboratory) crossed with Ai14 (C57BL/6 background, Strain 7908, The Jackson Laboratory) transgenic mice, hereafter ePet-cretdTomato and PV-cretdTomato, respectively, and PitX3GFP (C57BL/6

background, Strain 41479-JAX, The Jackson Laboratory) mice were used in this study. Mice were group housed with littermates within ventilated cages in temperature- and humidity-controlled rooms with ad libitum access to water and rodent standard chow on a 12 h light/dark cycle.

6.2.3 Sample preparation for single neuron via bottom-up proteomics

After being deeply anesthetized with ketamine, mice were perfused transcardially with N-methyl-D-glucamine (NMDG)-based slicing solution containing (in mM): 92 NMDG, 20 HEPES, 25 glucose, 30 NaHCO₃, 1.2 NaH₂PO₄, 2.5 KCl, 5 sodium ascorbate, 3 sodium pyruvate, 2 thiourea, 10 MgSO₄, and 0.5 CaCl₂, pH 7.4, and osmolarity of 303–308 mOsm. Brains were quickly removed and placed in ice-cold NMDG solution. Horizontal brain slices (250 μ m thick) containing the dorsal raphe nucleus (DRN) or the ventral tegmental area (VTA) or coronal slices containing the prefrontal cortex (PFC) were obtained using a vibratome (Leica VT1200, Leica Biosystems Inc., IL, USA). After cutting, brain slices were incubated for 1h in a holding chamber at 32°C degrees filled with a recovery solution containing (in mM): 92 NaCl, 20 HEPES, 25 glucose, 30 NaHCO₃, 1.2 NaH₂PO₄, 2.5 KCl, 5 sodium ascorbate, 3 sodium pyruvate, 2 thiourea, 1 MgSO₄, and 2 CaCl₂ (pH 7.4, 303–308 mOsm). After 1h, the holding chamber containing the slices was kept at room temperature. In sequence, a single slice was transferred to a chamber perfused at a rate of 1.5 to 2.0 mL/min with artificial cerebrospinal fluid (aCSF, in mM: 125 NaCl, 2.5 KCl, 1.25 NaH₂PO₄, 1 MgCl₂•6H₂O, 11 glucose, 26 NaHCO₃, 2.4 CaCl₂, pH 7.4, and osmolarity of 303–308 mOsm at 32°C. All solutions were saturated with 95% O₂ and 5% CO₂. tdTomato-positive neurons in the DRN (ePet-cretdTomato) or in the PFC (PV-cretdTomato) and GFP-positive neurons (PitX3GFP) in the VTA were located in brain slices,

initially using epifluorescence, followed by infrared differential interference contrast (IR-DIC) optics, using a Nikon Eclipse FN1 upright microscope.

tdTomato-positive and GFP-positive neurons were patched and held at -70 mV in whole-cell patch-clamp configuration using a Sutter integrated patch clamp amplifier (1 kHz low-pass Bessel filter and 10 kHz digitization) with Igor-pro 8.04 software (Sutter Instruments). Glass patch pipettes with resistance 2-3 MOhms were filled with internal solution containing NH_4HCO_3 50 mM. After obtaining a giga-ohm seal, a 60-second recording in the cell-attached configuration was obtained, and the dopaminergic identity of the neuron was confirmed by the presence of a slow pacemaker firing pattern (Figure 1). Following electrophysiological analysis, the microprobe entered the cell with a steady negative pressure applied at the outlet end of pipette with a syringe to aspirate a portion of neural soma. For single-cell protein expression profiling and analysis, the cytoplasm of the patched neuron was harvested into the recording pipette right after entering in whole-cell configuration. The total time harvesting the intracellular content did not exceed more than 3 min. Whole-cell access resistance (15-25 MOhms) and stability of the gigaseal (i.e. seal between the neuron and the pipette) was constantly monitored to avoid contamination from the extracellular medium. The content of the pipette tip containing the harvested cytoplasm was then expelled into a 500 μL microtube for further processing. A standard bottom-up proteomic workflow requires tissue lysis, reduction, alkylation and protein purification steps prior to trypsin digestion.¹⁸² However, in this study, we modified the protocol to minimize sample losses from added steps as described elsewhere.²³⁶ Each collected protein extract from dopaminergic neuron was combined with 5 μL of 50 mM ammonium bicarbonate containing 0.1 μg of trypsin protease for one-step digestion at 60 °C for 1 h. The resulting single-neuron protein digests were vacuum-dried and stored at -80 °C until CE-HRMS analysis.

6.2.4 Single-cell CE-nanoESI-HRMS

The resulting peptides were analyzed on a custom-built micro-loading CE platform that we recently reported^{30, 235}. The separation CE capillary was coaxially fed into a platinum emitter, which served as an electrospray (ESI) emitter (250/750 μm inner/outer diameter) with $\sim 10\text{--}15$ μm of CE protrusion. An ~ 20 nL (< 1 ng) of protein digest was separated by capillary zone electrophoresis in a 100-cm long capillary (40/110 μm inner/outer diameter) at ~ 220 V/cm field strength. The electrophoretically separated peptides were ionized by the ESI interface. In this design, the sheath solution (50% MeOH in 1% (v/v) FA) was supplied through the grounded metal blunt tip emitter. The emitter was positioned ~ 2 mm in front of a mass spectrometer for detection and the spray source was maintained in the cone-jet regime for efficient ion generation.¹¹²

For standard peptide measurements, peptide ions were mass analyzed from m/z 350 to 1,800 at 35,000 FWHM resolution (MS^1) using a hybrid quadrupole Orbitrap mass spectrometer equipped with a higher-energy collision dissociation (HCD) cell (Q Exactive plus, Thermo Scientific, Waltham, MA, USA).

For single neuron proteomics measurements, peptide ions were mass analyzed from m/z 100 to 1,700 using a trapped ion mobility mass spectrometry quadrupole orthogonal acceleration time-of-flight (TIMS-TOF, Bruker Daltonics, Billerica, MA, USA) with a collision-induced dissociation (CID) cell for fragmentation. The mass spectrometer was tuned and calibrated according to vendor specifications and operated at 40,000 FWHM resolution. To identify peptides, signals were fragmented via data-dependent acquisition with the following settings: data acquisition rate, 2 Hz for MS^1 and 1 Hz for MS^2 ; survey scan cycle time, 3 s; fragmentation

preference, top most-intense; MS² threshold, 250 counts per 1000 summations; active exclusion, exclude after 1 spectra and release after 0.5 min; charge state preference, 2-5; exclude singly and unknown; *m/z* window and CID energy, 2 Da and 20–70 eV depending on charge state; collision gas, nitrogen; and dynamic exclusion, applied; smart exclusion, applied with 5× threshold; number of PASEF MS/MS scans, 5–25; Charge range, 0–5; scheduling target intensity, 10,000–40,000; scheduling intensity threshold, 2,500; Collision energy, 38–45 eV; Active exclusion, reconsider precursor if current/previous intensity, 4; Mobilogram, summation widths, 25 pts; Max no. of peaks, 3; TIMS enabled, on.

6.2.5 Data analysis

Primary MS/MS–MS data were analyzed in MaxQuant ver. 1.6.7.0 (Max Planck Institute of Biochemistry) executing the Andromeda search engine ver. 1.6.7.0 search engine¹¹⁵ against the *Mus musculus* proteome (downloaded from UniProt on October 15th, 2019) as database with the following search parameters: type, TIMS-DDA; TIMS half width, 4; TIMS step, 3; TIMS resolution, 32,000; TIMS min ms/ms intensity, 1.5; TIMS remove precursor, on; TIMS collapse ms/ms, on; trypsin digestion, up to 2 missed cleavages; variable modification, methionine oxidation; fixed modification, cysteine carbamidomethylation; precursor mass tolerance (MS¹), 20 ppm; fragment mass tolerance (MS²), 4.5 ppm; minimum peptide length, 5. Peptides are reported with <1% false discovery rate (FDR), calculated against a reversed-sequence decoy database. The reported protein groups were clustered based on the parsimony principle. Common contaminants were manually removed from the reported protein list.

6.2.6 Safety consideration

Fused silica capillaries and borosilicate capillary emitters, which pose potential needle-stick hazard, were handled with care. Standard safety protocols were followed during the handling of chemicals. All electrically conductive parts of the CE-ESI interface were grounded or isolated to prevent electrical shock hazard.

6.3 Results and discussion

The goal of this study was to advance protein identification from a single neuron protein digest. We and others recently demonstrated that CE-HRMS offers sensitivity benefits for limited amounts of peptides and proteins. For example, custom-built CE has enabled us to identify ~225 proteins from ~500 pg of neuron digest²³⁵. In addition, we have recently coupled whole-patch electrophysiology with mass spectrometry to enable single neuron analysis.²³⁶ Using whole-patch electrophysiology, we were able to incorporate microsampling technique to aspirate small portion (~1–10 nL) of the neuronal soma to perform bottom-up proteomics analysis. Despite measuring only sub pg amounts of protein digest, the study identified ~160 protein IDs and quantified ~100 protein IDs in single dopaminergic neuron. However, there was a high salt concentration apparent in the sample when measuring these single neurons, which calls for new methodology to remove these salt contaminants to improve the protein coverage. Salt contamination is a major issue in mass spectrometry due to several conditions. One of which is that it can adversely affect the performance of native electrospray ionization by reducing the overall molecular ion abundances and distributing signal for any give charge state into many cationized forms. In addition, it causes ion suppression due to making ion formation less reproducible, causing severe adduction. To improve the sensitivity of the protein detection by

mass spectrometry, methodological or technological developments need to address the reduction of salt contaminants in the native sample, especially for a single neuron sample which contains high amounts of salt due to its buffer media which single neuron is being collected from during electrophysiology.

We proposed that chemical desalting can sufficiently reduce salt contaminant from the sample by combining ionophores with salt ions in the sample to make ionophore complexes. The reason for making such ionophore complexes is that salt ions migrate through the capillary at an earlier time (10-15 min separation window) and can extend to a separation range where peptide ions migrate. Therefore, having a heavier ionophore complex with salt ions would make them larger in size, thus migrating slower in the electrophoretic separation, having less of the interference with the electrophoretically separating peptide ions. Here, we suggested to use crown-5-ether (15-crown-5), which are well known Na^+ ionophores that have a high affinity for sodium cations.^{234, 237} Crown ethers are ethers with a closed structure that has a shape of a crown. The closed structure gives rise to a cavity and this is the origin of its interesting properties such as binding to different cations. The properties that give its uniqueness to binding with sodium ions are the interaction between the oxygen atoms in the crown ether and the cation in the cavity, which lowers the free energy for the complex constituents.²³⁸ Therefore, we proposed to use crown-5-ether to minimize the sodium ions in our native neuron digest sample prior to separation by CE. Schematics of the study are presented in Figure 6.1.

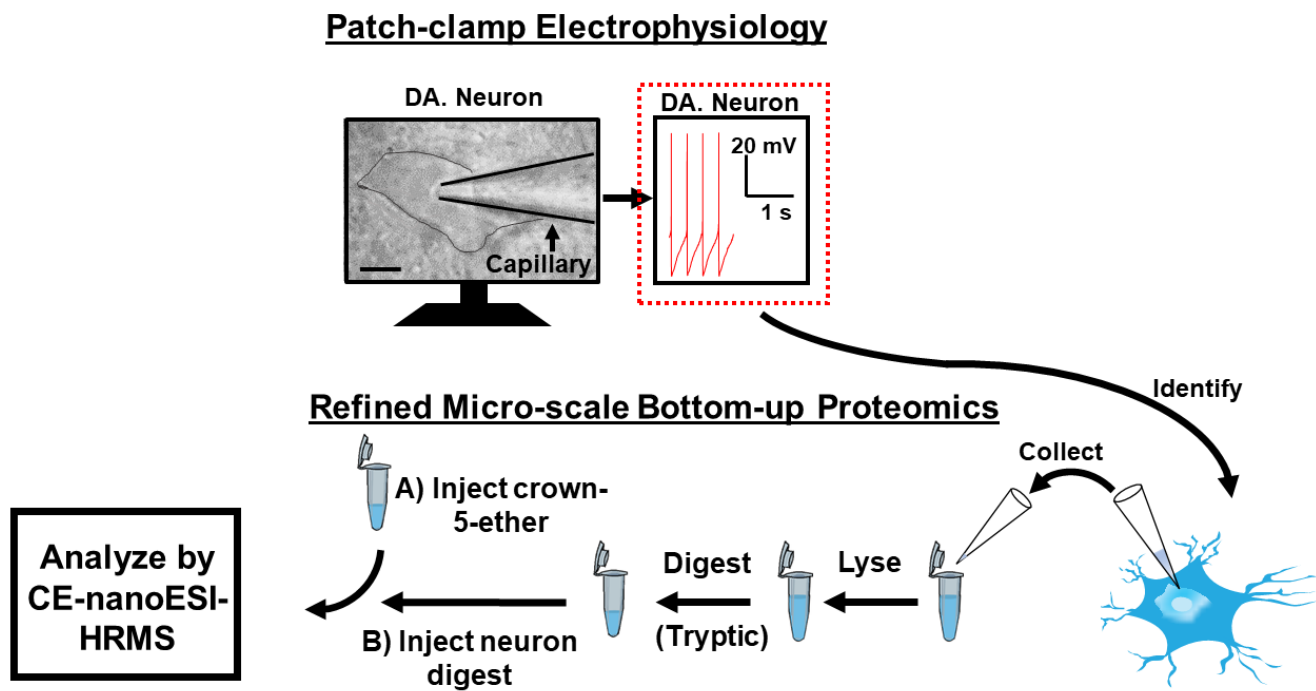


Figure 6.1 Detection of trace amounts of proteins from single neurons using microanalytical high-resolution mass spectrometry with chemical desalting methodology. **Top panel:** Neurons were putatively identified based on physiology and its location in the brain slice through electrophysiology measurement. **Bottom panel:** The collected neuronal soma was lysed and digested before analyzed by custom-built microanalytical capillary electrophoresis (CE) platform and detected using timsTOF-MS (trapped-ion mobility spectrometry time-of-flight mass spectrometer). Before the analysis, there was a prior injection of crown-5-ether to reduce salt contaminant that were present in each neuron digest.

After a whole-patch electrophysiological measurement, we aspirated small content of neuronal soma (~1–10 nL) after ensuring a good patch to the neuron confirmed by its action potential. The collected neuronal soma was then processed via bottom-up proteomics described elsewhere.²³⁶ Here, we injected crown-5-ether into the separation capillary before analyzing neuron digest. The reason here is that we wanted to stack the samples together, creating a reaction complex between crown-5-ether and sodium ions from neuron digest. First, we evaluated the overall effect of total sodium ions present in the native neuron digest sample (Fig. 6.2a). It is clear that salt ions are causing heavy interference with other peptide ions from being

detected by mass spectrometer. A major portion of the separation, starting from 15 min to 35 min separation window, suggests that salt ions are hindering the detection of other peptide ions that were migrating during that time. In fact, from this measurement, only 60 protein IDs were identified. We wanted to first understand how much sodium ions are present in the sample, and therefore created a calibration curve of sodium chloride with different concentration to understand how much sodium ions are present from a single neuron digest (Fig. 6.2b). Although it may not be the case for all of the single neurons to have same amounts of salt concentration, it provides as a good estimate to understand how much of the salt concentration is present in each neurons. By plotting the calibration curve, we found out that roughly 300-350 mM of NaCl concentration corresponded to the peak area of the salt peak under a single neuron measurement. Therefore, we wanted to evaluate crown-5-ether's effectiveness to reduce these salt contaminants by creating a mock sample with 300--350 mM NaCl added in to create the similar environment

as a single neuron digest.

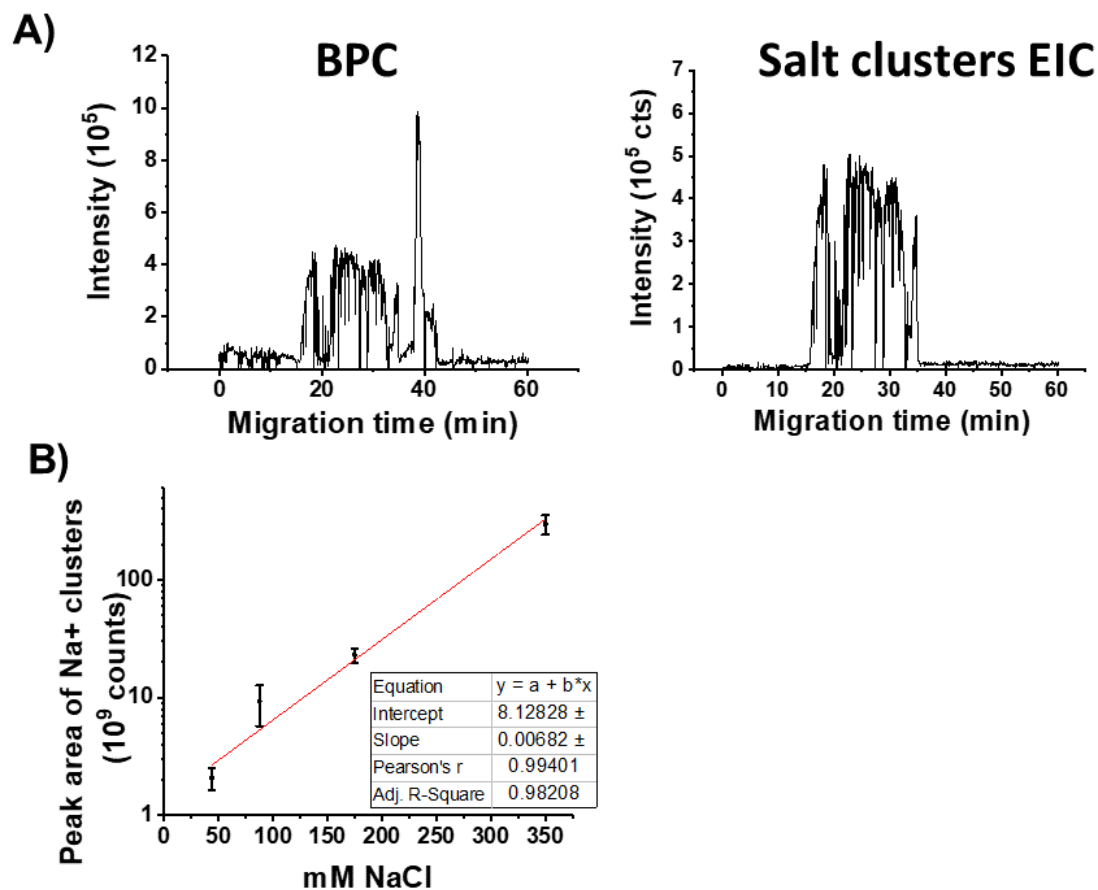


Figure 6.2. Salt contamination apparent towards single neuron proteomics. A) Base peak chromatogram (BPC) of a single neuron digest prior to any desalting methodology applied shows significant salt contaminant demonstrated by salt clusters extracted ion chromatogram (EIC). B) Calibration curve of NaCl to be used as rough estimate of salt contaminant concentration from the native single neuron digest.

Secondly, we evaluated the effect of crown-5-ether by calculating peak area under the sodium ion clusters for 350 mM NaCl before and after addition of crown-5-ether (Fig. 6.3a). Although, the amount of crown-5-ether to reach to known amount of NaCl was estimated to be 1-to-1 ratio, we started at higher concentration for crown-5-ether as this will be a small plug (10 nL) of injection into the capillary and the samples will be next to each other reacting with

another as electrophoresis happens. Therefore, we first tried with 1 M crown-5-ether solution to be injected prior to 350 mM NaCl mock single neuron sample. Before any injection of crown-5-ether, the peak area of sodium clusters was significantly large, $\sim 1.1 \times 10^9$ counts. When we added 1 M of crown-5-ether, the peak area of sodium clusters decreased by at least 70%, $\sim 3.0 \times 10^8$ counts. Additionally, 2.0 M and 2.5 M of crown-5-ether reduced the sodium clusters more by at least 85% and 90% respectively. Therefore, we chose 2 or 2.5 M crown-5-ether to be best suitable for samples containing 350 mM of NaCl.

To have a deeper understanding of the effect of crown-5-ether on peptides, we chose model peptide standards, Angiotensin I, II, IV and 1-9 to serve as a simulation for the real neuron digest sample. Again, we started with something lower in concentration for crown-5-ether and NaCl, 150 mM each respectively (Fig. 6.3b). We saw a sudden drop in signal-to-noise ratio of each peptide standards as we added more NaCl, increasing from 150 mM to 300 mM gave a detrimental effect, almost decreasing the signal-to-noise ratio by 95% or above. We then wanted to understand how the addition of crown-5-ether would affect the recovery of each peptides' signal-to-noise ratio, and therefore we added 150 mM and 500 mM of crown-5-ether to each 150 mM and 300 mM of NaCl containing peptide standards. Surprisingly, the addition of crown-5-ether improved the signal-to-noise ratio and almost recovered all of its lost signal back to original in some cases. This proves that adding crown-5-ether would significantly help reduce salt contaminant in the sample complex by forming sodiated complex with sodium ion clusters.

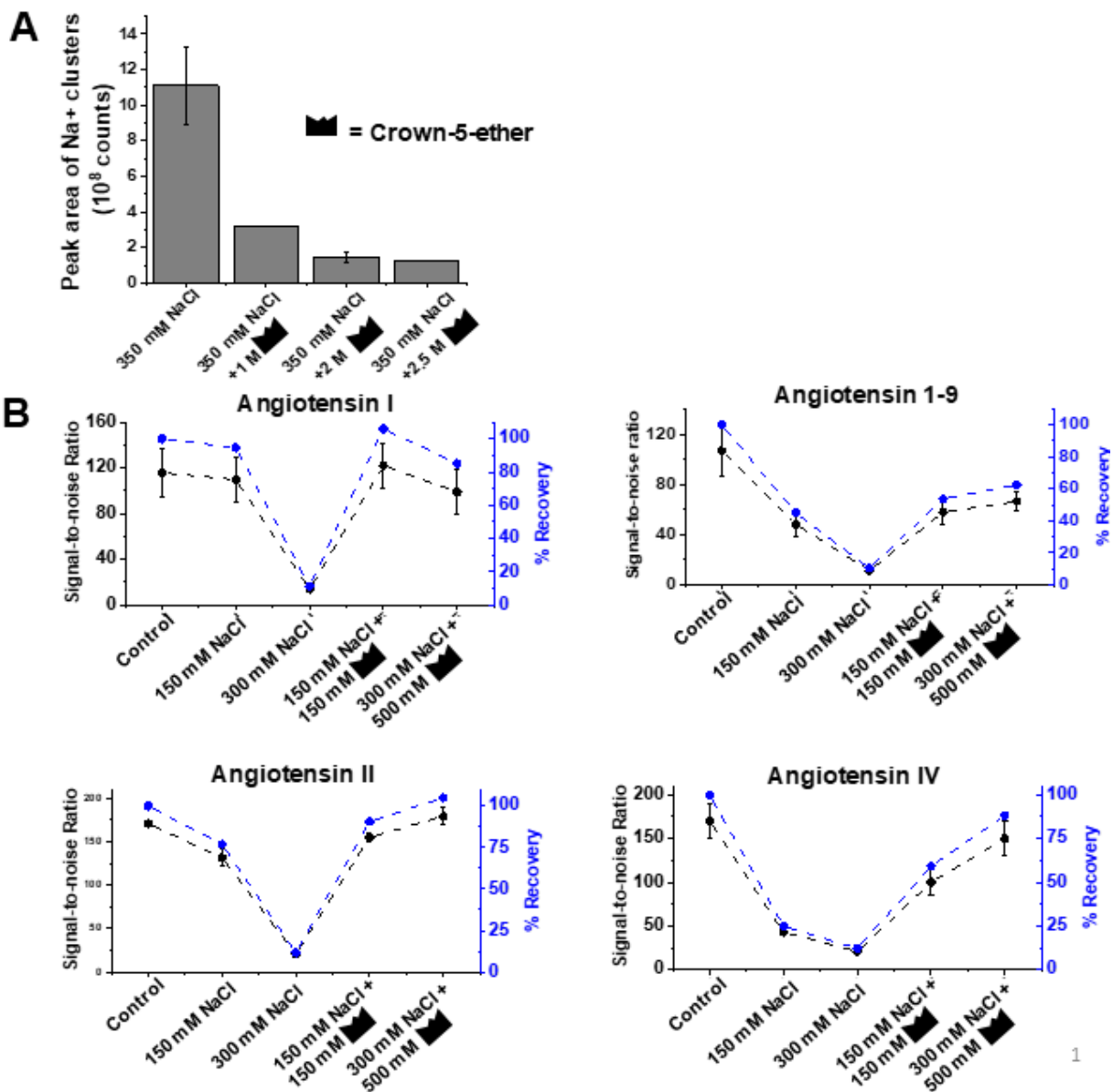


Figure 6.3. The effect of crown ether on desalting NaCl from model peptides. **A)** Peak area of the Na⁺ clusters for corresponding addition of crown-5-ether (denoted by the crown symbol). Na⁺ cluster peak area was significantly reduced as 1 M, 2 M and 2.5 M crown-5-ether was added prior to the 350 mM NaCl injection. **B)** Signal-to-noise (SN) ratio of each peptide standards. As NaCl is added to the peptide standards, the SN decreases dramatically while adding crown-5-ether. Increasing the concentration of crown-5-ether improved the SN recovery of each peptides.

Next, we applied this methodology to a mock sample solvent with 300 mM of NaCl spiked into a sample protein digest to inject 200 pg of the sample. We wanted to first apply this to a known concentration of NaCl with known amounts of protein digest to estimate the current state of the actual single neuron digest. The result demonstrated that by adding 2 M crown-5-ether, significant amounts of salt ions were removed from the measurement (Fig 6.4a). As depicted in grey, there was a large salt clusters peak starting from 15 min to 35 min separation window while, depicted in red, addition of crown-5-ether reduced its peak by at least half, enabling a better detection of peptide ions that are migrating during that time. The improvement in protein IDs were clearly visible when we added crown-5-ether. Notably, about 50% of the protein IDs were recovered from the control (without NaCl) protein digest (400 from 800 protein IDs). In comparison, only 15% of the protein IDs were recoverable from 350 m NaCl containing protein digest (120 from 800 protein IDs) (Fig. 6.4b). This finding suggests that injecting 2 M of crown-5-ether should be sufficient to help alleviate the salt contaminant from interfering and masking the proteins.

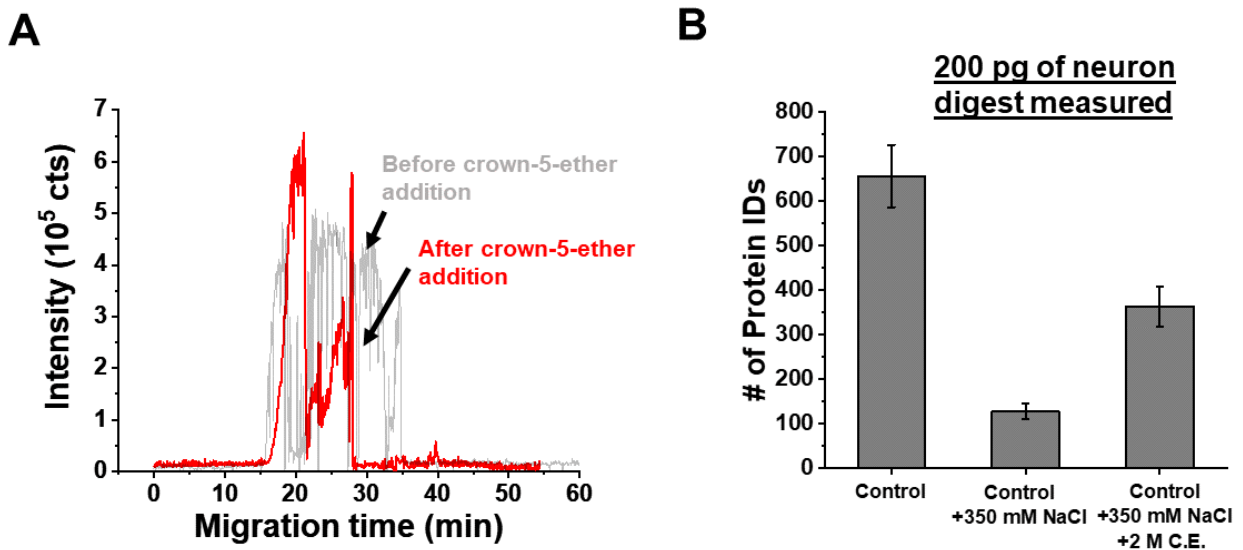


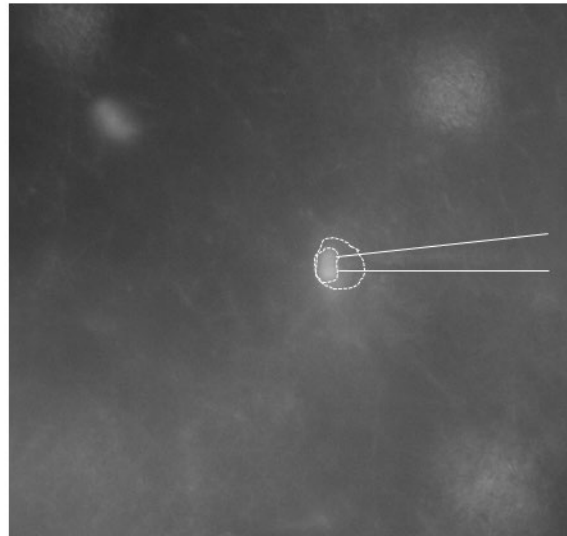
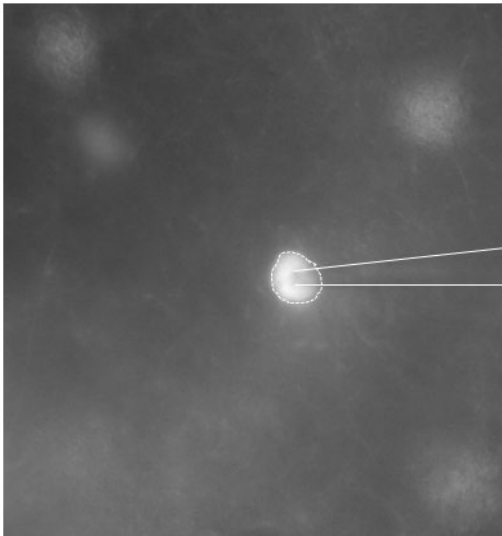
Figure 6.4 Protein ID improvements from using crown-5-ether. **A)** The EIC of salt cluster before adding crown-5-ether is depicted in grey while the one with addition of crown-5-

ether is depicted in red. After addition of crown-5-ether, the peak area of salt clusters reduced significantly, enabling enhanced sensitivity of our measurement. **B)** The number of protein IDs from 200 pg of neuron digest is compared with addition of 350 mM NaCl and with/without 2 M crown-5-ether. The recovery rate for protein IDs were about ~50% when compared to ~15% recovery rate without addition of crown-5-ether. 200 pg of neuron digest was measured to approximate the content from a single neuron digest.

Next, we assessed the performance of chemical desalting methodology to single neuron measurements. We wanted to first identify as many proteins as possible from a single neuron by employing the new generation trapped-ion mobility time-of-flight mass spectrometry (timsTOF MS, Bruker Daltonics). We have previously refined the operating settings to enable 800 protein IDs from an ~200 pg of neuron digest. From our previous studies, we estimated the protein content of a single neuron would be less than 500 pg.²³⁵ Therefore, by enabling protein characterization from 200 pg of neuron digest, we were confident to identify at least 200 protein IDs from each of the single neurons we collected as each single neuron is expected to have about ~500 pg of neuron digest. Here, our main goal of this study was to differentiate neuronal types by proteomic differences among different neurons. We wanted to first understand what types of proteins were characterized in each of the single neuron and to use that to differentiate different types of neurons. We have collected 3 different types of neurons: dopaminergic, serotonin and parvalbumin interneuron. With the help of electrophysiology and microscopy, we were able to differentiate these neurons before collecting the neuronal soma from each of them (Fig. 6.5).

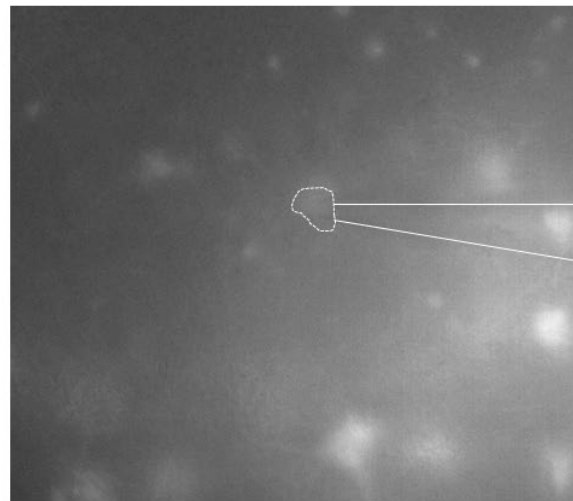
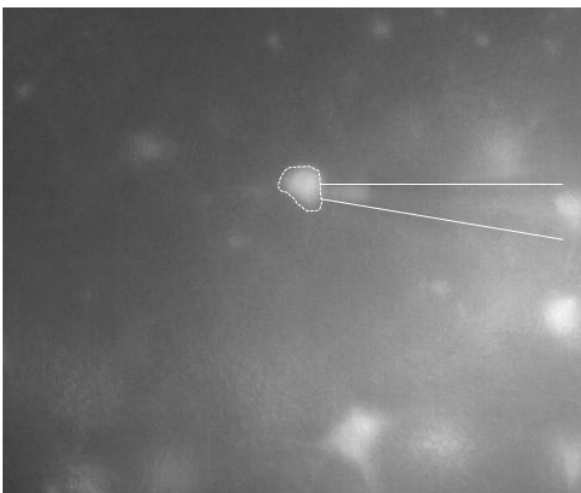
A.

PV neurons



B.

Dopamine neurons



C.

Serotonin neuron

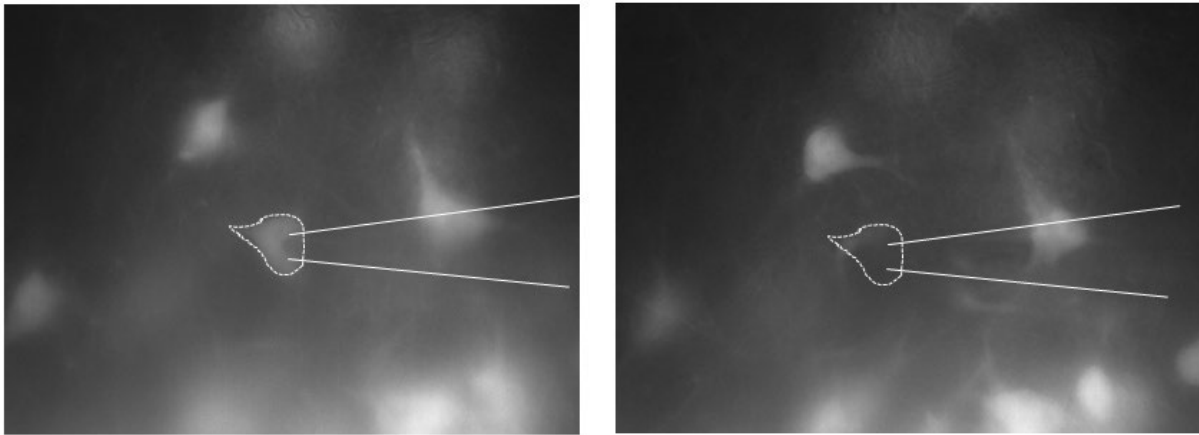


Figure 6.5 Neuronal soma extraction by microcapillary sampling. A) Identification and aspiration of parvalbumin neuron. B) Identification and aspiration of dopaminergic neuron. C) Identification and aspiration of serotonin neuron.

Once validated prior to our collection, each neuronal soma was collected in a 500 μL LoBind microtube that has trypsin protease for a quick 1 h digest at 60 $^{\circ}\text{C}$. This step was necessary as we only have finite amounts of sample which may dry with prolonged exposure to heat, thus disrupting digestion. After digestion, the samples were vacuum dried and stored at -80 $^{\circ}\text{C}$ until CE-HRMS analysis.

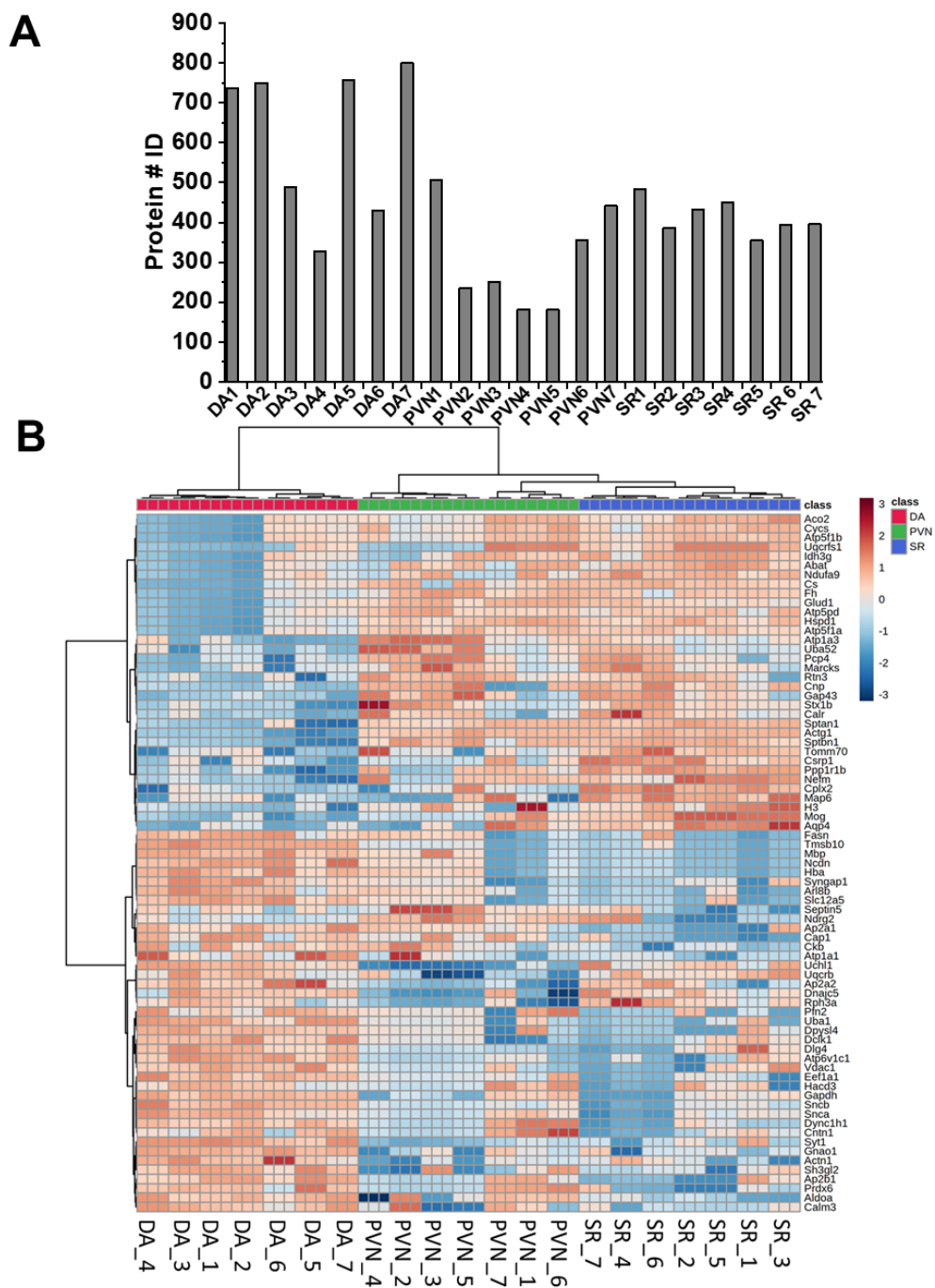


Figure 6.6 Protein identified among different types of neurons. **A)** Protein IDs from single dopaminergic neuron as an example of the application of c-desalting methodology. Dynamic concentration range demonstrates 3–4 log orders in magnitude. **B)** The hierarchical cluster analysis demonstrates the differences in proteomic expression from each single neuron was able to distinguish between different neuronal types. Dopaminergic neuron (DA) is depicted in red, parvalbumin (PVN) is depicted in green and serotonin neuron (SR) is depicted in blue. There is a

clear differences between all types of neurons, thus being able to identify a type of neuron based on proteomic expression is confirmed.

For every analysis steps, we injected 10 nL of 2 M crown-5-ether solution prior to injecting 10 nL of the sample reconstituted in 0.5 μ L sample solvent (50% ACN with 0,5% AcOH). We then used our timsTOF MS to do DDA-based data acquisition. We have collected technical triplicates of each single neurons and have data searched against MaxQuant (v. 1.6.7.0) executing Andromeda (v. 1.6.7.0) to identify proteins. When we employed c-desalting methodology, we saw many proteins from each of the single neurons (Fig. 6.6a). An average of 700 protein IDs were identified from single dopaminergic neurons and about 300-400 protein IDs were identified from both parvalbumin and serotonin neurons. This result was surprising when compared to our previous result, identifying fewer than 200 proteins per single neuron. When we combined the protein IDs from each of the single neurons and did an HCA analysis. Surprisingly, the HCA analysis was able to distinguish different types of neurons based on proteomic differences (Fig. 6.6b). This is the first time ever that proteomic differences are present at a single neuron level and can be used to distinguish different types of neurons. Our results suggest that proteins isolated are largely those associated with the soma and somatic organelles. This will make this technique a valuable tool for studying how proteins involved with basic cellular functions such as metabolism, cytoskeletal dynamics, and protein translation and processing interact to affect activity of the cell. While the broad categories of proteins isolated are the same between cell types (Fig. 6.7), there is substantial variation in the individual proteins found in each cell type. Intriguingly, protein expression was more similar between parvalbumin and serotonergic neurons than between dopaminergic and serotonergic, despite the fact that dopaminergic and serotonergic neurons are more closely genetically related (Fig. 6.6). This

highlights the potential usefulness of single-cell proteomics, as gene expression is only one step in determining the final complement of proteins that governs a cell's function. Measurement of proteins from single electrophysiologically-identified cells will allow a more direct comparison of protein expression and cellular function.

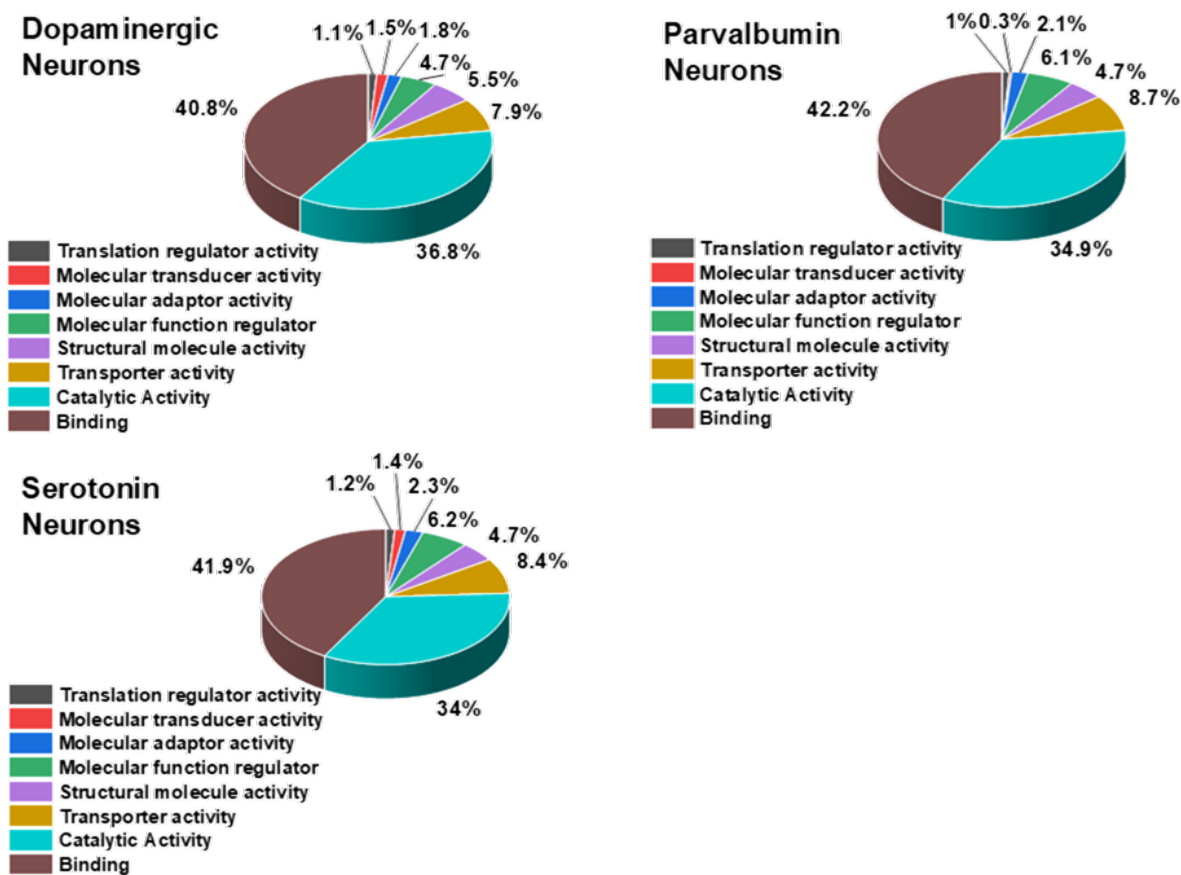


Figure 6.7 Gene ontology of the different neurons. Each neurons have similar gene ontology as they are from the same brain. However, individual proteins are varied from one to another.

6.4 Conclusions

Here, we have enabled single-neuron proteomics by integrating a novel c-desalting methodology with ultra-high-speed TIMS-TOF mass spectrometer with a PASEF workflow. By

integrating c-desalting, we were able to identify over 700 protein IDs from a single dopaminergic neurons and over 300-400 protein IDs from parvalbumin and serotonin neurons. In contrast to methodology without c-desalting, this enabled about 5-7 times more protein IDs from a single dopaminergic neurons. In addition, the fast CE separation was matched with the ultra-high-speed TIMS-TOF MS's DDA methodology, the PASEF methodology, which enabled even more sampling of ions as many peptides were separating during the busiest region of the separation window. By reducing salt contaminants, we achieved higher sensitivity for the measurement, where we found over 50% reduction of salt content to enable 5-7 times more protein IDs. Our proteomic experiments verify that the differences in proteomic expression between different neurons were able to be used to distinguish different types of neurons which were confirmed by electrophysiology. This adaptation of two different technology, electrophysiology and mass spectrometry, is a first step to enabling deep proteomic characterization of single neurons, which opens a new potential to single-cell proteomics analysis for developing brain or impaired brain sections to understand molecular mechanisms involved during those development. In the future, we imagine that incorporating c-desalting and microsampling approach using electrophysiology can be still optimized to further improve the protein IDs and quality of the information contained from the findings. For example, a refined microsampling approach could minimize aspirating salt contaminant from the media of the cell tissue and maximize the neuronal soma aspiration to increase protein content from the targeted cell. Furthermore, we note that applications of our single-neuron proteomics with c-desalting are not restricted to single neurons but also to different types of single cells which could extend its application for single-cell analysis to better understand molecular mechanisms involved during development of various cells one is investigating.

Chapter 7: Conclusions and future directions

7.1 Advancing single neuron proteomics and neuroscience

Single-neuron proteomics by MS provides an essential tool to study molecular mechanisms of action responsible for brain development and how neurons connect to each other to form an organization. Classical MS-based analytical workflows are mainly designed to understand and characterize biomolecules from a large population of cells, but it has been found that cell populations are not homogeneous. Therefore, to uncover the chemical diversity between neuron types, it is important to perform molecular profiling at the single neuron level. To this end, many analytical approaches have been revised to enable single-cell proteomics. However, due to large chemical diversity, limited sample material and chemical complexity of single neurons, there is still a need to improve the current technologies.

In this dissertation, I have made substantial advances towards the analysis of proteins in single neurons from the mouse brain. First, I developed a new generation ion source to enable ultrasensitive detection from a limited population of neurons (Chapter 2). This new generation ion source has improved the detection sensitivity by a factor of 20 compared to our previous generation ion source, enabling 230 zmol of lower limit of detection. In addition, I also incorporated a multidimensional separation approach to further improve the detectable proteins and peptides from a limited population of neurons (Chapter 3). Next, I integrated an iterative data dependent acquisition methodology to improve the duty cycle of the mass spectrometer to acquire more quality data on low-abundance peptides and proteins (Chapter 4). In addition, I integrated a microcapillary sampling technique with electrophysiology to enable single neuron proteomics (Chapter 5). Based on the effectiveness demonstrated by the microprobe to collect

neuronal soma from the live neurons, I utilized this approach to interrogate neuron-to-neuron heterogeneity using a new generation mass spectrometer equipped with ion mobility mass spectrometry (Chapter 6).

In this work, I demonstrated that combining electrophysiology with mass spectrometry enables single-neuron proteomics with ultra-sensitive CE-nanoESI-MS, which empowers the study of proteomics to understand the neuron-to-neuron heterogeneity. For instance, we were able to distinguish different types of neuronal types based on the MS data I obtained. This is the first time such differences was demonstrated using proteomic expression to differentiate different types of neurons that were validated by electrophysiology. While the active molecular mechanisms that drive the differences between these neurons remain elusive to us at this point, our established CE-nanoESI-MS analytical platform and findings can allow us and others to conceive new hypotheses and research strategies to understand how proteomic heterogeneity contributes to cell specification during their normal or impaired development.

Moreover, we found many proteins that are known to be associated with basic cellular functions such as metabolism, cytoskeletal dynamics, and protein translation and processing that interact to affect cell activity. Intriguingly, protein expression was more similar between parvalbumin and serotonergic neurons than between dopaminergic and serotonergic, despite the fact that dopaminergic and serotonergic neurons are more closely genetically related. Our findings highlight the potential usefulness of single-cell proteomics, as gene expression is only one step in determining the final composite of proteins that governs a cell's function. Our measurement of proteins from single electrophysiologically-identified cells will enable more direct comparison of protein expression and cellular function.

7.2 Technological advancements for single-cell proteomics

7.2.1 Improvements in proteomics detection

To facilitate the analysis of proteomics from single neurons, I developed a single-cell CE-nanoESI-MS platform that enables ultrasensitive detection from single neuron content. This analytical platform was able to detect over 800 proteins from single dopaminergic neurons and over 300 proteins from parvalbumin neurons and over 600 proteins from serotonin neurons. However, additional technological advances to our platform may be implemented to help with protein detection, identification, and sensitivity to continue improving single-neuron proteomics detection. To improve sensitivity, larger amounts of sample can be injected into the CE capillary with pressurized injection with an automated system. This approach is compatible with our platform and will likely yield improved detection sensitivity for peptide and protein detection and identification. Improvements in the CE interface and spray stabilization will also result in improved detection sensitivity. For example, the tapered-tip CE-ESI interface was able to reduce the sheath flowrate from 1 $\mu\text{L}/\text{min}$ to $< 300 \text{ nL}/\text{min}$, which enhanced the detection sensitivity by 20 \times . There are also alternatives such as electrokinetically pumped low-flow CE-nanoESI⁹⁸ and sheathless CE-ESI that will result in reduced analyte dilution in the electrospray plume. Altogether, these suggested improvements can lead to a deeper profiling of biomolecules in single cells.

7.2.2 Improvements in measurement throughput

In the current state of development, there is a major limitation for the analysis of single cells which originates from the minuscule amounts of starting material, which can be easily lost during sample preparation. The throughput at which single cells are analyzed can be improved,

thereby raising the potential to analyze higher numbers of individual cells and improve statistical results. One way to increase the throughput is using a nanodroplet-based processing platform that has recently been developed. Its feasibility to perform single-cell proteomics was demonstrated with a nanoPOTS autosampler allowing fully automated sample injection from nanowells to an LC-MS system.²³⁹ By combining the automated system with microfluidic devices fabricated to entail single-cells, ~77 cells were able to be measured per day, compared to ~5 cells per day using our interface. Combining the nanoPOTS with CE would increase the number of protein identifications and make the streamlined analysis more easily accessible.

7.2.3 Improvements in sample preparation

One of the major challenges in single-cell proteomics is the handling of individual cells to process them through a bottom-up proteomic workflow without worrying about sample loss. When dealing with single cells, one has to be adequately trained to microsample the cell. As described before, microsampling a neuron requires whole-cell patch-clamp electrophysiology to be recorded. However, microsampling with electrophysiological electrodes introduces substantial salt contamination which is detrimental for mass spectrometry analysis. Therefore, minimizing salt contaminants would be essential to providing a quality proteomics data. In order to minimize salt contaminants, more careful aspiration of the neuronal soma is required. Also, chemically desalting the collected sample would also decrease the salt contaminants as well.

7.2.4 Improvements in bottom-up data acquisition

One of the standing challenges in single-cell bottom-up proteomics is the missing data problem. It is commonly believed that protein identification relies on the successful fragmentation of one of a protein's unique peptide. Low peptide signals and limited duty cycle afforded by the mass

spectrometer hinders the identification of these low-abundance peptides and proteins. These existing problems are compounded by already limited protein amounts (from a single neuron) and by fast CE separation. However, several solutions have been introduced to facilitate these challenges. Firstly, the duration of CE separation could be increased by reducing the electroosmotic flow. A recent study suggested a lengthy separation by CE, ~140 min time window, that is comparable to nanoLC.²⁴⁰ Having a slower separation will increase the success rate at which peptides can be detected and be fragmented. Another solution has been to change the data acquisition parameters to limit redundant peptide fragmentation,^{184, 241-242} which will improve the duty cycle of the mass spectrometer as it will only attempt to fragment ions that are not redundant. Finally, development of faster scanning mass analyzers would enable faster fragmentation events for more peptide ions, and thereby increasing the identification rates. Most recently, trapped ion mobility mass spectrometer equipped with quadrupole and time-of-flight instrumentation has enabled 10 – 20× faster scanning rate, providing over 200 Hz acquisition rate to capture rapidly separating peptides. This new generation mass spectrometer has increased the acquisition duty cycle and the mass resolution with an added dimension of separation (ion mobility) to successfully identify peptides and proteins.²⁴³⁻²⁴⁴

7.3 Outlook

Combined advances in proteomic sample preparation, separation approaches and mass spectrometry technologies promise to enable deeper proteomic coverage from smaller and smaller single cells, such as mammalian neurons. This rapidly advancing technology opens a new gate to explore information on cellular heterogeneity in complex systems such as cancer cells, tumor cells in the brain and other organs. With new information, we can finally understand

the molecular mechanisms of action and develop effective treatment for such incurable diseases like Alzheimer's and Parkinson's diseases.

Appendices

Table 4.1. Protein identification from control, top 150 and top 250 excluded list. Total of 9 technical replicate measurements were made using 4.5 ng of protein digest.

Accession ID	Protein name	Gene name	Quantified?
Q9CWF2	Tubulin beta-2B chain	<i>Tubb2b</i>	Yes
P68369	Tubulin alpha-1A chain (Alpha-tubulin 1) (Alpha-tubulin isotype M-alpha-1) (Tubulin alpha-1 chain) [Cleaved into: Detyrosinated tubulin alpha-1A chain]	<i>Tuba1a</i>	Yes
Q7TMM9	Tubulin beta-2A chain	<i>Tubb2a</i>	Yes
P99024	Tubulin beta-5 chain	<i>Tubb5</i>	Yes
P68372	Tubulin beta-4B chain (Tubulin beta-2C chain)	<i>Tubb4b</i>	Yes
P05213	Tubulin alpha-1B chain (Alpha-tubulin 2) (Alpha-tubulin isotype M-alpha-2) (Tubulin alpha-2 chain) [Cleaved into: Detyrosinated tubulin alpha-1B chain]	<i>Tuba1b</i>	Yes
P63260	Actin, cytoplasmic 2 (Gamma-actin) [Cleaved into: Actin, cytoplasmic 2, N-terminally processed]	<i>Actg1</i>	Yes
Q9ERD7	Tubulin beta-3 chain	<i>Tubb3</i>	Yes
P68134	Actin, alpha skeletal muscle (Alpha-actin-1) [Cleaved into: Actin, alpha skeletal muscle, intermediate form]	<i>Acta1</i>	Yes
Q9D6F9	Tubulin beta-4A chain (Tubulin beta-4 chain)	<i>Tubb4a</i> <i>Hist1h2b</i>	Yes
Q8CGP2	Histone H2B type 1-P	<i>p</i>	Yes
Q6ZWY9	Histone H2B type 1-C/E/G	<i>H2bc4</i>	Yes
O08553	Dihydropyrimidinase-related protein 2 (DRP-2) (Unc-33-like phosphoprotein 2) (ULIP-2)	<i>Dpysl2</i>	Yes
Q62188	Dihydropyrimidinase-related protein 3 (DRP-3) (Unc-33-like phosphoprotein 1) (ULIP-1)	<i>Dpysl3</i>	Yes
Q8CGP6	Histone H2A type 1-H (H2A-clustered histone 12)	<i>H2ac12</i>	Yes
P16858	Glyceraldehyde-3-phosphate dehydrogenase (GAPDH) (EC 1.2.1.12) (Peptidyl-cysteine S-nitrosylase GAPDH) (EC 2.6.99.-)	<i>Gapdh</i>	Yes
P62806	Histone H4	<i>H4c1</i>	Yes
P03995	Glial fibrillary acidic protein (GFAP)	<i>Gfap</i>	Yes
P48962	ADP/ATP translocase 1 (ADP,ATP carrier protein 1) (ADP,ATP carrier protein, heart/skeletal muscle isoform T1) (Adenine nucleotide translocator 1) (ANT 1) (Solute carrier family 25 member 4)	<i>Slc25a4</i>	Yes
Q6PIC6	Sodium/potassium-transporting ATPase subunit alpha-3 (Na(+)/K(+) ATPase alpha-3 subunit) (EC 7.2.2.13) (Na(+)/K(+) ATPase alpha(III) subunit) (Sodium pump subunit alpha-3)	<i>Atp1a3</i>	Yes
P84244	Histone H3.3	<i>H3-3a</i>	Yes
P56480	ATP synthase subunit beta, mitochondrial (EC 7.1.2.2) (ATP synthase F1 subunit beta)	<i>Atp5f1b</i>	Yes
P63017	Heat shock cognate 71 kDa protein (EC 3.6.4.10) (Heat shock 70 kDa protein 8)	<i>Hspa8</i>	Yes

P51881	ADP/ATP translocase 2 (ADP,ATP carrier protein 2) (Adenine nucleotide translocator 2) (ANT 2) (Solute carrier family 25 member 5) [Cleaved into: ADP/ATP translocase 2, N-terminally processed]	<i>Slc25a5</i>	Yes
P97427	Dihydropyrimidinase-related protein 1 (DRP-1) (Collapsin response mediator protein 1) (CRMP-1) (Inactive dihydropyrimidinase) (Unc-33-like phosphoprotein 3) (ULIP-3)	<i>Crmp1</i>	Yes
P63101	14-3-3 protein zeta/delta (Protein kinase C inhibitor protein 1) (KCIP-1) (SEZ-2)	<i>Ywhaz</i>	Yes
P13595-2	Neural cell adhesion molecule 1 (N-CAM-1) (NCAM-1) (CD antigen CD56)	<i>Ncam1</i>	Yes
Q03265	ATP synthase subunit alpha, mitochondrial (ATP synthase F1 subunit alpha)	<i>Atp5fla</i>	Yes
P17182	Alpha-enolase (EC 4.2.1.11) (2-phospho-D-glycerate hydro-lyase) (Enolase 1) (Non-neural enolase) (NNE)	<i>Eno1</i>	Yes
P10126	Elongation factor 1-alpha 1 (EF-1-alpha-1) (Elongation factor Tu) (EF-Tu) (Eukaryotic elongation factor 1 A-1) (eEF1A-1)	<i>Eef1a1</i>	Yes
P62259	14-3-3 protein epsilon (14-3-3E)	<i>Ywhae</i>	Yes
P61982	14-3-3 protein gamma [Cleaved into: 14-3-3 protein gamma, N-terminally processed]	<i>Ywhag</i>	Yes
P0DP28	Calmodulin-3	<i>Calm3</i>	Yes
P05064	Fructose-bisphosphate aldolase A (EC 4.1.2.13) (Aldolase 1) (Muscle-type aldolase)	<i>Aldoa</i>	Yes
Q9CQV8-2	14-3-3 protein beta/alpha (Protein kinase C inhibitor protein 1) (KCIP-1) [Cleaved into: 14-3-3 protein beta/alpha, N-terminally processed]	<i>Ywhab</i>	Yes
O70456	14-3-3 protein sigma (Stratifin)	<i>Sfn</i>	Yes
Q3THW5	Histone H2A.V (H2A.F/Z) (H2A.Z variant histone 2)	<i>H2az2</i>	Yes
P18872-2	Guanine nucleotide-binding protein G(o) subunit alpha	<i>Gnao1</i>	Yes
P17742	Peptidyl-prolyl cis-trans isomerase A (PPIase A) (EC 5.2.1.8) (Cyclophilin A) (Cyclosporin A-binding protein) (Rotamase A) (SP18) [Cleaved into: Peptidyl-prolyl cis-trans isomerase A, N-terminally processed]	<i>Ppia</i>	Yes
P68254-2	14-3-3 protein theta (14-3-3 protein tau)	<i>Ywhaq</i>	Yes
P11499	Heat shock protein HSP 90-beta (Heat shock 84 kDa) (HSP 84) (HSP84) (Tumor-specific transplantation 84 kDa antigen) (TSTA)	<i>Hsp90ab1</i>	Yes
P20152	Vimentin	<i>Vim</i>	Yes
P68510	14-3-3 protein eta	<i>Ywhah</i>	Yes
P52480-2	Pyruvate kinase PKM (EC 2.7.1.40) (Pyruvate kinase muscle isozyme)	<i>Pkm</i>	Yes
Q60932-2	Voltage-dependent anion-selective channel protein 1 (VDAC-1) (mVDAC1) (Outer mitochondrial membrane protein porin 1) (Plasmalemmal porin) (Voltage-dependent anion-selective channel protein 5) (VDAC-5) (mVDAC5)	<i>Vdac1</i>	Yes
Q9EQF6	Dihydropyrimidinase-related protein 5 (DRP-5) (Collapsin response mediator protein 5) (CRMP-5)	<i>Dpysl5</i>	Yes
P01942	Hemoglobin subunit alpha (Alpha-globin) (Hemoglobin alpha chain)	<i>Hba</i>	Yes
P07901	Heat shock protein HSP 90-alpha (EC 3.6.4.10) (Heat shock 86 kDa) (HSP 86) (HSP86) (Tumor-specific transplantation 86 kDa antigen) (TSTA)	<i>Hsp90aa1</i>	Yes
Q6PIE5	Sodium/potassium-transporting ATPase subunit alpha-2 (Na ⁺)/K ⁺ ATPase alpha-2 subunit) (EC 7.2.2.13) (Na ⁺)/K ⁺ ATPase alpha(+)	<i>Atp1a2</i>	Yes
P08249	Malate dehydrogenase, mitochondrial (EC 1.1.1.37)	<i>Mdh2</i>	Yes

Q9R0P9	Ubiquitin carboxyl-terminal hydrolase isozyme L1 (UCH-L1) (EC 3.4.19.12) (Neuron cytoplasmic protein 9.5) (PGP 9.5) (PGP9.5) (Ubiquitin thioesterase L1)	<i>Uchl1</i>	Yes
P62984	Ubiquitin-60S ribosomal protein L40 (Ubiquitin A-52 residue ribosomal protein fusion product 1) [Cleaved into: Ubiquitin; 60S ribosomal protein L40 (CEP52)]	<i>Uba52</i>	Yes
Q68FD5	Clathrin heavy chain 1	<i>Cltc</i>	Yes
P18760	Cofilin-1 (Cofilin, non-muscle isoform)	<i>Cfl1</i>	Yes
Q91XV3	Brain acid soluble protein 1 (22 kDa neuronal tissue-enriched acidic protein) (Neuronal axonal membrane protein NAP-22)	<i>Baspl</i>	Yes
P06151	L-lactate dehydrogenase A chain (LDH-A) (EC 1.1.1.27) (LDH muscle subunit) (LDH-M)	<i>Ldha</i>	Yes
P11798	Calcium/calmodulin-dependent protein kinase type II subunit alpha (CaM kinase II subunit alpha) (CaMK-II subunit alpha) (EC 2.7.11.17)	<i>Camk2a</i>	Yes
P06837	Neuromodulin (Axonal membrane protein GAP-43) (Calmodulin-binding protein P-57) (Growth-associated protein 43)	<i>Gap43</i>	Yes
Q9DBJ1	Phosphoglycerate mutase 1 (EC 5.4.2.11) (EC 5.4.2.4) (BPG-dependent PGAM 1) (Phosphoglycerate mutase isozyme B) (PGAM-B)	<i>Pgam1</i>	Yes
P20029	Endoplasmic reticulum chaperone BiP (EC 3.6.4.10) (78 kDa glucose-regulated protein) (GRP-78) (Binding-immunoglobulin protein) (BiP) (Heat shock protein 70 family protein 5) (HSP70 family protein 5) (Heat shock protein family A member 5) (Immunoglobulin heavy chain-binding protein)	<i>Hspa5</i>	Yes
P43274	Histone H1.4 (H1 VAR.2) (H1e)	<i>H1-4</i>	Yes
P62880	Guanine nucleotide-binding protein G(I)/G(S)/G(T) subunit beta-2 (G protein subunit beta-2) (Transducin beta chain 2)	<i>Gnb2</i>	Yes
P28652	Calcium/calmodulin-dependent protein kinase type II subunit beta (CaM kinase II subunit beta) (CaMK-II subunit beta) (EC 2.7.11.17)	<i>Camk2b</i>	Yes
O08599	Syntaxin-binding protein 1 (Protein unc-18 homolog 1) (Unc18-1) (Protein unc-18 homolog A) (Unc-18A)	<i>Stxbp1</i>	Yes
Q8K0T0	Reticulon-1 (Neuroendocrine-specific protein)	<i>Rtn1</i>	Yes
P13595-3	Neural cell adhesion molecule 1 (N-CAM-1) (NCAM-1) (CD antigen CD56)	<i>Ncam1</i>	Yes
Q64523	Histone H2A type 2-C (H2A-clustered histone 20) (H2a-613B)	<i>H2ac20</i>	Yes
P62874	Guanine nucleotide-binding protein G(I)/G(S)/G(T) subunit beta-1 (Transducin beta chain 1)	<i>Gnb1</i>	Yes
P63038	60 kDa heat shock protein, mitochondrial (EC 5.6.1.7) (60 kDa chaperonin) (Chaperonin 60) (CPN60) (HSP-65) (Heat shock protein 60) (HSP-60) (Hsp60) (Mitochondrial matrix protein P1)	<i>Hspd1</i>	Yes
P17751	Triosephosphate isomerase (TIM) (EC 5.3.1.1) (Methylglyoxal synthase) (EC 4.2.3.3) (Triose-phosphate isomerase)	<i>Tpi1</i>	Yes
Q923T9-3	Calcium/calmodulin-dependent protein kinase type II subunit gamma (CaM kinase II subunit gamma) (CaMK-II subunit gamma) (EC 2.7.11.17)	<i>Camk2g</i>	Yes
Q9CZU6	Citrate synthase, mitochondrial (EC 2.3.3.1) (Citrate (Si)-synthase)	<i>Cs</i>	Yes
P16546-2	Spectrin alpha chain, non-erythrocytic 1 (Alpha-II spectrin) (Fodrin alpha chain)	<i>Sptan1</i>	Yes
Q01768	Nucleoside diphosphate kinase B (NDK B) (NDP kinase B) (EC 2.7.4.6) (Histidine protein kinase NDKB) (EC 2.7.13.3) (P18) (nm23-M2)	<i>Nme2</i>	Yes
P17183	Gamma-enolase (EC 4.2.1.11) (2-phospho-D-glycerate hydro-lyase) (Enolase 2) (Neural enolase) (Neuron-specific enolase) (NSE)	<i>Eno2</i>	Yes
P14094	Sodium/potassium-transporting ATPase subunit beta-1 (Sodium/potassium-dependent ATPase subunit beta-1)	<i>Atp1b1</i>	Yes

Q04447	Creatine kinase B-type (EC 2.7.3.2) (B-CK) (Creatine kinase B chain)	<i>Ckb</i>	Yes
Q0KK56	(Creatine phosphokinase B-type) (CPK-B)		
-2	Protein FAM184B	<i>Fam184b</i>	Yes
P18872	Guanine nucleotide-binding protein G(o) subunit alpha	<i>Gnao1</i>	Yes
	Macrophage migration inhibitory factor (MIF) (EC 5.3.2.1) (Delayed early response protein 6) (DER6) (Glycosylation-inhibiting factor) (GIF) (L-dopachrome isomerase) (L-dopachrome tautomerase) (EC 5.3.3.12)		
P34884	(Phenylpyruvate tautomerase)	<i>Mif</i>	Yes
Q61553	Fascin (Singed-like protein)	<i>Fscn1</i>	Yes
	Glucose-6-phosphate isomerase (GPI) (EC 5.3.1.9) (Autocrine motility factor) (AMF) (Neuroleukin) (NLK) (Phosphoglucose isomerase) (PGI)		
P06745	(Phosphohexose isomerase) (PHI)	<i>Gpi</i>	Yes
P35802	Neuronal membrane glycoprotein M6-a (M6a)	<i>Gpm6a</i>	Yes
Q99KI0	Aconitate hydratase, mitochondrial (Aconitase) (EC 4.2.1.3) (Citrate hydrolyase)	<i>Aco2</i>	Yes
P09411	Phosphoglycerate kinase 1 (EC 2.7.2.3)	<i>Pgk1</i>	Yes
P61294	Ras-related protein Rab-6B	<i>Rab6b</i>	Yes
	Peroxiredoxin-2 (EC 1.11.1.24) (Thiol-specific antioxidant protein) (TSA) (Thioredoxin peroxidase 1) (Thioredoxin-dependent peroxide reductase 1)		
Q61171	(Thioredoxin-dependent peroxiredoxin 2)	<i>Prdx2</i>	Yes
Q9R0P5	Destrin (Actin-depolymerizing factor) (ADF) (Sid 23)	<i>Dstn</i>	Yes
P35276	Ras-related protein Rab-3D	<i>Rab3d</i>	Yes
Q8BMJ7	Cell growth regulator with RING finger domain protein 1 (Cell growth regulatory gene 19 protein)	<i>Cgrrf1</i>	Yes
P14873	Microtubule-associated protein 1B (MAP-1B) (MAP1(X)) (MAP1.2)		
Q3ULB	[Cleaved into: MAP1B heavy chain; MAP1 light chain LC1]	<i>Map1b</i>	Yes
5	Serine/threonine-protein kinase PAK 6 (EC 2.7.11.1) (p21-activated kinase 6) (PAK-6)	<i>Pak6</i>	Yes
P63011	Ras-related protein Rab-3A	<i>Rab3a</i>	Yes
	Excitatory amino acid transporter 1 (Glial high affinity glutamate transporter) (High-affinity neuronal glutamate transporter) (GluT-1) (Sodium-dependent glutamate/aspartate transporter 1) (GLAST-1) (Solute carrier family 1 member 3)		
P56564		<i>Slc1a3</i>	Yes
Q9DBR	Protein phosphatase 1 regulatory subunit 12A (Myosin phosphatase-targeting subunit 1) (Myosin phosphatase target subunit 1)	<i>Ppp1r12a</i>	Yes
7-2			
P10637-	Microtubule-associated protein tau (Neurofibrillary tangle protein) (Paired helical filament-tau) (PHF-tau)	<i>Mapt</i>	Yes
4			
P70296	Phosphatidylethanolamine-binding protein 1 (PEBP-1) (HCNPPP) [Cleaved into: Hippocampal cholinergic neurostimulating peptide (HCNP)]	<i>Pebp1</i>	Yes
O54983	Ketimine reductase mu-crystallin (EC 1.5.1.25) (NADP-regulated thyroid-hormone-binding protein)	<i>Crym</i>	Yes
P84078	ADP-ribosylation factor 1	<i>Arf1</i>	Yes
	V-type proton ATPase catalytic subunit A (V-ATPase subunit A) (EC 7.1.2.2) (V-ATPase 69 kDa subunit) (Vacuolar proton pump subunit alpha)		
P50516	Vesicle-fusing ATPase (EC 3.6.4.6) (N-ethylmaleimide-sensitive fusion protein) (NEM-sensitive fusion protein) (Suppressor of K(+) transport growth defect 2) (Protein SKD2) (Vesicular-fusion protein NSF)	<i>Atp6v1a</i>	Yes
P46460		<i>Nsf</i>	Yes
P05063	Fructose-bisphosphate aldolase C (EC 4.1.2.13) (Aldolase 3) (Brain-type aldolase) (Scrapie-responsive protein 2) (Zebrin II)	<i>Aldoc</i>	Yes
P21619-			
2	Lamin-B2	<i>Lmnb2</i>	Yes

P14211	Calreticulin (CRP55) (Calregulin) (Endoplasmic reticulum resident protein 60) (ERp60) (HACBP)	<i>Calr</i>	Yes
Q64433	10 kDa heat shock protein, mitochondrial (Hsp10) (10 kDa chaperonin) (Chaperonin 10) (CPN10)	<i>Hspe1</i>	Yes
P50516-2	V-type proton ATPase catalytic subunit A (V-ATPase subunit A) (EC 7.1.2.2) (V-ATPase 69 kDa subunit) (Vacuolar proton pump subunit alpha)	<i>Atp6v1a</i>	Yes
Q91V12-2	Cytosolic acyl coenzyme A thioester hydrolase (EC 3.1.2.2) (Acyl-CoA thioesterase 7) (Brain acyl-CoA hydrolase) (BACH) (CTE-IIa) (CTE-II) (Long chain acyl-CoA thioester hydrolase)	<i>Acot7</i>	Yes
Q60931	Voltage-dependent anion-selective channel protein 3 (VDAC-3) (mVDAC3) (Outer mitochondrial membrane protein porin 3)	<i>Vdac3</i>	Yes
Q62277	Synaptophysin (BM89 antigen) (Major synaptic vesicle protein p38)	<i>Syp</i>	Yes
P08228	Superoxide dismutase [Cu-Zn] (EC 1.15.1.1)	<i>Sod1</i>	Yes
Q6PCZ4	Melanoma-associated antigen E1 (Alpha-dystrobrevin-associated MAGE Protein) (DAMAGE) (MAGE-E1 antigen)	<i>Magee1</i>	Yes
O88935-1	Synapsin-1 (Synapsin I)	<i>Syn1</i>	Yes
P05202	Aspartate aminotransferase, mitochondrial (mAspAT) (EC 2.6.1.1) (EC 2.6.1.7) (Fatty acid-binding protein) (FABP-1) (Glutamate oxaloacetate transaminase 2) (Kynurenine aminotransferase 4) (Kynurenine aminotransferase IV) (Kynurenine--oxoglutarate transaminase 4) (Kynurenine--oxoglutarate transaminase IV) (Plasma membrane-associated fatty acid-binding protein) (FABPpm) (Transaminase A)	<i>Got2</i>	Yes
P15532	Nucleoside diphosphate kinase A (NDK A) (NDP kinase A) (EC 2.7.4.6) (Metastasis inhibition factor NM23) (NDPK-A) (Tumor metastatic process-associated protein) (nm23-M1)	<i>Nme1</i>	Yes
P51880	Fatty acid-binding protein, brain (Brain lipid-binding protein) (BLBP) (Brain-type fatty acid-binding protein) (B-FABP) (Fatty acid-binding protein 7)	<i>Fabp7</i>	Yes
Q9DCX2	ATP synthase subunit d, mitochondrial (ATPase subunit d) (ATP synthase peripheral stalk subunit d)	<i>Atp5pd</i>	Yes
P46096	Synaptotagmin-1 (Synaptotagmin I) (Sytl) (p65)	<i>Syt1</i>	Yes
Q91VR2	ATP synthase subunit gamma, mitochondrial (ATP synthase F1 subunit gamma) (F-ATPase gamma subunit)	<i>Atp5flc</i>	Yes
P40142	Transketolase (TK) (EC 2.2.1.1) (P68)	<i>Tkt</i>	Yes
P14152	Malate dehydrogenase, cytoplasmic (EC 1.1.1.37) (Cytosolic malate dehydrogenase)	<i>Mdh1</i>	Yes
Q8VEM8	Phosphate carrier protein, mitochondrial (Phosphate transport protein) (PTP) (Solute carrier family 25 member 3)	<i>Slc25a3</i>	Yes
Q61598-2	Rab GDP dissociation inhibitor beta (Rab GDI beta) (GDI-3) (Guanosine diphosphate dissociation inhibitor 2) (GDI-2)	<i>Gdi2</i>	Yes
P63001	Ras-related C3 botulinum toxin substrate 1 (EC 3.6.5.2) (p21-Rac1)	<i>Rac1</i>	Yes
P43006-3	Excitatory amino acid transporter 2 (GLT-1) (Sodium-dependent glutamate/aspartate transporter 2) (Solute carrier family 1 member 2)	<i>Slc1a2</i>	Yes
O55042-2	Alpha-synuclein (Non-A beta component of AD amyloid) (Non-A4 component of amyloid precursor) (NACP)	<i>Snca</i>	Yes
Q60930	Voltage-dependent anion-selective channel protein 2 (VDAC-2) (mVDAC2) (Outer mitochondrial membrane protein porin 2) (Voltage-dependent anion-selective channel protein 6) (VDAC-6) (mVDAC6)	<i>Vdac2</i>	Yes
P39053-5	Dynamin-1 (EC 3.6.5.5)	<i>Dnm1</i>	Yes
P17710-3	Hexokinase-1 (EC 2.7.1.1) (Hexokinase type I) (HK I) (Hexokinase, tumor isozyme)	<i>Hk1</i>	Yes

P35564	Calnexin	<i>Canx</i>	Yes
P50396	Rab GDP dissociation inhibitor alpha (Rab GDI alpha) (Guanosine diphosphate dissociation inhibitor 1) (GDI-1)	<i>Gdi1</i>	Yes
Q02053	Ubiquitin-like modifier-activating enzyme 1 (EC 6.2.1.45) (Ubiquitin-activating enzyme E1) (Ubiquitin-activating enzyme E1 X) (Ubiquitin-like modifier-activating enzyme 1 X)	<i>Uba1</i>	Yes
Q64332-2	Synapsin-2 (Synapsin II)	<i>Syn2</i>	Yes
Q8R480	Nuclear pore complex protein Nup85 (85 kDa nucleoporin) (FROUNT) (Nucleoporin Nup85) (Pericentrin-1)	<i>Nup85</i>	Yes
Q9D6M3	Mitochondrial glutamate carrier 1 (GC-1) (Glutamate/H(+) symporter 1) (Solute carrier family 25 member 22)	<i>Slc25a22</i>	Yes
P26443	Glutamate dehydrogenase 1, mitochondrial (GDH 1) (EC 1.4.1.3)	<i>Ghud1</i>	Yes
Q9ES97-3	Reticulon-3	<i>Rtn3</i>	Yes
P43006-2	Excitatory amino acid transporter 2 (GLT-1) (Sodium-dependent glutamate/aspartate transporter 2) (Solute carrier family 1 member 2)	<i>Slc1a2</i>	Yes
Q9D0K2	Succinyl-CoA:3-ketoacid coenzyme A transferase 1, mitochondrial (EC 2.8.3.5) (3-oxoacid CoA-transferase 1) (Somatic-type succinyl-CoA:3-oxoacid CoA-transferase) (SCOT-s)	<i>Oxct1</i>	Yes
P54227	Stathmin (Leukemia-associated gene protein) (Leukemia-associated phosphoprotein p18) (Metablastin) (Oncoprotein 18) (Op18) (Phosphoprotein p19) (pp19) (Prosolin) (Protein Pr22) (pp17)	<i>Stmn1</i>	Yes
Q61548-3	Clathrin coat assembly protein AP180 (91 kDa synaptosomal-associated protein) (Clathrin coat-associated protein AP180) (Phosphoprotein F1-20)	<i>Snap91</i>	Yes
P08113	Endoplasmic reticulum resident protein 99 (ERp99) (Heat shock protein 90 kDa beta member 1) (Polymorphic tumor rejection antigen 1) (Tumor rejection antigen gp96)	<i>Hsp90b1</i>	Yes
Q9DB20	ATP synthase subunit O, mitochondrial (ATP synthase peripheral stalk subunit OSCP) (Oligomycin sensitivity conferral protein) (OSCP)	<i>Atp5po</i>	Yes
P62814	V-type proton ATPase subunit B, brain isoform (V-ATPase subunit B 2) (Endomembrane proton pump 58 kDa subunit) (Vacuolar proton pump subunit B 2)	<i>Atp6v1b2</i>	Yes
P12960	Contactin-1 (Neural cell surface protein F3)	<i>Cntn1</i>	Yes
P10852	4F2 cell-surface antigen heavy chain (4F2hc) (Solute carrier family 3 member 2) (CD antigen CD98)	<i>Slc3a2</i>	Yes
Q9D3D9	ATP synthase subunit delta, mitochondrial (ATP synthase F1 subunit delta) (F-ATPase delta subunit)	<i>Atp5fld</i>	Yes
Q9DBG3	AP-2 complex subunit beta (AP105B) (Adaptor protein complex AP-2 subunit beta) (Adaptor-related protein complex 2 subunit beta) (Beta-2-adaptin) (Beta-adaptin) (Clathrin assembly protein complex 2 beta large chain) (Plasma membrane adaptor HA2/AP2 adaptin beta subunit)	<i>Ap2b1</i>	Yes
P62743	AP-2 complex subunit sigma (Adaptor protein complex AP-2 subunit sigma) (Adaptor-related protein complex 2 subunit sigma) (Clathrin assembly protein 2 sigma small chain) (Clathrin coat assembly protein AP17) (Clathrin coat-associated protein AP17) (Plasma membrane adaptor AP-2 17 kDa protein) (Sigma-adaptin 3b) (Sigma2-adaptin)	<i>Ap2s1</i>	Yes
P00405	Cytochrome c oxidase subunit 2 (EC 7.1.1.9) (Cytochrome c oxidase polypeptide II)	<i>Mtco2</i>	Yes
P31786	Acyl-CoA-binding protein (ACBP) (Diazepam-binding inhibitor) (DBI) (Endozepine) (EP)	<i>Dbi</i>	Yes

O88569-3	Heterogeneous nuclear ribonucleoproteins A2/B1 (hnRNP A2/B1) Isocitrate dehydrogenase [NADP] cytoplasmic (IDH) (EC 1.1.1.42) (Cytosolic NADP-isocitrate dehydrogenase) (IDP) (NADP(+)-specific	<i>Hnrnpa2</i> <i>b1</i>	Yes
O88844	ICDH) (Oxalosuccinate decarboxylase) Fatty acid-binding protein 5 (Epidermal-type fatty acid-binding protein) (E-FABP) (Fatty acid-binding protein, epidermal) (Keratinocyte lipid-binding protein) (Psoriasis-associated fatty acid-binding protein homolog) (PA-FABP)	<i>Idh1</i>	Yes
Q05816	Visinin-like protein 1 (VILIP) (Neural visinin-like protein 1) (NVL-1)	<i>Fabp5</i>	Yes
P62761	(NVP-1)	<i>Vsnl1</i>	Yes
Q62261-2	Spectrin beta chain, non-erythrocytic 1 (Beta-II spectrin) (Embryonic liver fodrin) (Fodrin beta chain)	<i>Sptbn1</i>	Yes
Q8VEK3-2	Heterogeneous nuclear ribonucleoprotein U (hnRNP U) (Scaffold-attachment factor A) (SAF-A)	<i>Hnrnpu</i>	Yes
P60843	Eukaryotic initiation factor 4A-I (eIF-4A-I) (eIF4A-I) (EC 3.6.4.13) (ATP-dependent RNA helicase eIF4A-1)	<i>Eif4a1</i>	Yes
O55022	Membrane-associated progesterone receptor component 1 (mPR)	<i>Pgrmc1</i>	Yes
P26645	Myristoylated alanine-rich C-kinase substrate (MARCKS)	<i>Marcks</i>	Yes
P01831	Thy-1 membrane glycoprotein (Thy-1 antigen) (CD antigen CD90)	<i>Thy1</i>	Yes
Q61207	Prosaposin (Sulfated glycoprotein 1) (SGP-1) [Cleaved into: Saposin-A; Saposin-B-Val; Saposin-B; Saposin-C; Saposin-D]	<i>Psap</i>	Yes
O08749	Dihydrolipoyl dehydrogenase, mitochondrial (EC 1.8.1.4) (Dihydrolipoamide dehydrogenase)	<i>Dld</i>	Yes
Q01853	Transitional endoplasmic reticulum ATPase (TER ATPase) (EC 3.6.4.6) (15S Mg(2+)-ATPase p97 subunit) (Valosin-containing protein) (VCP)	<i>Vcp</i>	Yes
P50518	V-type proton ATPase subunit E 1 (V-ATPase subunit E 1) (V-ATPase 31 kDa subunit) (p31) (Vacuolar proton pump subunit E 1)	<i>Atp6v1e1</i>	Yes
P58252	Elongation factor 2 (EF-2)	<i>Eef2</i>	Yes
P56135	ATP synthase subunit f, mitochondrial (ATP synthase membrane subunit f) Cytoplasmic dynein 1 heavy chain 1 (Cytoplasmic dynein heavy chain 1)	<i>Atp5mf</i>	Yes
Q9JHU4	(Dynein heavy chain, cytosolic)	<i>Dync1h1</i>	Yes
P61979-3	Heterogeneous nuclear ribonucleoprotein K (hnRNP K) GTP-binding nuclear protein Ran (GTPase Ran) (Ras-like protein TC4)	<i>Hnrnpk</i>	Yes
P62827	(Ras-related nuclear protein)	<i>Ran</i>	Yes
Q9D1G1	Ras-related protein Rab-1B (EC 3.6.5.2)	<i>Rab1b</i>	Yes
Q9Z2X1-2	Heterogeneous nuclear ribonucleoprotein F (hnRNP F) [Cleaved into: Heterogeneous nuclear ribonucleoprotein F, N-terminally processed]	<i>Hnrnpf</i>	Yes
Q8K259-3	Gypsy retrotransposon integrase-like protein 1 (GIN-1) (Zinc finger H2C2 domain-containing protein)	<i>Gin1</i>	Yes
P63328-2	Serine/threonine-protein phosphatase 2B catalytic subunit alpha isoform (EC 3.1.3.16) (CAM-PRP catalytic subunit) (Calmodulin-dependent calcineurin A subunit alpha isoform) (CNA alpha)	<i>Ppp3ca</i>	Yes
Q9D6R2	Isocitrate dehydrogenase [NAD] subunit alpha, mitochondrial (EC 1.1.1.41) (Isocitric dehydrogenase subunit alpha) (NAD(+)-specific ICDH subunit alpha)	<i>Idh3a</i>	Yes
Q8BLK3	Limbic system-associated membrane protein (LSAMP)	<i>Lsamp</i>	Yes
P97300-3	Neuroplastin (Stromal cell-derived receptor 1) (SDR-1)	<i>Nptn</i>	Yes

Q91V61 -2	Sideroflexin-3 MARCKS-related protein (Brain protein F52) (MARCKS-like protein 1) (Macrophage myristoylated alanine-rich C kinase substrate) (Mac-	<i>Sfxn3</i>	Yes
P28667	MARCKS) (MacMARCKS) Prohibitin-2 (B-cell receptor-associated protein BAP37) (Repressor of	<i>Marcks11</i>	Yes
O35129 P35803- 3	estrogen receptor activity) Neuronal membrane glycoprotein M6-b (M6b)	<i>Phb2</i> <i>Gpm6b</i>	Yes Yes
P28738	Kinesin heavy chain isoform 5C (Kinesin heavy chain neuron-specific 2)	<i>Kif5c</i>	Yes
Q76MZ 3	Serine/threonine-protein phosphatase 2A 65 kDa regulatory subunit A alpha isoform (PP2A subunit A isoform PR65-alpha) (PP2A subunit A isoform R1-alpha)	<i>Ppp2r1a</i>	Yes
Q8R191	Synaptogyrin-3	<i>Syng3</i>	Yes
Q9CWZ 7	Gamma-soluble NSF attachment protein (SNAP-gamma) (N- ethylmaleimide-sensitive factor attachment protein gamma)	<i>Napg</i>	Yes
Q99J16 Q9CQD 1	Ras-related protein Rap-1b (EC 3.6.5.2) (GTP-binding protein smg p21B) Ras-related protein Rab-5A (EC 3.6.5.2)	<i>Rap1b</i> <i>Rab5a</i>	Yes Yes
Q8QZT1	Acetyl-CoA acetyltransferase, mitochondrial (EC 2.3.1.9) (Acetoacetyl-CoA thiolase)	<i>Acat1</i>	Yes
Q9JIW9	Ras-related protein Ral-B (EC 3.6.5.2)	<i>Ralb</i>	Yes
Q99L04	Dehydrogenase/reductase SDR family member 1 (EC 1.1.-.-) Plasma membrane calcium-transporting ATPase 2 (PMCA2) (EC 7.2.2.10) (Plasma membrane calcium ATPase isoform 2) (Plasma membrane calcium	<i>Dhrs1</i>	Yes
Q9R0K7	pump isoform 2) Stress-70 protein, mitochondrial (75 kDa glucose-regulated protein) (GRP- 75) (Heat shock 70 kDa protein 9) (Mortalin) (Peptide-binding protein 74)	<i>Atp2b2</i>	Yes
P38647	(PBP74) (p66 MOT) Fatty acid synthase (EC 2.3.1.85) (Type I Fatty Acid Synthase) [Includes: [Acyl-carrier-protein] S-acetyltransferase (EC 2.3.1.38); [Acyl-carrier- protein] S-malonyltransferase (EC 2.3.1.39); 3-oxoacyl-[acyl-carrier-protein] synthase (EC 2.3.1.41); 3-oxoacyl-[acyl-carrier-protein] reductase (EC 1.1.1.100); 3-hydroxyacyl-[acyl-carrier-protein] dehydratase (EC 4.2.1.59); Enoyl-[acyl-carrier-protein] reductase (EC 1.3.1.39); Acyl-[acyl-carrier- protein] hydrolase (EC 3.1.2.14)]	<i>Hspa9</i>	Yes
P19096	Thioredoxin-dependent peroxide reductase, mitochondrial (EC 1.11.1.24) (Antioxidant protein 1) (AOP-1) (PRX III) (Perioredoxin-3) (Protein MER5)	<i>Fasn</i>	Yes
P20108	(Thioredoxin-dependent peroxiredoxin 3)	<i>Prdx3</i>	Yes
P84099	60S ribosomal protein L19	<i>Rpl19</i>	Yes
O55131 Q91WS 0	Septin-7 (CDC10 protein homolog) CDGSH iron-sulfur domain-containing protein 1 (MitoNEET)	<i>Septin7</i> <i>Cisd1</i>	Yes Yes
P97792- 3	Coxsackievirus and adenovirus receptor homolog (CAR) (mCAR)	<i>Cxadr</i>	Yes
P62702	40S ribosomal protein S4, X isoform	<i>Rps4x</i>	Yes
Q8CAY 6	Acetyl-CoA acetyltransferase, cytosolic (EC 2.3.1.9) (Cytosolic acetoacetyl- CoA thiolase)	<i>Acat2</i>	Yes
P67778	Prohibitin (B-cell receptor-associated protein 32) (BAP 32)	<i>Phb</i>	Yes
P26883	Peptidyl-prolyl cis-trans isomerase FKBP1A (PPIase FKBP1A) (EC 5.2.1.8) (12 kDa FK506-binding protein) (12 kDa FKBP) (FKBP-12) (Calstabin-1)	<i>Fkbp1a</i>	Yes

	(FK506-binding protein 1A) (FKBP-1A) (Immunophilin FKBP12) (Rotamase)		
Q9JIS5	Synaptic vesicle glycoprotein 2A (Synaptic vesicle protein 2) (Synaptic vesicle protein 2A) (Calcium regulator SV2A)	<i>Sv2a</i>	Yes
P63321	Ras-related protein Ral-A (EC 3.6.5.2)	<i>Rala</i>	Yes
P70349	Histidine triad nucleotide-binding protein 1 (EC 3.-.-.-) (Adenosine 5'-monophosphoramidase) (Protein kinase C inhibitor 1) (Protein kinase C-interacting protein 1) (PKCI-1)	<i>Hint1</i>	Yes
P84104-2	Serine/arginine-rich splicing factor 3 (Pre-mRNA-splicing factor SRP20) (Protein X16) (Splicing factor, arginine/serine-rich 3)	<i>Srsf3</i>	Yes
Q9D0M5	Dynein light chain 2, cytoplasmic (8 kDa dynein light chain b) (DLC8) (DLC8b) (Dynein light chain LC8-type 2)	<i>Dynll2</i>	Yes
Q8BG05-2	Heterogeneous nuclear ribonucleoprotein A3 (hnRNP A3)	<i>Hnrnpa3</i>	Yes
Q8R081	Heterogeneous nuclear ribonucleoprotein L (hnRNP L)	<i>Hnrnpl</i>	Yes
Q9D0M3-2	Cytochrome c1, heme protein, mitochondrial (EC 7.1.1.8) (Complex III subunit 4) (Complex III subunit IV) (Cytochrome b-c1 complex subunit 4) (Ubiquinol-cytochrome-c reductase complex cytochrome c1 subunit) (Cytochrome c-1)	<i>Cyc1</i>	Yes
P53994	Ras-related protein Rab-2A	<i>Rab2a</i>	Yes
P62962	Profilin-1 (Profilin I)	<i>Pfn1</i>	Yes
Q8BVE3	V-type proton ATPase subunit H (V-ATPase subunit H) (Vacuolar proton pump subunit H)	<i>Atp6v1h</i>	Yes
Q61411-2	GTPase HRas (EC 3.6.5.2) (H-Ras-1) (Transforming protein p21) (c-H-ras) (p21ras) [Cleaved into: GTPase HRas, N-terminally processed]	<i>Hras</i>	Yes
Q5M8N0	CB1 cannabinoid receptor-interacting protein 1 (CRIP-1)	<i>Cnrip1</i>	Yes
O08709	Peroxiredoxin-6 (EC 1.11.1.27) (1-Cys peroxiredoxin) (1-Cys PRX) (Acidic calcium-independent phospholipase A2) (aiPLA2) (EC 3.1.1.4) (Antioxidant protein 2) (Glutathione-dependent peroxiredoxin) (Lysophosphatidylcholine acyltransferase 5) (LPC acyltransferase 5) (LPCAT-5) (Lyso-PC acyltransferase 5) (EC 2.3.1.23) (Non-selenium glutathione peroxidase) (NSGPx)	<i>Prdx6</i>	Yes
Q61879	Myosin-10 (Cellular myosin heavy chain, type B) (Myosin heavy chain 10) (Myosin heavy chain, non-muscle IIb) (Non-muscle myosin heavy chain B) (NMMHC-B) (Non-muscle myosin heavy chain IIb) (NMMHC II-b) (NMMHC-IIb)	<i>Myh10</i>	Yes
Q8BH95	Enoyl-CoA hydratase, mitochondrial (EC 4.2.1.17) (Enoyl-CoA hydratase 1) (Short-chain enoyl-CoA hydratase) (SCEH)	<i>Echs1</i>	Yes
P61027	Ras-related protein Rab-10 (EC 3.6.5.2)	<i>Rab10</i>	Yes
Q8BGY2	Eukaryotic translation initiation factor 5A-2 (eIF-5A-2) (eIF-5A2) (Eukaryotic initiation factor 5A isoform 2)	<i>Eif5a2</i>	Yes
P35486	Pyruvate dehydrogenase E1 component subunit alpha, somatic form, mitochondrial (EC 1.2.4.1) (PDHE1-A type I)	<i>Pdha1</i>	Yes
Q63810-2	Calcineurin subunit B type 1 (Protein phosphatase 2B regulatory subunit 1) (Protein phosphatase 3 regulatory subunit B alpha isoform 1)	<i>Ppp3r1</i>	Yes
Q80XN0	D-beta-hydroxybutyrate dehydrogenase, mitochondrial (EC 1.1.1.30) (3-hydroxybutyrate dehydrogenase) (BDH)	<i>Bdh1</i>	Yes
P63318	Protein kinase C gamma type (PKC-gamma) (EC 2.7.11.13)	<i>Prkcg</i>	Yes
Q60668-4	Heterogeneous nuclear ribonucleoprotein D0 (hnRNP D0) (AU-rich element RNA-binding protein 1)	<i>Hnrnpd</i>	Yes

Q501J6-2	Probable ATP-dependent RNA helicase DDX17 (EC 3.6.4.13) (DEAD box protein 17)	<i>Ddx17</i>	Yes
P11404	Fatty acid-binding protein, heart (Fatty acid-binding protein 3) (Heart-type fatty acid-binding protein) (H-FABP) (Mammary-derived growth inhibitor) (MDGI)	<i>Fabp3</i>	Yes
Q9R0S2	Matrix metalloproteinase-24 (MMP-24) (EC 3.4.24.-) (Matrix metalloproteinase-21) (MMP-21) (Membrane-type matrix metalloproteinase 5) (MT-MMP 5) (MTMMP5) (Membrane-type-5 matrix metalloproteinase) (MT5-MMP) (MT5MMP) [Cleaved into: Processed matrix metalloproteinase-24]	<i>Mmp24</i>	Yes
Q9CQW2	ADP-ribosylation factor-like protein 8B (EC 3.6.5.2) (ADP-ribosylation factor-like protein 10C) (Novel small G protein indispensable for equal chromosome segregation 1)	<i>Arl8b</i>	Yes
P62270	40S ribosomal protein S18 (Ke-3) (Ke3)	<i>Rps18</i>	Yes
P08226	Apolipoprotein E (Apo-E)	<i>ApoE</i>	Yes
Q8BH59	Calcium-binding mitochondrial carrier protein Aralar1 (Mitochondrial aspartate glutamate carrier 1) (Solute carrier family 25 member 12)	<i>Slc25a12</i>	Yes
Q9QYC0-2	Alpha-adducin (Erythrocyte adducin subunit alpha)	<i>Add1</i>	Yes
Q9JLM8-2	Serine/threonine-protein kinase DCLK1 (EC 2.7.11.1) (Doublecortin-like and CAM kinase-like 1) (Doublecortin-like kinase 1)	<i>Dclk1</i>	Yes
Q9DCN2-2	NADH-cytochrome b5 reductase 3 (B5R) (Cytochrome b5 reductase) (EC 1.6.2.2) (Diaphorase-1) [Cleaved into: NADH-cytochrome b5 reductase 3 membrane-bound form; NADH-cytochrome b5 reductase 3 soluble form]	<i>Cyb5r3</i>	Yes
Q61206	Platelet-activating factor acetylhydrolase IB subunit alpha2 (EC 3.1.1.47) (PAF acetylhydrolase 30 kDa subunit) (PAF-AH 30 kDa subunit) (PAF-AH subunit beta) (PAFAH subunit beta)	<i>Pafah1b2</i>	Yes
Q8R1M2	Histone H2A.J (H2a/j)	<i>H2aj</i>	Yes
Q8VDN2	Sodium/potassium-transporting ATPase subunit alpha-1 (Na(+)/K(+)) ATPase alpha-1 subunit (EC 7.2.2.13) (Sodium pump subunit alpha-1)	<i>Atp1a1</i>	Yes
P28481-2	Collagen alpha-1(II) chain (Alpha-1 type II collagen) [Cleaved into: Collagen alpha-1(II) chain; Chondrocalcin]	<i>Col2a1</i>	Yes
Q8C0N2	Glycerol-3-phosphate acyltransferase 3 (GPAT-3) (EC 2.3.1.15) (1-acyl-sn-glycerol-3-phosphate O-acyltransferase 10) (AGPAT 10) (1-acyl-sn-glycerol-3-phosphate O-acyltransferase 9) (1-AGP acyltransferase 9) (1-AGPAT 9) (EC 2.3.1.51) (Acyl-CoA:glycerol-3-phosphate acyltransferase 3) (mGPAT3) (Lysophosphatidic acid acyltransferase theta) (LPAAT-theta)	<i>Gpat3</i>	Yes
P20065-2	Thymosin beta-4 (T beta 4) [Cleaved into: Hematopoietic system regulatory peptide (Seraspenide)]	<i>Tmsb4x</i>	Yes
Q8BSL7	ADP-ribosylation factor 2	<i>Arf2</i>	Yes
O08648-2	Mitogen-activated protein kinase kinase kinase 4 (EC 2.7.11.25) (MAPK/ERK kinase kinase 4) (MEK kinase 4) (MEKK 4)	<i>Map3k4</i>	Yes
P11531	Dystrophin	<i>Dmd</i>	Yes
Q0VBL6-2	Hypoxia-inducible factor 3-alpha (HIF-3-alpha) (HIF3-alpha) (Basic-helix-loop-helix-PAS protein MOP7) (HIF3-alpha-1) (Inhibitory PAS domain protein) (IPAS) (Member of PAS protein 7) (Neonatal and embryonic PAS protein)	<i>Hif3a</i>	Yes

Q9JF6	EF-hand and coiled-coil domain-containing protein 1 (Coiled-coil domain-containing protein 48)	<i>Efcc1</i>	Yes
P84084	ADP-ribosylation factor 5	<i>Arf5</i>	Yes
Q8CG7			
1	Prolyl 3-hydroxylase 2 (EC 1.14.11.7) (Leprecan-like protein 1)	<i>P3h2</i>	Yes
G5E829	Plasma membrane calcium-transporting ATPase 1 (EC 7.2.2.10) (Plasma membrane calcium ATPase isoform 1) (PMCA1) (Plasma membrane calcium pump isoform 1)	<i>Atp2b1</i>	Yes
P27773	Protein disulfide-isomerase A3 (EC 5.3.4.1) (58 kDa glucose-regulated protein) (58 kDa microsomal protein) (p58) (Disulfide isomerase ER-60) (Endoplasmic reticulum resident protein 57) (ER protein 57) (ERp57) (Endoplasmic reticulum resident protein 60) (ER protein 60) (ERp60)	<i>Pdia3</i>	Yes
Q9CZ1	Cytochrome b-c1 complex subunit 1, mitochondrial (Complex III subunit 1) (Core protein I) (Ubiquinol-cytochrome-c reductase complex core protein 1)	<i>Uqcrc1</i>	Yes
3			
P35700	Peroxisiredoxin-1 (EC 1.11.1.24) (Macrophage 23 kDa stress protein) (Osteoblast-specific factor 3) (OSF-3) (Thioredoxin peroxidase 2) (Thioredoxin-dependent peroxide reductase 2) (Thioredoxin-dependent peroxiredoxin 1)	<i>Prdx1</i>	Yes
P18572	Basigin (Basic immunoglobulin superfamily) (HT7 antigen)	<i>Bsg</i>	Yes
-2	(Membrane glycoprotein gp42) (CD antigen CD147)		
P63005	Platelet-activating factor acetylhydrolase IB subunit beta	<i>Pafah1b</i>	
-2	(Lissencephaly-1 protein) (LIS-1) (PAF acetylhydrolase 45 kDa subunit) (PAF-AH 45 kDa subunit) (PAF-AH alpha) (PAFAH alpha)	<i>1</i>	Yes
O88445	Aurora kinase C (EC 2.7.11.1) (Aurora 3) (Aurora/IPL1-related kinase 3) (ARK-3) (Aurora-related kinase 3) (Aurora/IPL1/Eg2 protein 1) (Serine/threonine-protein kinase 13) (Serine/threonine-protein kinase aurora-C)	<i>Aurkc</i>	Yes
A2ASS			
6-3	Titin (EC 2.7.11.1) (Connectin)	<i>Ttn</i>	Yes
O35737	Heterogeneous nuclear ribonucleoprotein H (hnRNP H) [Cleaved into: Heterogeneous nuclear ribonucleoprotein H, N-terminally processed]	<i>Hnrnph</i> <i>1</i>	Yes
P63044	Vesicle-associated membrane protein 2 (VAMP-2) (Synaptobrevin-2)	<i>Vamp2</i>	Yes
P60879	Synaptosomal-associated protein 25 (SNAP-25) (Super protein)		
-2	(SUP) (Synaptosomal-associated 25 kDa protein)	<i>Snap25</i>	Yes
O88597	Beclin-1 (Coiled-coil myosin-like BCL2-interacting protein) [Cleaved into: Beclin-1-C 35 kDa; Beclin-1-C 37 kDa]	<i>Becn1</i>	Yes
Q9CVB	Actin-related protein 2/3 complex subunit 2 (Arp2/3 complex 34 kDa subunit) (p34-ARC)	<i>Arpc2</i>	Yes
6			
P61264	Syntaxin-1B	<i>Stx1b</i>	Yes
Q9CQQ	ATP synthase F(0) complex subunit B1, mitochondrial (ATP synthase peripheral stalk-membrane subunit b) (ATP synthase subunit b)		
7	(ATPase subunit b)	<i>Atp5pb</i>	Yes
Q8CI94	Glycogen phosphorylase, brain form (EC 2.4.1.1)	<i>Pygb</i>	Yes
Q9D05	Pyruvate dehydrogenase E1 component subunit beta, mitochondrial		
1	(PDHE1-B) (EC 1.2.4.1)	<i>Pdhb</i>	Yes

P62821	Ras-related protein Rab-1A (EC 3.6.5.2) (YPT1-related protein)	<i>Rab1A</i>	Yes
P63024	Vesicle-associated membrane protein 3 (VAMP-3) (Cellubrevin) (CEB) (Synaptobrevin-3)	<i>Vamp3</i>	Yes
Q9DCT1	1,5-anhydro-D-fructose reductase (AF reductase) (EC 1.1.1.263) (Aldo-keto reductase family 1 member C-like protein 2) (Aldo-keto reductase family 1 member E1) (Aldo-keto reductase family 1 member E2)	<i>Akr1e2</i>	Yes
Q8K3A2	tRNA 2'-phosphotransferase 1 (mTPT1) (EC 2.7.1.160)	<i>Trpt1</i>	Yes
P59279	Ras-related protein Rab-2B	<i>Rab2b</i>	Yes
P62855	40S ribosomal protein S26	<i>Rps26</i>	Yes
Q9JKD3	Secretory carrier-associated membrane protein 5 (Secretory carrier membrane protein 5)	<i>Scamp5</i>	Yes
Q9WUA3-2	ATP-dependent 6-phosphofructokinase, platelet type (ATP-PFK) (PFK-P) (EC 2.7.1.11) (6-phosphofructokinase type C) (Phosphofructo-1-kinase isozyme C) (PFK-C) (Phosphohexokinase)	<i>Pfkp</i>	Yes
P60766-1	Cell division control protein 42 homolog (EC 3.6.5.2) (G25K GTP-binding protein)	<i>Cdc42</i>	Yes
P31324	cAMP-dependent protein kinase type II-beta regulatory subunit	<i>Prkar2b</i>	Yes
Q9CR57	60S ribosomal protein L14	<i>Rpl14</i>	Yes
P99029-2	Peroxisomal antioxidant enzyme (EC 1.11.1.24) (Antioxidant enzyme B166) (AOEB166) (Liver tissue 2D-page spot 2D-0014IV) (PLP) (Peroxisomal antioxidant enzyme) (Thioredoxin peroxidase PMP20) (Thioredoxin-dependent peroxidase 5)	<i>Prdx5</i>	Yes
Q9QZQ8-2	Core histone macro-H2A.1 (Histone macroH2A1) (mH2A1) (H2A.y) (H2A/y)	<i>Macroh2a1</i>	Yes
Q9JLM8	Serine/threonine-protein kinase DCLK1 (EC 2.7.11.1) (Doublecortin-like and CAM kinase-like 1) (Doublecortin-like kinase 1)	<i>Dclk1</i>	Yes
Q9Z1G4-3	V-type proton ATPase 116 kDa subunit a1 (V-ATPase 116 kDa subunit a1) (Clathrin-coated vesicle/synaptic vesicle proton pump 116 kDa subunit) (Vacuolar adenosine triphosphatase subunit Acl16) (Vacuolar proton pump subunit 1) (Vacuolar proton translocating ATPase 116 kDa subunit a isoform 1)	<i>Atp6v0a1</i>	Yes
Q9Z0E0-2	Neurochondrin (M-Sema F-associating protein of 75 kDa) (Norbin)	<i>Ncdn</i>	Yes
Q64521	Glycerol-3-phosphate dehydrogenase, mitochondrial (GPD-M) (GPDH-M) (EC 1.1.5.3) (Protein TISP38)	<i>Gpd2</i>	Yes
P21956-2	Lactadherin (MFGM) (Milk fat globule-EGF factor 8) (MFG-E8) (SED1) (Sperm surface protein SP47) (MP47)	<i>Mfge8</i>	Yes
P62492	Ras-related protein Rab-11A (Rab-11) (EC 3.6.5.2)	<i>Rab11a</i>	Yes
Q9JJV2-3	Profilin-2 (Profilin II)	<i>Pfn2</i>	Yes
Q9JJI8	60S ribosomal protein L38	<i>Rpl38</i>	Yes
Q9CZM2	60S ribosomal protein L15	<i>Rpl15</i>	Yes

P61089	Ubiquitin-conjugating enzyme E2 N (EC 2.3.2.23) (Bendless-like ubiquitin-conjugating enzyme) (E2 ubiquitin-conjugating enzyme N) (Ubc13) (Ubiquitin carrier protein N) (Ubiquitin-protein ligase N)	<i>Ube2n</i>	Yes
Q99PT1	Rho GDP-dissociation inhibitor 1 (Rho GDI 1) (GDI-1) (Rho-GDI alpha)	<i>Arhgdia</i>	Yes
Q99JY9	Actin-related protein 3 (Actin-like protein 3)	<i>Actr3</i>	Yes
Q9QUI0	Transforming protein RhoA (EC 3.6.5.2)	<i>Rhoa</i>	Yes
Q9QZL6	Ubiquitin carboxyl-terminal hydrolase 21 (EC 3.4.19.12) (Deubiquitinating enzyme 21) (Ubiquitin thioesterase 21) (Ubiquitin-specific-processing protease 21)	<i>Usp21</i>	Yes
P62852	40S ribosomal protein S25	<i>Rps25</i>	Yes
Q8BFR5-2	Elongation factor Tu, mitochondrial	<i>Tufm</i>	Yes
Q9CQA3	Succinate dehydrogenase [ubiquinone] iron-sulfur subunit, mitochondrial (EC 1.3.5.1) (Iron-sulfur subunit of complex II) (Ip) Heterogeneous nuclear ribonucleoprotein A1 (hnRNP A1) (HDP-1) (Helix-destabilizing protein) (Single-strand-binding protein) (Topoisomerase-inhibitor suppressed) (hnRNP core protein A1)	<i>Sdhb</i>	Yes
P49312-2	[Cleaved into: Heterogeneous nuclear ribonucleoprotein A1, N-terminally processed]	<i>Hnrnpa1</i>	Yes
P62908	40S ribosomal protein S3 (EC 4.2.99.18)	<i>Rps3</i>	Yes
Q9CY27	Very-long-chain enoyl-CoA reductase (EC 1.3.1.93) (Synaptic glycoprotein SC2) (Trans-2,3-enoyl-CoA reductase) (TER)	<i>Tecr</i>	Yes
P80317	T-complex protein 1 subunit zeta (TCP-1-zeta) (CCT-zeta-1)	<i>Cct6a</i>	Yes
P59999	Actin-related protein 2/3 complex subunit 4 (Arp2/3 complex 20 kDa subunit) (p20-ARC)	<i>Arpc4</i>	Yes
Q9D855	Cytochrome b-c1 complex subunit 7 (Complex III subunit 7) (Complex III subunit VII) (Ubiquinol-cytochrome c reductase complex 14 kDa protein)	<i>Uqcrb</i>	Yes
P32883-2	GTPase KRas (EC 3.6.5.2) (K-Ras 2) (Ki-Ras) (c-K-ras) (c-Ki-ras) [Cleaved into: GTPase KRas, N-terminally processed]	<i>Kras</i>	Yes
P12382	ATP-dependent 6-phosphofructokinase, liver type (ATP-PFK) (PFK-L) (EC 2.7.1.11) (6-phosphofructokinase type B) (Phosphofructo-1-kinase isozyme B) (PFK-B) (Phosphohexokinase)	<i>Pfkl</i>	Yes
Q9D6U8	Protein FAM162A (E2-induced gene 5 protein homolog) (Growth and transformation-dependent protein) (HGTD-P)	<i>Fam162a</i>	Yes
P12023-2	Amyloid-beta A4 protein (ABPP) (APP) (Alzheimer disease amyloid A4 protein homolog) (Amyloid precursor protein) (Amyloid-beta precursor protein) (Amyloidogenic glycoprotein) (AG) [Cleaved into: N-APP; Soluble APP-alpha (S-APP-alpha); Soluble APP-beta (S-APP-beta); C99 (APP-C99) (Beta-secretase C-terminal fragment) (Beta-CTF); Amyloid-beta protein 42 (Abeta42) (Beta-APP42); Amyloid-beta protein 40 (Abeta40) (Beta-APP40); C83 (Alpha-secretase C-terminal fragment) (Alpha-CTF); P3(42); P3(40); C80; Gamma-secretase C-terminal fragment 59 (APP-C59) (Amyloid intracellular domain 59) (AID(59)) (Gamma-CTF(59)); Gamma-secretase C-terminal fragment 57 (APP-C57) (Amyloid intracellular domain 57) (AID(57)) (Gamma-CTF(57)); Gamma-secretase C-	<i>App</i>	Yes

	terminal fragment 50 (Amyloid intracellular domain 50) (AID(50)) (Gamma-CTF(50)); C31]		
P62754	40S ribosomal protein S6 (Phosphoprotein NP33)	<i>Rps6</i>	Yes
Q7TQI 3	Ubiquitin thioesterase OTUB1 (EC 3.4.19.12) (Deubiquitinating enzyme OTUB1) (OTU domain-containing ubiquitin aldehyde-binding protein 1) (Otubain-1) (Ubiquitin-specific-processing protease OTUB1)	<i>Otub1</i>	Yes
Q6PD M2-3	Serine/arginine-rich splicing factor 1 (ASF/SF2) (Pre-mRNA-splicing factor SRp30a) (Splicing factor, arginine/serine-rich 1)	<i>Srsf1</i>	Yes
Q8BL0 6	Inactive ubiquitin carboxyl-terminal hydrolase 54 (Inactive ubiquitin-specific peptidase 54)	<i>Usp54</i>	Yes
P09671	Superoxide dismutase [Mn], mitochondrial (EC 1.15.1.1)	<i>Sod2</i>	Yes
P80315	T-complex protein 1 subunit delta (TCP-1-delta) (A45) (CCT-delta) Cytochrome b-c1 complex subunit Rieske, mitochondrial (EC 7.1.1.8) (Complex III subunit 5) (Cytochrome b-c1 complex subunit 5) (Rieske iron-sulfur protein) (RISP) (Rieske protein UQCRFS1) (Ubiquinol-cytochrome c reductase iron-sulfur subunit) [Cleaved into: Cytochrome b-c1 complex subunit 9 (Su9) (Subunit 9) (8 kDa subunit 9) (Complex III subunit IX) (Cytochrome b-c1 complex subunit 11) (UQCRFS1 mitochondrial targeting sequence) (UQCRFS1 MTS) (Ubiquinol-cytochrome c reductase 8 kDa protein)]	<i>Cct4</i>	Yes
Q9CR6 8	Actin, cytoplasmic 1 (Beta-actin) [Cleaved into: Actin, cytoplasmic 1, N-terminally processed]	<i>Uqcrcfs1</i>	Yes
P60710 Q8BFZ 3	Beta-actin-like protein 2 (Kappa-actin)	<i>Actb</i>	Yes
P84228 P03995 -2	Histone H3.2 (H3-clustered histone 13) (H3-clustered histone 14) (H3-clustered histone 15) (H3-clustered histone 2) (H3-clustered histone 3) (H3-clustered histone 4) (H3-clustered histone 6) (H3-clustered histone 7)	<i>Actb12</i>	Yes
Q9Z0U 1	Glial fibrillary acidic protein (GFAP)	<i>H3c2</i>	Yes
A2ASS 6-2	Tight junction protein ZO-2 (Tight junction protein 2) (Zona occludens protein 2) (Zonula occludens protein 2)	<i>Gfap</i>	Yes
P10637 -5	Titin (EC 2.7.11.1) (Connectin)	<i>Tjp2</i>	Yes
Q8BRV 5	Microtubule-associated protein tau (Neurofibrillary tangle protein) (Paired helical filament-tau) (PHF-tau)	<i>Ttn</i>	Yes
Q9WTI 7-4	Uncharacterized protein KIAA1671	<i>Mapt</i> <i>Kiaa1671</i>	Yes
Q9JHE 3	Unconventional myosin-Ic (Myosin I beta) (MMI-beta) (MMIb) Neutral ceramidase (N-CDase) (NCDase) (EC 3.5.1.-) (EC 3.5.1.23) (Acylsphingosine deacylase 2) (N-acylsphingosine amidohydrolase 2) [Cleaved into: Neutral ceramidase soluble form]	<i>Myo1c</i>	Yes
Q9CR8 4	ATP synthase F(0) complex subunit C1, mitochondrial (ATP synthase lipid-binding protein) (ATP synthase membrane subunit c locus 1) (ATP synthase proteolipid P1) (ATPase protein 9) (ATPase subunit c)	<i>Asah2</i>	Yes
Q8CHG 3	GRIP and coiled-coil domain-containing protein 2 (185 kDa Golgi coiled-coil protein) (GCC185)	<i>Atp5mc</i> <i>1</i>	Yes
		<i>Gcc2</i>	Yes

P62897	Cytochrome c, somatic	<i>Cycc</i>	Yes
Q9QYF9	Protein NDRG3 (N-myc downstream-regulated gene 3 protein) (Protein Ndr3)	<i>Ndr3</i>	Yes
P11983-2	T-complex protein 1 subunit alpha (TCP-1-alpha) (CCT-alpha) (Tailless complex polypeptide 1A) (TCP-1-A) (Tailless complex polypeptide 1B) (TCP-1-B)	<i>Tcp1</i>	Yes
Q5DU05-2	Centrosomal protein of 164 kDa (Cep164)	<i>Cep164</i>	Yes
P19783	Cytochrome c oxidase subunit 4 isoform 1, mitochondrial (Cytochrome c oxidase polypeptide IV) (Cytochrome c oxidase subunit IV isoform 1) (COX IV-1)	<i>Cox4i1</i>	Yes
P24369	Peptidyl-prolyl cis-trans isomerase B (PPIase B) (EC 5.2.1.8) (CYP-S1) (Cyclophilin B) (Rotamase B) (S-cyclophilin) (SCYLP)	<i>Ppib</i>	Yes
P61164	Alpha-centractin (Centractin) (ARP1) (Actin-RPV) (Centrosome-associated actin homolog)	<i>Actr1a</i>	Yes
Q7TM B8-2	Cytoplasmic FMR1-interacting protein 1 (Specifically Rac1-associated protein 1) (Sra-1)	<i>Cyfp1</i>	Yes
Q8K2C9	Very-long-chain (3R)-3-hydroxyacyl-CoA dehydratase 3 (EC 4.2.1.134) (3-hydroxyacyl-CoA dehydratase 3) (HACD3) (Butyrate-induced protein 1) (B-ind1) (Protein-tyrosine phosphatase-like A domain-containing protein 1)	<i>Hacd3</i>	Yes
P63028	Translationally-controlled tumor protein (TCTP) (21 kDa polypeptide) (p21) (p23)	<i>Tpt1</i>	Yes
Q8CAQ8-3	MICOS complex subunit Mic60 (Mitochondrial inner membrane protein) (Mitofilin)	<i>Immt</i>	Yes
P35980	60S ribosomal protein L18	<i>Rpl18</i>	Yes
Q8JZU2	Tricarboxylate transport protein, mitochondrial (Citrate transport protein) (CTP) (Solute carrier family 25 member 1) (Tricarboxylate carrier protein)	<i>Slc25a1</i>	Yes
Q68FL4-2	Putative adenosylhomocysteinase 3 (AdoHcyase 3) (EC 3.3.1.1) (Long-IRBIT) (S-adenosyl-L-homocysteine hydrolase 3) (S-adenosylhomocysteine hydrolase-like protein 2)	<i>Ahcy12</i>	Yes
Q9D6R2-2	Isocitrate dehydrogenase [NAD] subunit alpha, mitochondrial (EC 1.1.1.41) (Isocitric dehydrogenase subunit alpha) (NAD(+)-specific ICDH subunit alpha)	<i>Idh3a</i>	Yes
Q9CZD3	Glycine--tRNA ligase (EC 6.1.1.14) (Diadenosine tetraphosphate synthetase) (Ap4A synthetase) (EC 2.7.7.-) (Glycyl-tRNA synthetase 1) (GlyRS)	<i>Gars1</i>	Yes
O08807	Peroxiredoxin-4 (EC 1.11.1.24) (Antioxidant enzyme AOE372) (Peroxiredoxin IV) (Prx-IV) (Thioredoxin peroxidase AO372) (Thioredoxin-dependent peroxide reductase A0372) (Thioredoxin-dependent peroxiredoxin 4)	<i>Prdx4</i>	Yes
Q2PFD7-3	PH and SEC7 domain-containing protein 3 (Exchange factor for ADP-ribosylation factor guanine nucleotide factor 6 D) (Exchange factor for ARF6 D) (Pleckstrin homology and SEC7 domain-containing protein 3)	<i>Psd3</i>	Yes
Q9DBE8	Alpha-1,3/1,6-mannosyltransferase ALG2 (EC 2.4.1.132) (EC 2.4.1.257) (Asparagine-linked glycosylation protein 2 homolog) (GDP-Man:Man(1)GlcNAc(2)-PP-Dol alpha-1,3-	<i>Alg2</i>	Yes

	mannosyltransferase) (GDP-Man:Man(1)GlcNAc(2)-PP-dolichol mannosyltransferase) (GDP-Man:Man(2)GlcNAc(2)-PP-Dol alpha-1,6-mannosyltransferase)		
	AP-2 complex subunit mu (AP-2 mu chain) (Adaptor protein complex AP-2 subunit mu) (Adaptor-related protein complex 2 subunit mu) (Clathrin assembly protein complex 2 mu medium chain) (Clathrin coat assembly protein AP50) (Clathrin coat-associated protein AP50)		
P84091	(Mu2-adaptin) (Plasma membrane adaptor AP-2 50 kDa protein)	<i>Ap2m1</i>	Yes
O35143	ATPase inhibitor, mitochondrial (ATP synthase F1 subunit epsilon) (Inhibitor of F(1)F(o)-ATPase) (IF(1)) (IF1)	<i>Atp5if1</i>	Yes
P32037	Solute carrier family 2, facilitated glucose transporter member 3 (Glucose transporter type 3, brain) (GLUT-3)	<i>Slc2a3</i>	Yes
P47857	ATP-dependent 6-phosphofructokinase, muscle type (ATP-PFK) (PFK-M) (EC 2.7.1.11) (6-phosphofructokinase type A) (Phosphofructo-1-kinase isozyme A) (PFK-A) (Phosphohexokinase)	<i>Pfkm</i>	Yes
Q8VCB			
3	Glycogen [starch] synthase, liver (EC 2.4.1.11)	<i>Gys2</i>	Yes
P62918	60S ribosomal protein L8	<i>Rpl8</i>	Yes
	Lysosome membrane protein 2 (85 kDa lysosomal membrane sialoglycoprotein) (LGP85) (Lysosome membrane protein II) (LIMP II) (Scavenger receptor class B member 2)		
O35114		<i>Scarb2</i>	Yes
Q62425	Cytochrome c oxidase subunit NDUF4A	<i>Ndufa4</i>	Yes
P21279	Guanine nucleotide-binding protein G(q) subunit alpha (Guanine nucleotide-binding protein alpha-q)	<i>Gnaq</i>	Yes
O54901	OX-2 membrane glycoprotein (MRC OX-2 antigen) (CD antigen CD200)	<i>Cd200</i>	Yes
P63330	Serine/threonine-protein phosphatase 2A catalytic subunit alpha isoform (PP2A-alpha) (EC 3.1.3.16)	<i>Ppp2ca</i>	Yes
	AP-2 complex subunit alpha-2 (100 kDa coated vesicle protein C) (Adaptor protein complex AP-2 subunit alpha-2) (Adaptor-related protein complex 2 subunit alpha-2) (Alpha-adaptin C) (Alpha2-adaptin) (Clathrin assembly protein complex 2 alpha-C large chain)		
P17427	(Plasma membrane adaptor HA2/AP2 adaptin alpha C subunit)	<i>Ap2a2</i>	Yes
P14148	60S ribosomal protein L7	<i>Rpl7</i>	Yes
Q9CX			
W4	60S ribosomal protein L11	<i>Rpl11</i>	Yes
	Proteasome subunit alpha type-6 (Macropain iota chain)		
Q9QU	(Multicatalytic endopeptidase complex iota chain) (Proteasome iota chain)	<i>Psm6</i>	Yes
M9			
Q3UU	GPI inositol-deacylase (EC 3.1.-.-) (Post-GPI attachment to proteins factor 1)	<i>Pgap1</i>	Yes
Q7			
	Guanine nucleotide-binding protein subunit alpha-11 (G alpha-11)		
P21278	(G-protein subunit alpha-11)	<i>Gna11</i>	Yes
	26S proteasome non-ATPase regulatory subunit 2 (26S proteasome regulatory subunit RPN1) (26S proteasome regulatory subunit S2)		
Q8VD			
M4	(26S proteasome subunit p97)	<i>Psm2</i>	Yes
Q9CQI			
3	Glia maturation factor beta (GMF-beta)	<i>Gmfb</i>	Yes

Q9DC				
W4	Electron transfer flavoprotein subunit beta (Beta-ETF)	<i>Etfb</i>	Yes	
P70268	Serine/threonine-protein kinase N1 (EC 2.7.11.13) (Protein kinase C-like 1) (Protein kinase C-like PKN) (Protein-kinase C-related kinase 1) (Serine-threonine protein kinase N)	<i>Pkn1</i>	Yes	
O70503	Very-long-chain 3-oxoacyl-CoA reductase (EC 1.1.1.330) (17-beta-hydroxysteroid dehydrogenase 12) (17-beta-HSD 12) (3-ketoacyl-CoA reductase) (KAR) (Estradiol 17-beta-dehydrogenase 12) (EC 1.1.1.62) (KIK-I)	<i>Hsd17b12</i>	Yes	
P14115	60S ribosomal protein L27a (L29)	<i>Rpl27a</i>	Yes	
P47754	F-actin-capping protein subunit alpha-2 (CapZ alpha-2)	<i>Capza2</i>	Yes	
O70133	ATP-dependent RNA helicase A (EC 3.6.4.13) (DEAH box protein 9) (mHEL-5) (Nuclear DNA helicase II) (NDH II) (RNA helicase A) (RHA)	<i>Dhx9</i>	Yes	
P14131	40S ribosomal protein S16	<i>Rps16</i>	Yes	
O88342	WD repeat-containing protein 1 (Actin-interacting protein 1) (AIP1)	<i>Wdr1</i>	Yes	
Q9D6J6	NADH dehydrogenase [ubiquinone] flavoprotein 2, mitochondrial (EC 7.1.1.2) (NADH-ubiquinone oxidoreductase 24 kDa subunit)	<i>Ndufv2</i>	Yes	
Q9D2G	Dihydrolipoyllysine-residue succinyltransferase component of 2-oxoglutarate dehydrogenase complex, mitochondrial (EC 2.3.1.61) (2-oxoglutarate dehydrogenase complex component E2) (OGDC-E2) (Dihydrolipoamide succinyltransferase component of 2-oxoglutarate dehydrogenase complex) (E2K)	<i>Dlst</i>	Yes	
Q61205	Platelet-activating factor acetylhydrolase IB subunit alpha1 (EC 3.1.1.47) (PAF acetylhydrolase 29 kDa subunit) (PAF-AH 29 kDa subunit) (PAF-AH subunit gamma) (PAFAH subunit gamma)	<i>Pafah1b3</i>	Yes	
P56395	Cytochrome b5	<i>Cyb5a</i>	Yes	
Q8C8R				
3-2	Ankyrin-2 (ANK-2) (Ankyrin-B) (Brain ankyrin)	<i>Ank2</i>	Yes	
Q91X9				
7	Neurocalcin-delta	<i>Ncald</i>	Yes	
Q99JR1	Sideroflexin-1	<i>Sfxn1</i>	Yes	
O35526	Syntaxin-1A (Neuron-specific antigen HPC-1)	<i>Stx1a</i>	No	
P48771	Cytochrome c oxidase subunit 7A2, mitochondrial (Cytochrome c oxidase subunit VIIa-liver/heart) (Cytochrome c oxidase subunit VIIa-L)	<i>Cox7a2</i>	No	
Q9DB77	Cytochrome b-c1 complex subunit 2, mitochondrial (Complex III subunit 2) (Core protein II) (Ubiquinol-cytochrome-c reductase complex core protein 2)	<i>Uqcrc2</i>	No	
Q9DCT	NADH dehydrogenase [ubiquinone] iron-sulfur protein 3, mitochondrial (EC 7.1.1.2) (Complex I-30kD) (CI-30kD) (NADH-ubiquinone oxidoreductase 30 kDa subunit)	<i>Ndufs3</i>	No	
2				
Q3UH				
K8	Trinucleotide repeat-containing gene 6A protein	<i>Tnrc6a</i>	No	
Q61301				
-2	Catenin alpha-2 (Alpha N-catenin)	<i>Ctnna2</i>	No	
Q922R	Protein disulfide-isomerase A6 (EC 5.3.4.1) (Thioredoxin domain-containing protein 7)	<i>Pdia6</i>	No	
8				
P19536	Cytochrome c oxidase subunit 5B, mitochondrial (Cytochrome c oxidase polypeptide Vb)	<i>Cox5b</i>	No	

P51863 Q3UH A3	V-type proton ATPase subunit d 1 (V-ATPase subunit d 1) (P39) (Physophilin) (V-ATPase 40 kDa accessory protein) (V-ATPase AC39 subunit) (Vacuolar proton pump subunit d 1)	<i>Atp6v0d 1</i>	No
Q8BRB 7-2 Q9QY X7-2	Spatacsin (Spastic paraplegia 11 protein homolog) Histone acetyltransferase KAT6B (EC 2.3.1.48) (MOZ, YBF2/SAS3, SAS2 and TIP60 protein 4) (MYST-4) (Protein querkopf) Protein piccolo (Aczonin) (Brain-derived HLMN protein) (Multidomain presynaptic cytomatrix protein)	<i>Spg11</i> <i>Kat6b</i> <i>Pclo</i>	No No No
P62242	40S ribosomal protein S8	<i>Rps8</i>	No
Q148V 7-3 Q9DA7 3	RAB11-binding protein RELCH (LisH domain and HEAT repeat- containing protein KIAA1468) (RAB11-binding protein containing LisH, coiled-coil, and HEAT repeats) Coiled-coil domain-containing protein 89 (Bc8 orange-interacting protein)	<i>Relch</i> <i>Ccdc89</i>	No No
Q9Z179	SHC SH2 domain-binding protein 1 (Protein expressed in activated lymphocytes) (mPAL) (SHC-binding protein)	<i>Shcbp1</i>	No
P10922	Histone H1.0 (Histone H1') (Histone H1(0)) (MyD196) [Cleaved into: Histone H1.0, N-terminally processed]	<i>H1-0</i>	No
P12970	60S ribosomal protein L7a (Surfeit locus protein 3) Dipeptidase 3 (EC 3.4.13.19) (Membrane-bound dipeptidase 3)	<i>Rpl7a</i>	No
Q9DA7 9	(MBD-3) (Protein expressed in male leptotene and zygotene spermatocytes 136) (MLZ-136)	<i>Dpep3</i>	No

Bibliography

1. Tyanova, S.; Temu, T.; Cox, J., The MaxQuant computational platform for mass spectrometry-based shotgun proteomics. *Nature Protocols* **2016**, *11* (12), 2301-2319.
2. Kim, M. S.; Pinto, S. M.; Getnet, D.; Nirujogi, R. S.; Manda, S. S.; Chaerkady, R.; Madugundu, A. K.; Kelkar, D. S.; Isserlin, R.; Jain, S.; Thomas, J. K.; Muthusamy, B.; Leal-Rojas, P.; Kumar, P.; Sahasrabudde, N. A.; Balakrishnan, L.; Advani, J.; George, B.; Renuse, S.; Selvan, L. D.; Patil, A. H.; Nanjappa, V.; Radhakrishnan, A.; Prasad, S.; Subbannayya, T.; Raju, R.; Kumar, M.; Sreenivasamurthy, S. K.; Marimuthu, A.; Sathe, G. J.; Chavan, S.; Datta, K. K.; Subbannayya, Y.; Sahu, A.; Yelamanchi, S. D.; Jayaram, S.; Rajagopalan, P.; Sharma, J.; Murthy, K. R.; Syed, N.; Goel, R.; Khan, A. A.; Ahmad, S.; Dey, G.; Mudgal, K.; Chatterjee, A.; Huang, T. C.; Zhong, J.; Wu, X.; Shaw, P. G.; Freed, D.; Zahari, M. S.; Mukherjee, K. K.; Shankar, S.; Mahadevan, A.; Lam, H.; Mitchell, C. J.; Shankar, S. K.; Satishchandra, P.; Schroeder, J. T.; Sirdeshmukh, R.; Maitra, A.; Leach, S. D.; Drake, C. G.; Halushka, M. K.; Prasad, T. S.; Hruban, R. H.; Kerr, C. L.; Bader, G. D.; Iacobuzio-Donahue, C. A.; Gowda, H.; Pandey, A., A draft map of the human proteome. *Nature* **2014**, *509* (7502), 575-81.
3. Wishart, D. S.; Feunang, Y. D.; Marcu, A.; Guo, A. C.; Liang, K.; Vázquez-Fresno, R.; Sajed, T.; Johnson, D.; Li, C.; Karu, N.; Sayeeda, Z.; Lo, E.; Assempour, N.; Berjanskii, M.; Singhal, S.; Arndt, D.; Liang, Y.; Badran, H.; Grant, J.; Serra-Cayuela, A.; Liu, Y.; Mandal, R.; Neveu, V.; Pon, A.; Knox, C.; Wilson, M.; Manach, C.; Scalbert, A., HMDB 4.0: the human metabolome database for 2018. *Nucleic acids research* **2018**, *46* (D1), D608-d617.
4. Eberwine, J.; Sul, J. Y.; Bartfai, T.; Kim, J., The promise of single-cell sequencing. *Nature methods* **2014**, *11* (1), 25-7.
5. Blainey, P. C.; Quake, S. R., Dissecting genomic diversity, one cell at a time. *Nature methods* **2014**, *11* (1), 19-21.
6. Yuan, G. C.; Cai, L.; Elowitz, M.; Enver, T.; Fan, G.; Guo, G.; Irizarry, R.; Kharchenko, P.; Kim, J.; Orkin, S.; Quackenbush, J.; Saadatpour, A.; Schroeder, T.; Shivdasani, R.; Tirosh, I., Challenges and emerging directions in single-cell analysis. *Genome biology* **2017**, *18* (1), 84.
7. Klein, A. M.; Mazutis, L.; Akartuna, I.; Tallapragada, N.; Veres, A.; Li, V.; Peshkin, L.; Weitz, D. A.; Kirschner, M. W., Droplet barcoding for single-cell transcriptomics applied to embryonic stem cells. *Cell* **2015**, *161* (5), 1187-1201.
8. Briggs, J. A.; Weinreb, C.; Wagner, D. E.; Megason, S.; Peshkin, L.; Kirschner, M. W.; Klein, A. M., The dynamics of gene expression in vertebrate embryogenesis at single-cell resolution. *Science (New York, N.Y.)* **2018**, *360* (6392).
9. Lombard-Banek, C.; Moody, S. A.; Nemes, P., Single-cell mass spectrometry for discovery proteomics: Quantifying translational cell heterogeneity in the 16-cell frog (*Xenopus*) embryo. *Angewandte Chemie (International ed. in English)* **2016**, *55* (7), 2454-8.
10. Cong, Y.; Motamedchaboki, K.; Misal, S. A.; Liang, Y.; Guise, A. J.; Truong, T.; Huguet, R.; Plowey, E. D.; Zhu, Y.; Lopez-Ferrer, D.; Kelly, R. T., Ultrasensitive single-cell proteomics workflow identifies >1000 protein groups per mammalian cell. *bioRxiv* **2020**, 2020.06.03.132449.
11. Wilson, R. S.; Nairn, A. C., Cell-type-specific proteomics: A neuroscience perspective. *Proteomes* **2018**, *6* (4), 51.
12. Qi, M.; Philip, M. C.; Yang, N.; Sweedler, J. V., Single cell neurometabolomics. *ACS chemical neuroscience* **2018**, *9* (1), 40-50.

13. Zhu, H.; Zou, G.; Wang, N.; Zhuang, M.; Xiong, W.; Huang, G., Single-neuron identification of chemical constituents, physiological changes, and metabolism using mass spectrometry. *Proceedings of the National Academy of Sciences* **2017**, *114* (10), 2586-2591.
14. Vogel, C.; Marcotte, E. M., Insights into the regulation of protein abundance from proteomic and transcriptomic analyses. *Nature reviews. Genetics* **2012**, *13* (4), 227-32.
15. Peshkin, L.; Wühr, M.; Pearl, E.; Haas, W.; Freeman, R. M., Jr.; Gerhart, J. C.; Klein, A. M.; Horb, M.; Gygi, S. P.; Kirschner, M. W., On the relationship of protein and mRNA dynamics in vertebrate embryonic development. *Developmental cell* **2015**, *35* (3), 383-94.
16. Larsen, M. R.; Trelle, M. B.; Thingholm, T. E.; Jensen, O. N., Analysis of posttranslational modifications of proteins by tandem mass spectrometry. *BioTechniques* **2006**, *40* (6), 790-798.
17. Han, X.; Aslanian, A.; Yates, J. R., 3rd, Mass spectrometry for proteomics. *Curr Opin Chem Biol* **2008**, *12* (5), 483-490.
18. Beck, M.; Claassen, M.; Aebersold, R., Comprehensive proteomics. *Current opinion in biotechnology* **2011**, *22* (1), 3-8.
19. Nagaraj, N.; Wisniewski, J. R.; Geiger, T.; Cox, J.; Kircher, M.; Kelso, J.; Pääbo, S.; Mann, M., Deep proteome and transcriptome mapping of a human cancer cell line. *Molecular systems biology* **2011**, *7*, 548.
20. Wilhelm, M.; Schlegl, J.; Hahne, H.; Gholami, A. M.; Lieberenz, M.; Savitski, M. M.; Ziegler, E.; Butzmann, L.; Gessulat, S.; Marx, H.; Mathieson, T.; Lemeer, S.; Schnatbaum, K.; Reimer, U.; Wenschuh, H.; Mollenhauer, M.; Slotta-Huspenina, J.; Boese, J.-H.; Bantscheff, M.; Gerstmair, A.; Faerber, F.; Kuster, B., Mass-spectrometry-based draft of the human proteome. *Nature* **2014**, *509* (7502), 582-587.
21. Geiger, T.; Velic, A.; Macek, B.; Lundberg, E.; Kampf, C.; Nagaraj, N.; Uhlen, M.; Cox, J.; Mann, M., Initial quantitative proteomic map of 28 mouse tissues using the SILAC mouse. *Molecular & Cellular Proteomics* **2013**, *12* (6), 1709-1722.
22. Wühr, M.; Freeman, R. M., Jr.; Presler, M.; Horb, M. E.; Peshkin, L.; Gygi, S.; Kirschner, M. W., Deep proteomics of the *Xenopus laevis* egg using an mRNA-derived reference database. *Current biology : CB* **2014**, *24* (13), 1467-1475.
23. Lombard-Banek, C.; Moody, S. A.; Manzini, M. C.; Nemes, P., Microsampling capillary electrophoresis mass spectrometry enables single-cell proteomics in complex tissues: Developing cell clones in live *xenopus laevis* and zebrafish embryos. *Analytical chemistry* **2019**, *91* (7), 4797-4805.
24. Lombard-Banek, C.; Choi, S. B.; Nemes, P., Chapter Thirteen - Single-cell proteomics in complex tissues using microprobe capillary electrophoresis mass spectrometry. In *Methods in Enzymology*, Allbritton, N. L.; Kovarik, M. L., Eds. Academic Press: 2019; Vol. 628, pp 263-292.
25. Budnik, B.; Levy, E.; Harmange, G.; Slavov, N., SCoPE-MS: mass spectrometry of single mammalian cells quantifies proteome heterogeneity during cell differentiation. *Genome biology* **2018**, *19* (1), 161.
26. Thompson, A.; Schäfer, J.; Kuhn, K.; Kienle, S.; Schwarz, J.; Schmidt, G.; Neumann, T.; Johnstone, R.; Mohammed, A. K.; Hamon, C., Tandem mass tags: a novel quantification strategy for comparative analysis of complex protein mixtures by MS/MS. *Analytical chemistry* **2003**, *75* (8), 1895-904.

27. Lombard-Banek, C.; Moody, S. A.; Nemes, P., Single-cell mass spectrometry for discovery proteomics: Quantifying translational cell heterogeneity in the 16-cell frog (*Xenopus*) embryo. *Angewandte Chemie International Edition* **2016**, *55* (7), 2454-2458.
28. Lombard-Banek, C.; Reddy, S.; Moody, S. A.; Nemes, P., Label-free quantification of proteins in single embryonic cells with neural fate in the cleavage-stage frog (*Xenopus laevis*) embryo using capillary electrophoresis electrospray ionization high-resolution mass spectrometry (CE-ESI-HRMS). *Molecular & Cellular Proteomics* **2016**, *15* (8), 2756-2768.
29. Choi, S. B.; Lombard-Banek, C.; Munoz-Llancao, P.; Manzini, M. C.; Nemes, P., Enhanced peptide detection toward single-neuron proteomics by reversed-phase fractionation capillary electrophoresis mass spectrometry. *J. Am. Soc. Mass Spectrom.* **2018**, *29* (5), 913-922.
30. Choi, S. B.; Zamarbide, M.; Manzini, M. C.; Nemes, P., Tapered-tip capillary electrophoresis nano-electrospray ionization mass spectrometry for ultrasensitive proteomics: the mouse cortex. *J. Am. Soc. Mass Spectrom.* **2017**, *28* (4), 597-607.
31. Zhang, Y.; Fonslow, B. R.; Shan, B.; Baek, M.-C.; Yates, J. R., Protein analysis by shotgun/bottom-up proteomics. *Chemical Reviews* **2013**, *113* (4), 2343-2394.
32. Yates, J. R., The revolution and evolution of shotgun proteomics for large-scale proteome analysis. *Journal of the American Chemical Society* **2013**, *135* (5), 1629-1640.
33. Washburn, M. P.; Wolters, D.; Yates, J. R., Large-scale analysis of the yeast proteome by multidimensional protein identification technology. *Nature Biotechnology* **2001**, *19* (3), 242-247.
34. Wolters, D. A.; Washburn, M. P.; Yates, J. R., An automated multidimensional protein identification technology for shotgun proteomics. *Analytical chemistry* **2001**, *73* (23), 5683-5690.
35. Gilar, M.; Olivova, P.; Daly, A. E.; Gebler, J. C., Two-dimensional separation of peptides using RP-RP-HPLC system with different pH in first and second separation dimensions. *Journal of separation science* **2005**, *28* (14), 1694-703.
36. Thompson, A.; Schäfer, J.; Kuhn, K.; Kienle, S.; Schwarz, J.; Schmidt, G.; Neumann, T.; Hamon, C., Tandem mass tags: a novel quantification strategy for comparative analysis of complex protein mixtures by MS/MS. *Analytical chemistry* **2003**, *75* (8), 1895-1904.
37. Ross, P. L.; Huang, Y. N.; Marchese, J. N.; Williamson, B.; Parker, K.; Hattan, S.; Khainovski, N.; Pillai, S.; Dey, S.; Daniels, S.; Purkayastha, S.; Juhasz, P.; Martin, S.; Bartlett-Jones, M.; He, F.; Jacobson, A.; Pappin, D. J., Multiplexed protein quantitation in *Saccharomyces cerevisiae* using amine-reactive isobaric tagging reagents. *Molecular & cellular proteomics : MCP* **2004**, *3* (12), 1154-69.
38. Frost, D. C.; Greer, T.; Li, L., High-resolution enabled 12-plex IiLeu isobaric tags for quantitative proteomics. *Analytical chemistry* **2015**, *87* (3), 1646-1654.
39. Cox, J.; Neuhauser, N.; Michalski, A.; Scheltema, R. A.; Olsen, J. V.; Mann, M., Andromeda: A peptide search engine Integrated into the MaxQuant environment. *J. Proteome Res.* **2011**, *10* (4), 1794-1805.
40. Cox, J.; Mann, M., MaxQuant enables high peptide identification rates, individualized p.p.b.-range mass accuracies and proteome-wide protein quantification. *Nature Biotechnology* **2008**, *26* (12), 1367-1372.
41. Altschuler, S. J.; Wu, L. F., Cellular heterogeneity: do differences make a difference? *Cell* **2010**, *141* (4), 559-63.

42. Booker, S. A.; Song, J.; Vida, I., Whole-cell patch-clamp recordings from morphologically- and neurochemically-identified hippocampal interneurons. *J. Vis. Exp.* **2014**, *91*, 1-11.
43. Cahoy, J. D.; Emery, B.; Kaushal, A.; Foo, L. C.; Zamanian, J. L.; Christopherson, K. S.; Xing, Y.; Lubischer, J. L.; Krieg, P. A.; Krupenko, S. A.; Thompson, W. J.; Barres, B. A., A transcriptome database for astrocytes, neurons, and oligodendrocytes: A new resource for understanding brain development and function. *J. Neurosci.* **2008**, *28* (1), 264-278.
44. Doyle, J. P.; Dougherty, J. D.; Heiman, M.; Schmidt, E. F.; Stevens, T. R.; Ma, G. J.; Bupp, S.; Shrestha, P.; Shah, R. D.; Doughty, M. L.; Gong, S. C.; Greengard, P.; Heintz, N., Application of a translational profiling approach for the comparative analysis of CNS cell types *Cell* **2009**, *139* (5), 1022-1022.
45. Kang, H. J.; Kawasawa, Y. I.; Cheng, F.; Zhu, Y.; Xu, X. M.; Li, M. F.; Sousa, A. M. M.; Pletikos, M.; Meyer, K. A.; Sedmak, G.; Guennel, T.; Shin, Y.; Johnson, M. B.; Krsnik, Z.; Mayer, S.; Fertuzinhos, S.; Umlauf, S.; Lisgo, S. N.; Vortmeyer, A.; Weinberger, D. R.; Mane, S.; Hyde, T. M.; Huttner, A.; Reimers, M.; Kleinman, J. E.; Sestan, N., Spatio-temporal transcriptome of the human brain. *Nature* **2011**, *478* (7370), 483-489.
46. Beck, M.; Schmidt, A.; Malmstroem, J.; Claassen, M.; Ori, A.; Szymborska, A.; Herzog, F.; Rinner, O.; Ellenberg, J.; Aebersold, R., The quantitative proteome of a human cell line. *Molecular systems biology* **2011**, *7*, 1-8.
47. Kim, M. S.; Pinto, S. M.; Getnet, D.; Nirujogi, R. S.; Manda, S. S.; Chaerkady, R.; Madugundu, A. K.; Kelkar, D. S.; Isserlin, R.; Jain, S.; Thomas, J. K.; Muthusamy, B.; Leal-Rojas, P.; Kumar, P.; Sahasrabudhe, N. A.; Balakrishnan, L.; Advani, J.; George, B.; Renuse, S.; Selvan, L. D. N.; Patil, A. H.; Nanjappa, V.; Radhakrishnan, A.; Prasad, S.; Subbannayya, T.; Raju, R.; Kumar, M.; Sreenivasamurthy, S. K.; Marimuthu, A.; Sathe, G. J.; Chavan, S.; Datta, K. K.; Subbannayya, Y.; Sahu, A.; Yelamanchi, S. D.; Jayaram, S.; Rajagopalan, P.; Sharma, J.; Murthy, K. R.; Syed, N.; Goel, R.; Khan, A. A.; Ahmad, S.; Dey, G.; Mudgal, K.; Chatterjee, A.; Huang, T. C.; Zhong, J.; Wu, X. Y.; Shaw, P. G.; Freed, D.; Zahari, M. S.; Mukherjee, K. K.; Shankar, S.; Mahadevan, A.; Lam, H.; Mitchell, C. J.; Shankar, S. K.; Satishchandra, P.; Schroeder, J. T.; Sirdeshmukh, R.; Maitra, A.; Leach, S. D.; Drake, C. G.; Halushka, M. K.; Prasad, T. S. K.; Hruban, R. H.; Kerr, C. L.; Bader, G. D.; Iacobuzio-Donahue, C. A.; Gowda, H.; Pandey, A., A draft map of the human proteome. *Nature* **2014**, *509* (7502), 575-581.
48. Sharma, K.; Schmitt, S.; Bergner, C. G.; Tyanova, S.; Kannaiyan, N.; Manrique-Hoyos, N.; Kongi, K.; Cantuti, L.; Hanisch, U.-K.; Philips, M.-A.; Rossner, M. J.; Mann, M.; Simons, M., Cell type- and brain region-resolved mouse brain proteome. *Nat. Neurosci.* **2015**, *18*, 1819-1831.
49. Wang, Y.; Fonslow, B. R.; Wong, C. C. L.; Nakorchevsky, A.; Yates, J. R., Improving the comprehensiveness and sensitivity of sheath less capillary electrophoresis-tandem mass spectrometry for proteomic analysis. *Anal. Chem.* **2012**, *84* (20), 8505-8513.
50. Chen, Q.; Yan, G. Q.; Gao, M. X.; Zhang, X. M., Direct digestion of proteins in living cells into peptides for proteomic analysis. *Anal. Bioanal. Chem.* **2015**, *407* (3), 1027-1032.
51. Houel, S.; Abernathy, R.; Renganathan, K.; Meyer-Arendt, K.; Ahn, N. G.; Old, W. M., Quantifying the impact of chimera MS/MS spectra on peptide identification in large-scale proteomics studies. *J. Proteome Res.* **2010**, *9* (8), 4152-4160.

52. Mosier, P. D.; Counterman, A. E.; Jurs, P. C.; Clemmer, D. E., Prediction of peptide ion collision cross sections from topological molecular structure and amino acid parameters. *Anal. Chem.* **2002**, *74* (6), 1360-1370.
53. Houel, S.; Abernathy, R.; Renganathan, K.; Meyer-Arendt, K.; Ahn, N. G.; Old, W. M., Quantifying the impact of chimera MS/MS spectra on peptide identification in large-scale proteomics studies. *J Proteome Res* **2010**, *9* (8), 4152-60.
54. Picotti, P.; Clément-Ziza, M.; Lam, H.; Campbell, D. S.; Schmidt, A.; Deutsch, E. W.; Röst, H.; Sun, Z.; Rinner, O.; Reiter, L.; Shen, Q.; Michaelson, J. J.; Frei, A.; Alberti, S.; Kusebauch, U.; Wollscheid, B.; Moritz, R. L.; Beyer, A.; Aebersold, R., A complete mass-spectrometric map of the yeast proteome applied to quantitative trait analysis. *Nature* **2013**, *494* (7436), 266-270.
55. Nagaraj, N.; Alexander Kulak, N.; Cox, J.; Neuhauser, N.; Mayr, K.; Hoerning, O.; Vorm, O.; Mann, M., System-wide perturbation analysis with nearly complete coverage of the yeast proteome by single-shot ultra HPLC runs on a bench top Orbitrap. *Molecular & Cellular Proteomics* **2012**, *11* (3), M111.013722.
56. Hebert, A. S.; Richards, A. L.; Bailey, D. J.; Ulbrich, A.; Coughlin, E. E.; Westphall, M. S.; Coon, J. J., The one hour yeast proteome. *Molecular & Cellular Proteomics* **2014**, *13* (1), 339-347.
57. McAlister, G. C.; Nusinow, D. P.; Jedrychowski, M. P.; Wühr, M.; Huttlin, E. L.; Erickson, B. K.; Rad, R.; Haas, W.; Gygi, S. P., MultiNotch MS3 enables accurate, sensitive, and multiplexed detection of differential expression across cancer cell line proteomes. *Analytical chemistry* **2014**, *86* (14), 7150-7158.
58. Kim, M.-S.; Pinto, S. M.; Getnet, D.; Nirujogi, R. S.; Manda, S. S.; Chaerkady, R.; Madugundu, A. K.; Kelkar, D. S.; Isserlin, R.; Jain, S.; Thomas, J. K.; Muthusamy, B.; Leal-Rojas, P.; Kumar, P.; Sahasrabudde, N. A.; Balakrishnan, L.; Advani, J.; George, B.; Renuse, S.; Selvan, L. D. N.; Patil, A. H.; Nanjappa, V.; Radhakrishnan, A.; Prasad, S.; Subbannayya, T.; Raju, R.; Kumar, M.; Sreenivasamurthy, S. K.; Marimuthu, A.; Sathe, G. J.; Chavan, S.; Datta, K. K.; Subbannayya, Y.; Sahu, A.; Yelamanchi, S. D.; Jayaram, S.; Rajagopalan, P.; Sharma, J.; Murthy, K. R.; Syed, N.; Goel, R.; Khan, A. A.; Ahmad, S.; Dey, G.; Mudgal, K.; Chatterjee, A.; Huang, T.-C.; Zhong, J.; Wu, X.; Shaw, P. G.; Freed, D.; Zahari, M. S.; Mukherjee, K. K.; Shankar, S.; Mahadevan, A.; Lam, H.; Mitchell, C. J.; Shankar, S. K.; Satishchandra, P.; Schroeder, J. T.; Sirdeshmukh, R.; Maitra, A.; Leach, S. D.; Drake, C. G.; Halushka, M. K.; Prasad, T. S. K.; Hruban, R. H.; Kerr, C. L.; Bader, G. D.; Iacobuzio-Donahue, C. A.; Gowda, H.; Pandey, A., A draft map of the human proteome. *Nature* **2014**, *509* (7502), 575-581.
59. Sharma, K.; Schmitt, S.; Bergner, C. G.; Tyanova, S.; Kannaiyan, N.; Manrique-Hoyos, N.; Kongi, K.; Cantuti, L.; Hanisch, U.-K.; Philips, M.-A.; Rossner, M. J.; Mann, M.; Simons, M., Cell type- and brain region-resolved mouse brain proteome. *Nature Neuroscience* **2015**, *18* (12), 1819-1831.
60. Tasic, B.; Menon, V.; Nguyen, T. N.; Kim, T. K.; Jarsky, T.; Yao, Z.; Levi, B.; Gray, L. T.; Sorensen, S. A.; Dolbeare, T.; Bertagnolli, D.; Goldy, J.; Shapovalova, N.; Parry, S.; Lee, C.; Smith, K.; Bernard, A.; Madisen, L.; Sunkin, S. M.; Hawrylycz, M.; Koch, C.; Zeng, H., Adult mouse cortical cell taxonomy revealed by single cell transcriptomics. *Nature Neuroscience* **2016**, *19* (2), 335-346.
61. Zeisel, A.; Muñoz-Manchado, A. B.; Codeluppi, S.; Lönnerberg, P.; La Manno, G.; Juréus, A.; Marques, S.; Munguba, H.; He, L.; Betsholtz, C.; Rolny, C.; Castelo-Branco, G.;

- Hjerling-Leffler, J.; Linnarsson, S., Cell types in the mouse cortex and hippocampus revealed by single-cell RNA-seq. *Science (New York, N.Y.)* **2015**, *347* (6226), 1138-1142.
62. Lanni, E. J.; Rubakhin, S. S.; Sweedler, J. V., Mass spectrometry imaging and profiling of single cells. *Journal of Proteomics* **2012**, *75* (16), 5036-5051.
63. Rubakhin, S. S.; Romanova, E. V.; Nemes, P.; Sweedler, J. V., Profiling metabolites and peptides in single cells. *Nat. Methods* **2011**, *8* (4), S20-S29.
64. Buchberger, A.; Yu, Q.; Li, L., Advances in mass spectrometric tools for probing neuropeptides. *Annual Review of Analytical Chemistry* **2015**, *8* (1), 485-509.
65. Wang, D.; Bodovitz, S., Single cell analysis: the new frontier in 'omics'. *Trends in Biotechnology* **2010**, *28* (6), 281-290.
66. Hofstadler, S. A.; Swanek, F. D.; Gale, D. C.; Ewing, A. G.; Smith, R. D., Capillary electrophoresis-electrospray ionization fourier transform ion cyclotron resonance mass spectrometry for direct analysis of cellular proteins. *Analytical chemistry* **1995**, *67* (8), 1477-1480.
67. Valaskovic, G. A.; Kelleher, N. L.; McLafferty, F. W., Attomole protein characterization by capillary electrophoresis-mass spectrometry. *Science (New York, N.Y.)* **1996**, *273* (5279), 1199-1202.
68. Mellors, J. S.; Jorabchi, K.; Smith, L. M.; Ramsey, J. M., Integrated microfluidic device for automated single cell analysis using electrophoretic separation and electrospray ionization mass spectrometry. *Analytical chemistry* **2010**, *82* (3), 967-973.
69. Bendall, S. C.; Simonds, E. F.; Qiu, P.; Amir, E.-a. D.; Krutzik, P. O.; Finck, R.; Bruggner, R. V.; Melamed, R.; Trejo, A.; Ornatsky, O. I.; Balderas, R. S.; Plevritis, S. K.; Sachs, K.; Pe'er, D.; Tanner, S. D.; Nolan, G. P., Single-cell mass cytometry of differential immune and drug responses across a human hematopoietic continuum. *Science (New York, N.Y.)* **2011**, *332* (6030), 687-696.
70. Waanders, L. F.; Chwalek, K.; Monetti, M.; Kumar, C.; Lammert, E.; Mann, M., Quantitative proteomic analysis of single pancreatic islets. *Proceedings of the National Academy of Sciences* **2009**, *106* (45), 18902-18907.
71. Wang, N.; Xu, M.; Wang, P.; Li, L., Development of mass spectrometry-based shotgun method for proteome analysis of 500 to 5000 cancer cells. *Analytical chemistry* **2010**, *82* (6), 2262-2271.
72. Chen, Q.; Yan, G.; Gao, M.; Zhang, X., Direct digestion of proteins in living cells into peptides for proteomic analysis. *Anal. Bioanal. Chem.* **2015**, *407* (3), 1027-1032.
73. Yue, G.; Luo, Q.; Zhang, J.; Wu, S.-L.; Karger, B. L., Ultratrace LC/MS Proteomic Analysis Using 10- μ m-i.d. Porous Layer Open Tubular Poly(styrene-divinylbenzene) Capillary Columns. *Analytical chemistry* **2007**, *79* (3), 938-946.
74. Luo, Q.; Yue, G.; Valaskovic, G. A.; Gu, Y.; Wu, S.-L.; Karger, B. L., On-line 1D and 2D porous layer open tubular/LC-ESI-MS using 10- μ m-i.d. poly(styrene-divinylbenzene) columns for ultrasensitive proteomic analysis. *Analytical chemistry* **2007**, *79* (16), 6174-6181.
75. Shen, Y.; Tolić, N.; Masselon, C.; Paša-Tolić, L.; Camp, D. G.; Hixson, K. K.; Zhao, R.; Anderson, G. A.; Smith, R. D., Ultrasensitive proteomics using high-efficiency on-line micro-SPE-NanoLC-NanoESI MS and MS/MS. *Analytical chemistry* **2004**, *76* (1), 144-154.
76. Li, S.; Plouffe, B. D.; Belov, A. M.; Ray, S.; Wang, X.; Murthy, S. K.; Karger, B. L.; Ivanov, A. R., An integrated platform for isolation, processing, and mass spectrometry-based

- proteomic profiling of rare cells in whole blood. *Molecular & Cellular Proteomics* **2015**, *14* (6), 1672-1683.
77. Smith, R. D.; Barinaga, C. J.; Udseth, H. R., Improved electrospray ionization interface for capillary zone electrophoresis-mass spectrometry. *Analytical chemistry* **1988**, *60* (18), 1948-1952.
78. Bonvin, G.; Schappler, J.; Rudaz, S., Capillary electrophoresis–electrospray ionization–mass spectrometry interfaces: Fundamental concepts and technical developments. *Journal of Chromatography A* **2012**, *1267*, 17-31.
79. Lindenburg, P. W.; Haselberg, R.; Rozing, G.; Ramautar, R., Developments in interfacing designs for CE–MS: Towards enabling tools for proteomics and metabolomics. *Chromatographia* **2015**, *78* (5), 367-377.
80. Maxwell, E. J.; Chen, D. D. Y., Twenty years of interface development for capillary electrophoresis–electrospray ionization–mass spectrometry. *Analytica Chimica Acta* **2008**, *627* (1), 25-33.
81. Bendahl, L.; Hansen, S. H.; Olsen, J., A new sheathless electrospray interface for coupling of capillary electrophoresis to ion-trap mass spectrometry. *Rapid Communications in Mass Spectrometry* **2002**, *16* (24), 2333-2340.
82. Chen, Y.-R.; Her, G.-R., A simple method for fabrication of silver-coated sheathless electrospray emitters. *Rapid Communications in Mass Spectrometry* **2003**, *17* (5), 437-441.
83. Ramsey, R. S.; McLuckey, S. A., Capillary electrophoresis/electrospray ionization ion trap mass spectrometry using a sheathless interface. *Journal of Microcolumn Separations* **1995**, *7* (5), 461-469.
84. Zamfir, A. D.; Dinca, N.; Sisu, E.; Peter-Katalinić, J., Copper-coated microsyringe interface for on-line sheathless capillary electrophoresis electrospray mass spectrometry of carbohydrates. *Journal of separation science* **2006**, *29* (3), 414-422.
85. Kriger, M. S.; Cook, K. D.; Ramsey, R. S., Durable gold-coated fused silica capillaries for use in electrospray mass spectrometry. *Analytical chemistry* **1995**, *67* (2), 385-389.
86. Moini, M., Simplifying CE–MS Operation. 2. interfacing low-flow separation techniques to mass spectrometry using a porous tip. *Analytical chemistry* **2007**, *79* (11), 4241-4246.
87. Faserl, K.; Sarg, B.; Kremser, L.; Lindner, H., Optimization and evaluation of a sheathless capillary electrophoresis–electrospray ionization mass spectrometry platform for peptide analysis: Comparison to liquid chromatography–electrospray ionization mass spectrometry. *Analytical chemistry* **2011**, *83* (19), 7297-7305.
88. Wang, C.; Lee, C. S.; Smith, R. D.; Tang, K., Capillary isotachopheresis-nanoelectrospray ionization-selected reaction monitoring MS via a novel sheathless interface for high sensitivity sample quantification. *Analytical chemistry* **2013**, *85* (15), 7308-7315.
89. Wang, Y.; Fonslow, B. R.; Wong, C. C. L.; Nakorchevsky, A.; Yates, J. R., Improving the comprehensiveness and sensitivity of sheath less capillary electrophoresis-tandem mass spectrometry for proteomic analysis. *Analytical chemistry* **2012**, *84* (20), 8505-8513.
90. Guo, X.; Fillmore, T. L.; Gao, Y.; Tang, K., Capillary electrophoresis–nanoelectrospray ionization selected reaction monitoring mass spectrometry via a true sheathless metal-coated emitter interface for robust and high-sensitivity sample quantification. *Analytical chemistry* **2016**, *88* (8), 4418-4425.

91. Han, X.; Wang, Y.; Aslanian, A.; Bern, M.; Lavallée-Adam, M.; Yates, J. R., Sheathless capillary electrophoresis-tandem mass spectrometry for top-down characterization of pyrococcus furiosus proteins on a proteome scale. *Analytical chemistry* **2014**, *86* (22), 11006-11012.
92. Zhao, Y.; Riley, N. M.; Sun, L.; Hebert, A. S.; Yan, X.; Westphall, M. S.; Rush, M. J. P.; Zhu, G.; Champion, M. M.; Medie, F. M.; Champion, P. A. D.; Coon, J. J.; Dovichi, N. J., Coupling capillary zone electrophoresis with electron transfer dissociation and activated ion electron transfer dissociation for top-down proteomics. *Analytical chemistry* **2015**, *87* (10), 5422-5429.
93. Bush, D. R.; Zang, L.; Belov, A. M.; Ivanov, A. R.; Karger, B. L., High resolution CZE-MS quantitative characterization of intact biopharmaceutical proteins: Proteoforms of interferon- β 1. *Analytical chemistry* **2016**, *88* (2), 1138-1146.
94. Bruins, A. P.; Covey, T. R.; Henion, J. D., Ion spray interface for combined liquid chromatography/atmospheric pressure ionization mass spectrometry. *Analytical chemistry* **1987**, *59* (22), 2642-2646.
95. Hashimoto, M.; Ishihama, Y.; Tomita, M.; Soga, T., Microelectrospray interface with coaxial sheath flow for high-resolution capillary electrophoresis/mass spectrometry separation. *Rapid Communications in Mass Spectrometry* **2007**, *21* (22), 3579-3584.
96. Sun, L.; Li, Y.; Champion, M. M.; Zhu, G.; Wojcik, R.; Dovichi, N. J., Capillary zone electrophoresis-multiple reaction monitoring from 100 pg of RAW 264.7 cell lysate digest. *Analyst* **2013**, *138* (11), 3181-3188.
97. Li, Y.; Wojcik, R.; Dovichi, N. J.; Champion, M. M., Quantitative multiple reaction monitoring of peptide abundance introduced via a capillary zone electrophoresis-electrospray interface. *Analytical chemistry* **2012**, *84* (14), 6116-6121.
98. Sun, L.; Zhu, G.; Zhao, Y.; Yan, X.; Mou, S.; Dovichi, N. J., Ultrasensitive and fast bottom-up analysis of femtogram amounts of complex proteome digests. *Angewandte Chemie International Edition* **2013**, *52* (51), 13661-13664.
99. Li, Y.; Compton, P. D.; Tran, J. C.; Ntai, I.; Kelleher, N. L., Optimizing capillary electrophoresis for top-down proteomics of 30–80 kDa proteins. *PROTEOMICS* **2014**, *14* (10), 1158-1164.
100. Sun, L.; Zhu, G.; Zhang, Z.; Mou, S.; Dovichi, N. J., Third-generation electrokinetically pumped sheath-flow nanospray interface with improved stability and sensitivity for automated capillary zone electrophoresis-mass spectrometry analysis of complex proteome digests. *J. Proteome Res.* **2015**, *14* (5), 2312-2321.
101. Ludwig, K. R.; Sun, L.; Zhu, G.; Dovichi, N. J.; Hummon, A. B., Over 2300 phosphorylated peptide identifications with single-shot capillary zone electrophoresis-tandem mass spectrometry in a 100 min separation. *Analytical chemistry* **2015**, *87* (19), 9532-9537.
102. Lapainis, T.; Rubakhin, S. S.; Sweedler, J. V., Capillary electrophoresis with electrospray ionization mass spectrometric detection for single-cell metabolomics. *Analytical chemistry* **2009**, *81* (14), 5858-5864.
103. Nemes, P.; Knolhoff, A. M.; Rubakhin, S. S.; Sweedler, J. V., Metabolic differentiation of neuronal phenotypes by single-cell capillary electrophoresis-electrospray ionization-mass spectrometry. *Analytical chemistry* **2011**, *83* (17), 6810-6817.
104. Nemes, P.; Rubakhin, S. S.; Aerts, J. T.; Sweedler, J. V., Qualitative and quantitative metabolomic investigation of single neurons by capillary electrophoresis electrospray ionization mass spectrometry. *Nature Protocols* **2013**, *8* (4), 783-799.

105. Nemes, P.; Knolhoff, A. M.; Rubakhin, S. S.; Sweedler, J. V., Single-cell metabolomics: Changes in the metabolome of freshly isolated and cultured neurons. *ACS chemical neuroscience* **2012**, *3* (10), 782-792.
106. Onjiko, R. M.; Moody, S. A.; Nemes, P., Single-cell mass spectrometry reveals small molecules that affect cell fates in the 16-cell embryo. *Proceedings of the National Academy of Sciences* **2015**, *112* (21), 6545-6550.
107. Onjiko, R. M.; Morris, S. E.; Moody, S. A.; Nemes, P., Single-cell mass spectrometry with multi-solvent extraction identifies metabolic differences between left and right blastomeres in the 8-cell frog (*Xenopus*) embryo. *Analyst* **2016**, *141* (12), 3648-3656.
108. González-Ruiz, V.; Codesido, S.; Far, J.; Rudaz, S.; Schappler, J., Evaluation of a new low sheath–flow interface for CE-MS. *ELECTROPHORESIS* **2016**, *37* (7-8), 936-946.
109. Craig, R.; Cortens, J. P.; Beavis, R. C., Open source system for analyzing, validating, and storing protein identification data. *J. Proteome Res.* **2004**, *3* (6), 1234-1242.
110. Smith, R. D.; Olivares, J. A.; Nguyen, N. T.; Udseth, H. R., Capillary zone electrophoresis-mass spectrometry using an electrospray ionization interface. *Analytical chemistry* **1988**, *60* (5), 436-441.
111. Schmidt, A.; Karas, M.; Dülcks, T., Effect of different solution flow rates on analyte ion signals in nano-ESI MS, or: when does ESI turn into nano-ESI? *J. Am. Soc. Mass Spectrom.* **2003**, *14* (5), 492-500.
112. Nemes, P.; Marginean, I.; Vertes, A., Spraying mode effect on droplet formation and ion chemistry in electrosprays. *Anal. Chem.* **2007**, *79* (8), 3105-3116.
113. Valaskovic, G. A.; Murphy, J. P.; Lee, M. S., Automated orthogonal control system for electrospray ionization. *J. Am. Soc. Mass Spectrom.* **2004**, *15* (8), 1201-1215.
114. Iavarone, A. T.; Williams, E. R., Mechanism of charging and supercharging molecules in electrospray ionization. *Journal of the American Chemical Society* **2003**, *125* (8), 2319-2327.
115. Cox, J.; Hein, M. Y.; Luber, C. A.; Paron, I.; Nagaraj, N.; Mann, M., Accurate proteome-wide label-free quantification by delayed normalization and maximal peptide ratio extraction, termed MaxLFQ. *Molecular & Cellular Proteomics* **2014**, *13* (9), 2513-2526.
116. Ferencz, B.; Gerritsen, L., Genetics and underlying pathology of dementia. *Neuropsychology review* **2015**, *25* (1), 113-24.
117. Manzini, M. C.; Rajab, A.; Maynard, T. M.; Mochida, G. H.; Tan, W.-H.; Nasir, R.; Hill, R. S.; Gleason, D.; Al Saffar, M.; Partlow, J. N.; Barry, B. J.; Vernon, M.; LaMantia, A.-S.; Walsh, C. A., Developmental and degenerative features in a complicated spastic paraplegia. *Annals of Neurology* **2010**, *67* (4), 516-525.
118. Sun, L.; Zhu, G.; Dovichi, N. J., Integrated capillary zone electrophoresis–electrospray ionization tandem mass spectrometry system with an immobilized trypsin microreactor for online digestion and analysis of picogram amounts of RAW 264.7 cell lysate. *Analytical chemistry* **2013**, *85* (8), 4187-4194.
119. Faserl, K.; Kremser, L.; Müller, M.; Teis, D.; Lindner, H. H., Quantitative proteomics using ultralow flow capillary electrophoresis–mass spectrometry. *Analytical chemistry* **2015**, *87* (9), 4633-4640.
120. Johnson, M. B.; Wang, P. P.; Atabay, K. D.; Murphy, E. A.; Doan, R. N.; Hecht, J. L.; Walsh, C. A., Single-cell analysis reveals transcriptional heterogeneity of neural progenitors in human cortex. *Nature Neuroscience* **2015**, *18* (5), 637-646.

121. Lengler, J.; Jug, F.; Steger, A., Reliable neuronal systems: The importance of heterogeneity. *PLOS ONE* **2013**, *8* (12), e80694.
122. Shekhar, K.; Lapan, S. W.; Whitney, I. E.; Tran, N. M.; Macosko, E. Z.; Kowalczyk, M.; Adiconis, X.; Levin, J. Z.; Nemesh, J.; Goldman, M.; McCarroll, S. A.; Cepko, C. L.; Regev, A.; Sanes, J. R., Comprehensive classification of retinal bipolar neurons by single-cell transcriptomics. *Cell* **2016**, *166* (5), 1308-1323.e30.
123. Dowell, J. A.; Frost, D. C.; Zhang, J.; Li, L., Comparison of two-dimensional fractionation techniques for shotgun proteomics. *Analytical chemistry* **2008**, *80* (17), 6715-6723.
124. Zhang, X.; Fang, A.; Riley, C. P.; Wang, M.; Regnier, F. E.; Buck, C., Multi-dimensional liquid chromatography in proteomics—A review. *Analytica Chimica Acta* **2010**, *664* (2), 101-113.
125. Wiśniewski, J. R.; Zougman, A.; Mann, M., Combination of FASP and stagetip-based fractionation allows in-depth analysis of the hippocampal membrane proteome. *J. Proteome Res.* **2009**, *8* (12), 5674-5678.
126. Wang, H.; Sun, S.; Zhang, Y.; Chen, S.; Liu, P.; Liu, B., An off-line high pH reversed-phase fractionation and nano-liquid chromatography–mass spectrometry method for global proteomic profiling of cell lines. *Journal of Chromatography B* **2015**, *974*, 90-95.
127. Gilar, M.; Olivova, P.; Daly, A. E.; Gebler, J. C., Two-dimensional separation of peptides using RP-RP-HPLC system with different pH in first and second separation dimensions. *Journal of separation science* **2005**, *28* (14), 1694-1703.
128. Gokce, E.; Andrews, G. L.; Dean, R. A.; Muddiman, D. C., Increasing proteome coverage with offline RP HPLC coupled to online RP nanoLC–MS. *Journal of Chromatography B* **2011**, *879* (9), 610-614.
129. Kulak, N. A.; Geyer, P. E.; Mann, M., Loss-less nano-fractionator for high sensitivity, high coverage proteomics. *Molecular & Cellular Proteomics* **2017**, *16* (4), 694-705.
130. Romanova, E. V.; Aerts, J. T.; Croushore, C. A.; Sweedler, J. V., Small-volume analysis of cell–cell signaling molecules in the brain. *Neuropsychopharmacology* **2014**, *39* (1), 50-64.
131. Harstad, R. K.; Johnson, A. C.; Weisenberger, M. M.; Bowser, M. T., Capillary Electrophoresis. *Anal. Chem.* **2016**, *88* (1), 299-319.
132. Dawod, M.; Arvin, N. E.; Kennedy, R. T., Recent advances in protein analysis by capillary and microchip electrophoresis. *Analyst* **2017**, *142* (11), 1847-1866.
133. Šlampová, A.; Malá, Z.; Gebauer, P.; Boček, P., Recent progress of sample stacking in capillary electrophoresis (2014–2016). *ELECTROPHORESIS* **2017**, *38* (1), 20-32.
134. Sun, L.; Hebert, A. S.; Yan, X.; Zhao, Y.; Westphall, M. S.; Rush, M. J. P.; Zhu, G.; Champion, M. M.; Coon, J. J.; Dovichi, N. J., Over 10 000 peptide identifications from the hela proteome by using single-shot capillary zone electrophoresis combined with tandem mass spectrometry. *Angewandte Chemie International Edition* **2014**, *53* (50), 13931-13933.
135. Zhao, Y.; Sun, L.; Zhu, G.; Dovichi, N. J., Coupling capillary zone electrophoresis to a Q Exactive HF mass spectrometer for top-down proteomics: 580 proteoform identifications from yeast. *J. Proteome Res.* **2016**, *15* (10), 3679-3685.
136. Hofstadler, S. A.; Severs, J. C.; Smith, R. D.; Swanek, F. D.; Ewing, A. G., Analysis of single cells with capillary electrophoresis electrospray ionization fourier transform ion cyclotron resonance mass spectrometry. *Rapid Communications in Mass Spectrometry* **1996**, *10* (8), 919-922.

137. Mellors, J. S.; Jorabchi, K.; Smith, L. M.; Ramsey, J. M., Integrated microfluidic device for automated single cell analysis using electrophoretic separation and electrospray ionization mass spectrometry
Analytical chemistry **2010**, *82* (3), 967-973.
138. Moini, M.; Demars, S. M.; Huang, H., Analysis of carbonic anhydrase in human red blood cells using capillary electrophoresis/electrospray ionization-mass spectrometry. *Analytical chemistry* **2002**, *74* (15), 3772-3776.
139. Comi, T. J.; Do, T. D.; Rubakhin, S. S.; Sweedler, J. V., Categorizing cells on the basis of their chemical profiles: progress in single-cell mass spectrometry. *Journal of the American Chemical Society* **2017**, *139* (11), 3920-3929.
140. Yan, X.; Sun, L.; Zhu, G.; Cox, O. F.; Dovichi, N. J., Over 4100 protein identifications from a *Xenopus laevis* fertilized egg digest using reversed-phase chromatographic prefractionation followed by capillary zone electrophoresis–electrospray ionization–tandem mass spectrometry analysis. *PROTEOMICS* **2016**, *16* (23), 2945-2952.
141. Chen, D.; Shen, X.; Sun, L., Capillary zone electrophoresis–mass spectrometry with microliter-scale loading capacity, 140 min separation window and high peak capacity for bottom-up proteomics. *Analyst* **2017**, *142* (12), 2118-2127.
142. Zhang, Z.; Yan, X.; Sun, L.; Zhu, G.; Dovichi, N. J., Detachable strong cation exchange monolith, integrated with capillary zone electrophoresis and coupled with pH gradient elution, produces improved sensitivity and numbers of peptide identifications during bottom-up analysis of complex proteomes. *Analytical chemistry* **2015**, *87* (8), 4572-4577.
143. Zhang, Z.; Sun, L.; Zhu, G.; Cox, O. F.; Huber, P. W.; Dovichi, N. J., Nearly 1000 protein identifications from 50 ng of *xenopus laevis* zygote homogenate using online sample preparation on a strong cation exchange monolith based microreactor coupled with capillary zone electrophoresis. *Analytical chemistry* **2016**, *88* (1), 877-882.
144. Sun, B.; Kovatch, J. R.; Badiou, A.; Merbouh, N., Optimization and modeling of quadrupole orbitrap parameters for sensitive analysis toward single-cell proteomics. *J. Proteome Res.* **2017**, *16* (10), 3711-3721.
145. Pollen, A. A.; Nowakowski, T. J.; Shuga, J.; Wang, X.; Leyrat, A. A.; Lui, J. H.; Li, N.; Szpankowski, L.; Fowler, B.; Chen, P.; Ramalingam, N.; Sun, G.; Thu, M.; Norris, M.; Lebofsky, R.; Toppani, D.; Kemp, D. W.; Wong, M.; Clerkson, B.; Jones, B. N.; Wu, S.; Knutsson, L.; Alvarado, B.; Wang, J.; Weaver, L. S.; May, A. P.; Jones, R. C.; Unger, M. A.; Kriegstein, A. R.; West, J. A. A., Low-coverage single-cell mRNA sequencing reveals cellular heterogeneity and activated signaling pathways in developing cerebral cortex. *Nature Biotechnology* **2014**, *32* (10), 1053-1058.
146. Grassi, D.; Plonka, F. B.; Oksdath, M.; Guil, A. N.; Sosa, L. J.; Quiroga, S., Selected SNARE proteins are essential for the polarized membrane insertion of igf-1 receptor and the regulation of initial axonal outgrowth in neurons. *Cell Discovery* **2015**, *1* (1), 15023.
147. Jurado, S.; Goswami, D.; Zhang, Y.; Molina, A. J.; Südhof, T. C.; Malenka, R. C., LTP requires a unique postsynaptic SNARE fusion machinery. *Neuron* **2013**, *77* (3), 542-58.
148. Menezes, J.; Luskin, M., Expression of neuron-specific tubulin defines a novel population in the proliferative layers of the developing telencephalon. *The Journal of Neuroscience* **1994**, *14* (9), 5399-5416.
149. Keays, D. A.; Tian, G.; Poirier, K.; Huang, G.-J.; Siebold, C.; Cleak, J.; Oliver, P. L.; Fray, M.; Harvey, R. J.; Molnár, Z.; Piñon, M. C.; Dear, N.; Valdar, W.; Brown, S. D. M.;

- Davies, K. E.; Rawlins, J. N. P.; Cowan, N. J.; Nolan, P.; Chelly, J.; Flint, J., Mutations in α -tubulin cause abnormal neuronal migration in mice and lissencephaly in humans. *Cell* **2007**, *128* (1), 45-57.
150. Doherty, P.; Cohen, J.; Walsh, F. S., Neurite outgrowth in response to transfected N-CAM changes during development and is modulated by polysialic acid. *Neuron* **1990**, *5* (2), 209-19.
151. Bukalo, O.; Fentrop, N.; Lee, A. Y. W.; Salmen, B.; Law, J. W. S.; Wotjak, C. T.; Schweizer, M.; Dityatev, A.; Schachner, M., Conditional ablation of the neural cell adhesion molecule reduces precision of spatial learning, long-term potentiation, and depression in the CA1 subfield of mouse hippocampus. *The Journal of Neuroscience* **2004**, *24* (7), 1565-1577.
152. Gonzalez-Billault, C.; Jimenez-Mateos, E. M.; Caceres, A.; Diaz-Nido, J.; Wandosell, F.; Avila, J., Microtubule-associated protein 1B function during normal development, regeneration, and pathological conditions in the nervous system. *Journal of Neurobiology* **2004**, *58* (1), 48-59.
153. Francis, F.; Koulakoff, A.; Boucher, D.; Chafey, P.; Schaar, B.; Vinet, M.-C.; Friocourt, G.; McDonnell, N.; Reiner, O.; Kahn, A.; McConnell, S. K.; Berwald-Netter, Y.; Denoulet, P.; Chelly, J., Doublecortin is a developmentally regulated, microtubule-associated protein expressed in migrating and differentiating neurons. *Neuron* **1999**, *23* (2), 247-256.
154. Nawabi, H.; Belin, S.; Cartoni, R.; Williams, P. R.; Wang, C.; Latremolière, A.; Wang, X.; Zhu, J.; Taub, D. G.; Fu, X.; Yu, B.; Gu, X.; Woolf, C. J.; Liu, J. S.; Gabel, C. V.; Steen, J. A.; He, Z., Doublecortin-like kinases promote neuronal survival and induce growth cone reformation via distinct mechanisms. *Neuron* **2015**, *88* (4), 704-19.
155. des Portes, V.; Francis, F.; Pinard, J.-M.; Desguerre, I.; Moutard, M.-L.; Snoeck, I.; Meiners, L. C.; Capron, F.; Cusmai, R.; Ricci, S.; Motte, J.; Echenne, B.; Ponsot, G.; Dulac, O.; Chelly, J.; Beldjord, C., Doublecortin is the major gene causing x-linked subcortical laminar heterotopia (SCLH). *Human Molecular Genetics* **1998**, *7* (7), 1063-1070.
156. Etherton, M.; Földy, C.; Sharma, M.; Tabuchi, K.; Liu, X.; Shamloo, M.; Malenka, R. C.; Südhof, T. C., Autism-linked neuroligin-3 R451C mutation differentially alters hippocampal and cortical synaptic function. *Proceedings of the National Academy of Sciences* **2011**, *108* (33), 13764-13769.
157. Bretin, S.; Reibel, S.; Charrier, E.; Maus-Moatti, M.; Auvergnon, N.; Thevenoux, A.; Glowinski, J.; Rogemond, V.; Prémont, J.; Honnorat, J.; Gauchy, C., Differential expression of CRMP1, CRMP2A, CRMP2B, and CRMP5 in axons or dendrites of distinct neurons in the mouse brain. *Journal of Comparative Neurology* **2005**, *486* (1), 1-17.
158. Heinzen, E. L.; Arzimanoglou, A.; Brashear, A.; Clapcote, S. J.; Gurrieri, F.; Goldstein, D. B.; Jóhannesson, S. H.; Mikati, M. A.; Neville, B.; Nicole, S.; Ozelius, L. J.; Poulsen, H.; Schyns, T.; Sweadner, K. J.; van den Maagdenberg, A.; Vilsen, B., Distinct neurological disorders with ATP1A3 mutations. *The Lancet Neurology* **2014**, *13* (5), 503-514.
159. Ghosh, A.; Giese, K. P., Calcium/calmodulin-dependent kinase II and Alzheimer's disease. *Molecular Brain* **2015**, *8* (1), 78.
160. Deák, F.; Schoch, S.; Liu, X.; Südhof, T. C.; Kavalali, E. T., Synaptobrevin is essential for fast synaptic-vesicle endocytosis. *Nature Cell Biology* **2004**, *6* (11), 1102-1108.
161. Chapman, E. R.; An, S.; Barton, N.; Jahn, R., SNAP-25, a t-SNARE which binds to both syntaxin and synaptobrevin via domains that may form coiled coils. *J. Biol. Chem.* **1994**, *269* (44), 27427-27432.

162. Südhof, T. C., Neurotransmitter release: the last millisecond in the life of a synaptic vesicle. *Neuron* **2013**, *80* (3), 675-90.
163. Picotti, P.; Clement-Ziza, M.; Lam, H.; Campbell, D. S.; Schmidt, A.; Deutsch, E. W.; Rost, H.; Sun, Z.; Rinner, O.; Reiter, L.; Shen, Q.; Michaelson, J. J.; Frei, A.; Alberti, S.; Kusebauch, U.; Wollscheid, B.; Moritz, R. L.; Beyer, A.; Aebersold, R., A complete mass-spectrometric map of the yeast proteome applied to quantitative trait analysis. *Nature* **2013**, *494* (7436), 266-270.
164. Altschuler, S. J.; Wu, L. F., Cellular Heterogeneity: Do Differences Make a Difference? *Cell* **2010**, *141* (4), 559-563.
165. Nisar, M. S.; Zhao, X., High resolution mass spectrometry for single cell analysis. *International Journal of Mass Spectrometry* **2020**, *450*, 116302.
166. Moshkovskii, S. A.; Lobas, A. A.; Gorshkov, M. V., Single cell proteogenomics — Immediate prospects. *Biochemistry (Moscow)* **2020**, *85* (2), 140-146.
167. Evers, T. M. J.; Hochane, M.; Tans, S. J.; Heeren, R. M. A.; Semrau, S.; Nemes, P.; Mashaghi, A., Deciphering metabolic heterogeneity by single-cell analysis. *Anal. Chem.* **2019**, *91* (21), 13314-13323.
168. He, Y.; Rshan, E. H.; Linke, V.; Shishkova, E.; Hebert, A. S.; Jochem, A.; Westphall, M. S.; Pagliarini, D. J.; Overmyer, K. A.; Coon, J. J., Multi-omic single-shot technology for integrated proteome and lipidome analysis. *Anal Chem* **2021**, *93* (9), 4217-4222.
169. Woo, J.; Williams, S. M.; Aguilera-Vazquez, V.; Sontag, R. L.; Moore, R. J.; Markillie, L. M.; Mehta, H. S.; Cantlon, J.; Adkins, J. N.; Smith, R. D.; Clair, G. C.; Pasa-Tolic, L.; Zhu, Y., High-throughput and high-efficiency sample preparation for single-cell proteomics using a nested nanowell chip. *bioRxiv* **2021**, 2021.02.17.431689.
170. Petelski, A. A.; Emmott, E.; Leduc, A.; Huffman, R. G.; Specht, H.; Perlman, D. H.; Slavov, N., Multiplexed single-cell proteomics using SCoPE2. *bioRxiv* **2021**, 2021.03.12.435034.
171. Gomes, F. P.; Yates, III, Recent trends of capillary electrophoresis mass spectrometry in proteomics research. *Mass Spectrom. Rev.* **2019**, *38* (6), 445-460.
172. Drouin, N.; van Mever, M.; Zhang, W.; Tobolkina, E.; Ferre, S.; Servais, A. C.; Gou, M. J.; Nyssen, L.; Fillet, M.; Lageveen-Kammeijer, G. S. M.; Nouta, J.; Chetwynd, A. J.; Lynch, I.; Thorn, J. A.; Meixner, J.; Lossner, C.; Taverna, M.; Liu, S.; Tran, N. T.; Francois, Y.; Lechner, A.; Nehm, R.; Banni, G. A. D.; Nasreddine, R.; Colas, C.; Lindner, H. H.; Faserl, K.; Neuss, C.; Nelke, M.; Lammerer, S.; Perrin, C.; Bich-Muracciolo, C.; Barbas, C.; Gonzalez, A. L.; Guttman, A.; Szigeti, M.; Britz-McKibbin, P.; Kroezen, Z.; Shanmuganathan, M.; Nemes, P.; Portero, E. P.; Hankemeier, T.; Codesido, S.; Gonzalez-Ruiz, V.; Rudaz, S.; Ramautar, R., Capillary electrophoresis mass spectrometry at trial by metabo-ring: Effective electrophoretic mobility for reproducible and robust compound annotation. *Anal. Chem.* **2020**, *92* (20), 14103-14112.
173. Wang, Y.; Fonslow, B. R.; Wong, C. C. L.; Nakorchevsky, A.; Yates, J. R., Improving the comprehensiveness and sensitivity of sheathless capillary electrophoresis–tandem mass spectrometry for proteomic analysis. *Anal. Chem.* **2012**, *84* (20), 8505-8513.
174. Lombard-Banek, C.; Moody, S. A.; Nemes, P., Single-cell mass spectrometry for discovery proteomics: quantifying translational cell heterogeneity in the 16-cell frog (*xenopus*) embryo. *Angew. Chem.-Int. Edit.* **2016**, *55* (7), 2454-2458.

175. Lombard-Banek, C.; Li, J.; Portero, E. P.; Onjiko, R. M.; Singer, C. D.; Plotnick, D.; Al Shabeeb, R. Q.; Nemes, P., *In vivo* subcellular mass spectrometry enables proteo-metabolomic single-cell systems biology in a chordate embryo developing to a normally behaving tadpole (*X. laevis*). *Angew. Chem.-Int. Edit.* **2021**, *60* (23), 12852-12858.
176. Lombard-Banek, C.; Moody, S. A.; Manzin, M. C.; Nemes, P., Microsampling capillary electrophoresis mass spectrometry enables single-cell proteomics in complex tissues: developing cell clones in live *Xenopus laevis* and zebrafish embryos. *Anal. Chem.* **2019**, *91* (7), 4797-4805.
177. Sun, L. L.; Zhu, G. J.; Zhao, Y. M.; Yan, X. J.; Mou, S.; Dovichi, N. J., Ultrasensitive and fast bottom-up analysis of femtogram amounts of complex proteome digests. *Angew. Chem.-Int. Edit.* **2013**, *52* (51), 13661-13664.
178. Sun, L. L.; Zhu, G. J.; Zhang, Z. B.; Mou, S.; Dovichi, N. J., Third-generation electrokinetically pumped sheath-flow nanospray interface with improved stability and sensitivity for automated capillary zone electrophoresis mass spectrometry analysis of complex proteome digests. *J. Proteome Res.* **2015**, *14* (5), 2312-2321.
179. Zhang, Z. B.; Hebert, A. S.; Westphall, M. S.; Qu, Y. Y.; Coon, J. J.; Dovichi, N. J., Production of over 27 000 peptide and nearly 4400 protein identifications by single-shot capillary zone electrophoresis mass spectrometry via combination of a very-low electroosmosis coated capillary, a third-generation electrokinetically-pumped sheath-flow nanospray interface, an orbitrap fusion lumos tribrid mass spectrometer, and an advanced-peak determination algorithm. *Anal. Chem.* **2018**, *90* (20), 12090-12093.
180. Liu, H. B.; Sadygov, R. G.; Yates, J. R., A model for random sampling and estimation of relative protein abundance in shotgun proteomics. *Anal. Chem.* **2004**, *76* (14), 4193-4201.
181. Tabb, D. L.; Vega-Montoto, L.; Rudnick, P. A.; Variyath, A. M.; Ham, A. J. L.; Bunk, D. M.; Kilpatrick, L. E.; Billheimer, D. D.; Blackman, R. K.; Cardasis, H. L.; Carr, S. A.; Clauser, K. R.; Jaffe, J. D.; Kowalski, K. A.; Neubert, T. A.; Regnier, F. E.; Schilling, B.; Tegeler, T. J.; Wang, M.; Wang, P.; Whiteaker, J. R.; Zimmerman, L. J.; Fisher, S. J.; Gibson, B. W.; Kinsinger, C. R.; Mesri, M.; Rodriguez, H.; Stein, S. E.; Tempst, P.; Paulovich, A. G.; Liebler, D. C.; Spiegelman, C., Repeatability and reproducibility in proteomic identifications by liquid chromatography-tandem mass spectrometry. *J. Proteome Res.* **2010**, *9* (2), 761-776.
182. Zhang, Y. Y.; Fonslow, B. R.; Shan, B.; Baek, M. C.; Yates, J. R., Protein analysis by shotgun/bottom-up proteomics. *Chem. Rev.* **2013**, *113* (4), 2343-2394.
183. Wang, N.; Li, L., Exploring the precursor ion exclusion feature of liquid chromatography-electrospray ionization quadrupole time-of-flight mass spectrometry for improving protein identification in shotgun proteome analysis. *Anal. Chem.* **2008**, *80* (12), 4696-4710.
184. Kreimer, S.; Belov, M. E.; Danielson, W. F.; Levitsky, L. I.; Gorshkov, M. V.; Karger, B. L.; Ivanov, A. R., Advanced precursor ion selection algorithms for increased depth of bottom-up proteomic profiling. *J. Proteome Res.* **2016**, *15* (10), 3563-3573.
185. Wu, W. W.; Shen, R. F.; Park, S. S.; Martin, B.; Maudsley, S., Precursor ion exclusion for enhanced identification of plasma biomarkers. *Proteom. Clin. Appl.* **2012**, *6* (5-6), 304-308.
186. Voisin, S. N.; Krakovska, O.; Matta, A.; DeSouza, L. V.; Romaschin, A. D.; Colgan, T. J.; Siu, K. W. M., Identification of novel molecular targets for endometrial cancer using a drill-down LC-MS/MS approach with iTRAQ. *PLoS One* **2011**, *6* (1), e16352.
187. Zhang, Z. Q., Automated precursor ion exclusion during LC-MS/MS data acquisition for optimal ion identification. *J. Am. Soc. Mass Spectrom.* **2012**, *23* (8), 1400-1407.

188. Hoopmann, M. R.; Merrihew, G. E.; von Haller, P. D.; MacCoss, M. J., Post analysis data acquisition for the iterative MS/MS sampling of proteomics mixtures. *J. Proteome Res.* **2009**, *8* (4), 1870-1875.
189. Bailey, D. J.; McDevitt, M. T.; Westphall, M. S.; Pagliarini, D. J.; Coon, J. J., Intelligent data acquisition blends targeted and discovery methods. *J. Proteome Res.* **2014**, *13* (4), 2152-2161.
190. Kaech, S.; Banker, G., Culturing hippocampal neurons. *Nat. Protoc.* **2006**, *1* (5), 2406-2415.
191. Pluskal, T.; Castillo, S.; Villar-Briones, A.; Oresic, M., MZmine 2: Modular framework for processing, visualizing, and analyzing mass spectrometry-based molecular profile data. *BMC Bioinformatics* **2010**, *11*, 11.
192. Chen, D. Y.; Shen, X. J.; Sun, L. L., Capillary zone electrophoresis-mass spectrometry with microliter-scale loading capacity, 140 min separation window and high peak capacity for bottom-up proteomics. *Analyst* **2017**, *142* (12), 2118-2127.
193. Chen, D.; Shen, X.; Sun, L., Strong cation exchange-reversed phase liquid chromatography-capillary zone electrophoresis-tandem mass spectrometry platform with high peak capacity for deep bottom-up proteomics. *Analytica Chimica Acta* **2018**, *1012* (5), 1-9.
194. Zhang, Z. B.; Yan, X. J.; Sun, L. L.; Zhu, G. J.; Dovichi, N. J., Detachable strong cation exchange monolith, integrated with capillary zone electrophoresis and coupled with ph gradient elution, produces improved sensitivity and numbers of peptide identifications during bottom-up analysis of complex proteomes. *Analytical chemistry* **2015**, *87* (8), 4572-4577.
195. Shen, X. J.; Kou, Q.; Guo, R. Q.; Yang, Z. C.; Chen, D. Y.; Liu, X. W.; Hong, H.; Sun, L. L., Native proteomics in discovery mode using size-exclusion chromatography capillary zone electrophoresis tandem mass spectrometry. *Analytical chemistry* **2018**, *90* (17), 10095-10099.
196. Zhu, H. Y.; Zou, G. C.; Wang, N.; Zhuang, M. H.; Xiong, W.; Huang, G. M., Single-neuron identification of chemical constituents, physiological changes, and metabolism using mass spectrometry. *Proc. Natl. Acad. Sci. U. S. A.* **2017**, *114* (10), 2586-2591.
197. Shi, W. X., Electrophysiological Characteristics of Dopamine Neurons: A 35-Year Update. *J. Neural Transm.-Suppl.* **2009**, (73), 103-119.
198. Hamill, O. P.; Marty, A.; Neher, E.; Sakmann, B.; Sigworth, F. J., Improved patch-clamp techniques for high-resolution current recording from cells and cell-free membrane patches. *Pflugers Arch.* **1981**, *391* (2), 85-100.
199. Booker, S. A.; Song, J.; Vida, I., Whole-cell Patch-clamp Recordings from Morphologically- and Neurochemically-identified Hippocampal Interneurons. *J. Vis. Exp.* **2014**, (91), 11.
200. Aerts, J. T.; Louis, K. R.; Crandall, S. R.; Govindaiah, G.; Cox, C. L.; Sweedler, J. V., Patch Clamp Electrophysiology and Capillary Electrophoresis–Mass Spectrometry Metabolomics for Single Cell Characterization. *Anal. Chem.* **2014**, *86* (6), 3203-3208.
201. Cadwell, C. R.; Palasantza, A.; Jiang, X. L.; Berens, P.; Deng, Q. L.; Yilmaz, M.; Reimer, J.; Shen, S.; Bethge, M.; Tolias, K. F.; Sandberg, R.; Tolias, A. S., Electrophysiological, transcriptomic and morphologic profiling of single neurons using Patch-seq. *Nat. Biotechnol.* **2016**, *34* (2), 199-+.
202. Camerino, D. C.; Tricarico, D.; Desaphy, J. F., Ion channel pharmacology. *Neurotherapeutics* **2007**, *4* (2), 184-198.

203. Sharma, K.; Schmitt, S.; Bergner, C. G.; Tyanova, S.; Kannaiyan, N.; Manrique-Hoyos, N.; Kongi, K.; Cantuti, L.; Hanisch, U. K.; Philips, M. A.; Rossner, M. J.; Mann, M.; Simons, M., Cell type- and brain region-resolved mouse brain proteome. *Nat. Neurosci.* **2015**, *18* (12), 1819-1831.
204. Choi, S. B.; Lombard-Banek, C.; Muñoz-LLancao, P.; Manzini, M. C.; Nemes, P., Enhanced Peptide Detection Toward Single-Neuron Proteomics by Reversed-Phase Fractionation Capillary Electrophoresis Mass Spectrometry. *J. Am. Soc. Mass Spectrom.* **2017**.
205. Sun, L. L.; Zhu, G. J.; Zhang, Z. B.; Mou, S.; Dovichi, N. J., Third-Generation Electrokinetically Pumped Sheath-Flow Nanospray Interface with Improved Stability and Sensitivity for Automated Capillary Zone Electrophoresis-Mass Spectrometry Analysis of Complex Proteome Digests. *J. Proteome Res.* **2015**, *14* (5), 2312-2321.
206. Trouillon, R.; Passarelli, M. K.; Wang, J.; Kurczyk, M. E.; Ewing, A. G., Chemical Analysis of Single Cells. *Anal. Chem.* **2013**, *85* (2), 522-542.
207. Onjiko, R. M.; Portero, E. P.; Moody, S. A.; Nemes, P., In Situ Microprobe Single-Cell Capillary Electrophoresis Mass Spectrometry: Metabolic Reorganization in Single Differentiating Cells in the Live Vertebrate (*Xenopus laevis*) Embryo. *Anal. Chem.* **2017**, *89* (13), 7069-7076.
208. Shi, T.; Gaffrey, M. J.; Fillmore, T. L.; Nicora, C. D.; Yi, L.; Zhang, P.; Shukla, A. K.; Wiley, H. S.; Rodland, K. D.; Liu, T.; Smith, R. D.; Qian, W.-J., Facile carrier-assisted targeted mass spectrometric approach for proteomic analysis of low numbers of mammalian cells. *Communications Biology* **2018**, *1* (1), 103.
209. Budnik, B.; Levy, E.; Harmange, G.; Slavov, N., SCoPE-MS: mass spectrometry of single mammalian cells quantifies proteome heterogeneity during cell differentiation. *Genome Biol.* **2018**, *19*, 12.
210. Lombard-Banek, C.; Moody, S. A.; Manzini, M. C.; Nemes, P., A microprobe single-cell mass spectrometer for spatially and temporally resolved single-cell proteomics in complex tissues and live embryos (Submitted). **2019**.
211. Neher, E.; Sakmann, B., Single-channel currents recorded from membrane of denervated frog muscle fibres. *Nature* **1976**, *260*, 799.
212. Markram, H.; Lubke, J.; Frotscher, M.; Roth, A.; Sakmann, B., Physiology and anatomy of synaptic connections between thick tufted pyramidal neurones in the developing rat neocortex. *J. Physiol.-London* **1997**, *500* (2), 409-440.
213. Shear, J. B.; Fishman, H. A.; Allbritton, N. L.; Garigan, D.; Zare, R. N.; Scheller, R. H., Single cells as biosensors for chemical separations. *Science* **1995**, *267* (5194), 74-77.
214. Polter, A. M.; Bishop, R. A.; Briand, L. A.; Graziane, N. M.; Pierce, R. C.; Kauer, J. A., Poststress Block of Kappa Opioid Receptors Rescues Long-Term Potentiation of Inhibitory Synapses and Prevents Reinstatement of Cocaine Seeking. *Biol. Psychiatry* **2014**, *76* (10), 785-793.
215. Ting, J. T.; Daigle, T. L.; Chen, Q.; Feng, G. P., Acute Brain Slice Methods for Adult and Aging Animals: Application of Targeted Patch Clamp Analysis and Optogenetics. In *Patch-Clamp Methods and Protocols, 2nd Edition*, Martina, M.; Taverna, S., Eds. Humana Press Inc: Totowa, 2014; Vol. 1183, pp 221-242.
216. Grace, A. A.; Onn, S. P., Morphology and electrophysiological properties of immunocytochemically identified rat dopamine neurons recorded invitro. *J. Neurosci.* **1989**, *9* (10), 3463-3481.

217. Lammel, S.; Hetzel, A.; Haeckel, O.; Jones, I.; Liss, B.; Roeper, J., Unique properties of mesoprefrontal neurons within a dual mesocorticolimbic dopamine system. *Neuron* **2008**, *57* (5), 760-773.
218. Feist, P.; Hummon, A. B., Proteomic Challenges: Sample Preparation Techniques for Microgram-Quantity Protein Analysis from Biological Samples. *Int J Mol Sci* **2015**, *16* (2), 3537-3563.
219. Suttapitugsakul, S.; Xiao, H. P.; Smeekens, J.; Wu, R. H., Evaluation and optimization of reduction and alkylation methods to maximize peptide identification with MS- based proteomics. *Mol. Biosyst.* **2017**, *13* (12), 2574-2582.
220. Altelaar, A. F. M.; Munoz, J.; Heck, A. J. R., Next-generation proteomics: towards an integrative view of proteome dynamics. *Nat. Rev. Genet.* **2013**, *14* (1), 35-48.
221. Larance, M.; Lamond, A. I., Multidimensional proteomics for cell biology. *Nature Reviews Molecular Cell Biology* **2015**, *16* (5), 269-280.
222. Aebersold, R.; Mann, M., Mass-spectrometric exploration of proteome structure and function. *Nature* **2016**, *537* (7620), 347-355.
223. Lombard-Banek, C.; Moody, S. A.; Manzini, M. C.; Nemes, P., Microsampling capillary electrophoresis mass spectrometry enables single-cell proteomics in complex tissues: developing cell clones in live xenopus laevis and zebrafish embryos. *Analytical chemistry* **2019**, *91* (7), 4797-4805.
224. Virant-Klun, I.; Leicht, S.; Hughes, C.; Krijgsveld, J., Identification of maturation-specific pProteins by single-cell proteomics of human oocytes. *Molecular & cellular proteomics : MCP* **2016**, *15* (8), 2616-27.
225. Zhu, Y.; Piehowski, P. D.; Zhao, R.; Chen, J.; Shen, Y.; Moore, R. J.; Shukla, A. K.; Petyuk, V. A.; Campbell-Thompson, M.; Mathews, C. E.; Smith, R. D.; Qian, W.-J.; Kelly, R. T., Nanodroplet processing platform for deep and quantitative proteome profiling of 10–100 mammalian cells. *Nature Communications* **2018**, *9* (1), 882.
226. Dou, M.; Clair, G.; Tsai, C.-F.; Xu, K.; Chrisler, W. B.; Sontag, R. L.; Zhao, R.; Moore, R. J.; Liu, T.; Pasa-Tolic, L.; Smith, R. D.; Shi, T.; Adkins, J. N.; Qian, W.-J.; Kelly, R. T.; Ansong, C.; Zhu, Y., High-throughput single cell proteomics enabled by multiplex isobaric labeling in a nanodroplet sample preparation platform. *Analytical chemistry* **2019**, *91* (20), 13119-13127.
227. Williams, S. M.; Liyu, A. V.; Tsai, C.-F.; Moore, R. J.; Orton, D. J.; Chrisler, W. B.; Gaffrey, M. J.; Liu, T.; Smith, R. D.; Kelly, R. T.; Pasa-Tolic, L.; Zhu, Y., Automated coupling of nanodroplet sample preparation with liquid chromatography-mass spectrometry for high-throughput single-cell proteomics. *Analytical chemistry* **2020**, *92* (15), 10588-10596.
228. Chen, A. T.; Franks, A.; Slavov, N., DART-ID increases single-cell proteome coverage. *PLoS Comput Biol* **2019**, *15* (7), e1007082-e1007082.
229. Specht, H.; Emmott, E.; Koller, T.; Slavov, N., High-throughput single-cell proteomics quantifies the emergence of macrophage heterogeneity. *bioRxiv* **2019**, 665307.
230. Metwally, H.; McAllister, R. G.; Konermann, L., Exploring the mechanism of salt-induced signal suppression in protein electrospray mass spectrometry using experiments and molecular dynamics simulations. *Analytical chemistry* **2015**, *87* (4), 2434-2442.
231. Hao, C.; March, R. E.; Croley, T. R.; Smith, J. C.; Rafferty, S. P., Electrospray ionization tandem mass spectrometric study of salt cluster ions. Part 1— Investigations of alkali metal chloride and sodium salt cluster ions. *J. Mass Spectrom.* **2001**, *36* (1), 79-96.

232. Rappsilber, J.; Mann, M.; Ishihama, Y., Protocol for micro-purification, enrichment, pre-fractionation and storage of peptides for proteomics using StageTips. *Nature Protocols* **2007**, *2* (8), 1896-1906.
233. Józwiak, M., Complex formation of crown ethers with cations in the water-organic solvent mixtures. Part VIII.1 Thermodynamic of interactions of Na⁺ ion with 15-crown-5 and benzo-15-crown-5 ethers in the mixtures of water with hexamethylphosphortriamide at 298.15 K. *Journal of Solution Chemistry* **2004**, *33* (9), 1073-1084.
234. Cole, M. L.; Jones, C.; Junk, P. C., Ether and crown ether adduct complexes of sodium and potassium cyclopentadienide and methylcyclopentadienide—molecular structures of [Na(dme)Cp][∞], [K(dme)0.5Cp][∞], [Na(15-crown-5)Cp], [Na(18-crown-6)CpMe] and the “naked Cp⁻” complex [K(15-crown-5)₂][Cp]. *Journal of the Chemical Society, Dalton Transactions* **2002**, (6), 896-905.
235. Choi, S. B.; Lombard-Banek, C.; Muñoz-Llancao, P.; Manzini, M. C.; Nemes, P., Enhanced peptide detection toward single-neuron proteomics by reversed-phase fractionation capillary electrophoresis mass spectrometry. *J. Am. Soc. Mass Spectrom.* **2018**, *29* (5), 913-922.
236. Lombard-Banek, C.; Choi, S. B.; Nemes, P., Single-cell proteomics in complex tissues using microprobe capillary electrophoresis mass spectrometry. *Methods Enzymol* **2019**, *628*, 263-292.
237. More, M. B.; Ray, D.; Armentrout, P. B., Intrinsic affinities of alkali cations for 15-crown-5 and 18-crown-6: Bond dissociation energies of gas-phase M⁺-crown ether complexes. *Journal of the American Chemical Society* **1999**, *121* (2), 417-423.
238. Petersson, F. Investigation of crown ether cation systems using electrophoretic NMR. Student thesis, 2012.
239. Williams, S. M.; Liyu, A. V.; Tsai, C. F.; Moore, R. J.; Orton, D. J.; Chrisler, W. B.; Gaffrey, M. J.; Liu, T.; Smith, R. D.; Kelly, R. T.; Pasa-Tolic, L.; Zhu, Y., Automated coupling of nanodroplet sample preparation with liquid chromatography-mass spectrometry for high-throughput single-cell proteomics. *Analytical chemistry* **2020**, *92* (15), 10588-10596.
240. Chen, D.; Shen, X.; Sun, L., Capillary zone electrophoresis-mass spectrometry with microliter-scale loading capacity, 140 min separation window and high peak capacity for bottom-up proteomics. *Analyst* **2017**, *142* (12), 2118-2127.
241. Bailey, D. J.; Rose, C. M.; McAlister, G. C.; Brumbaugh, J.; Yu, P.; Wenger, C. D.; Westphall, M. S.; Thomson, J. A.; Coon, J. J., Instant spectral assignment for advanced decision tree-driven mass spectrometry. *Proc Natl Acad Sci U S A* **2012**, *109* (22), 8411-6.
242. Hebert, A. S.; Thöing, C.; Riley, N. M.; Kwiecien, N. W.; Shiskova, E.; Huguet, R.; Cardasis, H. L.; Kuehn, A.; Eliuk, S.; Zabrouskov, V.; Westphall, M. S.; McAlister, G. C.; Coon, J. J., Improved precursor characterization for data-dependent mass spectrometry. *Analytical chemistry* **2018**, *90* (3), 2333-2340.
243. Vasilopoulou, C. G.; Sulek, K.; Brunner, A.-D.; Meitei, N. S.; Schweiger-Hufnagel, U.; Meyer, S. W.; Barsch, A.; Mann, M.; Meier, F., Trapped ion mobility spectrometry and PASEF enable in-depth lipidomics from minimal sample amounts. *Nature Communications* **2020**, *11* (1), 331.
244. Meier, F.; Brunner, A. D.; Koch, S.; Koch, H.; Lubeck, M.; Krause, M.; Goedecke, N.; Decker, J.; Kosinski, T.; Park, M. A.; Bache, N.; Hoerning, O.; Cox, J.; Räther, O.; Mann, M., Online parallel accumulation-serial fragmentation (PASEF) with a novel trapped ion mobility mass spectrometer. *Molecular & cellular proteomics : MCP* **2018**, *17* (12), 2534-2545.